Mountain pine beetle and forest harvest effects on hydrologic processes and streamflow in the Alberta Foothills

by

Amy Rachelle Goodbrand

A thesis submitted in partial fulfillment of the requirements for the degree of

Doctor of Philosophy

in

Water and Land Resources

Department of Renewable Resources

University of Alberta

ABSTRACT

The Alberta Foothills region has experienced an unprecedented mountain pine beetle (MPB) outbreak. The provincial management strategy is to contain the infestation with forest harvest. The landscape becomes a patchwork of dead (MPB grey-attack), alive, and harvested stands. MPB attack affects the water transport in trees and results in the gradual loss of the canopy structure, which has the potential to affect hydrologic processes. Therefore, there is a need to understand MPB and forest harvest effects on runoff generation and the streamflow response, especially in watersheds that provide habitat for the endangered Athabasca Rainbow Trout (ARTR). Research questions addressed in this thesis were: 1) what is the effect of varied canopy cover loss on stand water cycling in the Foothills; 2) what is the effect of forest harvest on streamflow in a Foothills watershed; and, 3) what is the effect of potential streamflow changes from MPB grey-attack and forest harvest scenarios on ARTR fry recruitment in a Foothills stream? Methods included a combination of statistical and hydrological modelling as well as data from the MPB Ecohydrology stand-level study and a long-term dataset from the Tri-Creeks Experimental Watershed (Tri-Creeks) near Robb, Alberta. Tri-Creeks has complex glacial deposits underlain by sedimentary bedrock; a geological setting with large potential for subsurface water storage. In addition, climate variability, especially meteorologically driven changes from the Pacific Decadal Oscillation (PDO), influence streamflow. Results from stand-level water balance models showed root zone drainage from the MPB grey-attack stands were similar to an undisturbed mature lodgepole pine stand. Compensatory increases in evapotranspiration from surviving vegetation (unaffected trees or understory vegetation) were predicted in the grey-attacked stands. The greatest root zone drainage occurred in the harvested stand. Results indicate regional differences in hydrologic processes that generate runoff in MPB and harvested stands. Historical clear-cut harvest within Tri-Creeks sub-watersheds was predicted to result in a significant measurable increase in rainfall-generated peak runoff events and summer runoff. However, increased runoff from harvested watersheds may have been attenuated by the drier antecedent watershed conditions in the warm PDO phase. Climate variability, in relation to antecedent watershed storage, remained a strong control on runoff generation in the watersheds. Watershed disturbance scenarios showed MPB grey-attack produced no effect on simulated streamflow response, while simulated clear-cut harvest (52% watershed area) resulted in 15% greater mean annual water yield than if grey-attack trees were left standing. Increased streamflow from forest harvest above the critical discharge threshold for streambed movement of ARTR spawning substrate during the incubation period was predicted to reduce fry recruitment, but annual fry recruitment was estimated to occur over the 50-year simulated streamflow record. Reduced fry recruitment from forest harvest was not likely to produce measurable change at the population level. Overall, results from this thesis provide better understanding of the MPB and forest harvest effects on hydrologic processes and streamflow in the Alberta Foothills and could factor into decisions about MPB strategies with respect to the endangered Athabasca Rainbow Trout.

PREFACE

This thesis is an original work by Amy R. Goodbrand.

Chapter 2 includes data collected and reported by others. The pre-treatment hydrometeorological data collection (2008 – 2009) was led by Dr. Pablo Piña[1]. I re-analyzed raw data for the pre-treatment period to ensure consistency between pre-and post-treatment periods, except for daily tree transpiration per unit leaf area. Pre-treatment (2008 – 2009) forest structure data collection was led by Dr. Anne McIntosh[2]. Post-treatment (2015 – 2016) forest structure data collection was led by Julie Steinke[3].

Chapter 3 includes data collected by the multi-decadal efforts of several organizations including Alberta Energy and Natural Resources, Alberta Recreation, Parks and Wildlife, Alberta Environment, Alberta Research Council, and Environment Canada. These data have been summarized in the grey literature[4,5].

Chapter 4 includes Athabasca Rainbow Trout (ARTR) population abundance data from Wampus Creek for the periods 1969 – 1985[6] and 1969 – 2013[7] collected by Alberta Fish and Wildlife. The relationship between fry density and the critical discharge threshold when ARTR spawning substrate begins to move downstream was developed by George Sterling[8].

---

[1] Piña (2013). PhD thesis, Univ. of Alberta, 162 pp. [2] McIntosh & Macdonald (2013). *Ecosphere*, 4(6), 1-28. [3] Steinke *et al.* (2020). *Forest Ecology and Management*, 474, 118373. [4] Andres *et al.* (1987). Alberta Research Council, Report No. SWE-87/01. Vol. 1. 418 pp. [5] Nip (1991). Research Branch Technical Report No. 4. Alberta Forestry, Lands and Wildlife. 66 pp. [6] Sterling (1990). Tri-Creeks Experimental Watershed, Research Report 10. Alberta Forestry Lands and Wildlife, Fish and Wildlife Division, 68 pp. [7] Alberta Athabasca Rainbow Trout Recovery Team. (2014). Alberta Species at Risk Recovery Plan No. 36. 111 pp. [8] Sterling (1992). MSc. Thesis, University of Alberta, 116 pp.

ACKNOWLEDGMENTS

People do not do big things alone, we do them together. My name is on the cover, but there are numerous people without whose help this thesis would not exist. Here are some of them:

I would like to sincerely thank Dr. Axel Anderson for his contributions to my development as a scientist, the autonomy, and opportunities. Thank you to Dr. Uldis Silins and Dr. Kevin Devito for the insightful conversations and guidance. I wish to thank each of them for their compassion and support as I navigated the last few years away from the University. I would also like to thank Dr. Justine Karst, Dr. Thian Yew Gan and Dr. David Olefeldt for participating in my Candidacy Exam and/or Final Examination. Thank you to Dr. Jim Buttle for serving as my external examiner.

The funding support of fRI Research through the Mountain Pine Beetle Ecology Program, the Forest Resources Improvement Association of Alberta (FRIAA) and West Fraser Mills Ltd. is gratefully acknowledged. I am also grateful for the financial support from a University of Alberta Doctoral Recruitment Scholarship, a Canadian Federation of University Women (Edmonton) bursary, and an Alberta Graduate Excellence Scholarship.

Thank you to Jamie Hynes and Shuhang Lu for their field assistance and efforts in transferring archived data into the digital world. Thank you to Milly Corrigan, Kelsey Ridley, Mathew Rayner and Connor Noyes for additional field help and tackling some snow surveys. I am indebted to Chris Williams for his help to fix and climb the towers. Thank you to Dr. Sheena Spencer for her feedback and support. To my other colleagues in the forest hydrology lab, thanks for the memories: Samantha Karpyshin, Amanda Martens, Mike Stewart, Dan Greenacre, Kali Herlein, Melissa Howard. Thank you to Dr. James Craig, Matt Chernos and Dr. Ryan MacDonald for their assistance with Raven. Thanks to Dr. Nicholas Zégre for the prediction interval R code. A special thank you to Ryan MacDonald for his encouragement to continue to pursue science when life got really hard.

This thesis would never have been written without the support of my other community. Thank you to the doctors and nurses I have crossed paths with at Tom Baker, High River, and the Cross Cancer Institute. Thank you to Wellspring and Survive & Thrive, where I have met some of the very best people. A very special thank you to the Owyhee River crew, Jenna & Matt F., Kirby P., Vito B., Tessa G. & Sarah L., Pat F. & Nancy P., George & Uyen, Trudy B., Danielle L., and Natalia H.S. – your words and actions will never be forgotten.

I dedicate this thesis to my family. Mom, Dad, Derek, Benton, Ian, Vicki, Tennessee, Dixie, Jack and Isabelle – there will never be the right words to express my heartfelt gratitude, and so I hope the words, thank you, will somehow be enough. Thank you for the love and support. Thank you, for everything. No matter how difficult some days have been, I am always aware of the blessing and privilege to obtain this level of education. To my parents, grandparents, and the parents of their parents – all their choices (or lack of), decisions, hardships, sacrifices and hard work they endured for me to eventually reach this moment in time…it took all of you, to make this happen. Thank you.

TABLE OF CONTENTS

LIST OF TABLES

LIST OF FIGURES

CHAPTER 1 – INTRODUCTION

1.1 Mountain Pine Beetle

Forested regions across western Canada and the United States have seen recent unprecedented epidemic levels of tree death (primarily lodgepole pine, *Pinus contorta*) due to mountain pine beetle (*Dendroctonus ponderoseae*; MPB), which has affected 5.10 million hectares in British Columbia (2001 – 2010) and 3.38 million hectares in the western United States (1997 – 2010; upper estimate; Meddens *et al.*, 2012). Outbreaks of MPB have occurred outside their previously considered natural ecological range and have expanded eastward out of the Rocky Mountain region to other pine forests (Carroll *et al.*, 2006). In Alberta, MPB has affected 43.6% of the susceptible pine (5.5 million total hectares; C. Whitehouse, pers. communications, December 22, 2020). The rapid spread of MPB in the Rocky Mountain region and into Alberta has been attributed to increases in minimum winter air temperature, increases in reproductive cycles and faster development of MPB, increased drought stress in forests and the decrease in natural tree defenses, and host availability in monoculture lodgepole pine stands (Raffa *et al.*, 2008; Mitton and Ferrenberg, 2012; Williams *et al.*, 2012).

Mountain pine beetles introduce blue-stain fungi that inhibit sap flow and kill host trees within one year (Hubbard *et al.*, 2013). The needles turn red (red-attack) at tree death, but can take up to three years after tree death before needles fall (Wulder *et al.*, 2006). Once needles have fallen, the trees are said to be in grey-attack phase. The branches begin to drop five years after stand death, and trees may start to fall after five years with 90% down after 14 years (Mitchell and Preisler, 1998). The gradual canopy cover loss that results from MPB attack differs from other forest disturbances like harvest and wildfire because MPB disturbance directly affects the overstory without disturbance to the understory or soil (Adams *et al.*, 2012). There is a need for forest managers to understand the interaction between the varied disturbances and remaining canopy cover and the effect on hydrologic processes that generate runoff and the subsequent streamflow response.

1.2 Mountain Pine Beetle and Forest Harvest Effects on Hydrologic Processes

Mountain pine beetle affects both the individual tree physiology related to water transport and the gradual loss of the canopy structure, which both have the potential to affect hydrologic processes. Changes to hydrologic processes in clear-cut harvested stands are relatively well known (Moore and Wondzell, 2005; Winkler *et al.*, 2010) compared to MPB-attacked stands prior to the epidemic. Forest harvest in watersheds with conifer forests and a seasonal snowpack can lead to decreased canopy interception and transpiration, increased precipitation reaching the ground surface, increased energy for snow ablation, and increased soil moisture input and groundwater recharge (Moore and Wondzell, 2005; Winkler *et al.*, 2010). More recently, field studies have been established in British Columbia and the Rocky Mountain regions of western United States in a range of live, MPB grey-attack, and clear-cut stands with the rapid outbreak of MPB. For these regions, the dominant hydrologic input to forests is winter precipitation; therefore, much attention has been on snow accumulation given that canopy snow interception was expected to decrease with canopy cover loss and snowmelt drives runoff generation in these snow-dominated watersheds (Winkler and Moore 2006; Boon 2007, 2009; Bewley *et al.*, 2010; Winkler *et al.*, 2010; Pugh and Small, 2012). These studies showed that MPB attacked stands accumulated more snow and melted faster than undisturbed mature stands, due to a combination of decreased canopy snow interception and increased shortwave radiation transmittance through the canopy. However, snow water equivalent (SWE) in MPB attacked stands versus undisturbed mature stands in British Columbia differed in low-snow years but not in high-snow years because the amount of snowfall likely exceeded the canopy interception capacity (Boon, 2012; Winkler *et al.*, 2014). Another study in the central Rocky Mountains found that SWE between stands did not change, and reduced sublimation of canopy snow interception was compensated by increased snowpack sublimation as a result of greater radiation reaching the understory in MPB grey-attacked stands (Biederman *et al.*, 2014b). MPB grey-attack stands have also shown an increase in soil moisture due to reduced canopy interception losses and decreased overstory transpiration with tree death (Morehouse *et al.*, 2008; Clow *et al.*, 2011; Reed *et al.*, 2016). However, studies in MPB grey-attack stands in British Columbia and the central Rocky Mountains have shown that decreased overstory transpiration and canopy interception losses may be compensated for with increased transpiration of surviving vegetation (non-affected MPB trees) and understory vegetation (seedling, saplings, shrubs) or increased soil evaporation as a result of increased radiation reaching the understory, which results in little change to the total net evapotranspiration in the stand (Brown *et al.*, 2013; Biederman *et al.*, 2014a; Reed *et al.*, 2014; Reed *et al.*, 2016; Meyer *et al.*, 2017). The increases and decreases of the individual components of total evapotranspiration (i.e. overstory transpiration, canopy interception loss, understory evapotranspiration, soil evaporation) may change dependent on the hydroclimate conditions of the region. For example, the Alberta Foothills receives a larger proportion of annual precipitation during the growing season and snowmelt does not produce the maximum annual peak streamflow. Therefore, further understanding of the hydrologic response to MPB grey-attack and forest management strategies (e.g. salvage harvest) is needed in other climatic regions, like the Foothills, to understand the regional differences in runoff generation across the geographical range of MPB infested watersheds.

1.3 Mountain Pine Beetle and Forest Harvest Effects on Streamflow

In a review of paired watershed studies located in the Rocky Mountain/Inland Intermountain region, measurable increases in annual water yield can be expected after harvest of only 15% watershed area, while 30% or more harvested can be expected to produce generally larger increases from 0 to 350 mm yr^{-1} (Stednick, 1996). The wide variation in streamflow response to forest harvest is due to the inherent differences in climate, geology, runoff generation, topography, soils, vegetation, and harvest operations between sites (Moore and Wondzell, 2005; Winkler *et al.*, 2010). A paired watershed experiment on the eastern slopes of the Alberta Rocky Mountains showed streamflow was not sensitive to forest harvest with no significant measurable change in annual water yield or peak flow magnitude (Harder *et al.*, 2015). These watersheds had low levels of harvest relative to their size and a large percentage of alpine area; an area shown to generate the majority of runoff for streamflow (Fang *et al.*, 2016). In contrast, the moderately steep slopes and rolling hills of the Foothills region adjacent to the eastern slopes of the Rocky Mountains typically have merchantable timber throughout the watershed due to their lower elevation. Conceptual models for forest harvest effects on streamflow in fully-forested watersheds would suggest Foothills watersheds have increased potential for changes in streamflow (Bosch and Hewlett, 1982; Stednick, 1996; Green and Alila, 2012).

Studies that document the streamflow response to MPB infestation have provided varied results. Historical paired watershed studies after previous MPB outbreaks in the central Rocky Mountains reported 14-26% greater annual streamflow (Love, 1955; Bethlahmy, 1974; Potts, 1984). However, multi-watershed observations post-MPB epidemic in the western United States show a mix of increased, decreased or unchanged streamflow (Biederman *et al.*, 2015; Slinski *et al.*, 2016). The authors concluded that any changes in streamflow were likely related to climate variability that drives precipitation, snowmelt timing, and streamflow pattern (Biederman *et al.*, 2015; Slinski *et al.*, 2016). The inherent variability makes it difficult to detect MPB disturbance from the background climate signal (Burt *et al.*, 2015), which complicates traditional paired watershed and observational field studies (e.g. Bethlahmy, 1974; Potts, 1984; Slinkski *et al.*, 2016). A hydrological modelling approach becomes important to detect the effect of MPB (or forest harvest) disturbance if differences are masked by background climate variability in long-term streamflow observations. Model simulations in snow-dominated watersheds (65 to 85% precipitation as snow) found annual streamflow volumes only increased 2% in Alberta (Pomeroy *et al.*, 2012) and 11% in Colorado (Penn *et al.*, 2016). The large snowmelt inputs from the alpine areas and addition of adjacent unaffected areas (i.e. healthy forest, non-forested area) likely resulted in the muted forest disturbance signal from MPB (Pomeroy *et al.*, 2012; Penn *et al.*, 2016). More specifically, the increases in streamflow were small relative to inter-annual variability because runoff contributions from unaffected areas muted the watershed-scale response, but also compensatory changes in snow and ET processes mitigated the hillslope-scale response (Penn *et al.*, 2016). However, there is still a need to integrate hydrological process knowledge with hydrological modelling to understand the streamflow response to MPB and current forest management strategies for non-alpine forested watersheds.

1.4 Methods to Detect Changes in Streamflow

Paired watershed experiments have been used in forest hydrology across a range of physiographic regions for a century to detect changes in streamflow due to forest harvest (Bates, 1921), which include an untreated control watershed and pre- and post-harvest data in an adjacent watershed. The limitations of paired watershed studies have been previously reviewed (e.g. Alila *et al.*, 2009; Zégre *et al.*, 2010) and alternative statistical and model-based approaches for single watershed analysis have been used to determine the effect of forest harvest on streamflow (Schnorbus and Alila, 2004; Seibert *et al.*, 2010; Seibert and McDonnell, 2010; Zégre *et al.*, 2010; Wei and Zhang, 2010). There is still debate on the best approach to detect change because the effects of forest harvest are difficult to isolate from background climate variability; however, review papers have suggested that a combination of statistical and hydrological modelling approaches would be better than one method alone (Moore and Wondzell, 2005; Wei *et al.*, 2013).

Recent studies on paired watershed experiments have shown that climate variability associated with the large-scale ocean-atmosphere circulation phases of the Pacific Decadal Oscillation (PDO) and El Niño Southern Oscillation Index (ENSO) may modify streamflow trends due to meteorological changes and potentially interact with forest harvest experiments (Moore and Scott, 2005; Wei and Zhang, 2010; Burt *et al.*, 2015; Harder *et al.*, 2015). For example, at H.J.

Andrews Experimental Forest in Oregon, the climate variability related to ENSO was found to be the dominant driver of the streamflow response that followed forest harvest treatments (Burt *et al.*, 2015). Interestingly, the timing of treatment application in several historical paired watershed experiments in the Pacific Northwest have coincided closely with a PDO phase shift in 1977 from cool to warm (Golding, 1980; King and Tennyson, 1984; Troendle and King, 1987; Andres *et al.*, 1987; Cheng, 1989; King, 1989), which was not well known or realized until the mid-1990s (Mantua *et al.*, 1997). Positive PDO (warm phase) values have been associated with increased air temperatures, decreased precipitation, decreased snow accumulation, and decreased streamflow (Whitfield *et al.*, 2010; Newton *et al.*, 2014; Shrestha *et al.*, 2016). Therefore, there is reason to re-examine historical paired watershed studies using alternative methods to evaluate the effect of climate variability and forest harvest on streamflow.

1.5 The Foothills

Alberta's Foothills region makes up 19% of the provincial forested land base (352,477 km^2). The Foothills is primarily managed for timber, non-renewable resource extraction (mining, oil and natural gas) and public wildlands, and 82% of the land base has been tenured for forest harvest (Strittholt *et al.*, 2007). In addition to the overlapping tenures and multiple stakeholders, the Foothills currently faces diverse forest management issues that include both managed and natural disturbances (e.g. insect infestation, wildfire, climate change). In addition, insect and pathogen attack, and wildfire frequency and severity are expected to increase with climate change (Westerling *et al.*, 2003; Fettig *et al.*, 2013). Forest integrity and water security in Foothills watersheds are important as their streams contribute to river flow that supplies the western Prairie Provinces agriculture, municipal, and industrial water use (Schindler and Donahue, 2006; St. Jaques *et al.*, 2010) and provide aquatic habitat for threatened (Bull Trout; COSEWIC, 2012) and endangered (Athabasca Rainbow Trout; Fisheries and Oceans, 2020) fish species.

The Foothills is a region with complex glacial deposits and extremely folded and faulted sedimentary bedrock strata; a geologic setting that has the potential for large subsurface water storage (Spencer *et al.*, 2019). Increased proportions of permeable or fractured sedimentary bedrock found along the eastern slopes of the Rocky Mountains, like that found in the Foothills, has also been suggested to attenuate precipitation inputs for streamflow generation (Jensco *et al.*, 2011; Harder *et al.*, 2015; Spencer *et al.*, 2019). In these Rocky Mountain watersheds, the annual hydrograph is dominated by the spring-early summer snowmelt from the alpine region, which reliably produces much of the annual flow volume and maximum annual peak flow (e.g. Wagner, 2010; Spencer *et al.*, 2019). In contrast, the non-alpine Foothills watersheds receive a larger proportion of precipitation in the growing season and streams have a lower predictability of seasonal flooding (i.e. maximum annual peak flow) given the stochastic nature of large summer rainfall events (Natural Regions Committee, 2006); a hydroclimatic condition more similar to that seen in the adjacent Boreal Plains region (e.g. Redding and Devito, 2011).

1.6 Mountain Pine Beetle Management Strategies

The rapid rate of MPB infestation across western Canada and the United States has prompted salvage harvest (BCMoFR, 2005; Collins *et al.*, 2010); however, as MPB extended eastward into Alberta, the provincial management strategy focused on control (i.e. single tree or stand-level harvest of infested pine trees), salvage (i.e. within one year of infestation) or prevention; all of which include forest harvest (ASRD, 2007). The preventative pine reduction strategy was to reduce the number of susceptible pine stands by 75% over the next 20 years through targeted forest harvest (ASRD, 2007). A temporary increase in the Annual Allowable Cut (AAC) was permitted. For example, a management plan in a Foothills region forest management unit (effective 2018) was approved to undertake a 125% accelerated harvest of AAC over the next decade (AAF, 2018). The landscape then becomes a mosaic of dead (MPB grey-attack), alive, and clear-cut harvested stands, with varied canopy cover between them. There is a need for forest managers to understand the interactions between varied canopy cover, the effect of current MPB management strategies on streamflow, and the potential negative effects to aquatic life, especially in fisheries-sensitive watersheds.

1.7 Implications for Athabasca Rainbow Trout

Athabasca Rainbow Trout (*Oncorhynchus mykiss*; ARTR) are a unique salmonid ecotype found only in the upper Athabasca River watershed and the only native population of rainbow trout in Alberta (COSEWIC, 2014). ARTR were assessed as endangered in 2014 (COSEWIC, 2014) and listed under the *Species at Risk Act* in 2019 (Fisheries and Oceans Canada, 2020). ARTR were found to be sensitive to streamflow changes for successful incubation of embryos in the streambed substrate (i.e. redd) and emergence of fry (Sterling, 1992). ARTR fry abundance was found to be inversely correlated with streamflow exceeding a critical discharge (0.731 $m^3 s^{-1}$; $r = -0.82$, $p = 0.0066$); the discharge when spawning gravel begins to move downstream and leads to crushing or exposure of embryos (hereafter “ARTR $Q_{0.731}$”; Sterling, 1992).

Studies have raised concern about the potential scour of redds due to more frequent high flows during the incubation period of salmonids as a result of anthropogenic threats, i.e. human changes to aquatic ecosystems. For example, altered streamflow regimes in future warmer climates may result in increased depth of scour during salmonid incubation that may affect individual year cohorts, but these studies found limited risk to salmonid population decline (Goode *et al.*, 2013; McKean and Tonina, 2013). The population decline in Bull Trout in an Idaho watershed could not be fully explained by an increase in the frequency and depth of scour due to streamflow changes from forest harvest (Tonina *et al.*, 2008). In Alberta, percent area disturbed from industrial activity (mainly forest harvest) and road density were found to negatively effect the abundance of salmonid species (Bull Trout, Rainbow Trout) compared to reference watersheds (Scrimgeour *et al.*, 2008), but the authors did not investigate the mechanisms by which forest harvest influenced population abundance. To my knowledge, no studies have documented the potential streamflow changes from MPB and subsequent MPB management strategies (i.e. forest harvest) and the direct effect on salmonid fry recruitment.

1.8 Research Questions

The goal of this thesis was to improve the understanding of the effects of MPB grey-attack and current MPB management strategies on stand-scale hydrologic processes and the streamflow response in the Alberta Foothills, which includes fisheries-sensitive watersheds that provide aquatic habitat for the endangered Athabasca Rainbow Trout. The research questions addressed in this thesis were:

- What is the effect of varied canopy cover loss (alive, MPB grey-attack, harvest) on stand water cycling in the Foothills?
- What is the effect of forest harvest on streamflow in a Foothills watershed?
- What is the effect of potential streamflow changes from MPB grey-attack and forest harvest scenarios on Athabasca Rainbow Trout fry recruitment in a Foothills stream?

The studies within this thesis start at the stand-scale (Chapter 2), then move to the watershed-scale (Chapter 3), and finally build on these studies to explore a watershed management question (Chapter 4). The objective of Chapter 2 was to use the MPB Ecohydrology before-after control-impact detailed stand-level study near Robb, Alberta (MPB Robb; Piña, 2013; Steinke *et al.*, 2020) to analyze three years of field data collected from stands of undisturbed mature lodgepole pine (i.e. alive), clear-cut salvage harvested, and two MPB stands with varied simulated grey-attack intensity. The detailed stand-level measurements were then used to parameterize water balance models that quantify the magnitude of responses exhibited by snowmelt, the individual components of total evapotranspiration and root zone drainage. I hypothesized that compared to an undisturbed mature stand, the loss of canopy cover increases snow accumulation, decreases total evapotranspiration, increases soil moisture, and increases root zone drainage. Alternatively, canopy cover loss may increase snowpack sublimation and understory evapotranspiration that may compensate for reduced canopy interception losses and overstory transpiration.

In Chapter 3, I used data from the historical, long-term Tri-Creeks Experiment Watershed (Tri-Creeks; 1967 – 1985; Sterling *et al.*, 2016) that included a control and two treated sub-watersheds with different calibration periods and harvest sequences. I examined the streamflow response to forest harvest using a combination of statistical and hydrological modelling methods to attempt to isolate the effect of forest harvest from climate variability, specifically the 1976/77 PDO regime shift. I hypothesized the meso-scale, non-alpine watersheds would have increased potential of changes in streamflow due to forest harvest. Alternatively, I hypothesized that climate variability in relation to large variations in subsurface storage and connectivity with heterogeneity in geology masked the streamflow response to forest harvest.

Chapter 4 objectives were to integrate stand-level hydrologic process knowledge from the MPB Robb stand-scale study (Chapter 2) into a watershed-scale hydrological model constructed for a sub-watershed in Tri-Creeks (Chapter 3) to predicted streamflow from scenarios that include a reference (pristine forest) condition and a combination of clear-cut harvest, MPB grey-attack and undisturbed mature, even-aged lodgepole pine. The last objective was to estimate fry recruitment over 50 years using the relationship between fry density and streamflow above the critical discharge threshold (ARTR $Q_{0.731}$) during the incubation period established in Tri-Creeks (Sterling, 1992). I hypothesized that reduced total evapotranspiration and increased net water inputs into the soil from clear-cut harvest would result in greater streamflow above the ARTR $Q_{0.731}$ during the incubation period compared to MPB grey-attack. I also hypothesized that streamflow above the ARTR $Q_{0.731}$ during the incubation period would be greater in a cool PDO than a warm PDO period.

CHAPTER 2 – MOUNTAIN PINE BEETLE AND FOREST HARVEST EFFECTS ON A LODGEPOLE PINE STAND WATER BALANCE

2.1 Introduction

Hydrologic processes that generate runoff are controlled by the individual tree physiology related to water transport and the overstory structure of trees. Changes in the overstory structure will control the extent to which canopy cover loss will alter interception, evapotranspiration and shading of the understory. The forest canopy opens when pine trees are attacked by mountain pine beetle (MPB; *Dendroctonus ponderoseae*), which introduce a blue-stain fungi that inhibits sap flow and kill hosts trees. After MPB attack (green-attack), root water uptake ceases within one year (Hubbard *et al.*, 2013). The needles turn red at tree death (red-attack), but can take up to three years after tree death before needles fall (Wulder *et al.*, 2006). Once needles have fallen, the trees are said to be in grey-attack phase. The branches begin to drop five years after stand death, and trees may start to fall after five years with 90% down after 14 years (Mitchell and Preisler, 1998). The gradual canopy cover loss that follows stand death differs from wildfire and forest harvest because it directly affects the overstory without disturbance to the understory (vegetation/litter layer) or soil (Adams *et al.*, 2012).

Forested regions across western Canada and the United States have seen unprecedented epidemic levels of tree death due to MPB (primarily lodgepole pine; *Pinus contorta*), which has affected 5.10 million hectares in British Columbia (2001 – 2010) and 3.38 million hectares in the western United States (1997 – 2010; upper estimate; Meddens *et al.*, 2012). Outbreaks of MPB have occurred outside their previously considered natural ecological range and have expanded eastward out of the Rocky Mountain region to other pine forests (Carroll *et al.*, 2006; ASRD, 2007). The rapid rate of MPB infestation throughout North America has prompted salvage harvest (BCMoFR, 2005; Collins *et al.*, 2010); however, pine reduction strategies to reduce the number of susceptible pine stands with increased annual allowable cut (AAC) levels with targeted forest harvest have been planned in other forest management areas (ASRD, 2007; AAF, 2018). The landscape has become a patchwork of dead (MPB grey-attack), alive, and clear-cut salvage harvested stands, with varied canopy cover between them. There is a need for forest managers to understand the interaction between varied canopy cover and the effect on runoff generation and streamflow.

Field studies have been established in British Columbia and the Rocky Mountain regions of the western United States in a range of live, MPB grey-attack, and clear-cut stands. For these regions the dominant hydrologic input to forests is winter precipitation. Therefore, much attention has been on snow accumulation given that canopy snow interception was expected to decrease with canopy cover loss and snowmelt drives runoff generation in these snow-dominated watersheds (Winkler and Moore 2006; Boon 2007, 2009; Bewley *et al.*, 2010; Winkler *et al.*, 2010; Pugh and Small, 2012). These studies showed that MPB attacked stands accumulated more snow and melted faster than undisturbed mature stands, due to a combination of decreased canopy snow interception and increased shortwave radiation transmittance through the canopy. However, snow water equivalent (SWE) in MPB attacked stands versus undisturbed mature stands in British Columbia differed in low-snow years but not in high snow years because the amount of snowfall likely exceeded the canopy interception capacity (Boon, 2012; Winkler *et al.*, 2014). Another study in the central Rocky Mountains found that SWE between stands did not change, and reduced sublimation of canopy snow interception was compensated by increased snowpack sublimation (Biederman *et al.*, 2014b). Snowpack becomes a less dominant hydrologic input in more continental climates further east of the Rocky Mountains, like in the Foothills region (Natural Regions Committee, 2006). However, differences in snow accumulation and melt between stands of varied canopy cover loss may be important to determine the input to soil storage and the water available for root water uptake during the growing season, where higher snow accumulation would have greater potential to fill soil storage and drain from the root zone, and thus a greater amount of water available for evapotranspiration. In the Foothills, the highest evapotranspiration rates coincide with the timing of the largest proportion of precipitation. Therefore, additional water inputs to the soil in the growing season may change the dependence on the increases or decreases of the individual components of total evapotranspiration (i.e. overstory transpiration, canopy interception loss, understory evapotranspiration/soil evaporation) with canopy cover loss (Goeking *et al.*, 2020). Changes in canopy cover due to MPB grey-attack has been shown to increase soil moisture due to reduced canopy rainfall interception losses and overstory transpiration with tree death (Morehouse *et al.*, 2008; Clow *et al.*, 2011; Reed *et al.*, 2016). However, studies in British Columbia and the central Rocky Mountains have shown that reduced overstory transpiration and canopy rainfall interception losses with MPB grey-attack may be compensated by increased transpiration of surviving vegetation (non-affected MPB trees) and understory vegetation (seedling, saplings, shrubs) or increased soil evaporation as a result of increased radiation reaching the understory (Brown *et al.*, 2013; Biederman *et al.*, 2014a; Reed *et al.*, 2014; Reed *et al.*, 2016; Meyer *et al.*, 2017). Therefore, further understanding of the hydrologic response to MPB grey-attack and MPB management strategies (e.g. salvage harvest) is needed in other climatic regions, like the Foothills, where snowpack is a less dominant hydrologic input.

Early stand-scale studies were conducted in less than ideal experimental conditions such as mixed-species stands (Winkler *et al.* 2014) or stands located 125 kilometers apart (Biederman *et al.*, 2014a; Biederman *et al.*, 2014b) or focused on snow accumulation and melt (Boon, 2009; Boon, 2012). In contrast, Piña (2013) reported on a before-after control-impact (BACI) study to characterize the growing season hydrologic dynamics in adjacent, even-aged, mature lodgepole pine stands in the green-attack and early-red attack phases of simulated MPB attack (herbicide treatment in June 2009). The BACI study, located in the Alberta Foothills (Figure 2.1), provides an opportunity to build on these concepts, data and study design to specifically address the potential effects of MPB grey-attack on hydrologic processes in a continental climate dominated by growing season precipitation and advance these insights using these data to parametrize stand-level water balance models.

Now with the aforementioned BACI study in the grey-attack phase, this chapter addresses the question: what was the effect of varied canopy cover loss on stand water cycling in the Alberta Foothills? The objective was to use this unique BACI study to analyze three years of field data collected from stands of undisturbed mature lodgepole pine, clear-cut salvage harvested, and two MPB stands with varied simulated grey-attack intensity. The detailed stand-level measurements were then used to parameterize water balance models that quantify the magnitude of responses exhibited by snowmelt, the individual components of evapotranspiration and root zone drainage (Figure 2.2). I hypothesized that compared to an undisturbed mature stand, the loss of canopy cover increases snow accumulation, decreases total evapotranspiration, increases soil moisture, and increases root zone drainage. Alternatively, canopy cover loss may increase snowpack sublimation and understory evapotranspiration that may compensate for reduced canopy interception losses and overstory transpiration. The degree to which the individual components of total evapotranspiration either increase or decrease will determine the amount of water that drains from the root zone and generates runoff. Regional difference in runoff generation across the geo-climatic range of MPB infested watersheds will be better understood with information on water cycling in MPB grey-attack and salvage harvest stands.

2.2 Methods

2.2.1 Site Description

The MPB Ecohydrology site (MPB Robb) is located 11 km east of Robb (53.241ºN, -116.826º W; 1,130 m.a.s.l.) in the Upper Foothills natural subregion of Alberta (Natural Regions Committee, 2006; Figure 2.1). The site represents a region of pure lodgepole pine (*Pinus contorta* var. *latifolia* Engelm.) forest with mixed conifer stands of white spruce (*Picea glauca* (Moench) Voss) and subalpine fir (*Abies lasiocarpa* (Hook.) Nutt.), where stands are typically younger than 100-120 years old due to wildfire (Beckingham *et al.*, 1996). The climate is characterized as temperate continental with mean monthly temperatures ranging from 15ºC in July to -10ºC in December. Winters are cold, except for occasions with chinook winds. The warm, dry chinook winds are generated as Pacific air masses ascend the leeward side of the Rocky Mountains. Mean annual precipitation is 586 mm with 27% falling as snow and the largest monthly precipitation occurs in June (Figure 2.3). Upslope airflow over the Foothills produces light, but prolonged precipitation during winter arctic anticyclones and heavy prolonged precipitation during frequent cold low events in spring and summer (Reinelt, 1970).

The soils are brunisolic gray luvisols with a silt-loam texture, ~10% coarse gravel, and soil bulk density of 1.2 g cm^{-3} (Piña, 2013). The overstory for all stands included only lodgepole pine. There were very few white spruce (*P. glauca* (Moench) Voss), black spruce (*Picea mariana* (Mill.)), trembling aspen (*Populus tremuloides* Michx.), and balsam fir (*Abies balsamea* (L.) Mill.) in the lower canopy (Table 2.1). Green alder (*Alnus crispa* (Aiton) Pursh) was a common shrub. The understory was dominated by feather mosses, creeping dogwood (*Cornus canadensis* L.), twinflower (*Linnea borealis* L.), prickly wild rose (*Rosa acicularis* Lindl.), common blueberry (*Vaccinium myrtilloides* Michx.), common labrador tea (*Ledum groenlandicum*), and fireweed (*Chamerion angustifolium*) (Steinke *et al.*, 2020).

2.2.2 Experimental Design

The study used a BACI randomized block design to construct controlled tree mortality treatments and simulate MPB "grey attack" stand level effects. The study had three blocks: North Ridge Hydro (NRH), Horse Train Loop (HTL) and Power Shack Hill (PSH; Figure 2.1). Within each block were four experimental units (i.e. stands) that were treated in early summer 2009

(McIntosh and Macdonald, 2013): (i) untreated control (hereafter “Control”), (ii) simulated moderate intensity MPB attack (hereafter “50% Kill”); (iii) simulated high intensity MPB attack (hereafter “100% Kill”); and (iv) clear-cut – salvage harvested to simulate a typical management treatment post-MPB attack (hereafter “Salvage”). The NRH block had the hydrometeorological instruments (each stand = 0.64 ha). Vegetation dynamics were measured in all three blocks. All stands were surrounded by a 20-m (1 tree height) treed buffer to prevent edge effects. Each stand contained nine nested sampling points (20 m apart) in a systematic grid to collect forest structure and vegetation data within a permanent quadrate (1 x 1 m) surrounded by an 8-m fixed radius circular subplot.

The focus was to study epidemic levels of MPB. Therefore, the target of simulated MPB attack was 50% and 100% to capture a gradient of mortality. Trees were chemically girdled with glyphosate (N- (phosphonomethyl)glycine) to mimic MPB attack from June 15-19, 2009 (method outlined in McIntosh and Macdonald, 2013). Glyphosate can act as a defoliation aid because the systemic herbicide inhibits an enzyme that affects protein synthesis, which subsequently reduces photosynthesis and degrades chlorophyll (Baylis, 2000). All trees >10 cm dbh were injected in the 100% Kill stand. For the 50% Kill stand, every third tree > 10 cm dbh was injected to account for the root-to-root transfer of glyphosate among neighbor trees (McIntosh and Macdonald, 2013).

Harvest operations for the Salvage stand were completed by West Fraser Timber Company from July 16 to July 24, 2009. A feller-processor unit was used for stump-side processing and delimbing, then a tracked forwarder removed the logs from the treatment area. Debris was left onsite. There was no site preparation or planting and vegetation could regenerate naturally (McIntosh and Macdonald, 2013).

2.2.3 Forest Structure

Standard forest mensuration data were collected for all trees (dbh ≥ 5 cm and height > 1.3 m) within each 8-m fixed radius subplot (Table 2.1). Tree species, dbh, tree height, dead woody material, ground cover composition and forest floor depth (Fibric-Humic layers) were reported in McIntosh and Macdonald (2013) and Steinke (2018). Canopy cover and LAI were estimated with hemispherical photographs taken in mid-July at each of the nine nested sampling points within each stand (Figure 2.4; McIntosh and Macdonald, 2013; Steinke, 2018). A digital Nikon Coolpix 4500 with FC-E8 fisheye lens was mounted and leveled on a tripod approximately 1.4 m above the forest floor. Photographs were analyzed using Spot Light Intercept Model v3.01 (Poisson, 45°

cone around the zenith, clumping factor = 1.6). The LAI values represent a plant area index as no correction was made to account for stems and branches. The thickness of the forest floor (Fibric-Humic layers) was measured in each corner of the 1 x 1 m permanent quadrates.

2.2.4 Measurements

Pre-treatment hydrometeorological measurements in the NRH block were collected by Piña (2013) in 2008 – 2009. This section describes the post-treatment measurements collected between 2014 – 2017 in the grey-attack phase in the NRH block (unless otherwise stated), which were collected using the same approach and equipment installation as Piña (2013) to ensure consistency between pre- and post-treatment periods (except for snow transects).

2.2.4.1 Micrometeorology

Air temperature (T_a, ºC), relative humidity (RH; HMP50 hygrometer, Campbell Scientific), wind speed (v, m^3 s^{-1}, wind sentry anemometer, Campbell Scientific), and net radiation (Q^*; W m^{-2}, NR-LITE net radiometer, Kipp & Zonen) were measured at 20 m (canopy height) on a centrally located tower in each stand. T_a, RH and v were also collected 3 m above ground. Soil temperature (ºC, type T, Campbell Scientific) was measured at 0.2, 0.4, and 0.6 m below the mineral soil surface. Meteorological variables were sampled every 5 s and averaged after 10 min using a CR1000 control system (Campbell Scientific).

Understory photosynthetically active radiation (PAR) was measured with a quantum sensor designed using a gallium arsenide phosphide (GaAsP) photodiode (mmoles m^{-2} s^{-1}, Fielder and Comeau, 2000). A sensor was installed 1 m above ground on a plexiglass levelling plate connected to a 4 x 4 wooden post with attached ground spike. Four sensors were installed in each forested stand in the four cardinal directions from the meteorological tower to sample a range of canopy cover. One sensor was installed in the Salvage stand to measure total incoming PAR (2.5 m height). Data were collected at 10-min intervals. Annually, all PAR sensors were attached to a leveled horizontal wood board within the Salvage stand and calibrated to a LI-COR quantum sensor (LI-190R) to ensure accuracy.

2.2.4.2 Precipitation

Precipitation data were collected in the Salvage stand with a Jarek tipping bucket gauge and Alter shield (Geoscientific, Vancouver, Canada; accuracy ± 2%). The Jarek was fit with an antifreeze overflow system for winter collection. Snowfall data were compared to an SR50 ultrasonic snow depth sensor (Campbell Scientific, Logan, UT, USA) installed in fall 2015.

Precipitation data were confirmed with comparison to the Edson climate station (45 km northeast, Environment and Climate Change Canada, climate ID 3062239).

2.2.4.3 Snow Accumulation

Snow surveys were completed during 2015 – 2017. Snow surveys in 2015 consisted of two snow courses in each stand of the NRH block, each 100 m long, and snow depth and density measured every 10 m along the transect. In fall 2015, snow survey grids were established in the NRH block to measure 2016 and 2017 snow depth and density (Burles and Boon, 2011). Grids were added in each stand of the HTL block (2.3 km southeast of NRH) for 2017 snow surveys due to suspected edge effects in the NRH 50% Kill stand, because of partial loss of the exterior buffer from pipeline activities (Figure 2.1).

Each stand was marked by a 6 x 6 grid of wooden stakes placed at 10 m intervals (total grid size 50 m x 50 m; Burles and Boon, 2011). The sampling technique depended on snowpack depth. Snow density was collected with a standard Federal snow tube and field scale at each stake (n = 36). For a shallow snowpack (<15 cm), a bulk sampling method was used that included a 50 cm long PVC pipe (5.08 cm radius) and avalanche shovel (Burles and Boon, 2011). Snow depth measurements (n = 96) were collected at 5 m intervals within the snow survey grid using a graduated avalanche probe. Average snow density and depth measurements were multiplied to calculate stand-scale snow water equivalent (SWE).

2.2.4.5 Throughfall

Throughfall (T_f) was measured from mid-May to end-September in 2015 and 2016. In each forested stand, four trough gauges (6 m long x 5 cm wide) were attached to wooden stakes 70 cm above ground and gently angled to allow rain water to drain through a funnel and hose into a covered tipping bucket rain gauge (Davis Instruments Corp. model 7852, Hayward, CA, USA) connected to a HOBO event data logger (Onset Computer Corporation, Bourne, MA, USA). Tipping buckets were calibrated prior to deployment each spring. Mean T_f for each forested stand was calculated for each individual rainfall event. A rainfall event was defined as a period with more than 0.5 mm of precipitation, separated by at least 8 hours with no measurable rainfall indicated by a precipitation gauge in the Salvage stand (Carlyle-Moses *et al.*, 2014). To ensure consistency between the pre- and post-treatment periods, mean T_f for each forested stand was recalculated for each individual rainfall event defined above using the raw throughfall data for 2008 collected by Piña (2013).

2.2.4.6 Stemflow

Stemflow (S_f) was measured from mid-May to end-September in 2015 and 2016 on trees of various size (17 to 37 cm dbh) within each forested stand. These trees were originally selected by Piña (2013) in the pre-treatment period. For each stemflow gauge, a garden house (split open lengthwise) was stapled in a spiral orientation around the tree trunk at 1.3 m height and caulked on one edge to produce a watertight seal. S_f was captured by the hose and routed into a covered calibrated tipping bucket rain gauge (Davis Instruments) connected to HOBO event data logger (Onset) at the base of the tree. S_f was measured from three dead trees within the 100% Kill stand and three alive trees within each of the 50% Kill and Control stands.

The method used to scale tree S_f to account for the full distribution of tree sizes at the stand-scale was similar to Williams *et al.* (2019). First, linear relationships between rainfall event and S_f volume (L) were constructed for each instrumented tree. Second, slopes from the linear relationships were regressed against the dbh of the instrumented trees to produce two stemflow regressions: live trees and dead trees. The live and dead tree regressions were used to predict S_f volume (L) for trees within each of the nine 8-m fixed radius circular subplots for each forested stand and rainfall event. For each event, mean S_f volumes within each stand were converted to a depth (mm) by dividing by the total fixed-radius circular subplot area (1810 m^2). Similar to throughfall measurements, mean S_f volumes within each stand were recalculated using raw data collected in 2008 by Piña (2013) to ensure consistency between pre- and post-treatment periods.

2.2.4.7 Tree Transpiration

Direct measurements of overstory tree transpiration were made within the forested stands in 2008 – 2010 by Piña (2013) using the thermal dissipation technique (Granier, 1985; Granier, 1987). Briefly, one constant-heat sap flow sensor (TDP-30, Dynamax Inc, TX, USA) was installed per tree on the south side at 1.3 m above ground during the snow-free period. Sap flux was measured in seven live (healthy) trees during the 2008 pre-treatment period in each forested stand. The next year, after herbicide treatment, the sensors were rotated into seven additional trees in the Control stand; however, sensors were installed into live (healthy) trees surrounding by treated trees in the 50% Kill stand.

Mean daily tree transpiration per unit leaf area (Q_L; mm d^{-1}) estimated by Piña (2013) was used to develop linear relationships for the 1 Oct 2014 to 30 Sep 2017 study period assuming no change to the rate of sap flux velocities over time. Q_L was related to the daily maximum vapour pressure deficit (vpd_x) calculated from mean hourly air temperature and relative humidity measured at 21 m above ground (Spittlehouse, 2006). Non-linear relationships for Q_L for trees surrounded by live (unaffected) trees [Control stand; $Q_L = 0.185(1\text{-}\exp(-0.570 \cdot vpd_x))$] and for live trees surrounded by dead trees [(50% Kill stand; $Q_L = 0.208(1\text{-}\exp(-0.765 \cdot vpd_x))$] were determined using days with no rain. Q_L was assumed to be zero in the 100% Kill stand. Daily Q_L was estimated using vpd_x measured during the study period. Daily Q_L was multiplied by stand LAI to determine the stand-scale transpiration (E_t) for the Control and 50% Kill stands.

2.2.4.8 Soil Water Content

Volumetric soil water content (θ; m^3 m^{-3}, CS616 Water Content Reflectometer, Campbell Scientific) was measured hourly at 0.2, 0.4, and 0.6 m below the mineral soil surface at each meteorological station. Default calibration constants were used to determine θ given the bulk density of the soil was less than 1.55 g m^{-3} and the clay content less than 30% (Campbell Scientific, 2015).

Mean daily θ (m^3 m^{-3}) was converted to a water depth (mm) by multiplying θ by a soil layer thickness (mm). Mineral soil layers include the root zone (0 – 0.4 m, i.e. the maximum depth of active roots) and soil layer 2 (0.4 – 0.6 m; Figure 2.2). Field observation of wind thrown lodgepole pine and soil pits indicated >90% roots were within 30 cm from the ground surface. An equally weighted average of the shallow sensors (0.2 and 0.4 m) were used to determine θ in the root zone.

During the growing seasons (2008 – 2010), Piña (2013) made weekly measurements of volumetric soil water content with time domain reflectometry (*TDR*; model 1502c, Textronix Inc) using the empirical relationship for mineral soils developed by Topp *et al.* (1980). *TDR* wave guide rods that measured 0.2, 0.4, and 0.6 m were installed vertically at eight locations within each stand. These measurements provide a direct measurement of the total soil water content from 0 – 0.2 m, 0 – 0.4 m and 0 – 0.6 m.

One challenge for water balance model evaluation was that the modelled soil moisture time series in the unsaturated zone was intended to represent an average over the stand (0.64 ha), whereas the observed continuous θ (CS616 sensors) was sampled at the point-scale. To address this inconsistency, the observed θ data for the 1 Oct 2014 – 30 Sep 2017 study period were adjusted. Linear regressions were constructed between the mean daily *TDR* (mm) and corresponding mean daily θ (mm) for the root zone (0 – 0.4 m) and soil layer 2 (0.4 – 0.6 m) in each stand, respectively (refer to Appendix A): Control ($r^2 = 0.32$ and $r^2 = 0.06$); 50% Kill ($r^2 = 0.33$ and $r^2 = 0.15$); 100% Kill ($r^2 = 0.33$ and $r^2 = 0.16$); and, Salvage ($r^2 = 0.47$ and $r^2 = 0.31$) stands. For the Salvage stand, only measurements taken post-treatment were included. The regressions described variability poorly; however, regression slopes were small (0.7 – 1.7), except for soil moisture measured within soil layer 2 in the Salvage stand (slope = 4.1; Figure A.1). However, the approach was deemed appropriate to account for the inconsistency between stand-scale modelled and one-point measurement of soil moisture. Adjustments to soil moisture measurements to address the inconsistency in scale between measured and modelled data have been made by others (Clark *et al.*, 2011).

2.2.4.9 Groundwater Level

Piezometers were installed in each stand in July 2008 and 2009 using a rotary auger drill rig from 1.30 to 3.17 m below ground surface (Figure 2.1; Piña, 2013). Stratigraphy notes taken during piezometer installation indicate alternate layers of hard pan and sandy-silt soil, which suggest perched water table systems in the area (Piña, 2013). For most (or all) of the year, the piezometers were dry. In half of the piezometers, water levels were measured during the annual snowmelt period or after large heavy rainstorm events. However, the interpretation of changes in groundwater response was strongly confounded by the heterogeneity and unknown depth of the surface aquifer. Therefore, groundwater data were not presented.

2.2.5 Potential Evapotranspiration

Micrometeorological data were used with the Penman combination equation (Penman, 1948) to provide potential evapotranspiration (PET_P, mm d^{-1}) from each stand:

$$PET_P = \frac{1}{\lambda_v \rho_w} \cdot \left[\frac{\Delta}{\Delta + \gamma}\, Q^* + \frac{\gamma \epsilon_v v}{\Delta + \gamma}\,(e_s - e)\right] \tag{2.1}$$

$$\epsilon_v = \frac{0.622\rho_a}{6.25 \cdot e\rho_w} \cdot \left(ln\left(\frac{z_{ref} - z_o}{z_{rough}}\right)^{-2}\right) \tag{2.2}$$

where λ_v (MJ kg^{-1}) is the latent heat of vaporization of water, ρ_w (kg m^{-3}) is the density of water, $\Delta = de_s/dT$ is the slope of the saturated vapour pressure curve, $Q^* = S_n + L_n$ (MJ m^{-2} d^{-1}) is the net radiation to the system equal to the sum of net incoming and outgoing shortwave and longwave radiation, ϵ_v is a vertical transport efficiency factor, ρ_a is the air density (kPa), e is the vapour pressure of the atmosphere, $e_s(T)$ (kPa) is the current saturated vapour pressure of the atmosphere, a function of temperature, γ (kPA K^{-1}) is the psychrometric constant, z_{ref} is the reference height (m) at which the wind velocity (v; m d^{-1}) is reported, z_o (m) is the zero-plane displacement height, z_{rough} is the roughness height (m). Refer to Craig *et al.* (2019) for equations to calculate $\lambda_{v,}$ Δ, $e_s(T)$, and γ.

2.2.6 Statistical Analysis

Measured variables pre-treatment and post-treatment were compared between the Control stand and 50% Kill, 100% Kill and Salvage stands using the "extra sum of squares" analysis of covariance (ANCOVA) approach (Moore and Scott, 2005). A regression model (Model 1) was fit to the entire data set of pre- and post-treatment periods:

$$y = \beta_0 + \beta_1 x_1 + \varepsilon \tag{2.3}$$

where y = the value of the meteorological variable for a given time in the stand, and x_1 is the corresponding value for the Control stand. A second model (Model 2) includes the dummy variable, x_2 (0 = pre-treatment, 1 = post-treatment):

$$y = \beta_0 + \beta_1 x_1 + \beta_2 x_2 + \beta_3 x_1 x_2 + \varepsilon \tag{2.4}$$

For the post-treatment period, $x_2 = 1$, which results in the model:

$$y = (\beta_0 + \beta_2) + (\beta_1 + \beta_3) x_1 + \varepsilon \tag{2.5}$$

The null hypothesis of no treatment effect is $H_0 = \beta_2 = \beta_3 = 0$. A partial F statistic was used to determine if the fit of Model 2 was significantly different ($p = 0.05$) from Model 1, i.e. simulated MPB attack/harvest influenced the relationship between the treated stands and Control stand for: air temperature, vapour pressure deficit, windspeed, net radiation, PAR, soil temperature (20 cm depth), soil moisture, throughfall and stemflow. All variables, except throughfall and stemflow, were averaged weekly over the growing season (1 May – 30 Sep) during the pre-treatment (July 13, 2008 – July 12, 2009) and post-treatment (May 3, 2015 – August 23, 2017) periods. Throughfall and stemflow collected during rainfall events in 2008 (n = 29) and 2015 – 2016 (n = 68) were analyzed.

Snow survey data were not available from the pre-treatment period. Only snow survey data collected in 2016 and 2017 were analyzed to evaluate the effect of canopy cover loss. One-way analysis of variance (ANOVA) was applied to snow depth and SWE data to determine significance of differences between stands and years. Shapiro-Wilks' W test confirmed normality of data distributions (Shapiro *et al.*, 1968) and Levene's test confirmed homogeneity of variances (Hill and Lewicki, 2007). Scheffe's test was applied as a *post hoc* analysis to identify which pairs of treatments were statistically different (Hill and Lewicki, 2007).

All statistical analyses were performed using R (v 4.0.1; R Core Team, 2020) with alpha = 0.05 as the threshold for statistical significance.

2.2.7 Analytical Actual Evapotranspiration

Actual evapotranspiration was estimated using an analytical approach (AET_A) via:

$$AET_A = I_r + I_s + T_c + I_{ff} + T_u \tag{2.6}$$

where I_r is evaporation of intercepted rainfall in the forest canopy, I_s is evaporation of the intercepted snowfall in the forest canopy, T_c is overstory tree transpiration, I_{ff} is evaporation of the intercepted rainfall in the forest floor, T_u is understory plant transpiration. Daily AET_A could not exceed PET_P. The approach assumed that evaporation of intercepted rainfall in the forest floor and understory plant transpiration only occurred if evaporation of canopy intercepted rainfall and overstory tree transpiration did not exceed PET_P. Evapotranspiration from the understory was assumed zero in the presence of a snowpack.

Intercepted rainfall by the forest canopy (I_r; mm d^{-1}) was determined indirectly with $I_r = P_g - (T_f + S_f)$. Non-linear functions were developed to describe I_r and gross rainfall events (<24 hour duration) for each forested stand. The relationships were used to determine I_r for individual rainfall events during the modelling period. Rain that remained stored in the canopy at day end reduced interception for the next day (Spittlehouse, 2006). The maximum amount of rainfall the canopy could store was determined from I_r regressions.

Intercepted snowfall by the canopy (I_s; mm d^{-1}) used the method described in Hedstrom and Pomeroy (1998), which accounts for interception efficiency with canopy snow load, canopy density, and snow unloading rates:

$$I_S = S_L \cdot LAI \tag{2.7}$$

$$S_L = S_P \left(0.27 + \frac{46}{\rho_S}\right) \tag{2.8}$$

where I_s is the maximum canopy snow load as a function of LAI, S_L (kg m^{-2}) is a tree species specific maximum snow load per unit branch area, S_P (kg m^{-2}) is the mean tree species value for snow load (5.96 kg m^{-2}; Schmidt and Gluns, 1991), and ρ_s (kg m^{-3}) is the density of snow related to air temperature (Schmidt and Gluns, 1991). Snow that remained stored in the canopy at day end reduced snow interception for the subsequent day. Intercepted snow was evaporated.

Daily overstory tree transpiration (T_c; mm d^{-1}) was determined with the non-linear relationships of Q_L and vpd_x (see section 2.2.4.7) and available potential evapotranspiration.

Intercepted rainfall by the forest floor (I_{ff}; mm d^{-1}) was estimated using an empirical relationship of forest floor percolation to the underlying mineral soil developed in 2010 within the Control stand ($Perc_{ff} = 0.0394P_n^2 + 0.2396P_n$; $r^2 = 0.98$, n = 19; P_n = net rainfall; Piña, 2013). Water input from snowmelt and rainfall that did not percolate to the mineral soil or evaporate remained in the forest floor and limited interception the next day. The maximum water holding capacity of the forest floor layer (fibric/humic; 16.3 – 24 mm) was determined in a 2010 experiment by Piña (2013). These values combined with forest floor thickness (Steinke, 2018) were used to calculate the soil parameters for the forest floor layer in each treatment.

Lastly, understory plant transpiration (T_u; mm d^{-1}) was a function of available PET_P and extractable soil moisture available in the root zone. If T_u was neither energy-limited or soil water-limited, a maximum understory transpiration rate was used for each treatment (MAX_CAP_RISE_RATE; Table 2.2). To estimate the maximum rate, transpiration rates from the literature were weighted to the proportion of ground cover species composition collected by Steinke (2018): lodgepole pine seedlings (3.5 mm d^{-1}, Millions, 2015); shrub/forb (0.5 mm d^{-1}, Baldocchi *et al.*, 1997); grass (5.8 mm d^{-1}, Adams, 1991); and, bryophytes (0.4 mm d^{-1}, Bond-Lamberty *et al.*, 2010). The product was used to rate-limit T_u.

2.2.8 Stand Water Balance Modelling

The hydrological modelling period included three water years (1 Oct 2014 – 30 Sep 2017) and each water balance model operated on a daily timestep. Table 2.2 provides parameter values used in the models.

2.2.8.1 Model Structure

The Raven Hydrological Modelling Framework (Raven; v2.9.2, Craig *et al.*, 2020) was chosen for this study given the flexibility in hydrologic process and algorithm implementation and a model structure that could efficiently address model sensitivity and uncertainty analysis. Raven has also demonstrated excellent emulation of the watershed conceptual hydrological model HBV-EC (Bergstrom *et al.*, 1995; Canadian Hydraulics Centre, 2010). Therefore, the HBV-EC model structure template in Raven was selected and customized with dominant processes associated with water cycling in MPB grey-attacked and salvage harvested stands (Figure 2.2).

The model structure was designed to determine the stand water balance equation that links the change in soil water content in the root zone over time (ΔS_{RZ}), gross precipitation (P_g), evaporation of canopy intercepted rainfall and snowfall [$E_c = P_g -$ throughfall (T_h) – stemflow (S_t)], overstory tree transpiration (E_t), understory evapotranspiration (E_u), sublimation of snowpack (S) and root zone drainage (D). Root zone drainage was defined as percolation from the root zone soil layer at -0.4 m depth into the soil layers below. (Figure 2.2). Evaporation from the mineral soil was considered negligible as forest floor vegetation cover surveys indicated little bare ground (Table 2.1; Steinke, 2018). Unsaturated lateral flow in the root zone and soil layer 2 was considered negligible given the flat topography and low unsaturated hydraulic conductivities (Figure 2.2). However, unsaturated lateral flow could move vertically and laterally in soil layer 3.

$$\Delta S_{RZ} = P - E_c - E_t - E_u - S - D \tag{2.9}$$

Precipitation was partitioned into rain or snow using the HBV-EC algorithm (Bergstrom, 1995) where a linear transition between all snow and rain is determined from the mean daily temperature using a rain/snow transition temperature (1ºC) and a range of rain-snow transition zone (2ºC). Rain and snow were captured by the overstory canopy. The amount captured was controlled by the storage capacity of the canopy (mm; Table 2.2; MAX_CANOPY, MAX_SNOW_CANOPY) and the precipitation interception rate (mm d^{-1}). Interception percentages were input as a transient parameter with a time series of user-specified parameter values at a daily interval (Craig *et al.*, 2019), which were calculated for individual storm events with canopy interception equations.

Captured moisture on the canopy evaporated at the potential evapotranspiration (PET; mm d^{-1}) rate provided storage was available via:

$$E_c = PET \cdot F_c \cdot (1 - f_s) \tag{2.10}$$

where F_c is the fraction of land covered by forest canopy (%; FOREST_COVERAGE), and f_s is the vegetation density of the forest cover (%; FOREST_SPARSENESS).

Monteith (1965) modified the Penman equation to represent the daily ET rate from a vegetated surface by incorporating canopy conductance:

$$PET_{PM} = \frac{1}{\lambda_v \rho_w} \cdot \left[\frac{\Delta}{\Delta + \gamma \cdot (1 + c_{atm}/c_{can})} R_n + \frac{\rho_a c_{atm} c_a}{\Delta + \gamma \cdot (1 + c_{atm}/c_{can})} (e_s - e) \right] \tag{2.11}$$

$$c_{atm} = v \cdot \frac{k^2}{ln\left(\frac{z_{ref} - z_o}{z_{rough}}\right) ln\left(\frac{z_{ref} - z_o}{z_{vap}}\right)} \tag{2.12}$$

$$c_{can} = 0.5 \cdot c_{leaf} \cdot LAI \tag{2.13}$$

where c_{atm} (m d^{-1}) is the atmospheric conductance, c_a is the specific heat of air (1.012 x 10^{-3} MJ kg^{-1} K^{-1}), c_{can} (m d^{-1}) is the canopy conductance, k is the Von Karman constant (0.42), c_{leaf} is the leaf conductance (m d^{-1}) and z_{vap} is the vapour roughness height (m).

Evapotranspiration from the canopy and understory were rate-limited by the availability of forest floor and root zone storage, and by the subsequent capacity of the atmosphere to absorb water vapour after intercepted moisture evaporated. E_t and E_u were at PET if storage exceeded the tension storage, then were linearly proportional (Bergstrom, 1995):

$$E_t, E_u = PET \cdot min\left(\frac{\phi_{soil}}{\phi_{tens}}, 1\right) \tag{2.14}$$

where φ_{soil} (mm) is the moisture content of the soil layer and φ_{tens} (mm) is the maximum tension storage. φ_{tens} equals φ_{max} ($S_{fc} - S_{wilt}$), where φ_{max} (mm) equals the product of soil layer thickness (mm), porosity (POROSITY) and stone fraction. S_{fc} (%) is the saturation at field capacity (FIELD_CAPACITY; Craig *et al.*, 2019). S_{wilt} (%) is the saturation at wilting point (SAT_WILT; Craig *et al.*, 2019). The model used an additional snow correction in which E_t and E_u were zero in non-forested areas when snow depth was greater than zero.

The algorithm for capillary rise rate in the HBV-EC model (Bergstrom, 1995) can be used conceptually to move water from lower to higher soil water stores (Craig *et al.*, 2019). For this study, *Rise* moved water from the root zone storage to the forest floor storage to represent water movement via evapotranspiration from the roots of lodgepole pine trees and understory vegetation (bryophytes, forbs, shrubs, grass, pine seedlings).

$$Rise = M_{Cmax}\left(1 - \frac{\phi_{soil}}{\phi_{max}}\right) \tag{2.15}$$

where M_{Cmax} is the maximum interflow rate (MAX_CAP_RISE_RATE).

Sublimation (*S*) of the snowpack was modelled with the approximation used in the Cold Regions Hydrological Model (CRHM; Pomeroy *et al.*, 1997):

$$S = 0.08 \cdot \left(0.18 + 0.098 \cdot v_{avg}\right) \cdot \left(P_{sat0} - P_{vap}\right) \tag{2.16}$$

where v_{avg} (m s^{-1}) is the wind velocity at 10 m, P_{sat0} (mb) is the saturation pressure at zero degrees, and P_{avg} (mb) is the atmospheric vapour pressure.

Potential snowmelt and snow balance algorithms were used to simulate the coupled mass and energy balance equations that control melt and refreeze of the snowpack and the liquid phase in the snow pores. The potential melt rate M_{CRHM} (mm d^{-1}) is a parameter-free energy-based potential snowmelt model from the Cold Regions Hydrological Model (CRHM; Pomeroy *et al.*, 2007):

$$M_{CRHM} = \frac{1}{\lambda_v \rho_w} \cdot \left(S_n + L_n + Q_h + Q_p\right) \tag{2.17}$$

$$Q_h = -0.92 + 0.076 \cdot v + 0.19 \cdot T_{max} \tag{2.18}$$

$$Q_P = c_p \rho_w \cdot R \cdot max(T, 0.0)/1000 \tag{2.19}$$

where Q_h (MJ m^{-2} d^{-1}) is the convective/conductive heat transfer, Q_p (MJ m^{-2} d^{-1}) is the energy content of the rainfall, *R* (mm d^{-1}) is the rainfall rate/1000 (m d^{-1}), *T* (ºC) is the air temperature, c_p (MJ kg^{-1} K^{-1}) is the specific heat capacity of water. M_{CRHM} was applied to the snowpack with a single-layer energy balance snow model that tracked liquid water content, SWE, and the energy in the snowpack as implemented in CRHM (Pomeroy *et al.*, 2007). The evolution of snow albedo was not explicitly modelled but accounted for in net radiation measurements.

The bulk transmittance approach was used to determine the fraction of shortwave radiation transmitted through the tree canopy with a Beer's law relationship (Dingman, 2002):

$$f_{can} = exp(-k\ (LAI + SAI)) \tag{2.20}$$

where *k* is the extinction coefficient (-; SVP_EXTINCTION), LAI is the leaf area index (m m^{-1}; MAX_LAI), and SAI is the stem area index (%; SAI_HT_RATIO). SAI was considered zero as measured LAI was considered an effective LAI.

All net precipitation infiltrated the forest floor because no surface runoff was observed in the stands. Water that exceeded the forest floor storage capacity percolated downward into the mineral soil layers proportional to soil saturation to a power:

$$Perc = M_{max}\left(\frac{\phi_{soil}}{\phi_{max}}\right)^{n} \tag{2.21}$$

where M_{max} is the soil parameter MAX_PERC_RATE and n is the soil parameter PERC_N.

2.2.8.2 Forcing Functions

Meteorological data collected during the study period were used to force the hydrological models, which included: daily maximum and minimum air temperature; total daily rainfall and snowfall; mean daily relative humidity, windspeed, and air pressure; and, total daily net radiation.

After seven years in operation, meteorological stations were temporarily shut down from January 29th to March 4th, 2015 to ensure proper working order. The stations were subsequently decommissioned August 23rd, 2017. For modelling purposes, data from the nearby Edson climate station were used to gap-fill missing data at the Salvage station for the modelling period. Linear regressions were used to gap-fill air temperature (month as factor; $r^2 = 0.96$) and relative humidity (month as factor; $r^2 = 0.72$), and wind speed ($r^2 = 0.89$). A linear regression of modelled (Dingman, 2002) and measured net radiation in the Salvage stand was used to gap-fill the record ($r^2 = 0.86$). Missing data for the forested stand stations were gap-filled using linear regressions with the Salvage station. In addition, the Control station collapsed twice (April 2015, November 2016) due to tree fall. Data records were filled as described above with the Salvage station.

To determine the amount of radiation transmitted through the tree canopy that reached the forest floor, net radiation measured in the overstory was reduced using an extinction coefficient (k), which expresses the reduction in transmitted light per leaf area (Brown *et al.*, 1994):

$$k = -ln\left(\frac{Q_i}{Q_o}\right)/LAI(csc\ a) \tag{2.22}$$

where Q_i is understory PAR (mmoles m^{-2} s^{-1}), Q_o is total incoming PAR (mmoles m^{-2} s^{-1}) measured in the Salvage stand, LAI (m m^{-1}) is the average stand LAI across the three blocks. Multiplying LAI by the cosecant of the solar elevation angle (a) corrects for variations in solar angle among daily measurements. Only PAR data measured between 11:00 – 14:00 and on non-rain days were used to calculate the daily geometric mean PAR. Mean k includes only the period from 1 May to 30 Sep 2016 and 2017 as snowfall on the sensors inhibited readings.

2.2.8.3 Parameter Optimization

Parameters were optimized with Ostrich (v17.12.19; Matott, 2019) for each model using dynamically dimensioned search (DDS; Tolson and Shoemaker, 2007). The mean absolute error (MAE) was minimized in the optimization procedure. Discrete SWE and continuous θ measurements in the root zone and soil layer 2 (ice-free period) were equally weighted as tied response variables. The mean percent bias error (PBIAS) was also calculated. Model performance was also evaluated with estimates of AET_A.

2.2.8.4 Parameter Uncertainty

The DDS – approximation of uncertainty (DDS-AU; Tolson and Shoemaker, 2008) algorithm quantified the prediction uncertainty by identifying behavioral parameter sets through repeatedly applying a DDS search from alternative random starting points in the parameter space. For each model, there were 60,000 model evaluations (150 optimization trials and 400 function evaluations per optimization trial). The number of model evaluations were selected based on the optimal parameter set known to achieve the minimum MAE (Tolson and Shoemaker, 2008). The parameter sets from the 100 lowest MAE optimization trials were selected to characterize the prediction bounds. Each selected parameter set was used to reconstruct time series of water balance components including actual evapotranspiration, snow accumulation, snowmelt, change of storage in the root zone and root zone drainage. The daily 97.5th and 2.5th percentiles of the 100 time series for each water balance component represent model uncertainty at each time step. The median time series was presented for each water balance component.

2.3 Results

2.3.1 Micrometeorology

Mean growing season canopy air temperature was greater in both MPB grey-attack stands compared to that predicted from the Control stand (Figure 2.5). The observed post-treatment canopy T_a was 1.3°C (9%) greater in the 50% Kill stand ($p<0.0001$) and 1.2°C (9%) greater in the 100% Kill stand ($p<0.0001$) compared to predicted values determined from the pre-treatment calibration period. In comparison, post-treatment mean growing season T_a was 1.4°C (10%) greater than expected in the Salvage stand ($p<0.0001$). There was no difference in the mean growing season canopy T_a between the pre-treatment (13.2°C) and post-treatment (13.4°C) periods within the Control stand ($p = 0.82$).

There was no significant change in below canopy T_a in the 50% Kill ($p = 0.4$) or 100% Kill stand ($p = 1$) compared to the Control stand (Figure 2.6). In the Salvage stand, the mean growing season T_a (measured 3 m above ground) was 0.20°C (2%) greater in the post-treatment period ($p<0.0001$). There was no difference in the mean growing season below canopy T_a between the pre-treatment (11.4°C) and post-treatment (12.7°C) periods within the Control stand ($p = 0.18$).

Mean canopy *VPD* increased in both MPB grey-attack stands during the growing season (Figure 2.5). The observed post-treatment *VPD* was 0.03 kPA (4%) greater in the both the 50% Kill and 100% Kill ($p<0.0001$) stands, while the Salvage stand was 0.05 kPA (7%) greater in canopy *VPD* ($p<0.0001$). There was no difference in the mean growing season *VPD* between the pre-treatment (0.79 kPA) and post-treatment (0.77 kPA) periods within the Control stand ($p = 0.79$).

There was no change in the observed below canopy *VPD* in both the 50% Kill ($p = 0.99$) and 100% Kill ($p = 1$) stands compared to the predicted values determined from the pre-treatment calibration period (Figure 2.6). The Salvage stand was 0.02 kPA (3%) greater in *VPD* measured 3 m above ground ($p<0.0001$). There was no difference in the mean growing season below canopy *VPD* between the pre-treatment (0.66 kPA) and post-treatment (0.68 kPA) periods within the Control stand ($p = 0.76$).

Windspeed changes within the canopy varied with the intensity of MPB grey-attack (Figure 2.5). There was no significant change in the 50% Kill stand ($p = 0.35$). In the 100% Kill stand, the mean growing season windspeed observed in the post-treatment period was significantly greater (47%) compared to predicted values, which changed from 0.26 m s^{-1} to 0.49 m s^{-1} in the post-treatment period ($p<0.0001$). In comparison, mean windspeed in the Salvage stand was 80% greater compared to predicted values, which changed from 0.28 m s^{-1} to 1.36 m s^{-1} in the post-treatment period ($p<0.0001$). The mean growing season windspeed in the Control stand was not different between the pre-treatment (0.25 m s^{-1}) and post-treatment (0.30 m s^{-1}) periods ($p = 0.15$).

Changes in the windspeed below canopy also varied with the intensity of MPB grey-attack (Figure 2.6). The post-treatment mean growing season windspeed was 0.03 m s^{-1} (17%) greater in the 50% Kill stand compared to predicted values ($p<0.001$). In contrast, the 100% Kill stand had a 29% lower below canopy mean windspeed predicted in the post-treatment period from 0.28 m s^{-1} to 0.22 m s^{-1} ($p<0.0001$). Windspeed measured 3 m above ground in the Salvage stand was 77% greater ($p<0.0001$) from 0.16 m s^{-1} to 0.68 m s^{-1} in the post-treatment period. However, there was also a significant increase in the mean growing season below canopy windspeed between the pre-treatment (0.11 m s^{-1}) and post-treatment (0.19 m s^{-1}) periods within the Control stand ($p<0.0001$). The clear-cut harvest adjacent to the Control stand and 100% Kill stand as well as the loss of treed buffer adjacent to the 50% Kill stand in winter 2009/2010 likely influenced wind patterns within the stands between the pre- and post-treatment measurement periods. Windthrown trees were observed in the stands during this time period and were not related to MPB effects (Piña, 2013). In addition, fallen trees could reduce wind velocity at ground level in the 100% Kill stand.

Changes in net radiation within the canopy varied with the intensity of MPB attack (Figure 2.5). The 100% Kill stand was 25% greater in Q^* post-treatment compared to predicted values ($p<0.0001$), which changed from 7.27 MJ m^{-2} d^{-1} to 9.62 MJ m^{-2} d^{-1} in the post-treatment period However, net radiation in the canopy of the 50% Kill stand was lower in the post-treatment period, decreasing from 9.57 MJ m^{-2} d^{-1} to 8.21 MJ m^{-2} d^{-1} (18%; $p<0.0001$). The change in Q^* within the canopy of the 50% Kill stand could have been the result of where the net radiometer was placed when a new instrument was installed in 2015. The mean growing season Q^* measured from 10:00 to 16:00 reduced from 8.79 MJ m^{-2} d^{-1} to 7.35 MJ m^{-2} d^{-1} between the pre- and post-treatment periods; however, given the needle loss and fallen trees near the meteorological tower in the 50% Kill stand, Q^* was expected to increase in the post-treatment period. The Salvage stand had 2.28 MJ m^{-2} d^{-1} (26%) lower mean growing season Q^* compared to predicted values ($p<0.0001$). There was no difference in mean growing season Q^* in the Control stand between the pre-treatment (9.85 MJ m^{-2} d^{-1}) and the post-treatment (10.0 MJ m^{-2} d^{-1}) periods ($p = 0.84$).

The amount of PAR reaching the forest floor increased in both the MPB grey-attack and clear-cut harvest stands (Figure 2.6). Mean PAR was 10% (12.5 mol m^{-2} s^{-1}) greater in the 50% Kill stand ($p<0.0001$) and 24% (32.5 mol m^{-2} s^{-1}) greater in the 100% Kill stand ($p<0.0001$) compared to predicted values. In comparison, mean growing season PAR measured in the Salvage stand was 71% (224 mol m^{-2} s^{-1}) greater when the canopy was removed ($p<0.0001$). An increase in PAR corresponded with the measured decrease in LAI and canopy cover within the stands (Table 2.1). Mean growing season PAR in the Control stand between the pre-treatment (119 mol m^{-2} s^{-1}) and post-treatment (93.6 mol m^{-2} s^{-1}) periods decreased over time ($p = 0.05$).

The change in soil temperature within the top 20 cm of soil observed in either stand with simulated MPB grey-attack was not significant ($p = 1$). Mean soil temperatures showed a small increase (0.20 °C, 2%) in the 50% Kill stand and a very small decrease (0.003°C, 0.3%) in the

100% Kill stand, compared to a mean soil temperature increase of 2.8°C (26%) observed in the Salvage stand after trees were removed ($p<0.0001$). There was no difference in mean growing season soil temperature between the pre-treatment (8.3°C) and post-treatment (9.4°C) periods in the Control stand ($p = 0.10$).

Post-treatment potential evapotranspiration varied with the intensity of MPB grey-attack (Figure 2.7). In the 100% Kill stand, mean weekly PET_P in the growing season was 29% greater ($p<0.001$), which changed from 1.8 mm d^{-1} to 2.6 mm d^{-1} in the post-treatment period. In contrast, PET_P was 11% lower (0.22 mm d^{-1}) in the 50% Kill stand ($p<0.0001$), which reflects the lower net radiation predicted post-treatment compared to the Control stand. Mean growing season PET_P calculated in the Salvage stand was 20% lower ($p<0.0001$), from 2.8 mm d^{-1} to 2.3 mm d^{-1}, in the post-treatment period ($p<0.0001$). There was no difference in mean growing season PET_P between the pre-treatment (2.6 mm d^{-1}) and post-treatment (2.7 mm d^{-1}) periods in the Control stand ($p = 0.90$).

2.3.2 Snow Accumulation and Ablation

Snow accumulation was greater in both MPB grey-attack stands compared to the Control stand. Peak SWE measured in the NRH block was significantly higher in the MPB stands for both years ($p<0.05$; Figure 2.8). In 2016, peak SWE was similar between the 50% Kill, 100% Kill, and Salvage stands ($p<0.05$); however, peak SWE was different between these three stands in 2017 ($p<0.05$). Snowfall was lower in 2016 [91% of the 10-year mean (140 mm)] compared to 2017 (117%). Relative to the Salvage stand, peak SWE was reduced by 50% in the Control stand (range 40 to 61%), 11% in the 50% Kill stand (range -2.7 to 21%) and 22% in the 100% Kill stand (range 8 to 30%). Despite more needle loss in the 100% Kill stand, there was greater snow accumulation in the NRH 50% Kill. A comparison between stands was made at the nearby HTL block in 2017 (Figure 2.8). At the HTL block, peak SWE in the 50% Kill stand was lower than the HTL 100% Kill stand, and not significantly different to the HTL Control stand (Figure 2.8).

The ratios of forest:clearcut (F:C) snow depth in the post-treatment period were greater in the 50% Kill stand (0.81 – 0.81) compared to the 100% Kill stand (0.61 – 0.73), while the reverse was observed in the HTL block with a greater F:C ratio in the 100% Kill stand (0.71) compared to the 50% Kill stand (0.61). For the control, the F:C ratio in the NRH block ranged from 0.39 to 0.57 and was 0.57 in the HTL block.

Differences in peak SWE between stands largely reflected differences in snow depth, although small differences in snow density were observed between treatments. Snow depth was significantly different between years for each stand ($p<0.05$); however, these differences were not significant when comparing peak SWE between years for each stand except for the Salvage stand (Figure 2.8).

For all years, the snowpack disappeared earliest in the Control stand, followed by the 100% Kill stand, while snow remained the longest in the Salvage stand. In addition, mid-winter rainfall events influenced the snow density; for example, the 11 mm mixed rain and snow event on February 11, 2016. Rapid reduction in the snowpack also occurred during mid-winter chinook events. For example, from Feb 12 – 16th, 2017, the mean daily air temperature ranged from 1.9°C to 6.5°C.

2.3.3 Throughfall and Stemflow

The amount of rainfall reaching the forest floor increased with intensity of MPB attack (Figure 2.9). Mean post-treatment throughfall measured in 100% Kill stand was 16% greater than predicted values, which resulted in an increase from 49% of gross rainfall to 65% ($p<0.001$). The change in the 50% Kill was not significant, but increased from 52% to 55% of gross rainfall ($p = 1$). For small events (<1 mm), observed throughfall in the 100% Kill stand increased from 35% of gross rainfall to 74% compared to predicted values from the pre-calibration period. In comparison, the 50% Kill stand increased from 35% to 49% of gross rainfall for small events. The change in throughfall was less for larger events (>10 mm) with observed throughfall increased from 57% to 63% of gross rainfall in the 100% Kill stand.

Despite needle loss, stemflow on dead trees was less than live trees during measured rainfall events (Figure 2.9). Large checks were observed on dead trees and tree bark had started to slough off, which increased the storage capacity of the boles. Mean post-treatment stemflow measured on dead trees within the 100% Kill stand decreased 1085% compared to predicted values from 0.621 L per rainfall event to 0.054 L ($p<0.0001$). Stemflow measured on live trees surrounded by dead trees within the 50% Kill stand decreased 89% from 0.464 L per rainfall event to 0.260 L ($p<0.0001$). Total stand-level stemflow was negligible in all stands. In the post-treatment period, mean stand-level stemflow was <0.01% of gross rainfall in the Control, 50% Kill, and 100% Kill stands.

Total rainfall intercepted by the canopy that was indirectly determined from observed throughfall and stemflow events indicates the 100% Kill stand intercepted less rainfall than the 50% Kill stand compared to the pre-treatment period (Figure 2.10).

2.3.4 Soil Water Content

Mean weekly soil moisture content measured during the growing season increased at all depths (20, 40 and 60 cm) with an increase in MPB intensity (Figure 2.11). In the 100% Kill, mean weekly soil moisture was 8% (11.8 mm), 6% (5.7 mm) and 3% (2.7 mm) greater in the post-treatment period compared to predicted values from the pre-calibration period ($p<0.001$) at the 20 cm, 40 cm and 60 cm depths, respectively. The increase in soil moisture was smaller in the 50% Kill stand. Mean weekly soil moisture was 2% (2.9 mm, $p = 0.27$) greater at 20 cm, 3% (3.2 mm, $p<0.001$) greater at 40 cm, and 2% (2.4 mm; $p<0.001$) greater at 60 cm. For the Salvage stand, mean weekly soil moisture did not change at 20 cm depth (0.39 m^3 m^{-3}; 116 mm, $p = 0.97$), was 2% (1.3 mm; $p<0.001$) greater at 40 cm, and 3% (2.2 mm; $p<0.001$) greater at 60 cm in the post-treatment period. In the Control stand, there was a significant difference between pre-treatment (0.35 m^3 m^{-3}; 105 mm) and post-treatment (0.33 m^3 m^{-3}; 99 mm) periods at the 20 cm depth ($p<0.001$); however, there was no change in mean weekly soil moisture at the 40 cm depth (0.47 m^3 m^{-3}; 94 mm) or 60 cm depth (0.34 m^3 m^{-3}; 68 mm).

2.3.5 Model Performance

Model performance was evaluated with mean absolute error (MAE) and percent bias (PBIAS) between measured and modelled: SWE, soil moisture in the root zone, and soil moisture in soil layer 2 (Table 2.3). The water balance models were able to track the measured SWE and scaled soil water content reasonably well (Figures 2.12 and 2.13).

Simulated SWE showed better agreement with observations during 2015 and 2017, while 2016 was more impacted by mid-winter rain events. The rapid reductions in snowpack due to mid-winter rainfall events or chinook events were not well represented. This is evident from the 11 mm mixed rain and snow event on February 11, 2016 and the chinook event in mid-February 2017 (Figure 2.12).

Simulated soil moisture storage had better overall performance statistics than SWE. Modelled soil moisture storage in the root zone of the 50% Kill and 100% Kill stands tended to be peakier compared to measured values. Measured soil moisture in these stands may have more buffered peaks compared to the Control or Salvage stands due to soil heterogeneity; however, parameters for soil texture were set the same for each water balance model. Good agreement between modelled and measured soil moisture in the root zone and soil layer 2 suggests the proportions of total evapotranspiration and root zone drainage were appropriate.

Monthly modelled AET and estimated AET_A time series for 1 Oct 2014 – 30 Sep 2017 were compared (Figure 2.14). The model explained >92% of the variance in monthly modelled AET and the slope of the regressions were not significantly different from 1.00 for all stands ($p = 0.974 – 1.00$).

2.3.6 Stand Water Balances

There were 298 rainfall events larger than 0.25 mm during the post-treatment period; 57% of the rainfall events were <2 mm, 76% were <5 mm and 96% were <20 mm. The frequency distribution of rainfall events during the post-treatment period was similar to that observed during the canopy interception measurements. Only 2% of the rainfall events exceeded the maximum gross rainfall observed during measurements.

There was less rainfall canopy interception with canopy cover loss (Figures 2.15 and 2.16). Mean annual rainfall canopy interception modelled for the post-treatment period was 143 mm yr^{-1} (125 – 168 mm yr^{-1}) in the Control stand (36% of gross rainfall), 132 mm yr^{-1} (114 – 154 mm yr^{-1}) in the 50% Kill stand (33% of gross rainfall), and 116 mm yr^{-1} (98 – 140 mm yr^{-1}) in the 100% Kill stand (29% of gross rainfall).

Snow falls more frequently as small events in the study region. There were 131 snowfall events larger than 0.25 mm during the post-treatment period; 54% of the snowfall events were <2 mm, 82% were <5 mm and 99% were <20 mm. Automated snow depth records from the Salvage stand corroborate this trend (data not shown).

There was less snowfall canopy interception with canopy cover loss. Mean annual snowfall canopy interception modelled for the post-treatment period was 26 mm yr^{-1} (24 – 29 mm yr^{-1}) in the Control stand (17% of gross snowfall), 21 mm yr^{-1} (20 – 22 mm yr^{-1}) in the 50% Kill stand (14% of gross snowfall), and 13 mm yr^{-1} (11 – 14 mm yr^{-1}) in the 100% Kill stand (8% of gross snowfall).

The combined overstory transpiration and understory evapotranspiration ($E_t + E_U$) water balance term increased with canopy cover loss (Figure 2.16). Mean annual $E_t + E_U$ for the post-treatment period was 84 mm yr^{-1} (68 – 95 mm yr^{-1}) in the Control stand (15% of P_G), 113 mm yr^{-1} (99 – 128 mm yr^{-1}) in the 50% Kill stand (21% of P_G), 132 mm yr^{-1} (127 – 142 mm yr^{-1}) in the

100% Kill stand (24% of P_G), and 164 mm yr^{-1} (163 – 166 mm yr^{-1}) in the Salvage stand (30% of P_G). Increased $E_t + E_U$ in the 100% Kill and Salvage stands reflected increased water loss from understory vegetation because overstory transpiration was assumed to be negligible.

Increased water loss from the living vegetation ($E_t + E_U$) made up a larger proportion of total AET in the 50% Kill (43%) and 100% Kill (51%) stands compared to the Control stand (33%), despite similar mean annual total AET ($E_C + E_t + E_U$) between stands. Mean annual total AET was 253 mm yr^{-1} (221 – 287 mm yr^{-1}) in the Control stand (46% of P_G), 266 mm yr^{-1} (235 – 302 mm yr^{-1}) in the 50% Kill stand (48% of P_G), 259 mm yr^{-1} (236 – 294 mm yr^{-1}) in the 100% Kill stand (47% of P_G). The Salvage stand mean annual AET was 164 mm yr^{-1} (163 – 166 mm yr^{-1}; 30% of P_G). The larger proportion of water loss from living vegetation ($E_t + E_U$) compensated for the decreased canopy interception (E_C) in the MPB stands.

Sublimation from the snowpack was small in all stands. The mean annual water loss from sublimation amounted to 2% of gross snowfall (3 mm y^{-1}) in the Control, 100% Kill and 50% Kill stands, while increased windspeed in the Salvage stand resulted in snowpack sublimation of 3% of gross snowfall (4 mm y^{-1}).

Root zone drainage in both MPB stands was lower than the Control stand over the three-year study period (Figure 2.16). Mean annual drainage for the post-treatment period was 287 mm yr^{-1} (240 – 313 mm yr^{-1}) in the Control (52% of P_G), 253 mm yr^{-1} (223 – 301 mm yr^{-1}) in the 50% Kill (46% of P_G), and 269 mm yr^{-1} (231 – 301 mm yr^{-1}) in the 100% Kill (49% of P_G). The mean annual root zone drainage in the Salvage stand, five to seven years post-harvest, was 376 mm yr^{-1} (328 – 422 mm yr^{-1}; 68% of P_G).

The greatest magnitude of root zone drainage occurred during the snowmelt period or after large rainfall events that exceeded the root zone soil moisture storage capacity (Figure 2.15). The timing of root zone drainage varied between stands, which was dependent on antecedent soil moisture conditions, the timing and intensity of snowmelt/rainfall, and the timing of high evaporative demand (Figure 2.15). High AET rates typically occurred in June, July and August; however, overstory transpiration and understory evapotranspiration were limited by PET during this period, especially observed in the Control stand. In addition, the Control stand had the shallowest snowpack, but the snowpack in the 100% Kill stand melted at a faster rate and contributed to root zone drainage earlier in 2016 and 2017.

2.4 Discussion

2.4.1 Evapotranspiration

The values of AET reported here were within range of those reported for other lodgepole pine forests. The undisturbed mature stand at MPB Robb had a mean annual AET of 253 mm yr^{-1} (46% of P_G), which was less than a high elevation forest in the warmer southern British Columbia interior (381 mm yr^{-1}; 57% of P_G; Spittlehouse, 2006). In northeast British Columbia, the mean annual AET in a MPB attacked stand with >95% grey boles was 285 mm yr^{-1} (44% of P_G), while a MPB attacked stand with 82% grey-attack was 232 mm yr^{-1} (35% of P_G; Brown *et al.*, 2014). The 100% Kill stand was within range of the British Columbia grey-attack stands with an annual AET of 259 mm yr^{-1} (47% of P_G). To compare, the annual AET of the Salvage (five to seven years post-harvest) was 30% of P_G (164 mm yr^{-1}). Lower AET from a clear-cut stand has been reported in other pine forests. A jack pine stand in central Saskatchewan, six years post-harvest, had a mean annual AET of 37% of P_G (212 mm yr^{-1}; Barr *et al.*, 2012), while a clear-cut stand in the southern British Columbia interior was 36% of P_G (236 mm yr^{-1}).

Canopy cover loss as a result of MPB treatment decreased overstory tree transpiration, but the available soil water was subsequently used by healthy canopy trees, sub-canopy trees or understory shrubs, herbs, grasses and mosses. As the canopy opened due to tree death, understory evapotranspiration was stimulated by increased availability in soil moisture, nutrients and radiation that reached the forest floor (Brown *et al.*, 2013; Biederman *et al.*, 2014a; Reed *et al.*, 2016; Meyer *et al.*, 2017). For example, the forest floor in the 100% Kill stand received 24% more PAR compared to the pre-treatment period. Now in the post-treatment period, increased water loss from the living vegetation ($E_t + E_u$) made up a larger proportion of total AET in the 50% Kill (43%) and 100% Kill (51%) stands compared to the Control stand (33%), despite similar total AET between stands. There was little change in annual AET over a four year period (range 226 – 237 mm yr^{-1}) in an 82% grey-attacked stand in northeastern British Columbia (Brown *et al.*, 2013). In other northern conifer forests, increased evapotranspiration in grey-attacked stands from the secondary structure, shrubs and moss has been reported (Mikkelson *et al.*, 2013; Biederman *et al.*, 2014a; Meyer *et al.*, 2017). The understory can play an important role in equalizing AET from stands of varied LAI (Kelliher *et al.*, 1993). In addition, stand thinning or partial-cut strips can increase transpiration per unit leaf area from healthy lodgepole pine trees (Reid *et al*, 2006; Bladon *et al.*, 2006; Piña, 2013; Karpyshin, 2019). The increased evaporative demand from live canopy trees and understory vegetation compensated for the decline in overstory tree transpiration and canopy interception losses, which maintained annual total AET in MPB treated stands.

2.4.2 Rainfall Interception Losses

Rainfall canopy interception in the undisturbed mature forest stand was higher than lodgepole pine forests located outside of Alberta. In central Alberta, two undisturbed mature stands (>110 yr lodgepole pine) had canopy interception losses of 33% and 37% of R_G (Brabender, 2005), which was similar to the Control stand at MPB Robb (36% of R_G). However, rainfall canopy interception values from MPB Robb were higher than a southern interior British Columbia stand (23 to 31% of R_G; >125 yr lodgepole pine; Winkler *et al.*, 2010). Compared to British Columbia, MPB Robb receives a larger proportion of annual precipitation that falls as rain (70%) and frequently falls as small events (73% events <5 mm), which could result in higher water loss from rainfall captured in the canopies.

When the rainfall canopy interception storage capacity was exceeded, forest floor interception reduced the amount of net rainfall that infiltrated to the mineral soil. An experiment conducted in the Control stand in 2010 suggested 2.4 mm of rainfall could be intercepted per centimeter of forest floor (Piña, 2013), which was higher than the amount of forest floor interception measured for a young lodgepole pine forest in Alberta (1.8 mm cm^{-1} of forest floor thickness; Golding and Stanton, 1971). Despite variability in forest floor interception values, research suggests rainfall captured by the forest floor in lodgepole pine forests could constitute a larger portion of the water balance. Indeed, modelled rainfall interception results for the study period indicate mean annual forest floor interception was 104 mm y^{-1} (26% of R_G) compared to 140 mm y^{-1} (35% of R_G) of rainfall captured in the canopy of the Control stand. Loss of canopy in the 100% Kill stand resulted in similar interception captured by the canopy (119 mm y^{-1}; 30% of R_G) and forest floor (111 mm y^{-1}; 28% of R_G). As a result, the relatively infrequent, large rainfall events were important to replenish soil moisture and contribute to root zone drainage due to the high rainfall interception storage capacities in both the forest floor and canopy.

Despite canopy cover loss in the grey-attack stands, the canopies continued to provide high interception storage capacity. The storage capacity within the large branches and trunks of the standing dead trees resulted in only a 3% and 7% decrease in rainfall canopy interception in the 50% Kill and 100% Kill stands compared to the Control stand, respectively. Interception data in even-aged grey-attack stands are limited, as well as literature to directly compare grey-attack stands to stand-replacing disturbances like wildfire and regenerating harvest. However, compared to the Salvage stand, the 100% Kill stand continued to intercept >90% of the rainfall that would be caught in a live canopy. The loss of needles and fine branches reduced the canopy storage, but the large branches/trunks combined with increased windspeeds (i.e. increased potential evaporative demand) in the grey-attack canopy provided more storage capacity than one would likely observe after a stand-replacing disturbance.

2.4.3 Snow Accumulation and Ablation

MPB grey-attack stands showed a snow accumulation response in range between that observed in the undisturbed mature forest and clear-cut harvest. Snowpack accumulation typically increases with reduced interception (Boon, 2009; Boon, 2012; Pugh and Small, 2012). However, snow accumulation between the 50% Kill and 100% Kill stands was different between the HTL and NRH blocks. Greater snow accumulation in the NRH 50% Kill stand compared to the NRH 100% Kill stand may be due to increased blowing snow redistribution due to the loss of treed buffer (pipeline activities) and subsequent windfall in the stand. Relative to the Salvage stand (i.e. an open clearing), peak SWE was reduced 50% in the Control stand (40 to 61% depending on year) and 22% in the 100% Kill stand (8 to 30% depending on year). Research in MPB affected stands in British Columbia found that snow depth and SWE varied as a function of canopy cover loss (grey-attack versus alive) and interannual variability in meteorological conditions (i.e. high versus low-to-average snow years; Boon, 2012; Winkler *et al.*, 2014). They found greater differences in accumulation in years of low SWE, but canopy storage capacity would be exceeded in high snow years. However, snow depth and SWE in MPB Robb also varied in response to mid-winter rainfall and chinook events (i.e. strong, warm, dry winds), which are common in the Foothills region and results in snowpack removal via blowing snow, evaporation, and sublimation.

Compared to the undisturbed mature stand, the grey-attack stands were observed to have higher ablation rates (Boon, 2009; Boon, 2012; Pugh and Small, 2012). Ablation rate variability was primarily a function of net radiation transmittance to the ground and basal area, which contrasts clear-cut and regenerating stands where the dominant snowmelt energy is from sensible heat flux with the increased wind speeds (Winkler *et al.*, 2010; Mikkelson *et al.*, 2013). Below canopy wind speeds decreased in the 100% Kill stand (the stand not potentially influenced by buffer removal) and sublimation from the snowpack was small (2% of gross snowfall). Therefore, the increased radiation transmitted to the ground was likely the most important contribution to snowmelt in the grey-attack stands (Biederman *et al.*, 2014b), which altered snowmelt magnitude and timing.

2.4.4 Soil Moisture Response

The increased radiation transmittance and soil moisture in the upper soil horizons resulted in increased understory evapotranspiration in the grey-attack stands. Post-treatment soil moisture may increase because of decreased transpiration and canopy interception losses from overstory trees (Morehouse *et al.*, 2008; Clow *et al.*, 2011). However, increased evaporative demand driven by increased radiation transmitted to the forest floor may decrease the soil moisture (Brown *et al.*, 2013; Biederman *et al.*, 2014a; Meyer *et al.*, 2017). The changes in soil moisture measured in the 100% Kill and 50% Kill stands were smaller than expected due to increased transpiration from the live canopy trees (i.e. 50% Kill stand) and increased evapotranspiration from understory vegetation.

The post-treatment competing responses of individual components of evapotranspiration indicate no evidence of increased root zone drainage with MPB attack. Water balance results show only slightly less mean annual root zone drainage in the 50% Kill stand (46% of P_G) and 100% Kill stand (49% of P_G) compared to the Control stand (52% of P_G). As expected, the total loss of canopy cover as a result of clear-cut harvest resulted in more root zone drainage in the Salvage stand (68% of P_G). However, root zone drainage results did not follow the expected continuum based on canopy cover loss (least Control – 50% Kill – 100% Kill – Salvage most) as a result of varied increases and decreases in the individual components of total evapotranspiration driven largely by changes in net radiation reaching the understory. However, despite similar root zone drainage between an undisturbed mature forest stand and MPB grey-attack stands, it is still important that MPB affected stands be considered distinct cover types, because within watersheds the topographic aspect controls the effect of trees on shortwave radiation (e.g. Ellis *et al.*, 2011). Therefore, these results from stand water cycling from varied canopy cover loss should be explored at a watershed scale with different topographic slopes and aspects.

The extent of canopy cover loss and available unsaturated zone soil capacity (i.e. depth to water table and antecedent moisture content) may influence the amount of root zone drainage and recharge, and subsequently the groundwater response. Most water inputs at MPB Robb occur after snowmelt as well as in June, July and August, which coincides with the timing of high ET rates. These conditions result in little surplus water for groundwater recharge after unsaturated soil capacity is filled with water. Results show that small increases in soil moisture were observed after infrequent large rainfall events, but the dominant input to soil moisture was snowmelt, which influenced antecedent soil moisture conditions and soil storage after the snowmelt period. The function of snowmelt input may be to satisfy soil storage prior to summer rainfall events (Redding and Devito, 2011). Snowmelt and rainfall input depth and intensity, in relation to available soil storage capacity, were observed to be strong controls on the occurrence of groundwater response in glacial till soils (Redding and Devito 2008; 2010; Smith *et al.*, 2014). The deep soils developed from glacial tills found in MPB Robb (at least 3 m deep based on auger holes) may result in a threshold-type groundwater response, where extent of canopy cover loss, net evapotranspiration and available unsaturated zone storage capacity strongly control the groundwater response, which would need to be further explored.

2.4.5 Management Implications

The results of this chapter together with previous studies (e.g. Brown *et al.*, 2013; Meyer *et al.*, 2017) suggest that the management practice of clear-cut salvage harvesting MPB attacked stands that have sufficient live overstory trees or understory would not minimize the hydrologic effects on stand water cycling. The regenerating lodgepole pine canopy cover, even seven years post-harvest, had not re-established adequate canopy cover (i.e. LAI) for hydrologic recovery, or the return to pre-disturbance water cycling. If hydrologic recovery is assumed to be driven primarily by the return of the canopy to pre-disturbance levels, a study on lodgepole pine forests in southern interior British Columbia found rainfall interception losses were not similar to an adjacent mature forest until 25-years post-harvest (4 m tall lodgepole pine; Winkler *et al.*, 2010). In addition, maximum SWE was 43% recovered and mean ablation rate was 29% recovered (4.5 m tall lodgepole pine; 28% canopy cover; Winkler *et al.*, 2005). The results of this study highlight the need for further research to interpolate stand-level results to the watershed-scale to assess the effects on runoff timing and magnitude in watersheds with varied canopy cover loss.

How interaction among forest disturbance, climate change and forest management will affect water for forests and downstream water resources remains a concern for forest managers. If the forest management goal were to rehabilitate post-MPB attacked stands with stocked lodgepole pine, significant silviculture intervention would be required at MPB Robb (McIntosh and Macdonald, 2013). Research conducted in MPB Robb found minimal advance regeneration, no natural recruitment post-attack, and the highest recruitment rates of lodgepole pine seedlings on mineral soil and decayed wood, which were insufficient across all stand treatments (McIntosh and Macdonald, 2013). These results contrast with research from the Colorado Rocky Mountains, which found that post-MPB attacked stands should recover without silviculture intervention due to sufficient advance regeneration beneath uncut grey-attack stands with largely intact soils (Rhoades *et al.*, 2020). Differences in forest floor vegetation structure (i.e. increased moss) may be the reason for differences in advance regeneration and natural recruitment rates. Although recruitment of lodgepole pine will be higher in clear-cut salvage harvested stands, it is important that forest managers consider how salvage operations influence other natural resources apart from stocking as the forest management goal.

2.4.6 Conclusions

The results of this chapter add to the literature that provides context for the stand-scale hydrologic response to MPB that range across the geo-climatic regions within the MPB epidemic from British Columbia (e.g. Winkler *et al.*, 2014) to Arizona (Morehouse *et al.*, 2008), and can be used to better understand interrelated feedbacks on nutrient cycling and water quality (Mikkelson *et al.*, 2013). Forests affected by MPB attack should be considered a distinct cover type because these stands exhibit a range of hydrologic responses between an undisturbed mature stand and a clear-cut harvest stand. However, hydrometeorological data and water balance modelling results for this geo-climatic region do not support the hypothesis that root zone drainage increases in MPB grey-attack in even-aged mature lodgepole pine stands. As expected, compared to an undisturbed mature stand, within the canopy cover of the MPB grey-attack stands, canopy interception decreased and canopy windspeed increased, while radiation transmitted to the forest floor increased, and soil moisture in the upper soil horizons increased. Compensatory increases in understory evapotranspiration where predicted. Within the 50% Kill stand, the increase in available soil moisture due to partial overstory mortality led to increased transpiration from the neighboring live trees within the stand (Piña, 2013). For the 100% Kill stand, decreased overstory transpiration and canopy rainfall interception losses were compensated by increased understory evapotranspiration as a result of increased net radiation reaching the forest floor, which resulted in minimal change to total evapotranspiration. In all stands, the highest evapotranspiration rates occurred in the summer months, which resulted in snowmelt as the dominant input to soil moisture with additional small increases observed after infrequent large rainfall events. Rainfall and snowmelt depth and intensity, in relation to soil storage capacity (i.e. antecedent conditions), are likely strong controls on groundwater response, similar to that observed in soils developed from deep glacial tills (Redding and Devito 2008; 2010; Smith *et al.*, 2014). However, this requires further study in MPB Robb due to the heterogeneity and unknown depth of the surface aquifer. Further research is also needed to interpolate the stand-level hydrologic response to MPB grey-attack and forest management strategies to the watershed-scale to assess the effects on runoff generation and potential changes in streamflow. The results of this chapter show that the regional differences in water cycling within MPB grey-attack and salvage harvest stands need to be considered to better understand changes in runoff generation in other geo-climatic regions as MPB spreads outside its natural ecological range.

Table 2.1 Stand attributes measured during pre-treatment (2008) and post-treatment (2016) years within fixed area subplots. Herbicide application and harvest occurred in summer, 2009. Forest floor (FF) depth, average canopy cover, leaf area index (LAI), FF thickness and percentage of FF vegetation type is the average across all three blocks (see Figure 2.1; McIntosh and Macdonald, 2013; Steinke, 2018); dbh, diameter at breast height. Numbers in brackets are the standard error of the mean.

Stand Treatment	Control		50% Kill		100% Kill		Salvage	
Year	2008	2016	2008	2016	2008	2016	2008	2016
Basal Area (m^2 ha^{-1})	436	429	418	347	447	383	-	-
Dead Trees (%)	20	29	20	48	21	62	-	-
Declining Trees (%)	7.7	12	6.5	11	4.1	12	-	-
Density (stems ha^{-1})	1633	1372	1578	1111	1439	1133	-	-
Overstory height (m)[A]	22 - 26	25 - 30	23 - 25	25 - 30	23 - 32	26 - 31	20 - 28	0.75 - 2
Avg dbh (cm)	19	21	19	21	21	20	16	-
Range dbh (cm)	0.9 - 32	8.2 - 35	1.2 - 33	3.9 - 35	4.7 - 35	4.5 - 36	5.2 - 31	-
Avg Canopy Cover (%)	60 (0.8)	54 (1.3)	59 (2.0)	44 (4.1)	58 (1.0)	37 (1.6)	-	-
LAI (m^2 m^{-2})	2.48 (0.11)	1.82 (0.07)	2.97 (0.25)	2.19 (0.15)	2.33 (0.06)	1.44 (0.06)	2.50 (0.10)	-
PAR Transmittance (%)	22 (0.9)	33 (0.4)	28 (0.8)	47 (0.6)	22 (0.9)	48 (0.7)	-	-
Extinction Coefficient (-)	0.52 (0.06)	0.44 (0.02)	0.45 (0.04)	0.39 (0.02)	0.54 (0.05)	0.25 (0.01)	-	-
Forest Floor Depth (mm)	91 (4.1)	70 (3.9)	105 (6.4)	73 (4.5)	89 (4.5)	63 (3.5)	82 (4.1)	52 (2.3)
% Total FF Cover	121 (6.6)	92 (5.4)	139 (8.5)	115 (6.8)	115 (7.6)	132 (5.9)	133 (8.3)	113 (6.5)
% Tree (< 1.3 m)	0 (0)	0 (0)	0.3 (0.2)	0.0 (0.0)	0.1 (0.1)	7.8 (4.8)	1.1 (1.1)	4.4 (1.3)
% Shrub	22 (5.0)	18 (3.2)	38 (6.9)	27 (5.2)	25 (5.0)	33 (3.9)	45 (7.8)	27 (4.3)
% Forbes	32 (4.1)	29 (2.6)	33 (4.8)	32 (2.9)	35 (2.5)	43 (3.5)	40 (4.3)	22 (3.0)
% Grass	6.8 (3.1)	5.7 (1.9)	14 (3.8)	15 (4.0)	8.1 (2.6)	18 (2.9)	7.6 (2.2)	34 (3.6)
% Bryophyte	55 (4.5)	37 (3.4)	51 (4.5)	38 (3.9)	45 (5.4)	26 (3.1)	29 (4.5)	24 (3.7)

[A] Upper quartile range.

Table 2.2. List of model parameters, parameter values and range of calibrated parameters (100 parameters) for each stand. Parameter values and ranges were used in the modified HBV-EC model structure template in Raven to simulate the stand water balance and quantify the 95th percentile parameter uncertainty bounds. FF, forest floor; RZ, root zone; S, soil; ALL, all soil layers.

Parameter Name	Units	Site			
		Control	50% Kill	100% Kill	Salvage
		Vegetation Parameters			
MAX_HEIGHT[1]	m	23.5	23.5	0.5	1.3
MAX_LAI[1,2]	$m^2\ m^{-2}$	3.11-3.60	4.01-4.16	3.58-3.96	0.50-0.51
MAX_LEAF_COND[2,3,A]	$mm\ s^{-1}$	20.3-23.7	16.9-18.0	4.4-4.7	6.2-6.3
SVF_EXTINCTION[1,B]	-	0.41-0.48	0.36-0.42	0.23-0.27	-
MAX_CAPACITY[1,4,C]	mm	18-20	20-21	20-23	-
MAX_SNOW_CAPACITY[1,D]	mm	16-17	21-22	17-18	-
		Landuse Parameters			
FOREST_ SPARSENESS[1,E]	%	0.44-0.47	0.56-0.57	0.65-0.66	-
SNOW_SWI[5,F]	[0..1]	0.05	0.05	0.05	0.05
		Soil Parameters			
POROSITY (FF)[4]	[0..1]	0.24	0.24	0.24	0.24
FIELD_CAPACITY (FF)[4,6]	[0..1]	0.266	0.257	0.297	0.359
SAT_WILT (FF)[4,6]	[0..1]	0.09	0.086	0.1	0.121
POROSITY (RZ)[4,7]	[0..1]	0.40-0.46	0.41-0.48	0.40-0.43	0.40-0.47
POROSITY (S2)[4,7]	[0..1]	0.28-0.35	0.35-0.35	0.35-0.35	0.35-0.35
POROSITY (S3)[4,7]	[0..1]	0.30	0.30	0.30	0.30
FIELD_CAPACITY (ALL)[7]	[0..1]	0.22	0.22	0.22	0.22
SAT_WILT (ALL)[7]	[0..1]	0.073	0.073	0.073	0.073
MAX_CAP_RISE_RATE[6]	$mm\ d^{-1}$	0.4-0.6	0.7-0.7	1.0-1.0	1.9-2.7
MAX_PERC_RATE (RZ)[1]	$mm\ d^{-1}$	11-30	11-30	12-30	11-30
MAX_PERC_RATE (S2)[8]	$mm\ d^{-1}$	3.3-15	1.8-2.4	4.2-5.5	6.5-8.0
PERC_N (RZ)[8,G]	-	8.5-10	7.0-10	12-18	8.0-10
PERC_N (S2)[8]	-	5.4-9.8	9.6-10	19-20	9.6-10

Parameter sources: [1]this study; [2]Adams, 1990; [3]Meyer *et al.*, 2017; [4]Piña, 2013; [5]Gray and Male, 1980; [6]Steinke, 2018; [7]Dingman, 2002; [8]Craig *et al.*, 2019.

Description of parameters: [A]maximum leaf (stomatal) conductance; [B]coefficient to calculate the skyview factor; [C]maximum canopy storage capacity; [D]maximum canopy storage capacity as snow water equivalent; [E]canopy cover; [F]water saturation fraction of snow; [G]percolation exponent.

Table 2.3 Performance statistics mean percent bias error (PBIAS) and mean absolute error (MAE) calculated for snow water equivalent (SWE), soil moisture storage in the root zone (ΔS_{RZ}) and soil layer 2 for simulated stand water balances using a modified HBV-EC model structure template in Raven as outlined in Figure 2.2. Standard error is presented in brackets.

Stand Treatment	SWE		Root Zone		Soil Layer 2	
	PBIAS	MAE	PBIAS	MAE	PBIAS	MAE
Control	11.8 (0.009)	18.1 (0.003)	1.4 (0.02)	4.7 (0.01)	1.9 (0.03)	2.5 (0.003)
50% Kill	-39.4 (0.006)	31.4 (0.002)	1.8 (0.04)	7.3 (0.03)	-4.7 (0.07)	5.3 (0.02)
100% Kill	-35.1 (0.002)	23.1 (0.001)	0.84 (0.02)	6.1 (0.03)	-2.5 (0.04)	3.9 (0.01)
Salvage	-9.8 (0.000)	25.0 (0.000)	-6.6 (0.01)	6.3 (0.01)	-6.6 (0.05)	7.2 (0.01)

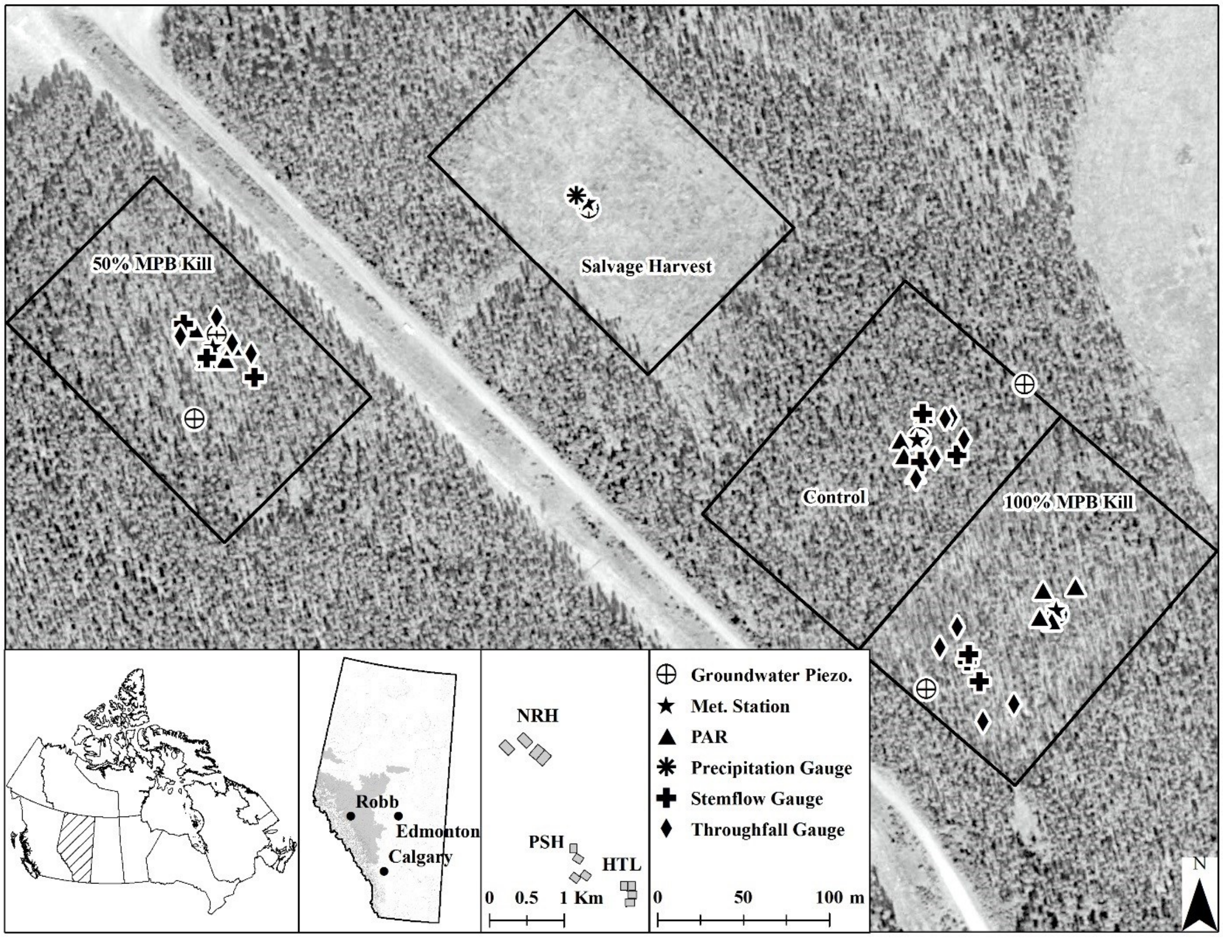

Figure 2.1 Study area and location of the mountain pine beetle (MPB) before-after control-impact (BACI) randomized block design located near Robb, Alberta, Canada within the Foothills region (dark grey) where there are three blocks: North Ridge Hydro (NRH), Horse Train Loop (HTL) and Power Shack Hill (PSH). Within each block were four treated experimental units (i.e. stands). The NRH stands are enlarged in the map, which had the hydrometeorological instruments (stand = 0.64 ha). The HTL stands were used for additional snow surveys in 2017. Harvest outside of the Salvage stand during 2009/2010 was unrelated to the study, which includes the loss of treed buffer adjacent to the 50% MPB Kill stand.

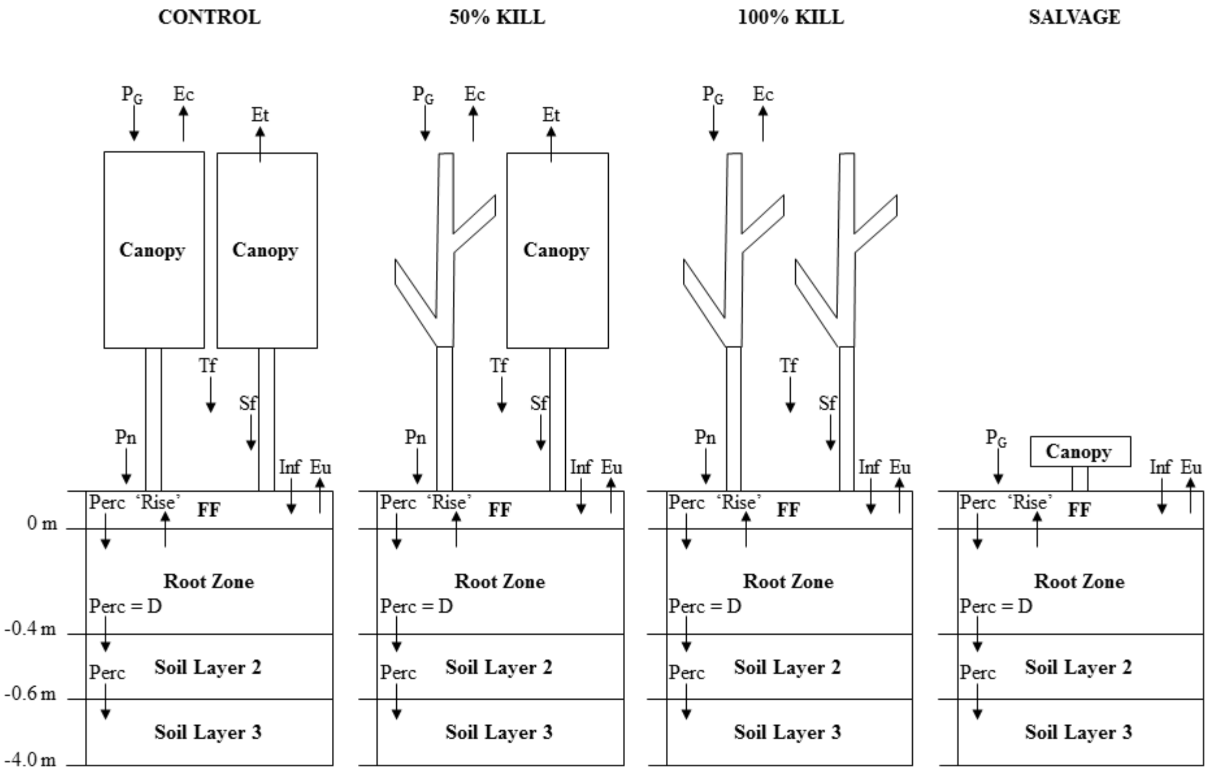

Figure 2.2 Conceptual model of hydrologic processes in MPB Robb stands. Needle loss is represented without the 'canopy box'. Unsaturated lateral flow in the root zone and soil layer 2 was considered negligible given the flat topography and low unsaturated hydraulic conductivities. P_G is gross precipitation. Net precipitation (P_n) equaled throughfall (T_f) plus stemflow (S_f). P_n that infiltrated (*Inf*) into the forest floor (*FF*) fibric/humic layer may percolate (*Perc*) vertically into the mineral soil. The hydrologic process *Rise* was used conceptually to move water from root zone storage to forest floor storage, which is the HBV-EC algorithm for capillary rise and linearly proportional to soil saturation in the forest floor layer. Total evapotranspiration included the sum of evaporation of canopy intercepted rain and snow (E_c), overstory tree transpiration (E_t), and understory evapotranspiration (E_u). Intercepted water by lodgepole pine seedlings in the salvage harvest stand was considered negligible. Sublimation was only removed from the snowpack (not shown). Root zone drainage (D) was defined as percolation from the Root Zone layer at -0.4 m depth into the soil layers below.

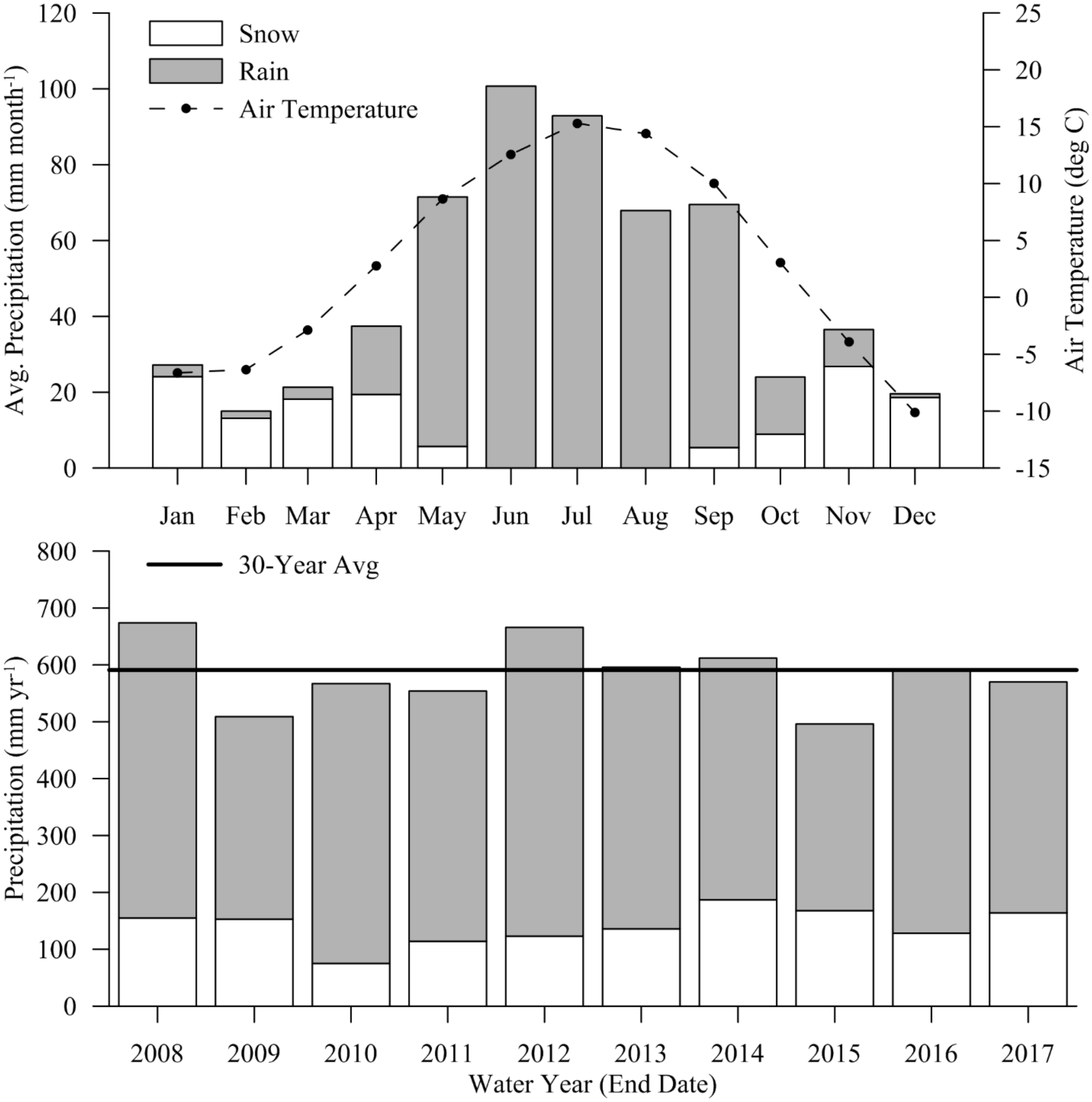

Figure 2.3 Average monthly precipitation and air temperature from 2008 – 2017 measured in the Salvage stand (top panel). The bottom panel shows total annual precipitation for each water year (October 1 to September 31) and the 30-year average (1967 – 1996) from the historical Robb meteorological station (Environment and Climate Change Canada, Climate ID 3065505, 1,130 m.a.s.l., 9.2 km from Salvage stand). The pre-treatment period includes Apr 2008 to Jul 2009, while post-treatment includes Oct 2014 to Sep 2017.

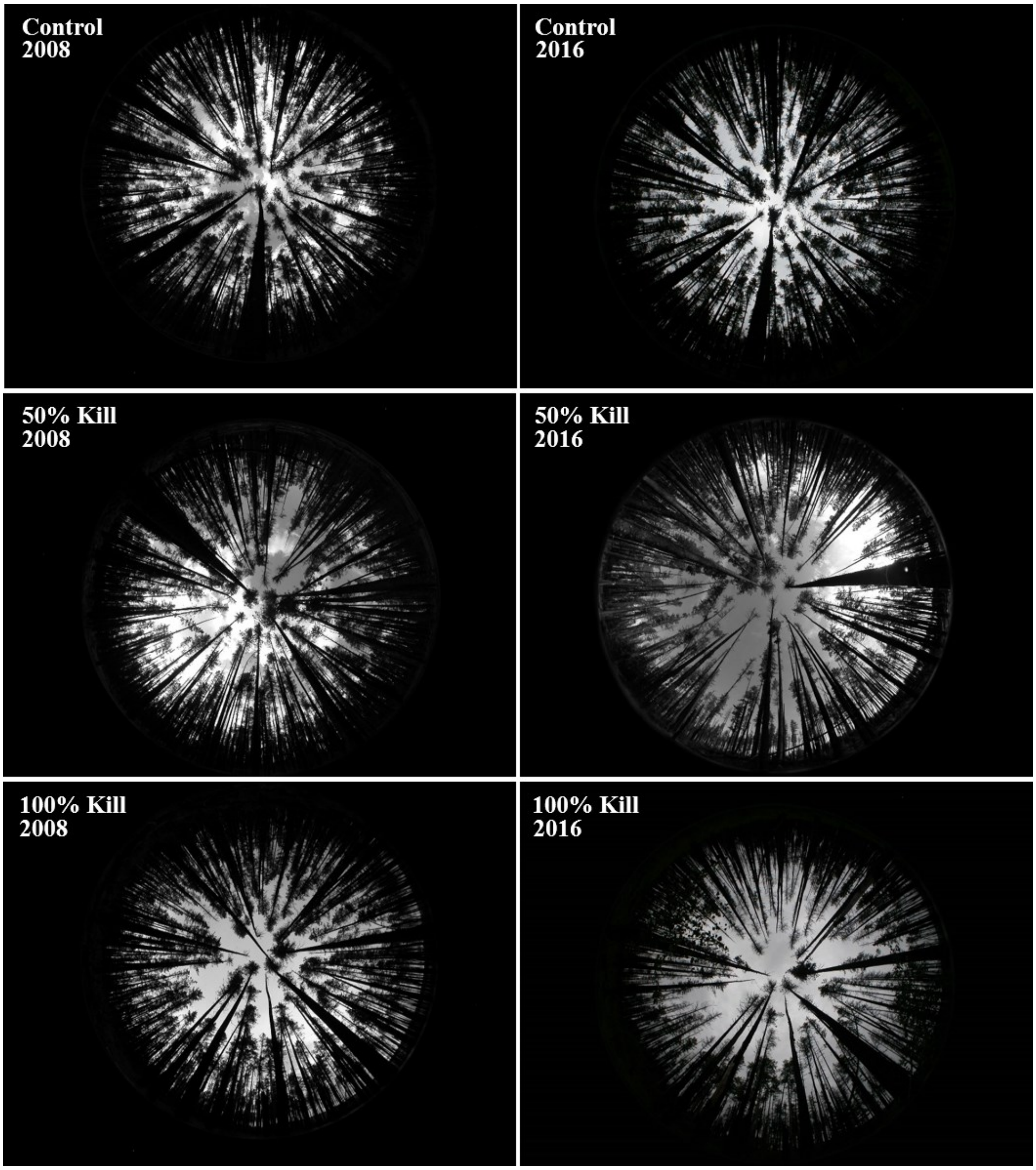

Figure 2.4 Typical hemispherical photographs to show canopy structure in the Control, 50% Kill and 100% Kill stands taken in July pre-treatment (2008) and post-treatment (2016).

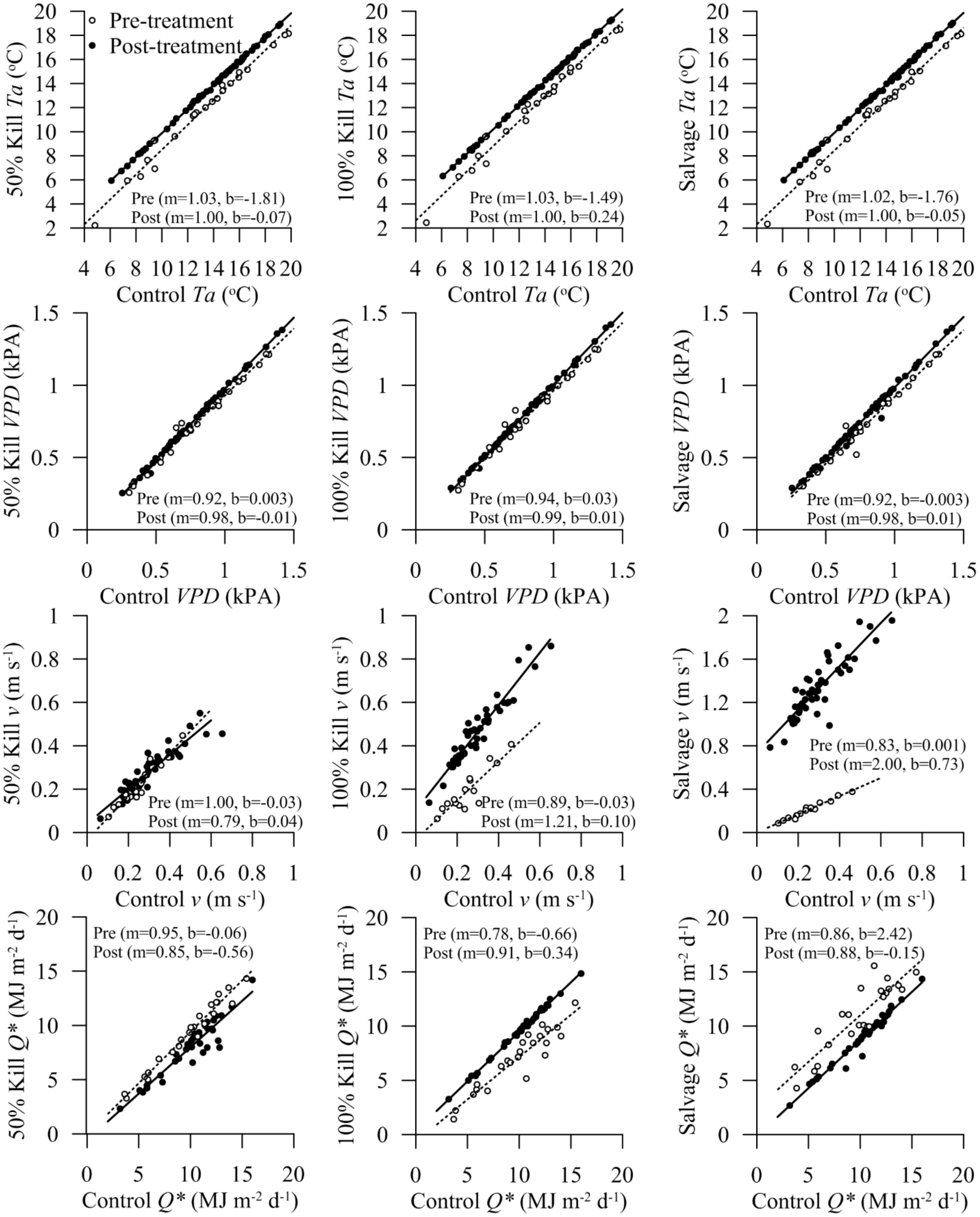

Figure 2.5 Within canopy (20 m height) relationships of mean weekly growing season (1 May – 30 Sep) air temperature (T_a), vapour pressure deficit (*VPD*), windspeed (v) and net radiation (Q*) within the stands, pre- and post-treatment. Shown with slope (m) and intercept (b).

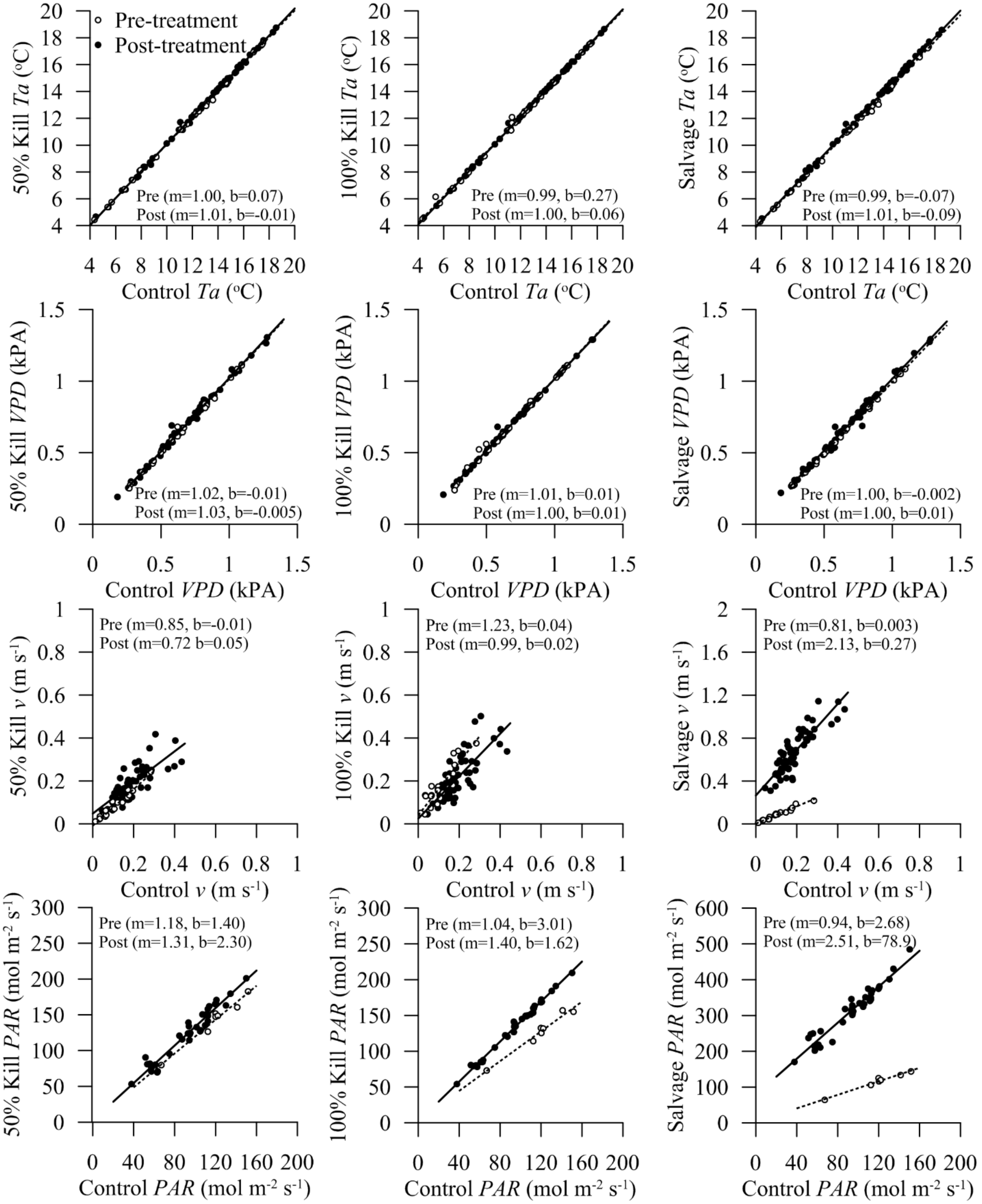

Figure 2.6 Below canopy (3 m height) relationships of mean weekly growing season (1 May – 30 Sep) air temperature (T_a), vapour pressure deficit (*VPD*), windspeed (*v*) and photosynthetically active radiation (*PAR*) within the stands, pre- and post-treatment. Shown with slope (m) and intercept (b).

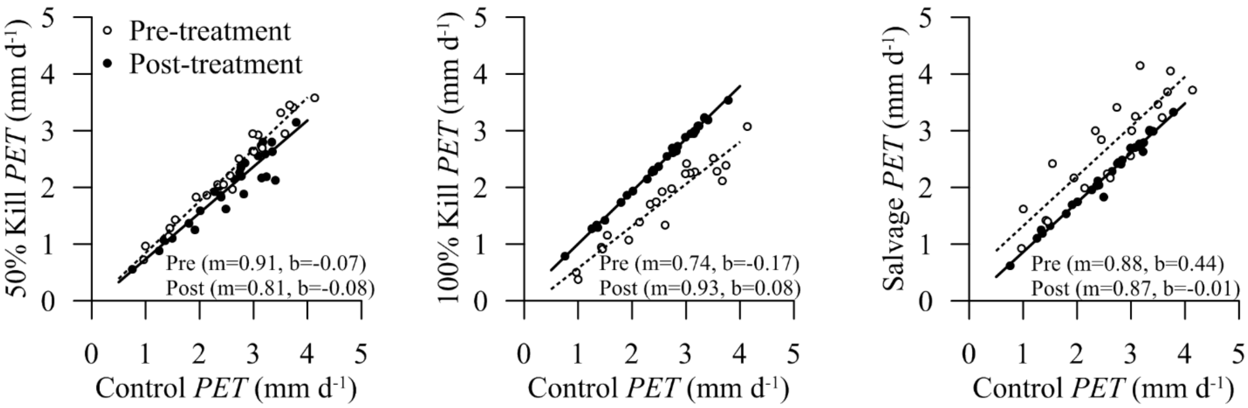

Figure 2.7 Relationship of mean weekly potential evapotranspiration (*PET*) during the growing season (1 May to 30 Sep) within the 50% Kill, 100% Kill and Salvage stands compared to the Control stand, pre- and post-treatment. Shown with slope (m) and intercept (b).

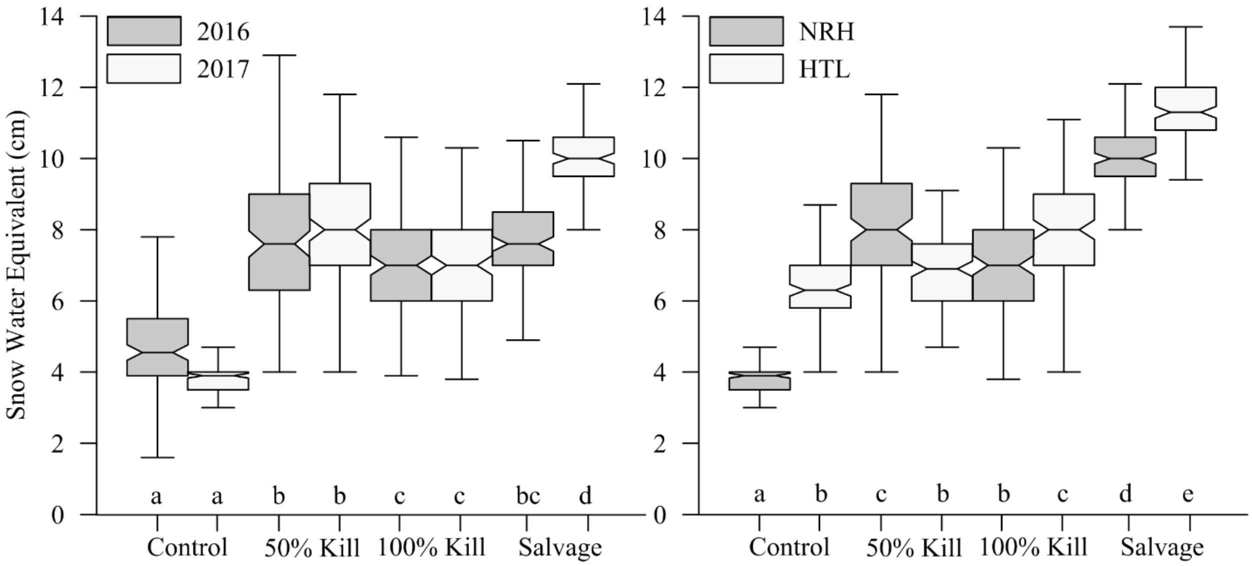

Figure 2.8 Notched box plots of 1 March snow water equivalent collected in each stand in: A) the NRH block during 2016/2017; and B) the NRH and HTL blocks during 2017. For each sample population (n = 36), the notch marks the median, the box ends mark the 25th and 75th percentile, and the bars show non-outlier maximum and minimum values. Means with the same letter are not significantly different.

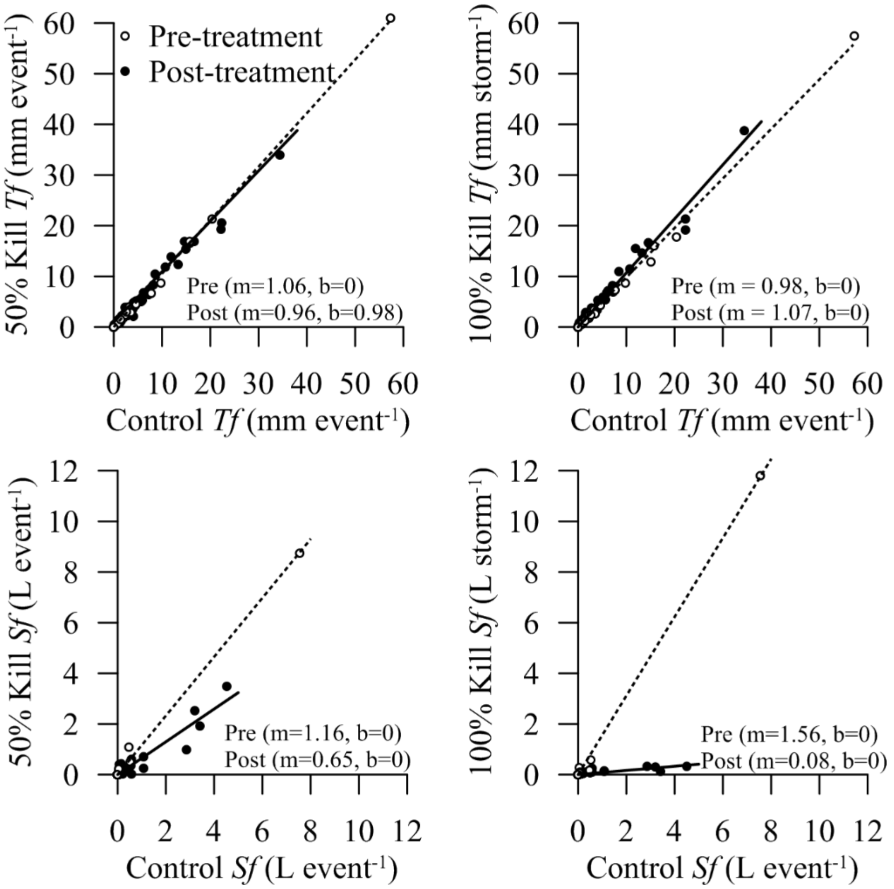

Figure 2.9 Relationship of throughfall (*Tf*) and stemflow (*Sf*) for individual rainstorms over the growing season (1 May – 30 Sep) within the 50% Kill and 100% Kill stands compared to the Control stands, pre- and post-treatment. Shown with slope (m) and intercept (b).

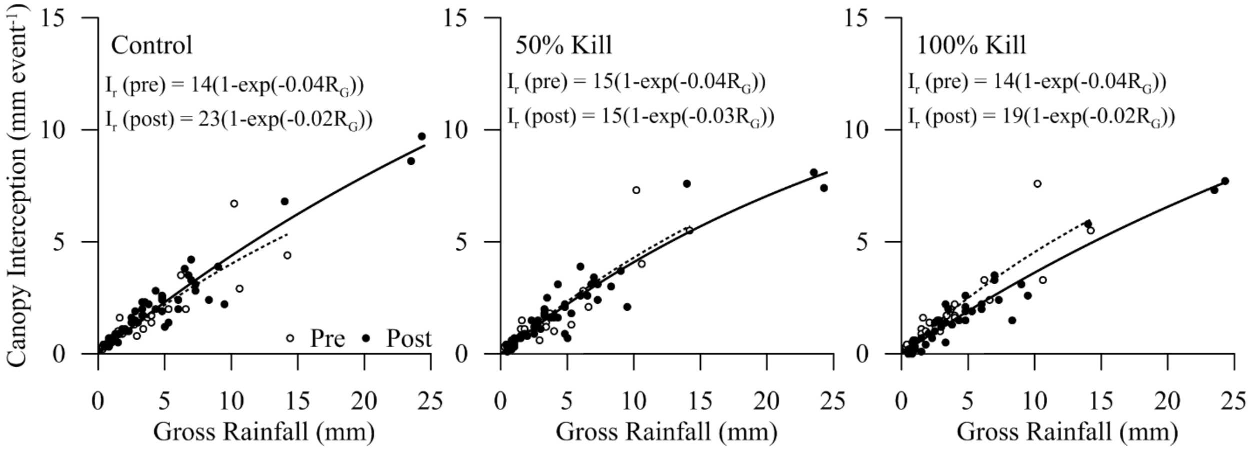

Figure 2.10 Relationships between gross rainfall (R_G) and canopy interception (I_r) in the Control, 50% Kill and 100% Kill stands, pre-treatment (2008 – 2009, dashed line) and post-treatment (2014 – 2017; solid line).

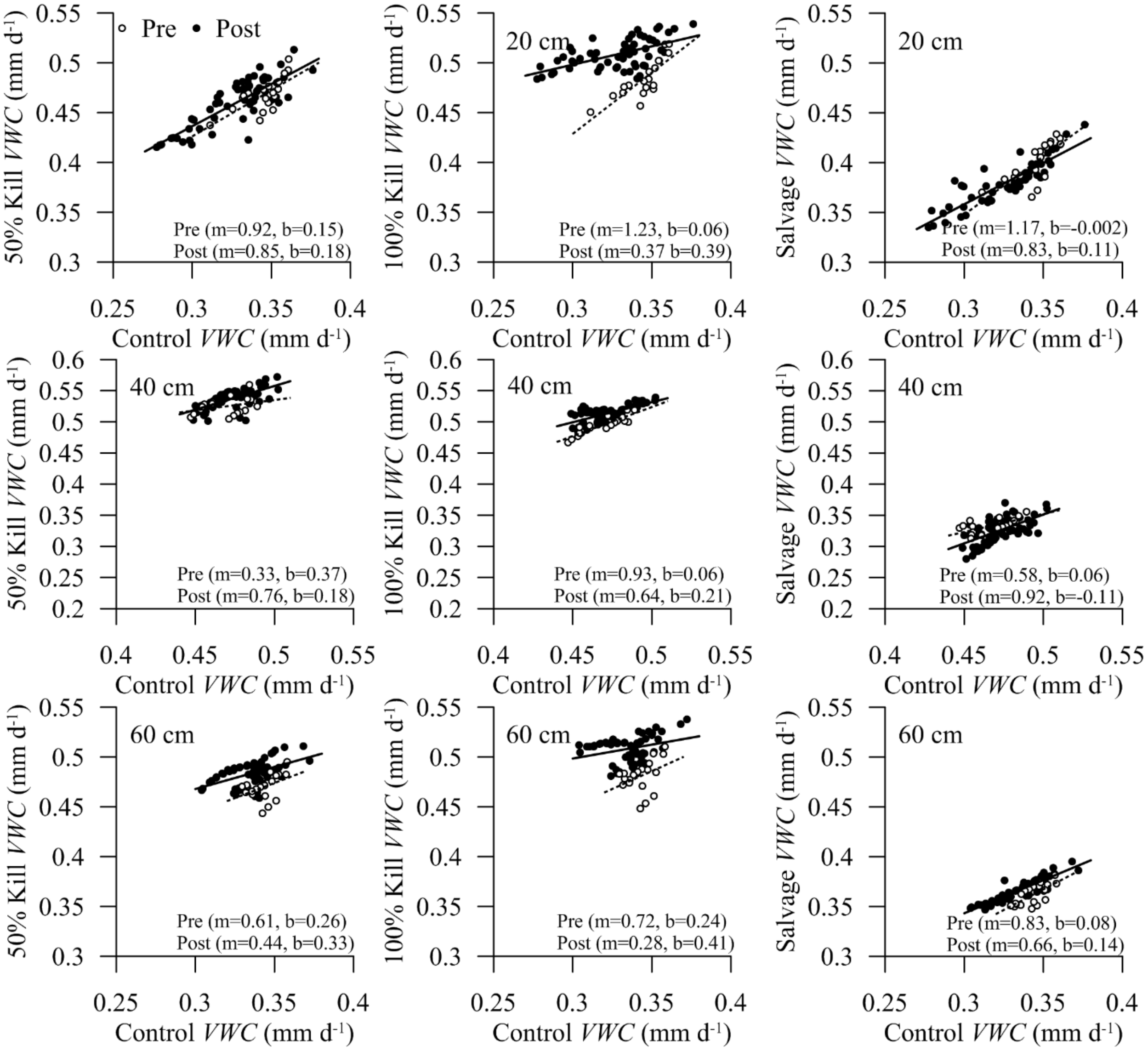

Figure 2.11 Relationship of mean weekly growing season (1 May – 30 Sep) volumetric soil water content (*VWC*) at 20, 40, and 60 cm below the mineral surface within the 50% Kill, 100% Kill, and Salvage stands compared to the Control stand, pre- and post-treatment.

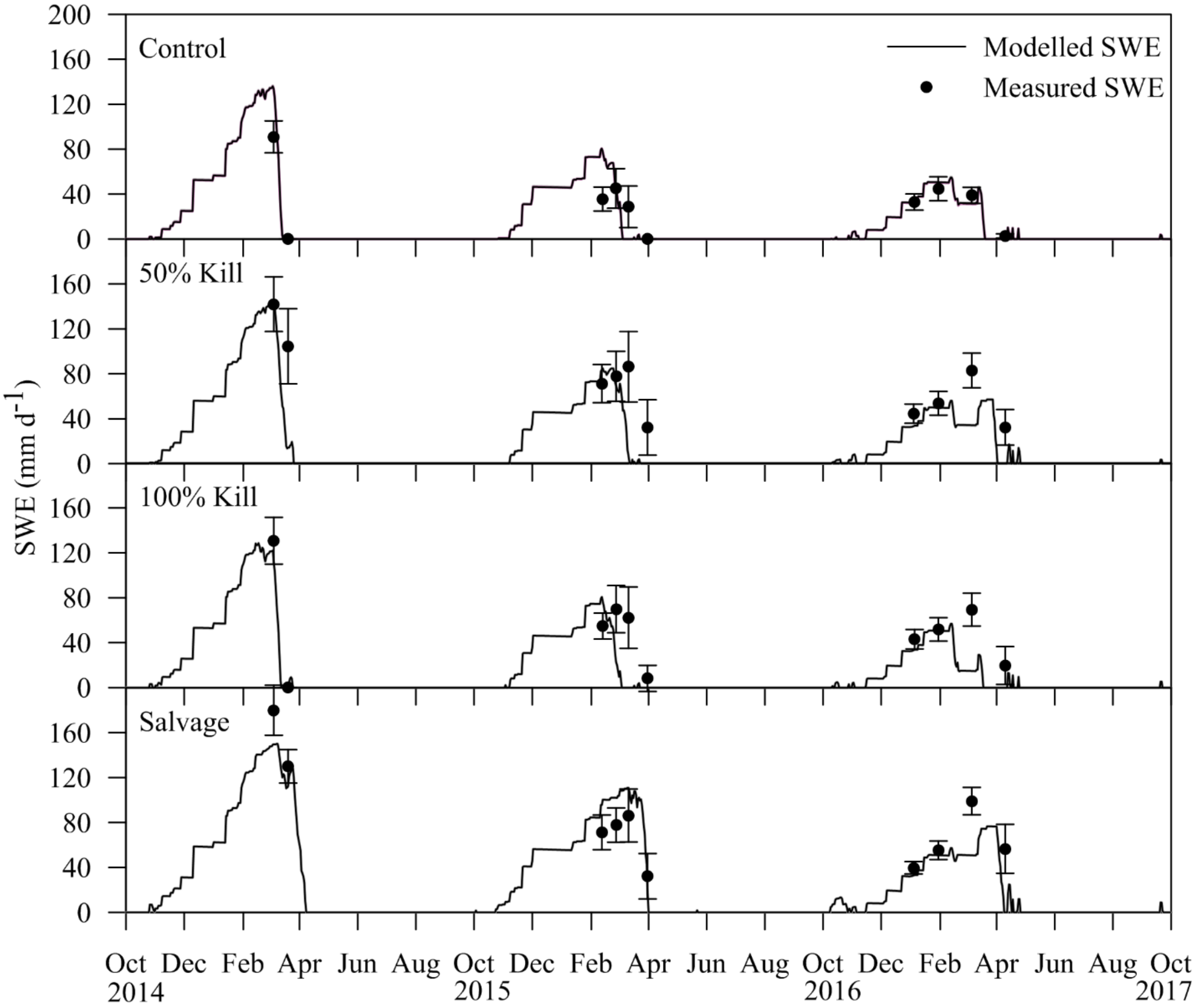

Figure 2.12 Predictions of SWE compared to observed snow survey data for each model combination in the treatment stands for the study period (1 Oct 2014 to 30 Sep 2017). The 95th percentile parameter uncertainty bounds (grey bands) were very similar to the modelled SWE because the Cold Regions Hydrological Model energy-based potential snowmelt algorithm used in the stand water balances was parameter-free (Pomeroy *et al.*, 2007). Therefore, the grey bands are not visible.

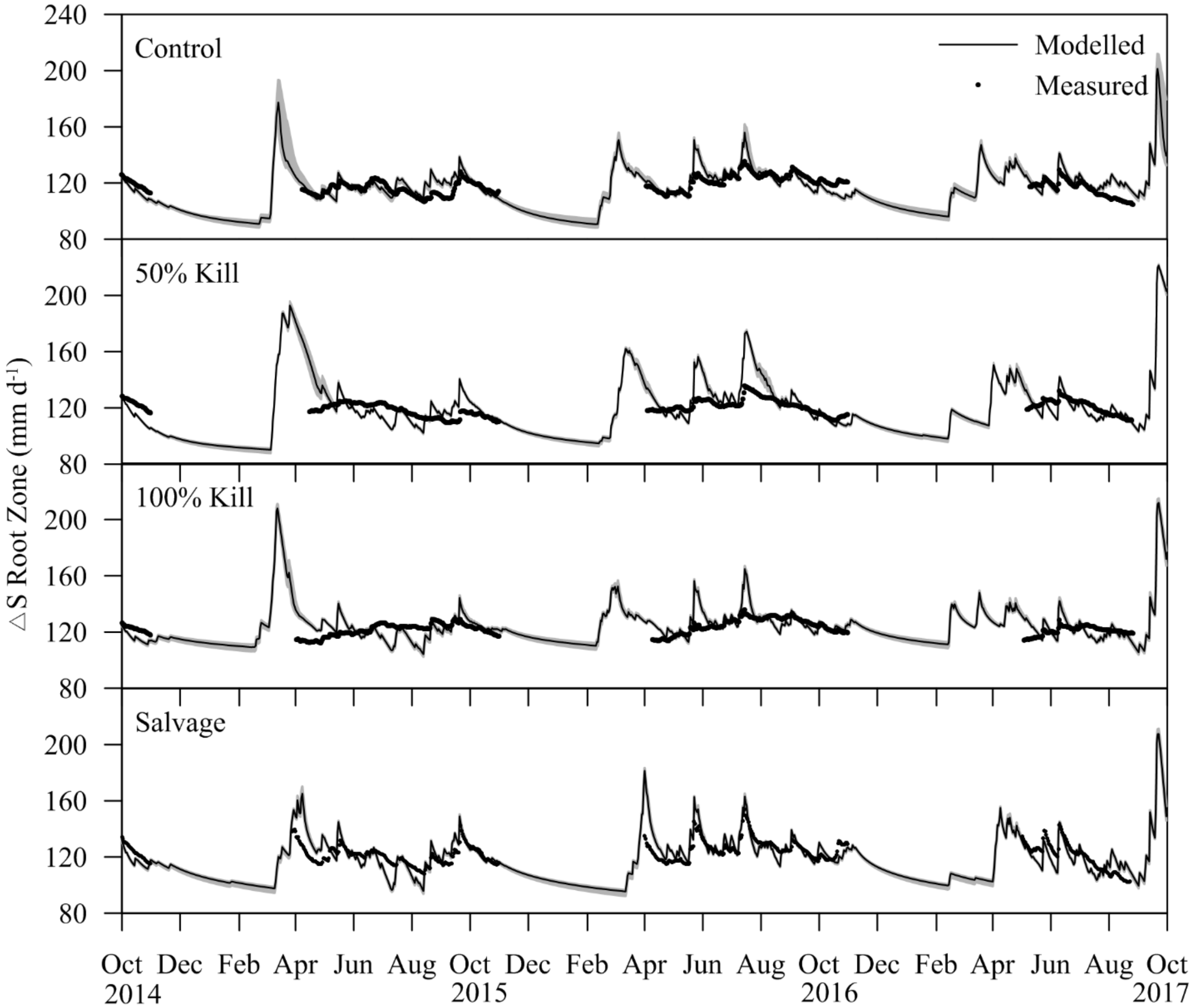

Figure 2.13 Predictions of change in storage in the root zone compared to observed soil water content in the stands for the study period (1 Oct 2014 to 30 Sep 2017). Grey bands indicate the 95th percentile parameter uncertainty bounds for modelled soil moisture. Measured soil water content when soil temperature was below 0ºC was excluded due to inaccuracy associated with the presence of frozen soil water.

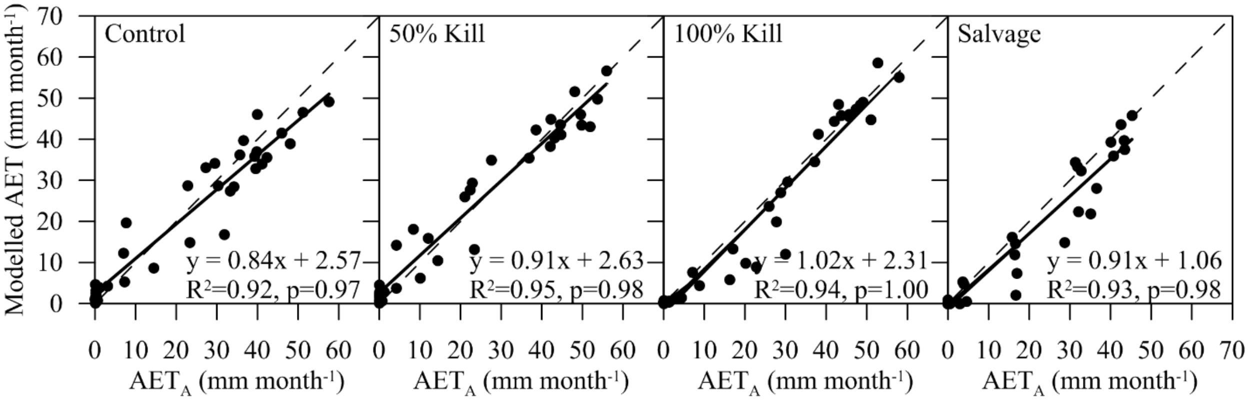

Figure 2.14 Predictions of monthly actual evapotranspiration using Penman Monteith algorithm compared to AET_A estimated using an analytical method with measured data for each stand over the study period (1 Oct 2014 to 30 Sep 2017). Dashed line indicates 1:1 line. The reported p-values are a result from t-tests performed at the 5% significance level.

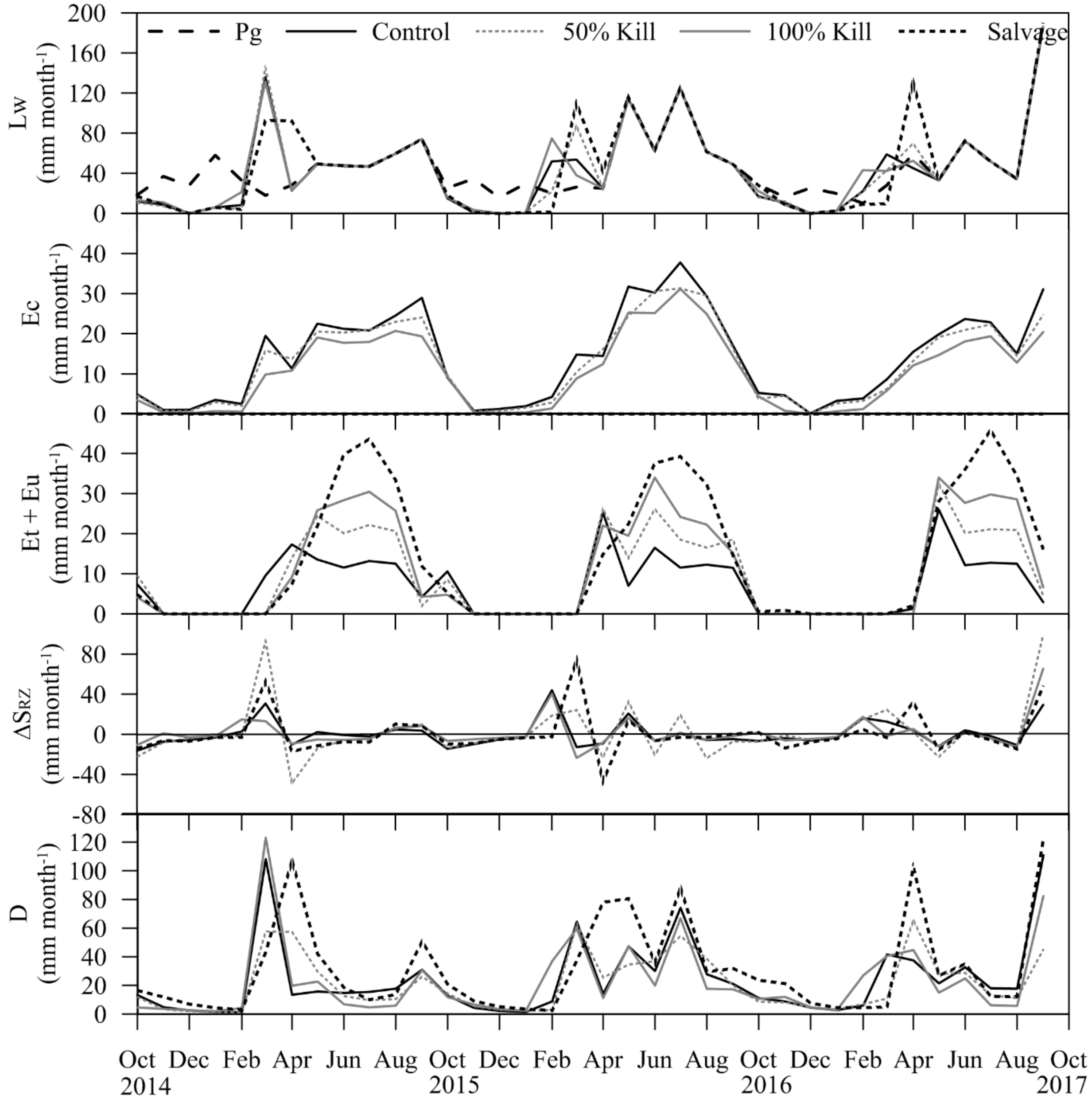

Figure 2.15 Mean monthly water balance components from 1 Oct 2014 to 30 Sep 2017: measured gross precipitation (P_g); liquid water (L_w), measured as rain plus modelled snowmelt and equals P_g on a water year basis; modelled evaporation of canopy intercepted rain and snow (E_c); modelled overstory transpiration and understory evapotranspiration ($E_t + E_u$); modelled change in soil water storage in the Root Zone (0.4 m thick; ΔS_{RZ}); and modelled Root Zone drainage (D, percolation below -0.4 m depth; see Figure 2.2).

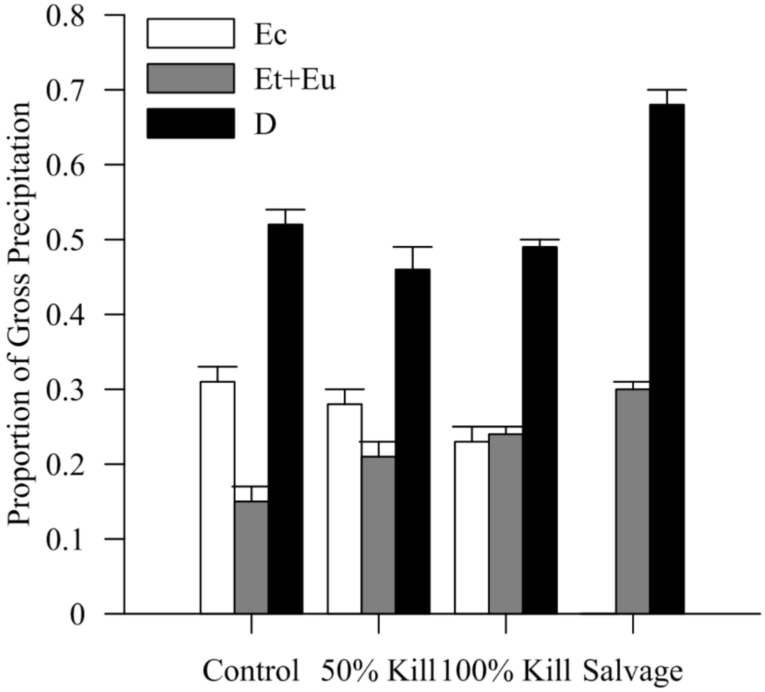

Figure 2.16 Three-year mean annual water balance components for the four stands. Bars represent the standard error of the mean. Water balance components are represented as a percentage of mean annual gross precipitation (552 mm). Total percentages do not sum to 100% due to changes in storage of water in the Root Zone ($\Delta S_{RZ,}$ 0.4 m thick; not presented in plot). E_c, evaporation of canopy intercepted rain and snow; E_t, overstory tree transpiration; E_u, understory evapotranspiration; and D, Root Zone drainage (percolation below -0.4 m depth; Figure 2.2).

CHAPTER 3 – FOREST HARVEST EFFECTS ON STREAMFLOW IN ALBERTA FOOTHILLS WATERSHEDS

3.1 Introduction

Forest harvest in snowmelt-dominated watersheds with conifer forests can lead to decreased canopy interception and transpiration, increased precipitation reaching the ground surface, increased energy for snow ablation, and increased soil moisture input and groundwater recharge (Winkler *et al.*, 2010). The loss of forest cover would presumably result in more net precipitation that enters the soil and the transfer of these water inputs to the stream is governed by the amount of storage and partitioning of flow paths within the subsurface, and in turn, influence the runoff generated for streamflow (Redding and Devito 2008; 2010; Smith *et al.*, 2014). A paired watershed experiment on the eastern slopes of the Alberta Rocky Mountains showed streamflow was not sensitive to forest harvest (Harder *et al.*, 2015). These watersheds had low levels of harvest relative to their size and a large area of sparsely vegetated alpine talus slopes and exposed bedrock; an area shown to generate the majority of runoff for streamflow (Fang *et al.*, 2016). In contrast, the moderately steep slopes and rolling hills of the foothills adjacent to the eastern slopes of the Rocky Mountains typically have merchantable timber throughout due to their lower elevation. Conceptual models for forest harvest effects on streamflow in fully-forested watersheds would suggest Foothills watersheds may be more sensitive to forest harvest and have increased potential for changes in streamflow (Bosch and Hewlett, 1982; Green and Alila, 2012).

Similar to the eastern slopes of the Alberta Rocky Mountains, the Foothills are in a region of complex geology made up of a history of glacial deposition underlain by folded and faulted sedimentary bedrock. The geologic setting suggests there is potential for large subsurface water storage (Spencer *et al.*, 2019) and is unique relative to other paired watershed experiments from the Pacific Northwest (e.g. Cheng, 1989; King and Tennyson, 1984; Troendle and King, 1985 and 1987). Characteristics of the complex glacial deposits, the sedimentary bedrock structure and permeability, and the effects on subsurface processes that dominate streamflow generation could attenuate the streamflow response to forest harvest in watersheds located in this geological setting (Jensco *et al.*, 2011; Harder *et al.*, 2015; Fang *et al.*, 2016; Spencer *et al.*, 2019).

Climate variability associated with the large-scale ocean-atmosphere circulation phases of the Pacific Decadal Oscillation (PDO) and El Niño Southern Oscillation Index (ENSO) may modify streamflow trends due to meteorological changes and potentially interact with forest harvest experiments (Moore and Scott, 2005; Wei and Zhang, 2010; Burt *et al.*, 2015; Harder *et al.*, 2015). For example, at H.J. Andrews Experimental Forest in Oregon, the climate variability related to ENSO was found to be the dominant driver of the streamflow response that followed forest harvest treatments (Burt *et al.*, 2015). Interestingly, the timing of treatment application in several historical paired watershed experiments in the Pacific Northwest have coincided closely with a PDO phase shift in 1977 from cool to warm (Golding, 1980; King and Tennyson, 1984; Troendle and King, 1987; Andres *et al.*, 1987; Cheng, 1989; King, 1989), which was not well known or realized until the mid-1990s (Mantua *et al.*, 1997). Positive PDO (warm phase) values have been associated with increased air temperatures, decreased precipitation, decreased snow accumulation, and decreased streamflow (Whitfield *et al.*, 2010; Newton *et al.*, 2014; Shrestha *et al.*, 2016). The streamflow response in treatment watersheds may not simply be the result of forest harvest experiments, because the paired watershed design does not control for the integrated hydrologic response to climate variability within the control watershed. The non-stationarity in climate within the control watershed has largely been overlooked because the intended purpose of the paired watershed experimental design was to 'control' for climate variability (Burt *et al.*, 2015). Therefore, there is reason to re-examine historical paired watershed studies using alternative methods to evaluate the effect of climate variability and forest harvest on streamflow.

The limitations of paired watershed studies have been previously reviewed (e.g. Alila *et al.*, 2009; Zégre *et al.*, 2010) and alternative statistical and model-based approaches for single watershed analysis have been used to determine the effect of forest harvest on streamflow (Schnorbus and Alila, 2004; Seibert and McDonnell, 2010; Zégre *et al.*, 2010; Wei and Zhang, 2010). There is still debate on the best approach to detect change because the effects of forest harvest are difficult to isolate from background climate variability; however, review papers have suggested that a combination of statistical and hydrological modelling approaches would be better than one method alone (Moore and Wondzell, 2005; Wei *et al.*, 2013). A hydrological modelling approach becomes important in larger watersheds (>10 km^2) where paired watershed studies are limited due to variation in precipitation inputs and watershed conditions between adjacent watersheds (soil and geology conditions, topography: Seibert and McDonnell, 2010; Zégre *et al.*, 2010). However, for both statistical and hydrological modelling approaches, a calibration period should be long enough to capture the range of climate variability, especially when the streamflow regime is influenced by meteorological changes associated with PDO and ENSO in forested watersheds.

Here we examine the streamflow response to forest harvest using a combination of statistical and hydrological modelling methods to attempt to isolate the effect of forest harvest from climate variability in a region with complex glacial deposits and extremely folded and faulted sedimentary bedrock strata. Increased proportions of permeable or fractured sedimentary bedrock found along the eastern slopes of the Rocky Mountains adjacent to the Foothills region have been suggested to attenuate precipitation inputs for streamflow generation (Jensco *et al.*, 2011; Harder *et al.*, 2015; Spencer *et al.*, 2019). I used data from a historical long-term paired watershed experiment in the west-central Alberta Foothills that included a control and two treated watersheds with different calibration periods and harvest sequences (Andres *et al.*, 1987). I hypothesized that meso-scale, non-alpine watersheds would have increased potential of changes in streamflow due to forest harvest. Alternatively, I hypothesized that climate variability in relation to large variations in subsurface storage and connectivity with heterogeneity in geology masks the streamflow response to forest harvest. The specific objectives of this chapter were to: 1) determine if there was a significant relationship between PDO, ENSO and hydrometeorological data; and, 2) evaluate the streamflow response to forest harvest and climate variability using modified double mass curves and change-detection hydrological modelling on single watersheds. Understanding the streamflow response to forest harvest will provide insight into the dominant controls on runoff generation and provide information to refine forest disturbance thresholds that guide management plans in meso-scale Foothills watersheds.

3.2 Methods

3.2.1 Study Site

The Tri-Creeks Experimental Watershed (Tri-Creeks) is located 40 km southeast of Hinton, Alberta (53.157°N, 117.262°W) in the Upper Foothills natural subregion of Alberta, which is adjacent to the Lower Foothills and mixed-wood Boreal subregion (east) and sub-alpine Rocky Mountain subregion (west; Natural Regions Committee, 2006; Figure 3.1). Tri-Creeks consists of three sub-watersheds: Wampus, Deerlick and Eunice Creeks (Table 3.1). Tri-Creeks is almost entirely forested with limited bedrock outcropping and small areas of grass and shrub adjacent to stream channels. Major tree species include lodgepole pine (*Pinus contorta* var. *latifolia Dougl.*), alpine fir (*Abies lasiocarpa* (Hook.) *Nutt.*), black spruce (*Pinus mariana*), and white spruce (*Picea* *glauca*). Lodgepole pine is predominant in the headwaters, while black spruce occurs in the valley bottoms, and mature stands consist of white spruce-fir associations that vary with aspect and elevation throughout Tri-Creeks (Winkler and Rothwell, 1983).

Topography of the area is gentle to moderate, with slopes of 1 – 40% and elevations range 1249 – 1690 m.a.s.l. This region consists of folded and fractured sedimentary bedrock that primarily alternates between sandstone, siltstone and shale bedrock (Currie, 1969; Figure 3.2). The bedrock is overlain at depths of 3 – 21 m with glaciolacustrine deposits at elevations less than 1380 m.a.s.l. and local sandy loam till deposits between elevations of 1380 – 1440 m.a.s.l. (Currie, 1969). At elevations above 1440 m.a.s.l., bedrock is overlain with glacial till deposits at depths of 1.5 m from surface or exposed. Soils are predominantly brunisols and luvisols, with some gleysols and organics (Dumanski *et al.*, 1972). An intensive soil sampling campaign in Tri-Creeks found soils were fine-textured with average soil porosity and bulk density of 33% and 1.28 g/cm^3 with a soil water storage capacity between 60 and 103 mm (Winkler and Rothwell, 1983). Mean steady soil infiltration rates for lodgepole pine stands are 200 mm/hr (range 47 – 444 mm/hr) and 12 mm/h (range 2.2 – 21 mm/h) for spruce-fir stands (Singh, 1983).

The climate is characterized as continental sub-humid, with long cold winters modified by short periods of chinook winds, and short cool summers with mean monthly temperatures ranging from 11°C in July to -13°C in January (Hillman *et al.*, 1978). The warm, dry chinook winds are generated as Pacific air masses ascend the leeward side of the Rocky Mountains and can increase the air temperature 20ºC or more within hours and drop again as rapidly (Jablonski, 1978). Mean annual precipitation is 615 mm with 39% falling as snow. The largest amount of precipitation falls in July and is highly variable from 36 to 177 mm month^{-1} (1967 – 1988).

Water year (WY, 1 October – 30 September) runoff can range from 117 to 441 mm in Eunice Creek (Table 3.1), and largely consists of baseflow (determined by digital filter hydrograph separation discussed in Table 3.1). Ice-free stream sections are observed throughout winter. Snowmelt does not typically generate the maximum annual peak flows, which rather occur in the summer with large variability in their magnitude and timing due to the stochastic nature of large rainfall events.

Historical samples of water isotopes, water chemistry and radioactive tritium isotopes collected in Tri-Creeks (1984 – 1986) indicate a groundwater flow system with active local and intermediate flow paths and short residence times (i.e. duration of time groundwater remains in subsurface) within the glacial till and sedimentary bedrock units (Andres *et al.*, 1987).

3.2.2 Data Sources and Processing

The Tri-Creeks forestry experiment included detailed meteorological observations of air temperature, relative humidity, precipitation, and snow accumulation (Sterling *et al.*, 2016). Air temperature (°C) and relative humidity (%) were measured by hygrothermographs located in Stevenson screens with a maximum and minimum thermometer for more accurate daily temperature readings at Wampus-A, Wampus-C, and Eunice-B (Figure 3.1). Total daily precipitation was measured and recorded using a Q12M Sacramento automatic weighing gauge at Wampus-C (mm d^{-1}). Seasonal precipitation was also recorded in Sacramento gauges for accumulated rainfall (May – Oct) and snowfall (Oct – May). Precipitation data were not corrected for gauge under-catch because wind speed data were not available; however, precipitation gauges were equipped with Alter shields. Snow courses consisted of ten points, 30 m long, at various elevations (1280 – 1580 m) and with varying tree cover to quantify snow water equivalent (mm SWE) across the watershed. Peak SWE values were measured near March 1, which were typically close to the peak accumulation for each winter season.

Daily climate data (maximum and minimum temperatures, and precipitation) were available from the Tri-Creeks forestry experiment from June 1967 to Dec 1985 at Wampus-C (Figure 3.1). Long-term climate data from nearby Environment Canada meteorological stations were used to gap-fill missing data and supplement climate data after monitoring in Tri-Creeks was decommissioned. For the study period June 1, 1967 to September 30, 1988, air temperature was gap-filled with monthly linear regressions (79% data completeness) using data available at Wampus-A ($r^2 = 0.95$; Figure 3.1) and a nearby meteorological station at Hinton ($r^2 = 0.90$; Climate ID 3063340, 1,014 m.a.s.l., 40 km northwest). Daily precipitation was gap-filled (64% data completeness) using the relative (percentage) difference in monthly precipitation between Wampus-C and nearby precipitation gauges at Hinton and Robb (Climate ID 3065505, 1,130 m.a.s.l., 25 km east).

Streamflow measurements occurred at the sub-watershed outlets from April – November and were gauged at rectangular weirs by the Water Survey of Canada (IDs 07AF003, 07AF004, 07AF005). Streamflow monitoring began in September 1966 at all three stations. The gauging station at Wampus Creek is still in operation, while Eunice and Deerlick Creeks were decommissioned in 1992 and 1990, respectively. Seasonal station operation required winter flow to be gap-filled using a baseflow recession constant to estimate the recession limb of the annual hydrograph for every year in the flow record by treating the watershed as a linear reservoir (Vogel and Kroll, 1996):

$$Q_t = Q_o(K_b)^t e^{\varepsilon t} \tag{3.1}$$

where Q_t is baseflow after t days, Q_o is equal to the initial baseflow value, K_b is the baseflow recession constant, and $e^{\varepsilon t}$ are independent normally distributed errors with constant variance and mean of zero.

3.2.3 Forestry Experiment

Prior to the Tri-Creeks forestry experiment, there was select and clear-cut logging conducted in the watersheds (Table 3.1). The small percentage of forest disturbance was assumed to not impact the forestry experiment (Andres *et al.*, 1987). The Alberta Forest Service harvesting ground rules (1973) were applied to the harvesting operations. After a 10-year calibration period, 52% of Wampus Creek was clear-cut logged over a six-year period (1978 – 1983). Treed buffer strips were left along the cutblock streamside of Wampus Creek. Deerlick Creek was clear-cut logged with streamside timber removal through 64% of the watershed over a three-year period (1981 – 1983). Cutblock size ranged from 13 – 200 ha in Wampus Creek and 20 – 114 ha in Deerlick Creek (Nip, 1991). Harvesting was done in the winter to minimize soil disturbance. Silvicultural treatments for reforestation of the cutblocks included drag, ripper or Bracke scarification, which was completed within one year of harvest (Nip, 1991).

The period of study included 1967 to 1988. The study period includes the 1976/77 PDO regime shift and excludes the 1988/89 PDO regime shift (Yasunaka *et al.*, 2003). Hydrologic recovery of clear-cut stands was assumed to be minimal given the slow growth of conifer trees (Winkler *et al.* 2005), and similar post-harvest time periods have been used for analysis in other forest harvest studies (see review by Moore and Wondzell, 2005).

3.2.4 Hydrometeorological Analyses

Previous studies that linked interannual and interdecadal climate variability to hydrometeorology in Alberta (Harder *et al.*, 2015, St. Jacques *et al.*, 2010) motivated an analysis of the relationship between PDO, ENSO, and hydrometeorological data series over the study period in Tri-Creeks. Data series included: mean annual, winter (November – March) and growing season (May – September) air temperature; total annual, winter, growing season precipitation; ratio of rain to total water year precipitation; peak SWE; and, total annual streamflow. PDO data were collected from Mantua (2016) and Southern Oscillation Index (SOI) data from the Australian Bureau of Meteorology (2016). The mean annual index for ENSO was used in the analysis, while mean winter averages (November to March) of PDO were related to the variable of interest in the subsequent year. Generalized least square (GLS) statistical models were developed using the *nlme* package (Pinheiro *et al.*, 2017) in the R statistical software (v3.6.1). GLS was used to fit statistical models, because autocorrelated residuals may occur and GLS regression can incorporate a correlation structure such as an auto-regressive moving average process (ARMA). The Akaike Information Criterion (AIC) statistic compared models and identified best fit. A likelihood-ratio test compared models with and without the forcing term to determine the statistical significance of trend (Harder *et al.*, 2015). A pseudo-r^2 was calculated for GLS regression models using the *nagelkerke* function in the *rcompanion* package (Mangiafico, 2017).

Plots of differences in mean daily runoff between the control and treated watersheds were constructed to visualize shifts in timing and magnitude before and after harvest and the PDO climate shift. Differences in mean daily runoff between the control watershed and Deerlick Creek were compared for three different time periods: pre-harvest (PDO cool phase), pre-harvest (PDO warm phase); and, post-harvest (PDO warm phase). The shorter calibration period of Wampus Creek only allowed the comparison of pre-harvest (PDO cool phase) and post-harvest (PDO warm phase) periods.

3.2.5 Modified Double Mass Curves

The modified double mass curve (MDMC) method developed by Wei and Zhang (2010) was used to isolate forest harvest effects on streamflow from background climate variability. The single watershed analysis fits a linear regression model to pre-harvest data to predict the expected streamflow response in the post-harvest period if there was no forest harvest. The MDMC plots accumulated annual runoff versus accumulated annual effective precipitation (annual precipitation minus actual evapotranspiration). All values were calculated based on a water year.

Actual evapotranspiration (ET) was estimated from the hydrological model simulations (see section 3.2.6.2; Hargreaves and Samani, 1985). Actual ET includes the total losses to the atmosphere (i.e. canopy interception loss, evapotranspiration, soil evaporation). The hydrological models for the treatment watersheds dynamically accounted for forest cover change using the land use change command in the Raven Hydrological Modelling Framework (Craig *et al.*, 2019).

Forested hydrologic response units (HRUs) that were historically harvested were changed to cutblock HRUs. Parameters for cutblock HRUs represented grassland vegetation and reflect changes in the snowmelt and infiltration rates associated with increased solar radiation and decreased canopy interception. Cutblock HRUs were cumulatively added annually to the model simulations over the harvest period.

Breaks in the MDMC were qualitatively assessed to evaluate the effect of climate variability and forest harvest. Regression calibration periods differed for Eunice (1969-1976), Wampus (1969-1977), and Deerlick (1969 – 1976). An additional linear regression model was fit to the entire pre-harvest period in Deerlick Creek (14 years), which included years during both the warm and cool PDO phases (1969 – 1981). The MDMC method assumes the change in soil water storage is a small part of the annual water balance (5-10%) and constant through time, the estimates of regression parameters were stable between effective precipitation and runoff, and all climate variability is lumped into precipitation and evapotranspiration (Wei and Zhang, 2010).

3.2.6 Change-Detection Hydrological Modelling

3.2.6.1 Overview

Conceptual rainfall-runoff models have been used to detect watershed-scale changes in forest hydrology, because the objective was to detect volumetric changes in streamflow (e.g. Zégre *et al.* 2010; Seibert and McDonnell, 2010, Mahat *et al.*, 2015). For this study, a process-based conceptual model rather than a physically-based model was used, because it had lower parameter requirements, and could more efficiently address model sensitivity and uncertainty analyses.

There are two main change-detection methods in the literature to analyze streamflow. The first method uses linear regression models in the pre-harvest period with daily observed streamflow and simulated streamflow ("virtual control") to predict post-harvest changes in streamflow (hereafter "change-detection regression method"; Zégre *et al.*, 2010). This is a similar method to the traditional paired watershed approach, but with a virtual control watershed rather than an adjacent physical control watershed. In contrast, instead of using linear regression models, observed streamflow from different periods is used to calibrate the hydrological model to produce pre-harvest and post-harvest parameter sets (hereafter "change-detection calibration method"; Seibert and McDonnel, 2010; Seibert *et al.*, 2010). Parameter values differed when models were calibrated for different periods when one period had significant forest cover loss from wildfire (Seibert *et al.*, 2010; Seibert and McDonnell, 2010; Mahat *et al.*, 2015). This method assumes that the different parameter sets capture the watershed response for pre- and post-disturbance conditions (Seibert and McDonnell, 2010). However, changes in parameter values between different periods can be difficult to interpret because of parameter interactions in a model. To overcome the problems of parameter interactions, model simulations that use different parameter sets are compared to assess the integrated watershed response to forest harvest. The change-detection calibration method is less sensitive to errors in precipitation or observed peak flow events, which can be problematic when the difference between observed and simulated flow are compared (i.e. model residuals; Seibert *et al.*, 2010).

3.2.6.2 Watershed Hydrological Model

The Raven Hydrological Modelling Framework (v2.9.2, Craig *et al.*, 2019) was used to simulate streamflow in each watershed using a modified version of the HBV-EC model (Bergstrom *et al.*, 1995; Canadian Hydraulics Centre, 2010). Daily air temperature (minimum, maximum and average) and precipitation were spatially distributed across the watershed using inverse-distance weighting. The model was discretized using HRUs that group areas of similar elevation, aspect, slope and landcover. Vertical climate gradients were represented by subdividing the basin into 100 m elevation bands.

Precipitation was partitioned into rain or snow using the HBV-EC algorithm (Bergstrom, 1995) where a linear transition between all snow and rain is determined from the average daily temperature using a rain/snow transition temperature and a rain-snow transition zone (2ºC). Precipitation intercepted by the forest canopy was removed by evaporation and controlled by the leaf area index and vegetation cover in each HRU (Bergstrom, 1995; Hedstrom and Pomeroy, 1998). Snowmelt was simulated using a corrected degree-day approach (Bergstrom, 1995). Rain and snowmelt infiltrated a conceptualized three-layer soil structure based on available water storage. Storm runoff that did not contribute to the topsoil reservoir (stored water that could eventually evaporate), either contributed to streamflow as rapid flow to the stream channel (fast reservoir) or through groundwater recharge (slow reservoir). Groundwater recharge was a function of soil moisture, while soil evaporation and transpiration were a function of soil moisture and potential *ET*. Slight variations to the HBV-EC model included algorithms for forest canopy snow interception (Hedstrom and Pomeroy, 1998), calculation of daily potential evapotranspiration (Hargreaves and Samani, 1985), and the Variable Infiltration Capacity routine for non-linear baseflow response in the slow reservoir (Clark *et al.*, 2008).

3.2.6.3 Model Calibration, Verification, Uncertainty

Model calibration and verification followed a similar hydrological modelling workflow to Chernos *et al.* (2017). For all models, at least two years were used as the 'warm up' period. The model was calibrated automatically with Ostrich (v17.12.19; Matott, 2019) for each watershed using dynamically dimensioned search (DDS) optimization (Tolson and Shoemaker, 2007). Weight was given to streamflow observations during the ice-free period. Insensitive parameters during the calibration period may be sensitive in the prediction period (either as individual parameters or as a subset of parameters); therefore, all parameters considered uncertain were calibrated and their uncertainty quantified in the prediction uncertainty analyses (Tolson and Shoemaker, 2007). Snow surveys, accumulated seasonal precipitation in Sacramento gauges, and an additional meteorological station (Eunice 'B') were used to check model performance.

The DDS – approximation of uncertainty (DDS-AU) algorithm quantified the prediction uncertainty by identifying behavioral parameter sets through repeatedly applying a DDS search from alternative random starting points in the parameter space (Tolson and Shoemaker, 2008). There were 60,000 model evaluations (150 optimization trials and 400 function evaluations per optimization trial). The number of model evaluations was selected based on the optimal parameter set known to achieve the maximum Nash Sutcliffe model efficiency value (NSE; Tolson and Shoemaker, 2008). The parameter sets from the 100 highest NSE optimization trials were selected to characterize the prediction bounds (e.g. Zégre *et al.*, 2010; Seibert *et al.*, 2010). Selected parameter sets were then used to reconstruct streamflow. Simulated streamflow from the upper 97.5th and lower 2.5th percentiles per day indicate the 95% uncertainty bounds for a daily streamflow model (Zégre *et al.*, 2010).

3.2.6.4 Change-Detection Regression Method

Similar to the methods outlined in Zégre *et al.* (2010), pre-harvest linear regression models for each watershed were constructed with daily observed streamflow and simulated streamflow ("virtual control") from April 1969 to October 1975 with:

$$y_d = \beta_0 + \beta_1 x_{1,d} + \varepsilon \tag{3.2}$$

where y_d is the observed daily streamflow and $x_{1,d}$ is the lower (2.5th), median and upper (97.5th) daily streamflow simulations generated from the DDS-AU uncertainty percentiles. A log_{10}-transformation of daily streamflow was applied to stabilize the variance (Som *et al*, 2012). Mean monthly streamflow was subtracted from each observation to achieve stationarity in model residuals (Som *et al*, 2012). Sinusoidal trigonometric coefficients were included to account for seasonality (Watson *et al.*, 2001; Gomi *et al.*, 2006); however, only terms that were statistically significant were retained. Generalized GLS regression was used to account for residual autocorrelation. The error term, ε, was modelled as an autoregressive process of order *k*. The order k was determined by examining partial autocorrelation functions and plots of the preharvest residuals. Comparison of the resulting models with the AIC statistic identified best fit.

The GLS regressions were used to predict streamflow during the post-harvest period without harvesting effects ($\hat{y_t}$). To determine statistical evidence of treatment effects, autocorrelation from the model residuals was removed using the AR time series model to provide an estimate of post-harvest innovations, $\widehat{u_t}$ (Watson *et al.*, 2001; Gomi *et al.*, 2006; Zégre *et al.*, 2010):

$$\widehat{u_t} = (y_t - \hat{y_t}) - \widehat{\Phi_t}(y_{t-1} - \widehat{y_{t-1}}) \ldots.. \tag{3.3}$$

where y_t is the observed daily streamflow during the post-harvest period, $\widehat{\Phi_t}$ is an estimate of the lag k autocorrelation coefficient from the GLS regression fit. Innovations are independent and approximately normally distributed. The 95% prediction intervals (*PI*) at time *j* are calculated by:

$$PI_j = 0 \pm 1.96\sqrt{var(\hat{u}_j)} \tag{3.4}$$

where $var(\widehat{u_j})$ is the prediction variance (Zégre *et al.*, 2010; Som *et al.*, 2012). Post-harvest innovations were compared to the 95% prediction intervals (based on the pre-harvest period) to determine if a significant number of innovations fall outside the prediction limits. Greater than 5% innovations that fall outside the prediction intervals in the post-harvest period would indicate a significant change in streamflow following harvest (Zégre *et al.*, 2010).

A hydrological model of the control watershed was constructed to evaluate if the change-detection method was robust to detect the absence of forest harvest. The ‘treatment’ period was initiated during November 1976, which corresponds to the timing of the PDO climate shift. In addition, the long calibration period of Deerlick Creek (“Deerlick Creek-14Yr”) provided an opportunity to detect the absence of forest harvest in the warm PDO phase (November 1976 – October 1981).

The change-detection hydrological regression method assumes: model parameters represent the integration of hydrological processes across space and time for watersheds;

hydrological model and linear regression parameters were consistent throughout pre- and post-harvest periods; similar structure for autocorrelation variance of model residuals for pre and post-harvest periods; and, prediction of future hydrologic response lies within the range of values observed in pre-harvest (Zégre *et al.*, 2010).

3.2.6.5 Change-Detection Calibration Method

Similar to the method in Seibert *et al.* (2010), Tri-Creeks streamflow was reconstructed using model parameter sets calibrated for the pre-harvest condition (hereafter "pre-parameters") and post-harvest condition (hereafter "post-parameters"). To deal with parameter uncertainty, a distribution of parameter sets from the 100 highest NSE optimization trials using the DDS-AU approach were produced. Pre-parameters sets produced for the change-detection calibration method (see section 3.2.6.4) were used in this analysis, while post-harvest hydrological models were calibrated for Wampus Creek (April 1983 – October 1988) and Deerlick Creek (April 1984 – October 1988). This produced post-parameters that reflected the forest cover change in the treated watersheds, which also coincided with the warm PDO phase. Eunice Creek was also calibrated from April 1983 to October 1988. The control watershed was included in the analysis to evaluate whether model parameters were consistent between the warm and cool PDO phases and as a test to detect false change, because Eunice Creek had no harvest activity.

To detect changes in streamflow, model simulations of daily runoff were reconstructed using the pre-parameter (Q_{pre}) and post-parameter (Q_{post}) sets. A series of peak runoff events was selected for each watershed and classified as either rainfall or snowmelt-generated. Each annual snowmelt peak runoff event and largest annual rainfall peak runoff event were included, as well as additional distinct rainfall-generated peak runoff events. The relative percent difference in simulated peak events (D_{peak}) were calculated with the median runoff values (mm d^{-1}) reconstructed from the 100 pre- and post-parameters sets:

$$D_{peak} = \frac{Q_{post,i} - Q_{pre,i}}{(Q_{post,i} + Q_{pre,i})/2} \cdot 100 \tag{3.5}$$

The relative percent difference in reconstructed daily runoff using the median Q_{pre} and Q_{post} was also quantified to compare the difference in average spring (April, May, June), summer (July, August), fall (September, October), baseflow period (November – March), and water year runoff between the pre- and post-harvest periods. The non-parametric Wilcoxon rank-sum test (two-way) was used to test if there was no change in the values of D_{peak} and seasonal runoff between the different periods.

3.3 Results

3.3.1 Hydrometeorological Analyses

In Tri-Creeks, positive (warm) winter PDO values were significantly associated with warmer winter air temperatures, lower winter precipitation, and less snowpack accumulation (Table 3.2; Figure 3.3). Despite less winter precipitation, there was no significant difference in total annual or monthly precipitation between cool and warm PDO phases over the study period (Wilcoxon, $p>0.05$), but rather a shift in precipitation phase to more larger rainstorms in July and September in the warm PDO phase (Figure 3.3D). There was a significant increasing trend in the ratio of rainfall to annual precipitation, where the percentage of rainfall increased from 56% during the cool PDO phase to 64% in the warm phase. The warm PDO phase also had significantly warmer annual mean air temperatures compared to the cool PDO phase (Wilcoxon, $p = 0.02$).

There was no relationship between PDO and Tri-Creeks streamflow, and no trends were detected in the streamflow records (Table 3.2). There was a significant relationship between ENSO and Deerlick and Eunice Creek streamflow; however, the relationship was weak. The hydrograph of average daily streamflow in Eunice Creek during the warm PDO phase shows an earlier snowmelt, a delayed rising limb period of spring freshet, and increased baseflow compared to the cool PDO phase (Figure 3.4). Given the lack of forest disturbance in Eunice Creek, the shift in the hydrograph can be attributed to the meteorological changes associated with the climate regime shift and the subsequent response of hydrological processes that dominate streamflow generation.

Differences in average daily streamflow in Wampus Creek post-harvest showed earlier snowmelt, lower snowmelt peak flow, and increased baseflow (Figure 3.5). The post-harvest period in Wampus coincided with decreased snowfall and increased September rainfall compared to the pre-harvest period (Figure 3.5).

The differences in average daily streamflow in Deerlick Creek showed earlier snowmelt both in the pre-harvest (warm PDO phase) and the post-harvest period (Figure 3.6), which suggests the earlier snowmelt timing could be an effect of climate variability and not forest harvest. The post-harvest period in Deerlick showed increased baseflow; however, increased streamflow in the fall also coincided with increased precipitation. In addition, the adjacent Deerlick and Eunice watersheds behaved differently in response to the PDO phase change. Comparison of the difference in daily streamflow between Deerlick and Eunice Creeks during the pre-harvest period indicates a different streamflow response to warmer winter air temperatures, lower winter precipitation, and lower snowpack in the warm PDO phase (Figure 3.6).

3.3.2 Modified Double Mass Curves

The watersheds responded differently to the changes in water input timing associated with the PDO phase change. After the climate regime shift, the increase in accumulated annual runoff in the warm PDO phase was larger in Deerlick Creek (prior to forest harvest) than Eunice Creek (Figure 3.7). For both watersheds, the increase in accumulated annual runoff was not associated with changes in actual evapotranspiration (ET). The average annual actual ET in Eunice Creek calculated using Hargreaves and Samani (1985) was not significantly different between the cool PDO phase (358 mm yr^{-1}) and warm PDO phase (371 mm yr^{-1}, Wilcoxon, $p = 0.20$). Similarly, the warm PDO phase showed increased average annual ET in Deerlick Creek (401 mm yr^{-1}) but was not different from the cool PDO phase (374 mm yr^{-1}, $p = 0.053$). The climate regime shift produced a break in slope from the predicted linear relation between annual runoff and annual effective precipitation. Given that the predicted linear regression was produced with no/prior to forest disturbance, it was expected that the observed curve would follow the linear relationship. The break in slope observed in Eunice Creek and Deerlick Creek (in the absence of forest harvest) suggests that the climate variability associated with the PDO regime shift could not be captured in precipitation and evapotranspiration alone, but rather the changes in soil water storage are needed to predict the watershed response in the Tri-Creek watersheds.

The length of the calibration period to predict the watershed response in the post-harvest period influenced the MDMCs. In addition to the climate regime shift, the region experienced more than 100 mm above normal precipitation in 1977, 1978 and 1980. For Deerlick Creek, results indicate that the shorter calibration period, which included a smaller range of climate variation to predict the watershed response (i.e. no warm PDO phase data and missing high precipitation years) showed a break in slope prior to forest harvest. The harvest period for Wampus Creek coincided more closely to the climate regime shift; however, the calibration period did include a high precipitation, warm PDO phase year (1977). Therefore, the MDMCs for both Deerlick Creek (14-year calibration) and Wampus Creek may have controlled for climate variability.

The MDMCs for both Deerlick Creek (14-year calibration) and Wampus Creek showed that accumulated annual runoff changed consistently with variation in effective precipitation during the post-harvest period (Figure 3.7). The post-harvest decrease in actual ET and associated increase in water input should result in increased accumulated annual runoff and a break in slope (Wei and Zhang, 2010). However, a break in slope from the predicted linear relationship between annual runoff and effective precipitation did not occur, despite a decrease in actual ET. Average annual actual ET was significantly different between pre-harvest (349 mm yr^{-1}) and post-harvest (266 mm yr^{-1}) in Wampus Creek ($p = 0.002$), which was also observed between pre-harvest (380 mm yr^{-1}) and post-harvest (285 mm yr^{-1}) in Deerlick Creek ($p = 0.003$). The MDMC results in Deerlick and Wampus Creeks suggest that the runoff response to increased water inputs as a result of forest harvest will likely be a function of the buffering capacity of soil storage and groundwater.

3.3.3 Change-Detection Hydrological Modelling

3.3.3.1 Model Performance

Hydrological model performance measured during the pre-harvest and post-harvest calibration periods indicate good agreement in model efficiency and volumetric error between observed and simulated streamflow (Table 3.3). Simulated SWE showed good agreement with observations, while maximum daily air temperatures and accumulated seasonal precipitation were also well-emulated (Table 3.3). In general, the models under-simulated runoff, particularly the rising limb and peak flow of the snowmelt period as well as June peak flows when antecedent conditions between years are highly variable (Figure 3.8). The observed runoff fell within uncertainty bounds 72% (Eunice), 66% (Wampus) and 67% (Deerlick) of days during the pre-harvest calibration period (Figure 3.8). However, for the post-harvest calibration period the number of days observed runoff fell within the uncertainty bounds was 43% (Eunice), 37% (Wampus) and 33% (Deerlick; Figure 3.9). The discrepancies between observed and simulated runoff could be attributed to several factors. Some of these factors include the representation of physical processes in the model structure, parameterization (e.g. soil and vegetation parameters), and measured input uncertainties (precipitation and air temperature). For example, meteorological data collected in Tri-Creeks were only available until 1985; therefore, uncertainties in the gap-filled precipitation and air temperature input would add to the discrepancies between observed and simulated hydrographs in the post-harvest calibration period. In addition, the lower percentage of observed runoff that fell within the uncertainty bounds was partially influenced by the “observed” baseflow period, which was estimated with a baseflow recession constant. Despite these factors, the hydrological models were able to capture the rainfall-runoff relationship to reconstruct runoff, which is most important in the change-detection hydrological modelling approach.

3.3.3.2 Change-Detection Regression Method

Hydrological models of Deerlick Creek and Eunice Creek were used to evaluate if the change-detection method was robust to detect the absence of forest harvest in the warm PDO phase. Less than 5% of the warm PDO phase innovations at both Deerlick and Eunice Creeks fell within the calculated predictions intervals (Table 3.4; Figure 3.10). This result would suggest the regression models adequately described the natural variability between simulated and observed streamflow after the climate regime shift (Zégre *et al.*, 2010).

Results indicate less than 5% of the post-harvest median model innovations for Wampus Creek and Deerlick Creek exceed the 95% predication intervals, which would suggest no significant change in daily streamflow due to forest harvest (Table 3.4, Figure 3.10). The lower (2.5th percentile) and upper (97.5th percentile) models do not exceed prediction limits and indicates a similar range of detection under model uncertainty.

The regression approach assumes the hydrological model and regression parameters are consistent throughout the pre- and post-harvest periods. However, the pre-harvest streamflow record shows Eunice Creek and Deerlick Creek did not have a consistent integrated watershed response between the cool and warm PDO phases (prior to forest harvest). Despite the longer pre-harvest calibration period for Deerlick-14Yr, the PDO driven meteorological changes and subsequent runoff generation may obscure the streamflow response and make it difficult to detect the effect of forest harvest from background climate variability with the regression approach.

3.3.3.3 Change-Detection Calibration Method

The precipitation regime varied between the two hydrological model calibration periods and subsequently resulted in different antecedent soil moisture conditions. The cool PDO calibration period (1969 – 1975) had 100% more 1-day rainfalls >10 mm (10 events), 76% more 2-day rainfalls >20 mm (17 events), and 67% more 3-day rainfalls >30 mm (3 events) compared to the warm PDO calibration period (1983 – 1988). The calibration periods did not have significantly different total annual precipitation ($p = 0.284$; Wilcoxon) and the warm PDO calibration period had 19% more average growing season rainfall (56 mm; $p = 0.432$). However, average annual snowfall was 49% more (91 mm; $p = 0.10$) in the cool calibration period. For the cool calibration period, the greater snowmelt input combined with more frequent, larger intensity rainfall events would have resulted in wetter antecedent soil moisture conditions across the watersheds.

Within the control watershed, the wetter, cooler PDO calibration period had 67% smaller maximum water holding capacity in the topsoil reservoir associated with lower median field capacity (FIELD_CAPACITY) and a shallower median topsoil reservoir depth (TOPSOIL; Figure 3.11; Table 3.5). The decrease in topsoil storage capacity reflects a watershed that has wetter antecedent soil conditions and expansion of saturated areas contributing to storm runoff, either as rapid flow to the stream channel or through groundwater recharge. In addition, the parameter that controls the division of water input that either contributes to soil storage or storm runoff (HBV_BETA) had a 27% lower median value in the cool calibration period. A lower HBV_BETA meant that for a certain modelled soil storage a smaller portion of water input was added to soil storage (i.e. that can eventually evaporate), while a larger portion contributed to storm runoff. In contrast, the drier, warm PDO calibration period had a higher maximum water holding capacity in the topsoil reservoir (Figure 3.11; Table 3.6). These parameter values suggest more water input contributed to soil storage and less of the watershed area contributed to storm runoff in order to match the watershed response in the observed hydrograph during the warm PDO calibration period. The warm calibration period for the treated watersheds resulted in a decrease in the maximum water holding capacity in the topsoil reservoir relative to the control watershed (Figure 3.11). This change implies that compared to the control watershed, there was less available watershed storage and a post-harvest increase in routed storm runoff.

Runoff reconstructed with pre- and post-parameters sets during the 1969 – 1975 period (absence of forest harvest) show the watersheds responded differently to the PDO driven meteorological changes in the snowmelt period (Figure 3.12). Based on test model simulations with median parameter values, the shift in snowmelt timing and peak flow was primarily a result of a decreased forest melt correction factor (HBV_MELT_FOR_CORR) and slower maximum potential melt rate (MELT_FACTOR). The melt rate was 41% and 50% slower in the warm PDO calibration period compared to the cool calibration period when the median pre- and post-parameters were compared in Eunice Creek and Deerlick Creek, respectively. In contrast, Wampus Creek had a 2.5% difference in the maximum potential melt rate between calibration periods, which suggest streamflow in Wampus Creek is less responsive to meteorological changes that influence snowmelt timing and peak flow.

Median parameter values for the treated watersheds that interact to contribute storm runoff through the soil response routine showed an increase in the runoff rate from the fast reservoir (i.e. rapid flow to the stream channel), but similar change in the slow reservoir runoff rate (i.e. storm runoff through groundwater recharge) compared to Eunice Creek. For the control watershed, the post-harvest (warm PDO) calibration period had an 8% greater fast reservoir runoff rate, compared to 174% in Wampus Creek and 66% in Deerlick Creek. In addition, the post-harvest (warm PDO) calibration period median slow reservoir runoff rates for the control watershed (177% greater) were within range of Wampus Creek (129% greater) and Deerlick Creek (200% greater). The parameterization of the storm runoff soil routine generated higher peak runoff events compared to pre-parameters when simulated with the same meteorological events, even in the control watershed (98% of rainfall-generated events).

Runoff reconstructed with pre- and post-parameters sets during the 1984 – 1988 period (post-harvest) show higher average annual spring and summer runoff (Figure 3.13) and simulated rainfall-generated peak runoff events increased due to forest harvest (Figure 3.14). Compared to the pre-harvest period, rainfall-generated peak runoff events showed greater variability in the magnitude of difference (Figure 3.14). The average relative difference in post-harvest peak runoff events were 54% higher in Wampus Creek compared to the pre-harvest period, while in Deerlick Creek post-harvest peak runoff events were 30% higher. The relative difference in peak runoff events was similar in Deerlick Creek when model simulations were reconstructed with pre-parameters calibrated with short (1969 – 1975) and longer (1969 – 1981) pre-harvest periods. For Deerlick-14Yr, the average relative difference in post-harvest peak runoff events was 28% higher than in the pre-harvest period. To compare, there was no significant change in the average relative difference in peak runoff events (0.1%) between the cool PDO phase and warm PDO phase periods in the control watershed ($p = 0.713$). By applying the same change detection approach to the control watershed, it was possible to attribute the increase in peak runoff events detected from forest harvest with greater certainty.

Changes in simulated snowmelt-generated peak runoff events due to forest harvest were difficult to evaluate due to the influence of climate variability on the spring snowmelt period. The PDO driven parameter changes in precipitation and winter air temperatures between the two calibration periods resulted in differences in the timing of snowmelt peak runoff between model simulations reconstructed with pre- and post-parameters, particularly for Eunice Creek (65% of events), Deerlick Creek (56% of events), and Deerlick-14Yr (61% of events). For example, snowmelt peak runoff events reconstructed with the post-parameters arrived 0 to 10 days later than peak events reconstructed with pre-parameters (Figure 3.12). For Wampus Creek, the timing of snowmelt generated peak runoff events reconstructed with the post-parameters were less delayed (up to 3 days) and accounted for only 27% of peak events, which may reflect the watershed's efficiency (i.e. synchronization) of snowmelt delivery to the stream channel. Without considering snowmelt peak timing, there was no significant change in the average relative difference in snowmelt-generated peak runoff events between periods (Table 3.7). Therefore, changes in the magnitude of snowmelt-generated peak runoff events were difficult to interpret due to PDO driven parameter changes between the two calibration periods.

Daily spring and summer runoff increased in the post-harvest period in the treated watersheds, while there was little change in daily fall and baseflow runoff (Figure 3.13; Table 3.7). However, the change-detection calibration approach detected a change in spring runoff in the control watershed (no harvest) as a result of the PDO driven changes in precipitation and winter air temperatures. The PDO regime shift again made it difficult to isolate the effect of forest harvest from background climate variability.

3.4 Discussion

3.4.1 Streamflow Response to Climate Variability

The observed hydrologic regime of the control watershed was not stationary during the study period due to the PDO phase change in 1977 from negative (cool) to positive (warm). Positive winter PDO values were significantly associated with warmer winter air temperatures, lower winter precipitation and less snowpack in Tri-Creeks, which is similar in other western Canadian forested watersheds (Moore and Scott, 2005; Harder *et al.*, 2015; Shrestha *et al.*, 2016). Meteorological changes driven by the warm PDO phase resulted in an earlier snowmelt, a delayed rising limb period of spring freshet, and increased runoff during the baseflow period. Increased baseflow was a result of more frequent, larger rainstorms in the summer/fall, especially in 1977, 1978 and 1980. After 1977, there was more annual runoff generated than predicted based on the modified double mass curve for Eunice Creek.

The PDO was not a significant predictor of streamflow in Tri-Creeks; a result also observed in a long-term monitored watershed located on the eastern slopes of the Alberta Rocky Mountains (Harder *et al.* 2015). Streamflow in southeastern British Columbia and other parts of southern

Alberta showed a significant decreasing trend in the warm PDO phase (Moore and Scott, 2005; St. Jacques *et al.*, 2010). The decreasing trend was not observed in Eunice Creek, but rather there was more inter-annual variability observed in annual streamflow. The streamflow variability was associated with large annual storage changes (1-33% of precipitation) during this phase, which means runoff was more variable with drier antecedent soil moisture condition. Antecedent soil moisture and the effects on subsurface processes that generate streamflow can create lagged effects in streamflow response in some forested watersheds (Jones and Post, 2004), and likely plays an important role in attenuating the PDO driven changes in precipitation inputs.

Larger annual peak streamflow later in the year indicate rain events and antecedent storage drive peak flow generation in Tri-Creeks. In Eunice Creek, the distribution of daily annual peak flow maxima shows that over the period of record (1968 – 1990), half occur after the day of year 167 (June 17). Prior to June, peak flows have a mean of 7.9 mm d^{-1}, while those after the median date have a mean flow of 9.3 mm d^{-1}. Given that snow in Tri-Creeks is typically melted by June, annual peak flows in Tri-Creeks are not typically driven by snowmelt runoff. Rather, snowmelt input satisfies soil storage prior to summer rain events; a hydrologic response like that observed in the Boreal Plains (e.g. Devito *et al*, 2005; Redding and Devito, 2011) and differs from alpine (e.g. Schnorbus and Alila, 2004; Fang *et al*; 2016; Spencer *et al.*, 2019) or montane watersheds (e.g. Moore and Scott, 2005).

The streamflow variability observed in the control watershed is likely controlled by its geological setting and large potential for subsurface water storage. The distribution of deep (>8 m) glacial soil permeability and water input timing and intensity may exert greater control than topography on runoff generation (Redding and Devito, 2008, 2010; Smith *et al,* 2014; Hokanson *et al.*, 2019). Subsurface runoff from the glacial till was shown to be a large component of streamflow from historical water quality and isotopes samples in Tri-Creeks and is likely an important storage reservoir that fills and drains on a multi-annual basis to deliver water to streamflow and underlying bedrock aquifers (Andres *et al.*, 1987). In addition, increased proportions of permeable or fractured sedimentary bedrock found along the eastern slopes of the Rocky Mountains, like that found in the Foothills, has been suggested to attenuate precipitation inputs for streamflow generation (Jensco *et al.*, 2011; Harder *et al.*, 2015; Spencer *et al.*, 2019). Therefore, how Tri-Creeks watersheds respond to forest harvest will likely be a function of climate variability and antecedent watershed storage that acts as a buffer between water inputs and streamflow to attenuate or enhance the response.

3.4.2 Streamflow Response to Forest Harvest

The long-term Tri-Creeks forest harvest experiments coincided with the timing of a PDO phase change and provided an opportunity to compare the results of statistical and hydrological modelling change-detection methods. Paired watershed methods (e.g. Moore and Scott, 2005; Alila *et al.*, 2009) were not used in Tri-Creeks because the large, adjacent watersheds responded differently to the PDO driven changes in precipitation and air temperature. Therefore, unexplained spatial and temporal variation was reduced with methods that detect change in a single watershed. However, methods that used a regression approach (i.e. pre-harvest linear regression to predict post-harvest 'control' streamflow) showed that the calibration period needs to be sufficiently long enough to capture the range of variability in meteorological changes and streamflow response in an effort to minimize bias in predication estimates post-harvest and reduce uncertainty in analyses outcomes (Zégre *et al.*, 2010). The influence of varied calibration length was evident in the Deerlick Creek MDMCs, even when the shorter calibration period had high and low precipitation years relative to the long-term average. In addition, the MDMC in Eunice Creek made it clear that climate variability could not be captured in precipitation and ET alone, because runoff generation is also driven by antecedent soil storage. When changes in antecedent soil conditions were modelled as part of the change-detection regression method, the ability to detect the effect of forest harvest from background climate variability remained uncertain. The uncertainty in model results were reduced when the model structure was evaluated to detect change in the control watershed. The effect of climate variability on streamflow was also evaluated in the warm PDO period prior to forest harvest in Deerlick Creek, and GLS regression models were constructed based on observed, lower, median and upper time series to incorporate natural variability and model uncertainty. However, results remained uncertain because the change-detection regression method assumes the hydrological model and linear regression parameters are consistent throughout the pre- and post-harvest periods, but observed streamflow showed Deerlick Creek had a different watershed response in the cool versus warm PDO periods prior to forest harvest. A significant forest harvest signal was detected when a hydrological modelling approach was used that accounted for antecedent soil storage and did not assume consistent parameters between the pre- and post-harvest periods. Pre- and post-parameters sets used to reconstruct streamflow driven by the same meteorological data in the post-harvest period assessed the integrated watershed response and could remove additional uncertainty as a result of climate variability (Seibert and McDonnell, 2010). However, climate variation continued to mask the streamflow record during the snowmelt period due to the dominant influence of the PDO driven meteorological changes in Tri-Creeks. This suggests that greater caution is needed to evaluate the effect of forest harvest on streamflow when the response is not solely the result of forest harvest operations. To detect forest harvest effects on streamflow, the length of the initial control period with respect to climate variation (e.g. PDO, ENSO) and antecedent storage within watersheds should not be overlooked.

Despite up to 52% and 64% harvest, streamflow in Tri-Creeks did not show a significant measurable change to forest harvest using the MDMC and change-detection regression method. However, additional modelling analyses that further reduced climate variability suggest there was a significant change to rainfall-generated peak runoff events and an increase in water year runoff as a result of increased spring and summer runoff. During the growing season, reduced transpiration and canopy interception that follows forest harvest should allow soils to wet up to a greater depth than would be observed under a forest canopy (Elliot *et al.*, 1998; Moore and Wondzell, 2005; Winkler *et al.*, 2010). The transfer of these net soil water inputs to the stream is governed by the amount of storage and partitioning of flow paths within the subsurface (Redding and Devito, 2008, 2010; Smith *et al*; 2014). The modelled soil response in the post-harvest (warm PDO phase) period indicates the treatment watersheds had wetter antecedent soil moisture conditions and increased subsurface runoff rates to the stream channel. Significant increases in annual streamflow and peak flows in the treatment watersheds does support the conceptual models for meso-scale, non-alpine conifer forested watersheds with greater than 20 – 25% of harvested area (Bosch and Hewlett, 1982; Green and Alila, 2012); however, those conceptual models do not explicitly include the function of climate variability, in relation to antecedent watershed storage, and subtle differences in actual watershed storage due to heterogeneity in the geological setting.

The percent of harvested watershed area is a common attribute used to predict a change in streamflow response; however, review studies have shown that above the 20 – 30% harvested area threshold the streamflow response is highly variable as the portion of harvested area increases (Bosch and Hewlett, 1982; Stednick, 1996; Guillemette *et al.*, 2005). For example, in a review of paired watershed studies located in the Rocky Mountain/Inland Intermountain region, measurable increases in annual water yield could be expected after harvest of only 15% watershed area, while

30% or more harvested could be expected to produce generally larger increases from 0 to 350 mm yr^{-1} (Stednick, 1996). The wide variation in streamflow response to disturbance is due to the inherent differences in climate, geology, runoff generation, topography, soils, vegetation, and harvest operations (e.g. cutblock distribution) between sites (Moore and Wondzell, 2005; Winkler *et al.*, 2010). The current threshold of 20 – 30% of disturbed watershed area used in forest management planning has not been confirmed for Foothills watersheds where climate variation and antecedent watershed storage play large roles in runoff generation. Results from Tri-Creeks suggest that climate variability masked the streamflow record and the buffering capacity provided by the antecedent watershed storage in the warm PDO phase may have attenuated the forest harvest signal in the streamflow response. Therefore, further research is needed to explore the effect of forest harvest on the streamflow response over a range of meteorological forcing and antecedent soil moisture conditions using a hydrological modelling approach.

The agreement of streamflow observations and hydrological model simulations was assumed acceptable to detect change with the calibration method given that the simulations captured the rainfall-runoff relationship (Seibert and McDonnell, 2010). For Tri-Creeks, the rainfall and snowmelt depth and intensity, in relation to antecedent soil conditions, were strong controls on runoff generation, which resembles a threshold-like response observed in soils developed from deep glacial tills (>8 m; Redding and Devito 2008; 2010; Smith *et al.*, 2014). Therefore, the addition of a simple threshold-based soil routine may improve model performance and should be explored in the future.

3.4.3 Streamflow Response to Projected Climate Change

This study provided an opportunity to test the ability of a hydrological model to simulate the streamflow regime between different historical PDO states as an analogue to anticipated projected climate change effects on snow-dominated streamflow in western North America. Concerns focused on the effects of climate change on streamflow include an increase in drought and flood frequencies and intensities as a result of increased air temperatures, increased frequency and intensity of heavy precipitation events, advanced snowmelt, and decreased snow cover (Jones *et al.*, 2012; IPCC, 2013). Projected climate changes in precipitation and air temperature may be less than those observed in the historical warm PDO phase in Tri-Creeks; however, hydrological model results found a moderate ability of the control watershed model to simulate the magnitude and timing of climate-driven differences in the warm PDO condition when streamflow was reconstructed with parameters calibrated in the cool PDO phase (pre-parameters). For example, pre-parameters used to reconstruct streamflow for the warm PDO period (1977 – 1988) in Eunice Creek under-predicted spring streamflow and did not capture the timing of advanced snowmelt. Changes in the timing of snowmelt-generated and increased summer streamflow could influence fish spawning cues or the availability and suitability of aquatic organism habitat. In addition, watershed management may rely on a hydrological model's ability to simulate future hydrologic changes based on potential climate change scenarios (e.g. environmental surface water baseline assessments; environmental flow needs studies). The results of this chapter demonstrate that caution is needed when using a hydrological model to assess potential future climate change on streamflow regimes in the Alberta Foothills, especially when quantifying values of ecological flow needs for forest management planning or infrastructure design.

3.4.4 Implications for Watershed Management

Alberta's Foothills region makes up 19% of the provincial forested land base (352,477 km^2; 'Green Zone') and is primarily managed for timber, non-renewable resource extraction (mining, oil and natural gas) and public wildlands. In addition to the overlapping tenures and multiple stakeholders, the Foothills region currently faces diverse forest management issues that include both managed and natural disturbances (e.g. insect infestation, wildfire, climate change). For example, a management plan in a Foothills region forest management unit (effective 2018) was approved to undertake a 125% accelerated harvest of annual allowable cuts over the next decade primarily to provide an opportunity for the forestry company to reduce areas within their defined forest area that are susceptible to mountain pine beetle infestation (AAF, 2018). The results from this chapter suggest that there is an effect of forest harvest on streamflow in Foothills watersheds, but the potential changes to streamflow can be concealed in natural climate variability. Therefore, there is an urgent need for further research to refine disturbance thresholds in Foothills watersheds to guide forest management planning in an effort to minimize negative effects to water resources and aquatic ecosystems, especially in fisheries-sensitive watersheds with spring spawning species (Sterling, 1992).

3.4.5 Conclusions

This chapter used a combination of statistical and hydrological modelling methods to reanalyze the effect of forest harvest on streamflow in the long-term historical paired watershed study in Tri-Creeks. The forest harvest experiment coincided with a PDO phase change. The watersheds were observed to respond differently to the PDO driven changes in precipitation and air temperature in the warm versus cool PDO phase. The background climate variability made it difficult to detect measurable change in the streamflow response to forest harvest using linear regression models in the pre-harvest period to predict post-harvest streamflow. However, a change-detection hydrological modelling approach that calibrated parameters separately in the pre- and post-harvest periods resulted in a significant measurable change in rainfall-generated peak runoff events and summer runoff in the post-harvest period, which was not detected in the control watershed. By applying the same change detection approach to the control watershed, it was possible to eliminate unexplained variation as the cause for changes in runoff and attribute the increases detected from forest harvest with greater certainty. Storm runoff increased in the treatment watersheds in the post-harvest period, but may have been attenuated by the drier antecedent conditions in the warm PDO phase and large potential for subsurface storage given Tri-Creeks' geologic setting. How the watersheds respond to forest harvest will likely be a function of antecedent watershed storage and climate variability. The relatively large interannual variation in precipitation and subtle differences in actual watershed storage may act as a buffer between water inputs and streamflow response, which confound the influence of forest harvest and comparison within paired-watershed studies. Further research is needed to evaluate the sensitivity of streamflow to harvested area and cutblock distribution within the watershed and varied antecedent moisture conditions to refine disturbance thresholds. Understanding the transient hydrologic response of these watersheds located in this geologic setting is paramount for land-use management (i.e. cumulative effects) and assessing climate change in the Alberta Foothills.

Table 3.1 Study design and watershed characteristics.

Watershed	Wampus Creek	Deerlick Creek	Eunice Creek
Area (km^2)	28.3	15.2	16.8
Experiment Status	Treatment	Treatment	Control
Prior Disturbance	Select/Clear-cut – 0.6% (1959)	Select/Clear-cut – 3% (1959)	Select/Clear-cut – 1.6% (1959)
Pre-Treatment Period	1967 – 1977	1967 – 1981	-
Treatment Type	Clearcut – 52%	Streamside Timber Removal – 64%	-
Post-Treatment Period	1983 – 1988	1984 – 1988	-
Mean Annual Runoff (mm)[A]	253	250	232
Runoff Coefficient (-)[A]	0.40	0.39	0.36
Avg. Baseflow (%)[AB]	71	71	74
Road Density (km/km^2)	0.46	0.30	0.37

[A] For 1967 – 1977 water years prior to forest treatment.

[B] Baseflow was estimated using Eckhardt (2012) two parameter recursive digital filter and calculated as the percentage of water year (WY) streamflow.

Table 3.2 Statistical association between Tri-Creeks hydrometeorological variables and the Pacific Decadal Oscillation (PDO) and El Nino Southern Oscillation (ENSO). Winter season includes November to March and the growing season ("Grow") from May to September. The variables include maximum, minimum and mean air temperature (T), precipitation (P), snow water equivalent (SWE), water year (WY) ratio of rain to total precipitation (Rain:P) and streamflow (Q).

Variable	Sig. Model Terms	Adj. r^2	tau
Annual T_{mean}	Trend	0.35	0.456
Grow T_{max}	-	0.02	0.222
Grow T_{min}	Trend	0.46^A	0.354
Winter T_{max}	PDO	0.49^A	0.246
Winter T_{min}	PDO, Trend	0.64^A	0.368
Annual P	-	0.05^A	-0.148
Grow P	ENSO	0.19	0.029
Winter P	PDO, Trend	0.33^A	-0.362
Peak SWE	PDO	0.36	-0.207
WY Rain:P	Trend	0.28	0.337
Eunice Q	ENSO	0.18	0.000
Deerlick Q	ENSO	0.23	0.053
Wampus Q	-	0.03	0.005

^{A}Pseudo-r^2 calculated with the *nagelkerke* function in *rcompanion* package in R statistical software because GLS regression was used to account for autocorrelation in the model residuals.

Table 3.3 Model performance statistics for the Tri-Creeks watershed hydrological models during the pre-harvest/cool PDO calibration period (1969 – 1975) and the post-harvest/warm PDO calibration period (1983/84 – 1988) including Nash-Sutcliffe Efficiency (NSE), mean percent bias error (PBIAS) and coefficient of determination (r^2). PBIAS was calculated using the average of the absolute values for snow surveys (SWE) and accumulated precipitation in the Sacramento gauges (PGAUGE).

Watershed	Optimal NSE	Optimal PBIAS	Range NSE	SWE		PGAUGE	T_{max}
				r^2	PBIAS	PBIAS	NSE
Pre-Harvest							
Eunice	0.79	-0.6	0.70 – 0.79	0.65	27	11	0.95
Wampus	0.76	1.4	0.72 – 0.78	0.68	18	9.5	-
Deerlick	0.75	0.5	0.66 – 0.74	0.62	27	9.3	-
Deerlick – 14Yr[A]	0.62	-0.7	0.55 – 0.63	0.62	24	11	-
Post-Harvest[B]							
Eunice	0.69	-0.5	0.60 – 0.68	0.31	26	11	0.91
Wampus	0.75	1.0	0.70 – 0.77	0.28	27	4.6	-
Deerlick[C]	0.75	-3.9	0.69 – 0.74	0.27	10	7.3	-

[A] Deerlick – 14Yr was calibrated for the entire pre-harvest period (1969 – 1981; cool and warm PDO phase).

[B] Tri-Creeks observed data were only available until December 1985.

[C] Deerlick Creek was calibrated 1984 – 1988, while Wampus and Eunice Creeks were calibrated 1983 – 1988.

Table 3.4 GLS regression and AR modeling results for the treated and control watersheds using the change-detection hydrological modelling regression method. Coefficients Φ_1, Φ_2, Φ_3, Φ_4 are estimated autocorrelation coefficients selected by AIC; β_0, β_1 are estimated via regression; *k* is the order of autocorrelation; *df* are the degrees of freedom; and *se* is the standard error of the estimate. "Lower" corresponds to the 2.5th percentile uncertainty simulation in GLS regression model, while "Upper" is the 97.5th percentile uncertainty simulation.

Model	*df*	*k*	Φ_1	Φ_2	Φ_3	Φ_4	β_0	β_1	*se*	% Post-Harvest[A]	% Warm PDO Phase[A]
						Eunice					
Lower[C]	2755	2	0.96	-0.11	-	-	0.00	0.37	0.14	-	3.8
Median	2755	2	0.94	-0.08	-	-	0.00	0.85	0.12	-	4.3
Upper	2755	2	0.91	-0.08	-	-	0.00	0.83	0.12	-	4.4
						Wampus					
Lower	3120	4	0.97	-0.15	0.04	-0.06	0.00	0.34	0.15	3.1	-
Median	3120	4	0.92	-0.12	0.09	-0.10	0.00	0.77	0.12	4.4	-
Upper	3120	4	0.88	-0.08	0.08	-0.10	0.00	0.78	0.12	4.9	-
						Deerlick					
Lower	2755	2	0.93	-0.11	-	-	0.00	0.33	0.19	3.5	2.7
Median	2755	2	0.94	-0.12	-	-	0.00	0.76	0.16	3.9	2.9
Upper	2755	3	0.90	-0.02	-0.08	-	0.00	1.0	0.15	4.7	3.3
						Deerlick – 14Yr					
Lower	4581	3	0.95	-0.07	-0.05	-	0.00	0.38	0.19	3.6	-
Median	4581	3	0.95	-0.06	-0.06	-	0.00	1.0	0.15	4.2	-
Upper	4581	3	0.92	-0.04	-0.07	-	0.00	1.0	0.15	4.8	-

[A] warm PDO phase and post-harvest innovations exceedance of 95% prediction limits. The selected significance level was $\alpha = 0.05$, where 5% of estimated innovations should fall outside the 95% intervals due to random error.

Table 3.5 List of model parameters, parameter ranges of 100 calibrated parameters (median in brackets) for each watershed in the pre-harvest calibration period. Parameter ranges were used in the modified HBV-EC model structure template in Raven to simulate streamflow and quantify the 95th percentile uncertainty bounds.

Parameter Name	Definition	Units	Site			
			Eunice	Wampus	Deerlick	Deerlick14
ADIABATIC_LAPSE	Adiabatic temp. lapse rate	°C km^{-1}	5.0 - 7.0 (6.3)	5.0 - 7.0 (6.2)	5.0 - 7.0 (5.2)	5.0 - 6.9 (5.3)
RAINSNOW_TEMP	Rain/snow transition temp	°C	0.51 - 3.5 (1.5)	0.52 - 3.5 (1.2)	0.50 - 1.9 (0.73)	2.6 - 3.5 (3.4)
MAX_LAI	Maximum leaf area index	m^2 m^{-2}	3.5 - 6.0 (4.5)	3.5 - 6.0 (4.6)	3.8 - 6.0 (5.8)	3.5 - 6.0 (4.6)
MAX_LAI	Max. leaf area index (CUT)	m^2 m^{-2}	-	-	-	-
FOREST_ SPARSENESS	Canopy cover	%	0.60 - 0.90 (0.88)	0.60 - 0.90 (0.85)	0.60 - 0.90 (0.79)	0.65 - 0.90 (0.87)
MELT_FACTOR	Maximum snowmelt factor	mm/d °C	3.2 - 4.0 (3.9)	3.1 - 4.0 (3.9)	3.0 - 4.0 (3.9)	3.5 - 4.0 (3.9)
MELT_FACTOR	Max. snowmelt factor (CUT)		-	-	-	-
MIN_MELT	Minimum snowmelt factor	mm/d °C	0.00 - 2.0 (1.9)	0.40 - 2.0 (1.9)	0.03 - 2.0 (1.7)	0.11 - 2.0 (1.8)
MIN_MELT	Min. snowmelt factor (CUT)		-	-	-	-
HBV_MELT_FOR_CORR	Snowmelt forest correction	-	0.74 - 0.90 (0.88)	0.81 - 0.90 (0.89)	0.75 - 0.90 (0.89)	0.76 - 0.90 (0.89)
HBV_MELT_ASP_CORR	Snowmelt aspect correction	-	0.10 - 1.0 (0.94)	0.33 - 1.0 (0.96)	0.13 - 1.0 (0.97)	0.12 - 1.0 (0.98)
REFREEZE	Maximum refreeze factor	mm/d °C	0.000 - 2.7 (0.04)	0.000 - 0.32 (0.03)	0.001 - 2.0 (0.04)	0.000 - 2.2 (0.03)
REFREEZE	Max. refreeze factor (CUT)	mm/d °C	-	-	-	-
FIELD_CAPACITY	Field capacity saturation	[0..1]	0.28 - 1.0 (0.91)	0.37 - 1.0 (0.96)	0.17 - 1.0 (0.86)	0.21 - 1.0 (0.92)
SAT_WILT	Minimum saturation	[0..1]	0.00 - 0.78 (0.11)	0.00 - 0.66 (0.09)	0.00 - 0.83 (0.17)	0.00 - 0.57 (0.06)
TOPSOIL	Thickness soil layer	m	0.10 - 0.50 (0.49)	0.10 - 0.50 (0.40)	0.10 - 0.50 (0.33)	0.11 - 0.50 (0.48)
SOIL 1 (Fast Reservoir)	Thickness soil layer	m	0.51 - 2.5 (1.3)	0.50 - 2.5 (1.4)	0.52 - 2.5 (1.5)	0.51 - 2.5 (1.6)
SOIL 2 (Slow Reservoir)	Thickness soil layer	m	0.50 - 1.3 (0.60)	0.50 - 0.90 (0.57)	0.50 - 1.1 (0.54)	0.50 - 0.9 (0.89)
HBV_BETA	Infiltration exponent	-	0.04 - 1.6 (0.65)	0.03 - 1.1 (0.52)	0.07 - 1.3 (0.44)	0.03 - 1.2 (0.57)
MAX_CAP_RISE_RATE	Max. capillary rise rate	mm d^{-1}	0.50 - 5.7 (0.73)	0.50 - 6.0 (0.83)	0.50 - 4.0 (0.59)	0.50 - 2.7 (0.59)
MAX_PERC_RATE	Maximum percolation rate	mm d^{-1}	2.2 - 10 (8.8)	3.4 - 10 (8.9)	3.4 - 10 (9.7)	3.8 - 10 (9.6)
BASEFLOW_COEFF	Linear baseflow storage	-	0.01 - 1.0 (0.35)	0.01 - 1.0 (0.47)	0.03 - 1.0 (0.38)	0.003 - 1.0 (0.31)
BASEFLOW_N	Baseflow exponent (SOIL 1)	-	1.0 - 10 (1.2)	1.0 - 9.1 (1.3)	1.0 - 10 (1.2)	1.0 - 9.3 (1.4)
BASEFLOW_N	Baseflow exponent (SOIL 2)		1.0 - 10 (7.2)	1.0 - 10 (8.4)	1.0 - 10 (1.3)	1.0 - 9.9 (7.5)
MAX_BASEFLOW_RATE	Maximum baseflow rate	mm d^{-1}	1.3 - 10 (8.7)	1.0 - 10 (9.3)	1.5 - 10 (9.6)	3.7 - 10 (9.0)

Table 3.6 List of model parameters, parameter ranges of 100 calibrated parameters (median in brackets) for each watershed in the post-harvest calibration period. Parameter ranges were used in the modified HBV-EC model structure template in Raven to simulate streamflow and quantify the 95th percentile uncertainty bounds.

Parameter Name	Definition	Units	Site		
			Eunice	Wampus	Deerlick
ADIABATIC_LAPSE	Adiabatic temp. lapse rate	°C km^{-1}	5.2 - 7.0 (6.7)	5.0 - 6.6 (5.1)	5.0 - 6.9 (5.4)
RAINSNOW_TEMP	Rain/snow transition temp	°C	0.50 - 3.5 (0.66)	0.50 - 2.7 (0.60)	0.50 - 2.0 (0.60)
MAX_LAI	Maximum leaf area index	m^2 m^{-2}	3.5 - 6.0 (4.3)	3.5 - 5.8 (3.7)	3.5 - 5.7 (3.8)
MAX_LAI	Max. leaf area index (CUT)	m^2 m^{-2}	-	0.51 - 2.0 (1.2)	0.52 - 2.0 (1.2)
FOREST_ SPARSENESS	Canopy cover	%	0.84 - 0.90 (0.90)	0.68 - 0.90 (0.89)	0.73 - 0.90 (0.89)
MELT_FACTOR	Maximum snowmelt factor	mm/d °C	2.0 - 3.8 (2.6)	2.1 - 4.0 (3.8)	2.0 - 4.0 (2.4)
MELT_FACTOR	Max. snowmelt factor (CUT)		-	2.0 - 4.0 (2.7)	2.0 - 4.0 (2.7)
MIN_MELT	Minimum snowmelt factor	mm/d °C	0.03 - 2.0 (1.3)	0.10 - 2.0 (1.3)	0.11 - 2.0 (1.8)
MIN_MELT	Min. snowmelt factor (CUT)		-	0.09 - 2.0 (1.1)	0.12 - 2.0 (1.5)
HBV_MELT_FOR_CORR	Snowmelt forest correction	-	0.60 - 0.89 (0.70)	0.61 - 0.90 (0.87)	0.60 - 0.90 (0.75)
HBV_MELT_ASP_CORR	Snowmelt aspect correction	-	0.10 - 1.0 (0.90)	0.30 - 0.9 (0.86)	0.36 - 0.91 (0.84)
REFREEZE	Maximum refreeze factor	mm/d °C	0.003 - 3.0 (1.1)	0.002 - 3.0 (1.2)	0.003 - 3.0 (1.7)
REFREEZE	Max. refreeze factor (CUT)	mm/d °C	-	0.01 - 2.9 (0.26)	0.001 - 3.0 (2.3)
FIELD_CAPACITY	Field capacity saturation	[0..1]	0.64 - 1.0 (0.98)	0.51 - 1.0 (0.96)	0.67 - 1.0 (0.96)
SAT_WILT	Minimum saturation	[0..1]	0.00 - 0.35 (0.02)	0.00 - 0.68 (0.03)	0.00 - 0.24 (0.04)
TOPSOIL	Thickness soil layer	m	0.92 - 1.5 (1.4)	0.68 - 1.0 (0.92)	0.59 - 1.0 (0.79)
SOIL 1 (Fast Reservoir)	Thickness soil layer	m	0.52 - 2.5 (1.6)	0.55 - 2.5 (1.4)	0.56 - 2.5 (1.6)
SOIL 2 (Slow Reservoir)	Thickness soil layer	m	0.50 - 1.3 (0.53)	0.50 - 0.65 (0.52)	0.50 - 0.89 (0.52)
HBV_BETA	Infiltration exponent	-	0.14 - 1.3 (0.89)	0.47 - 2.0 (1.3)	0.34 - 1.3 (0.76)
MAX_CAP_RISE_RATE	Max. capillary rise rate	mm d^{-1}	0.50 - 3.2 (0.64)	0.50 - 1.8 (0.65)	0.50 - 1.6 (0.68)
MAX_PERC_RATE	Maximum percolation rate	mm d^{-1}	1.8 - 10 (9.8)	0.51 - 10 (8.9)	0.55 - 10 (9.7)
BASEFLOW_COEFF	Linear baseflow storage	-	0.001 - 0.98 (0.28)	0.003 - 1.0 (0.43)	0.001 - 1.0 (0.40)
BASEFLOW_N	Baseflow exponent (SOIL 1)	-	1.0 - 9.8 (1.5)	1.0 - 9.6 (4.0)	1.0 - 10 (1.8)
BASEFLOW_N	Baseflow exponent (SOIL 2)		1.0 - 10 (9.8)	1.0 - 10 (9.8)	1.0 - 10 (9.8)
MAX_BASEFLOW_RATE	Maximum baseflow rate	mm d^{-1}	1.0 - 10 (9.5)	1.2 - 10 (9.4)	1.0 - 10 (4.2)

Table 3.7 The relative percent difference in simulated median daily runoff reconstructed with pre- and post-parameter sets during the study period. A positive value indicates post-parameter simulated runoff was greater than pre-parameter simulated runoff. Values represent the average relative difference within the period, while the ranges in annual runoff are in brackets. Bold values indicate a significant change in average relative percent difference between periods (% Change; p<0.01; Wilcoxon). Only Deerlick Creek (14Yr) was presented as the calibration period captured more climate variability over the 14 pre-harvest years in both the cool and warm PDO phases.

Streamflow	Eunice Creek			Wampus Creek			Deerlick Creek (14Yr)		
	Cool PDO	Warm PDO	% Change	Pre-Harvest	Post-Harvest	% Change	Pre-Harvest	Post-Harvest	% Change
Snowfall Peaks	-9.6 (-61–65)	20 (-100–67)	30	5.5 (-69–159)	19 (-41–74)	13	-15 (-113–36)	28 (-48–88)	43
Spring (4, 5, 6)	-11 (-22–32)	10 (-31–6.1)	**21**	-28 (-45– -16)	32 (23–46)	**60**	-14 (-40–3.2)	32 (20–45)	**46**
Summer (7, 8)	11 (-15–25)	20 (-1.1–50)	8.6	-15 (-30– -4.9)	13 (-5.9–24)	**29**	-3.1 (-26–8.8)	21 (16–28)	**24**
Fall (9, 10)	14 (-3.2–22)	7 (-12–37)	-7.0	-19 (-30– -8)	-10 (-30–2.6)	8.7	-1.6 (-10–4.2)	-1.1 (-9.5–5.6)	0.5
Baseflow	-16 (-27– -3.5)	-23 (-40– -6.8)	-6.8	-21 (-43– -11)	-27 (-47– -13)	-5.8	-12 (-19– -5.9)	-16 (-22– -8.3)	-3.4
Water Year	-5.3 (-14–11)	-2.2 (-12–1.5)	3.1	-21 (-14–30)	-3.4 (-11–4.2)	**18**	-9.5 (-19– -1.5)	4.2 (-1.4–8.9)	**14**

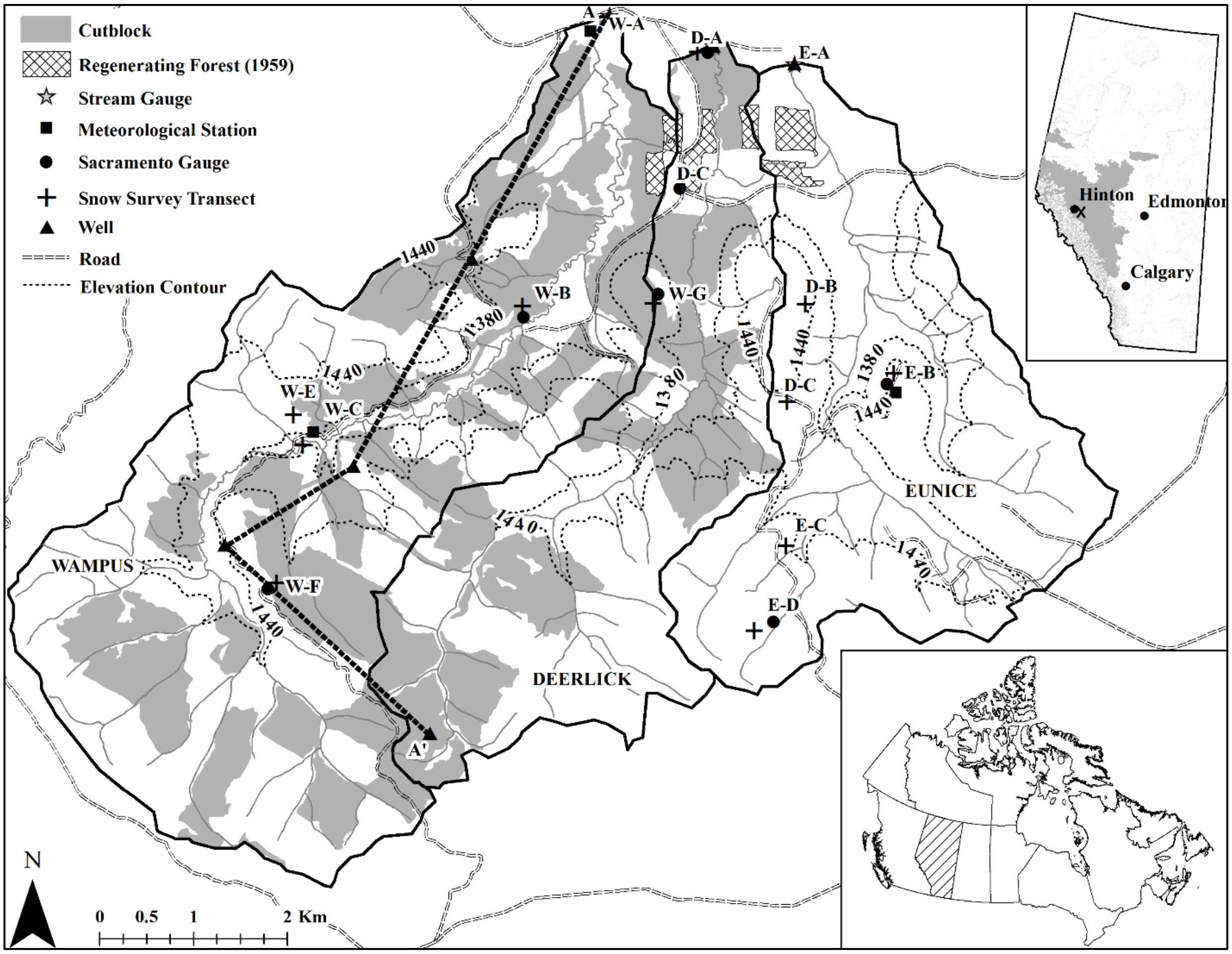

Figure 3.1 Study area and location of Tri-Creeks Experimental Watersheds (marked by an X on the provincial map) located near Hinton, Alberta, Canada within the Foothills Natural Sub-Region (dark grey). Eunice Creek (E) is the control watershed. Deerlick (D) and Wampus (W) Creeks are the treatment watersheds. Hydrometeorological instruments and snow survey transects are presented with historical labels. Cutblocks were harvested between 1978 and 1983. Elevation contours are labelled 1380 and 1440 m.a.s.l. and correspond to boundaries of glaciolacustrine deposits (<1380 m.a.s.l.), local sandy loam till (>1380 – <1440 m.a.s.l.), and glacial till deposits at depth 1.5 m from surface or exposed (>1440 m.a.s.l.). Geological cross-section through Wampus Creek from A to A' (thick dashed line) represents the stratigraphy of groundwater wells (black triangles; Figure 3.2).

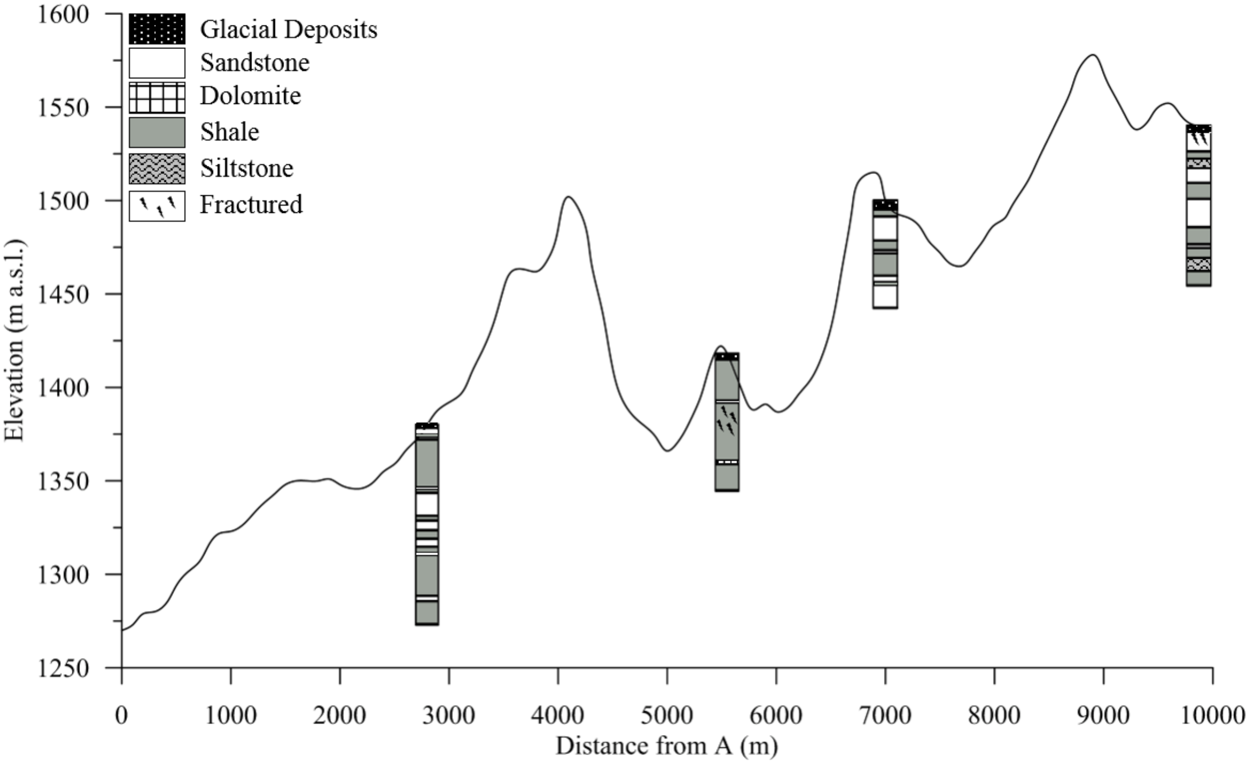

Figure 3.2 Geological cross-section through Wampus Creek from A to A' (see Figure 3.1 for mapped transect and locations of groundwater wells). The bedrock geology is composed of sedimentary layers of alternating sandstone and shale/siltstone, which can be fractured. The bedrock is overlain by 1.5 – 22 m of glacial deposits dependent on elevation with some exposed bedrock above 1440 m.a.s.l.

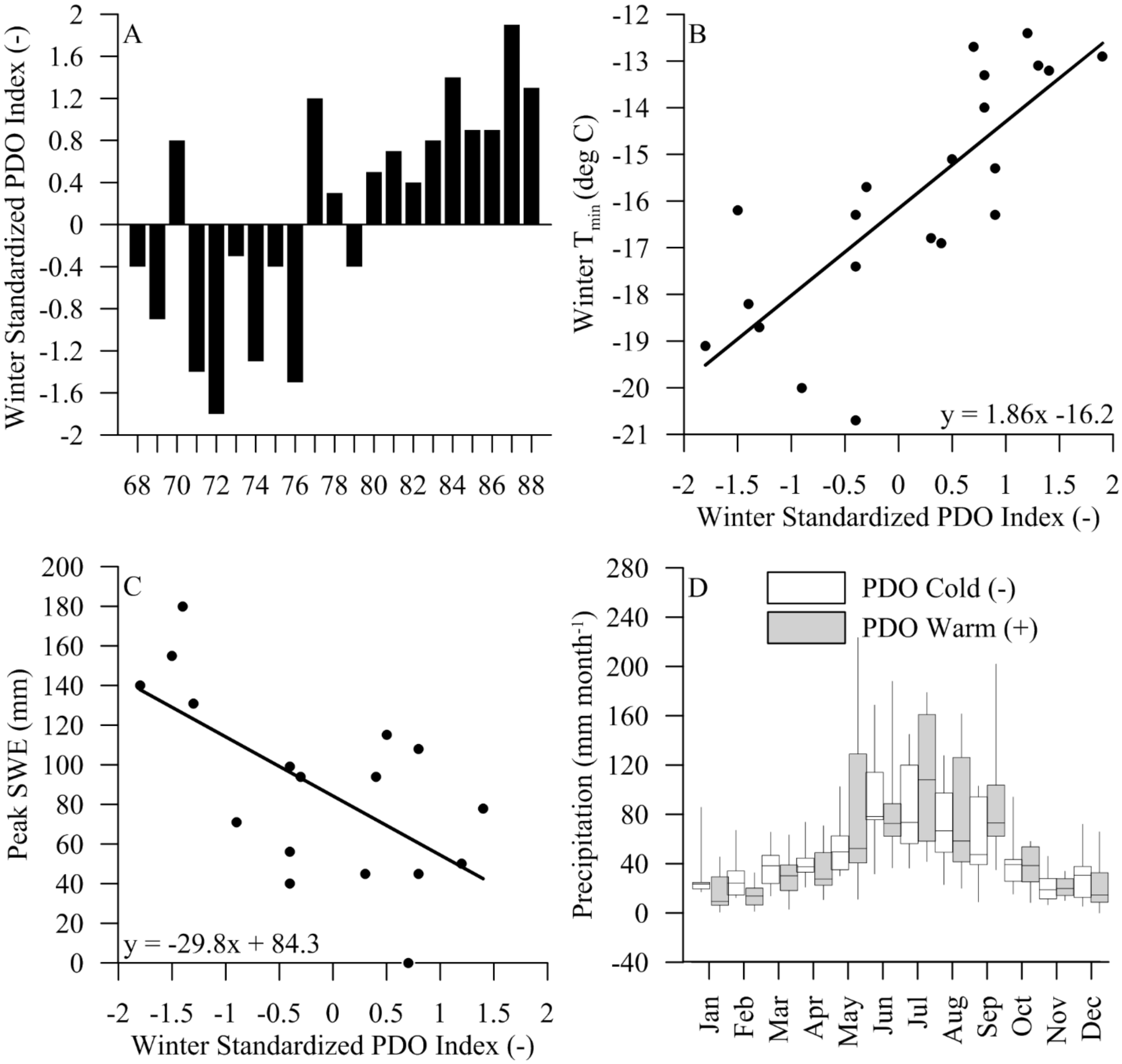

Figure 3.3 Mean winter (November – March) standardized PDO index (Mantua, 2016) plotted over the study period (A), with mean winter maximum air temperature (B), and peak snow water equivalent measured along transects in forested stands (SWE; C). Black lines indicate the best-fit regression line. The boxplot graph (D) compares total monthly precipitation in the cool PDO phase (1967-1976) to warm PDO phase (1977-1988).

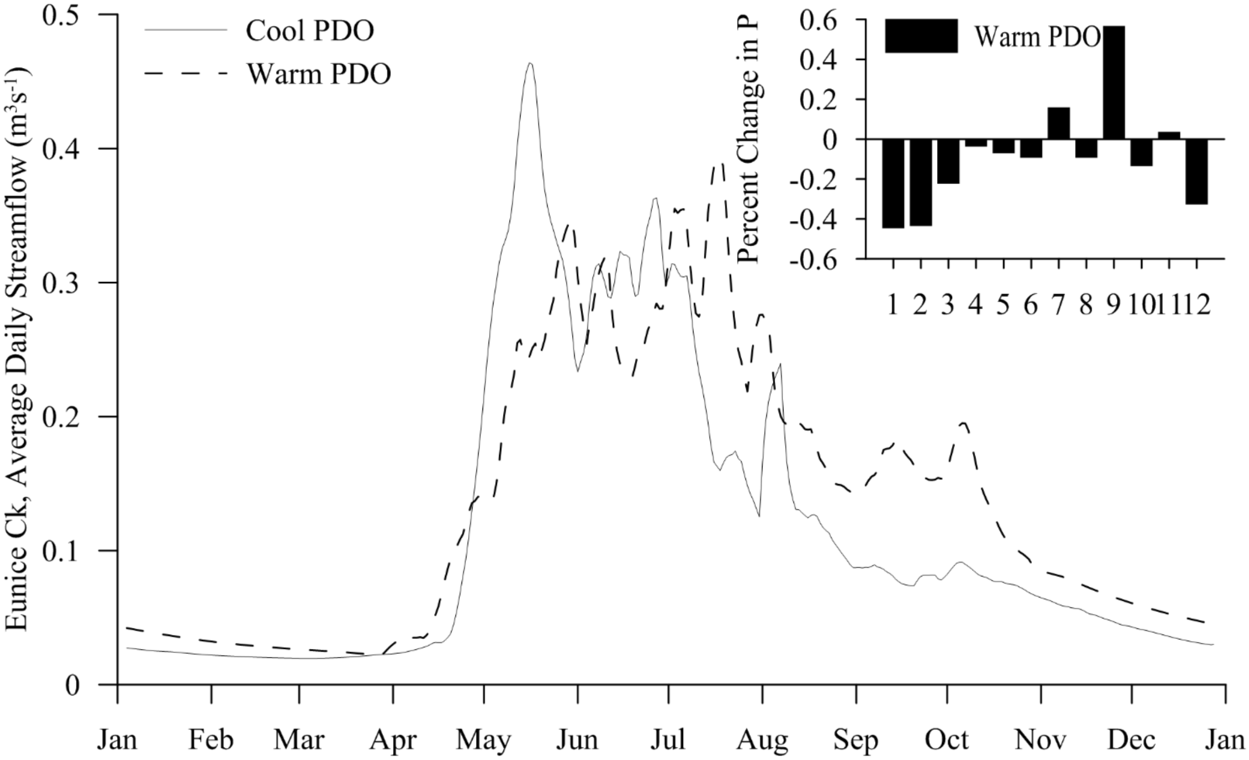

Figure 3.4 Average daily streamflow for Eunice Creek comparing cool PDO phase (1967-1976) to warm PDO phase (1977-1988). A 7-day moving average was used for better visualization of trend. The plot excludes the maximum annual peak in June 1980 because it skews the average hydrograph. The value for June 6th, 1980 with the maximum annual peak was 0.51 m^3 s^{-1}. The inlay plot is the percent change in monthly total precipitation between the cool and warm PDO periods.

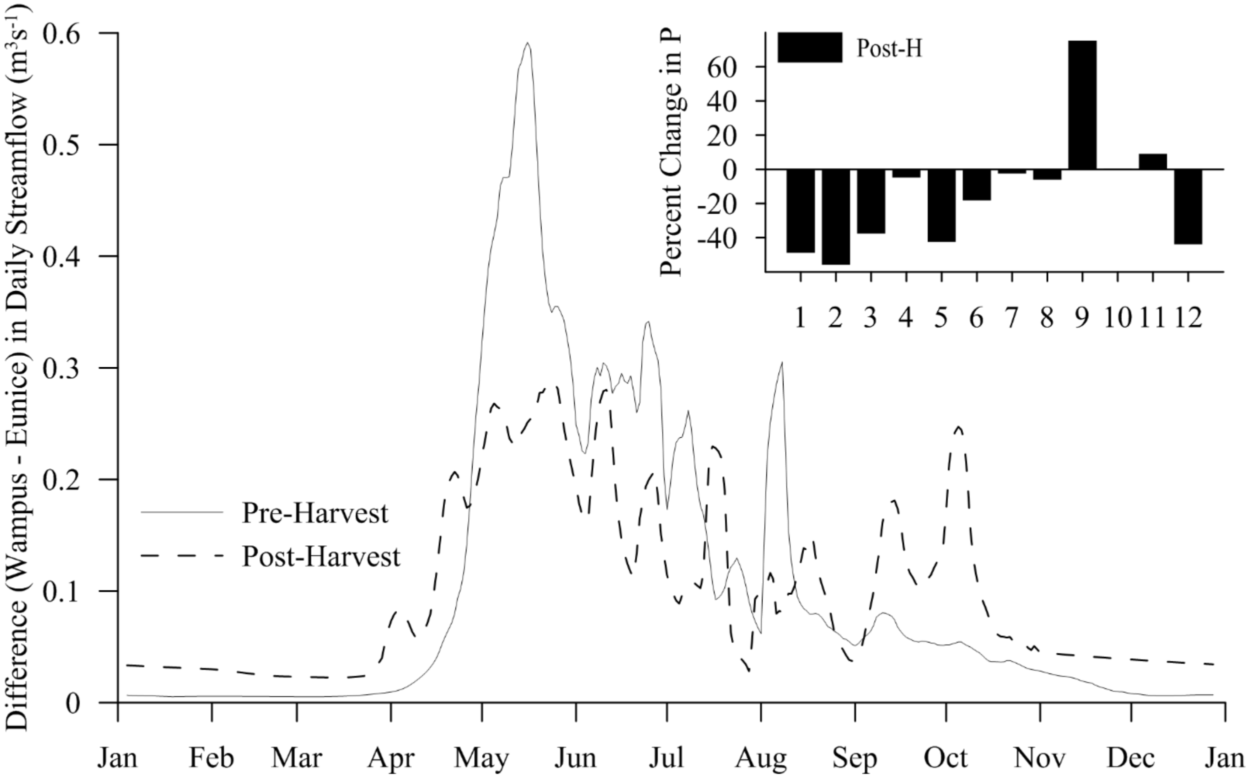

Figure 3.5 Difference in average daily discharge between Eunice and Wampus Creeks prior to harvest (1967 – 1977) and the post-harvest period (1983 – 1988) after 52% clearcut. A 7-day moving average was used for better visualization of trend, but not to calculate the difference in daily streamflow. The inlay plot is the percent change in monthly total precipitation between the pre-harvest and post-harvest period.

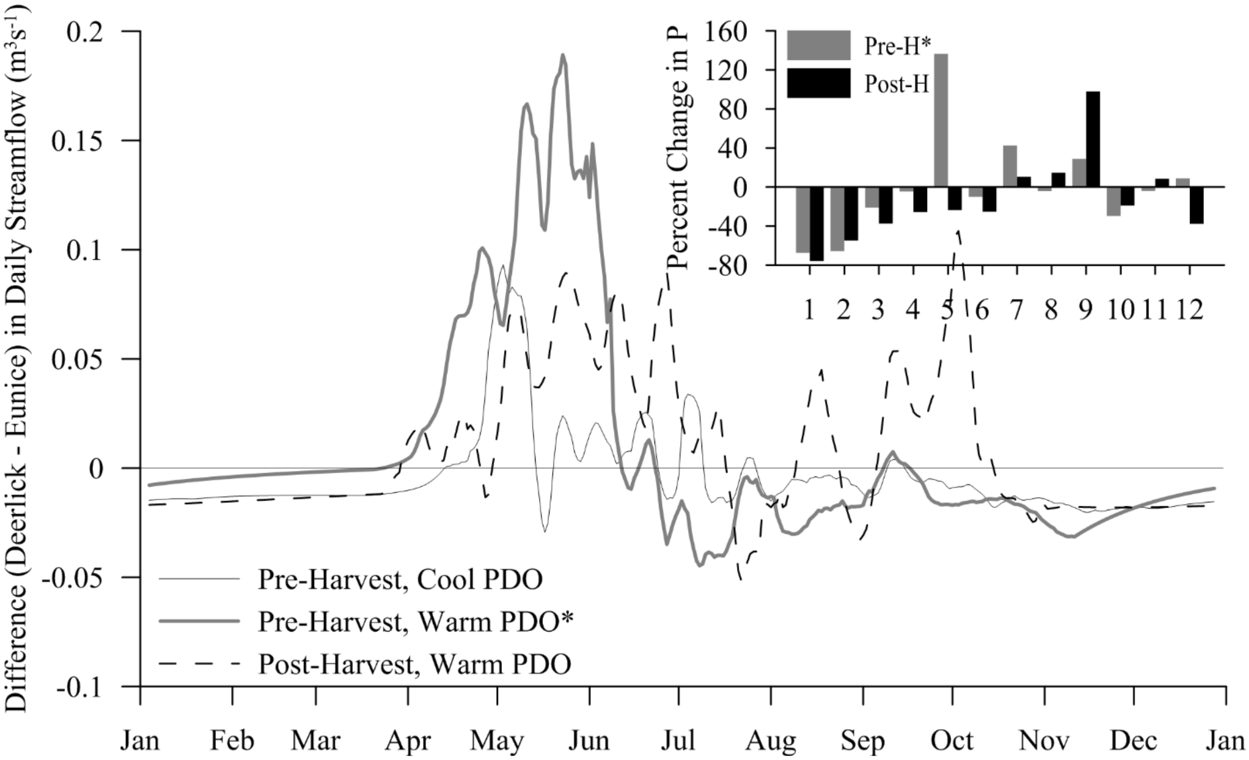

Figure 3.6 Difference in average daily discharge between Eunice and Deerlick Creeks during the pre-harvest period during the cool PDO phase (1967 – 1976) and the warm PDO warm (1977 – 1981), and the post-harvest period (1982 – 1988) after 64% clearcut harvest with streamside timber removal. A 7-day moving average was used for better visualization of trend, but not to calculate the difference in daily streamflow. The inlay plot is the percent change in monthly total precipitation between the pre-harvest (cool PDO) to the pre-harvest (warm PDO) and post-harvest period.

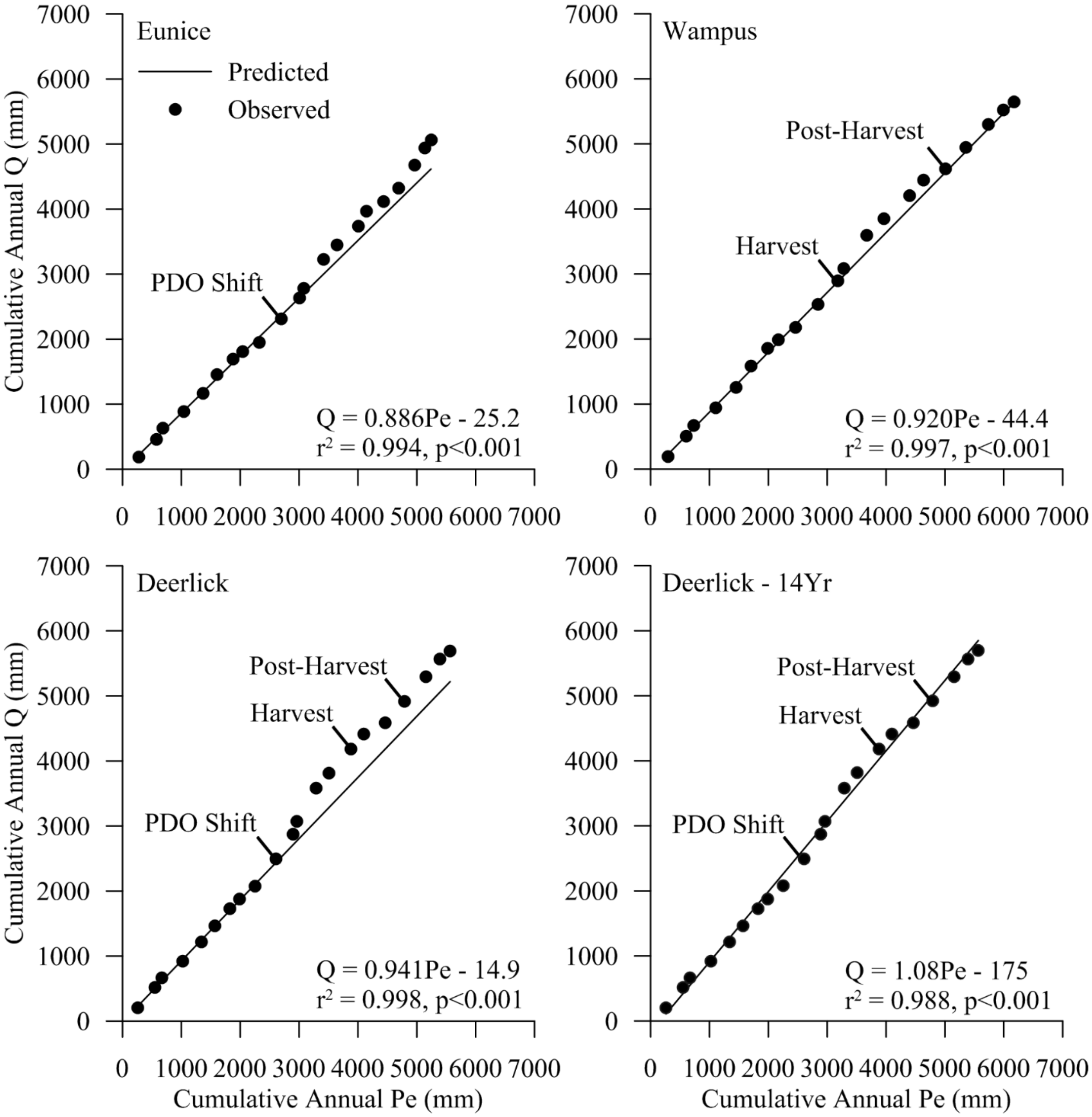

Figure 3.7 Modified double mass curve of accumulated annual runoff (Q) and accumulated annual effective precipitation (Pe) for the Tri-Creek watersheds. Regression calibration periods differed for Eunice Creek (1969-1976), Wampus Creek (1969-1977), and Deerlick Creek (1969 – 1976). An additional linear regression model was fit to the entire pre-harvest period in Deerlick Creek (14 years), which included years during both the warm and cold PDO phases (1969 – 1981).

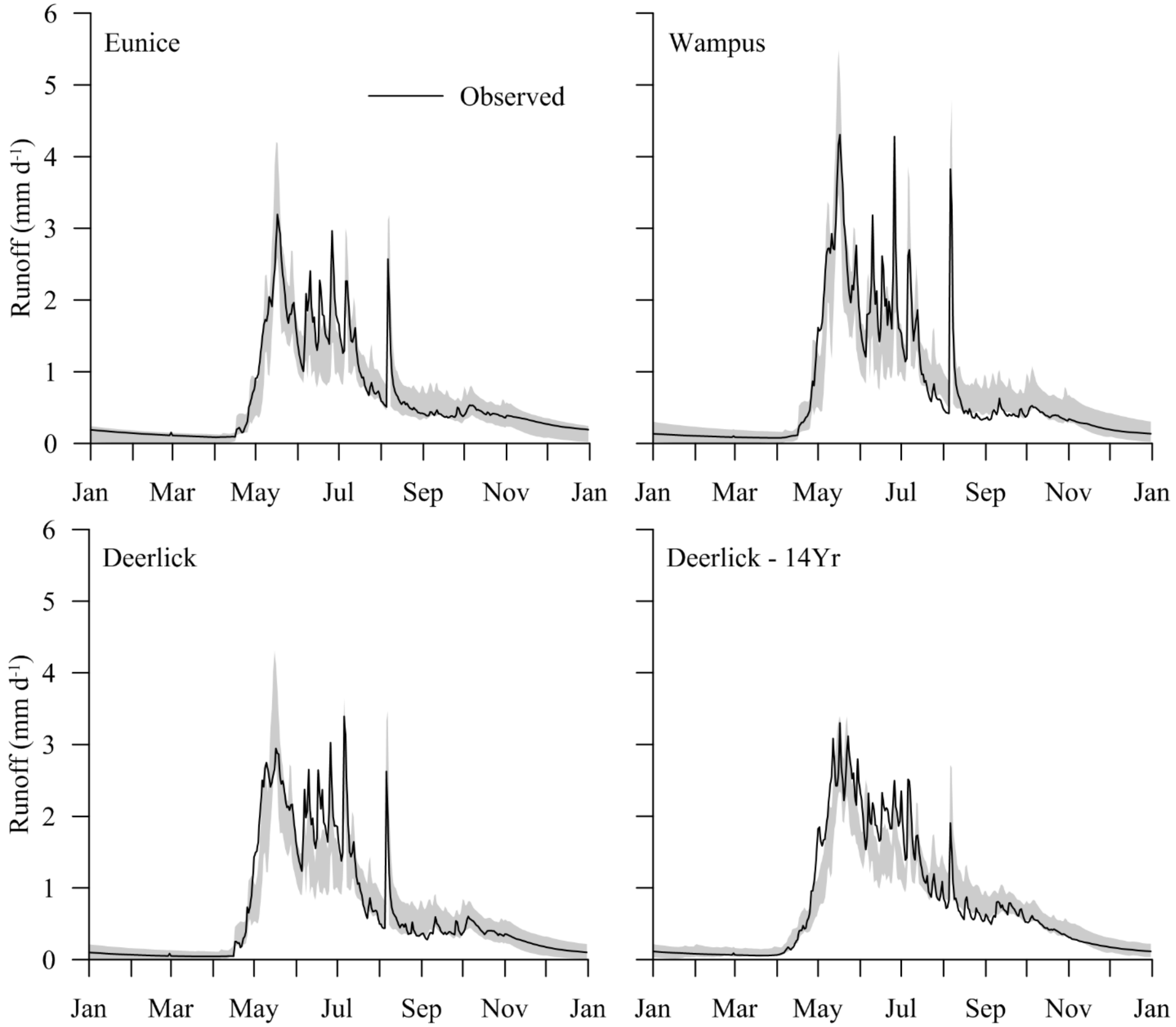

Figure 3.8 The average daily observed runoff and 95th percentile uncertainty bounds (grey) in Tri-Creeks during the model calibration period in Eunice Creek, Wampus Creek, and Deerlick Creek (1969 – 1975; pre-harvest and cool PDO phase). Deerlick – 14Yr includes a 14-year calibration period that occurs during both the cool and warm PDO phases (1969 – 1981).

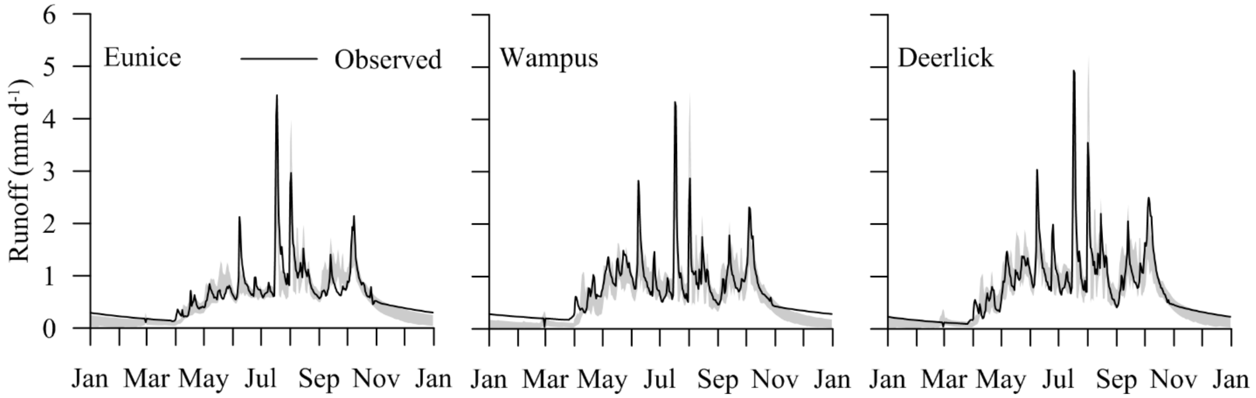

Figure 3.9 The average daily observed runoff and 95th percentile uncertainty bounds (grey) in Tri-Creeks during the model calibration period (plotted 1984 – 1988; post-harvest and warm PDO phase).

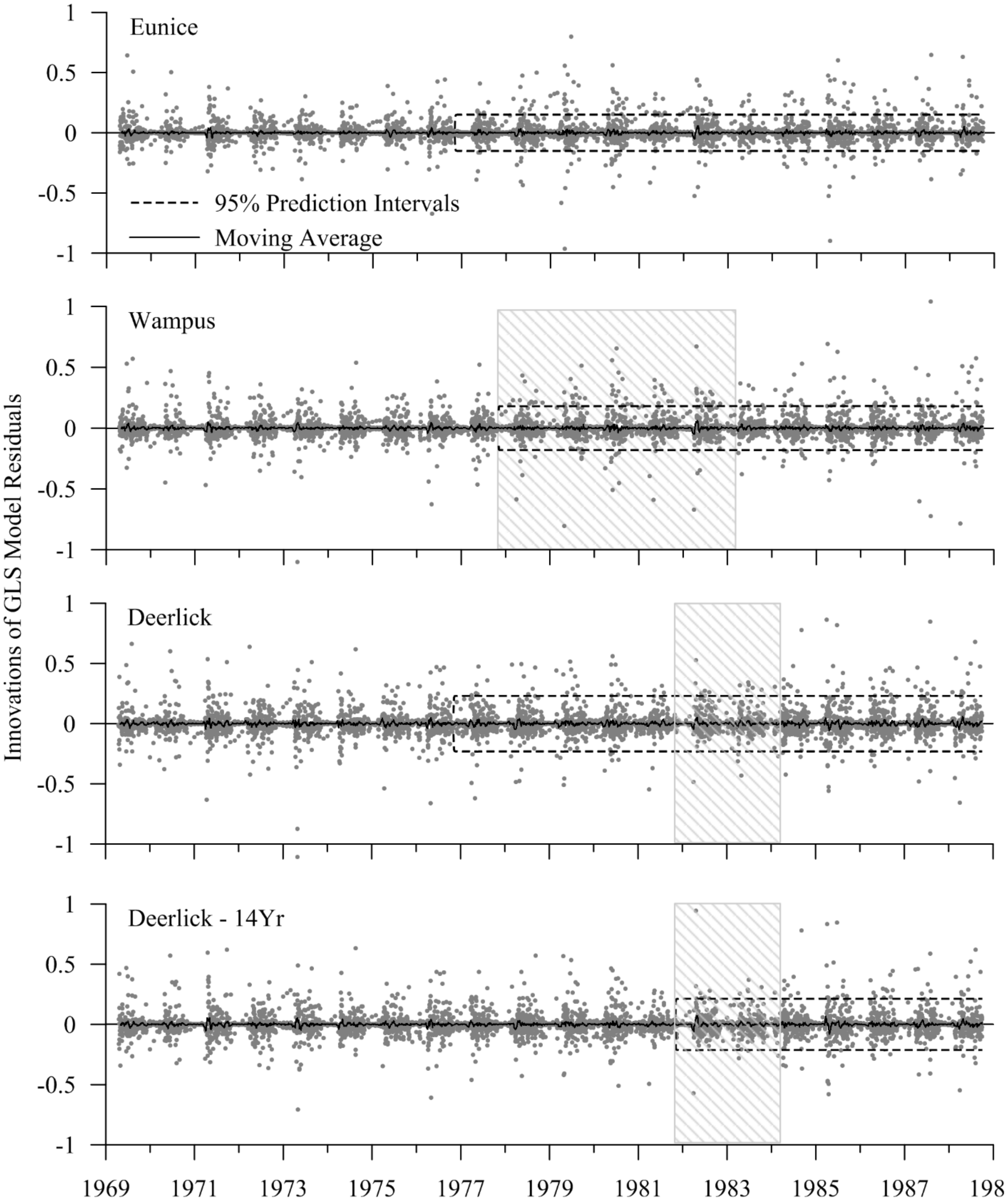

Figure 3.10 Time series of innovations of median GLS model residuals for Tri-Creek watersheds from change detection hydrological modelling and the regression method. The grey hatched box indicates the harvest period. The monthly moving average is shown to facilitate visualization of trend.

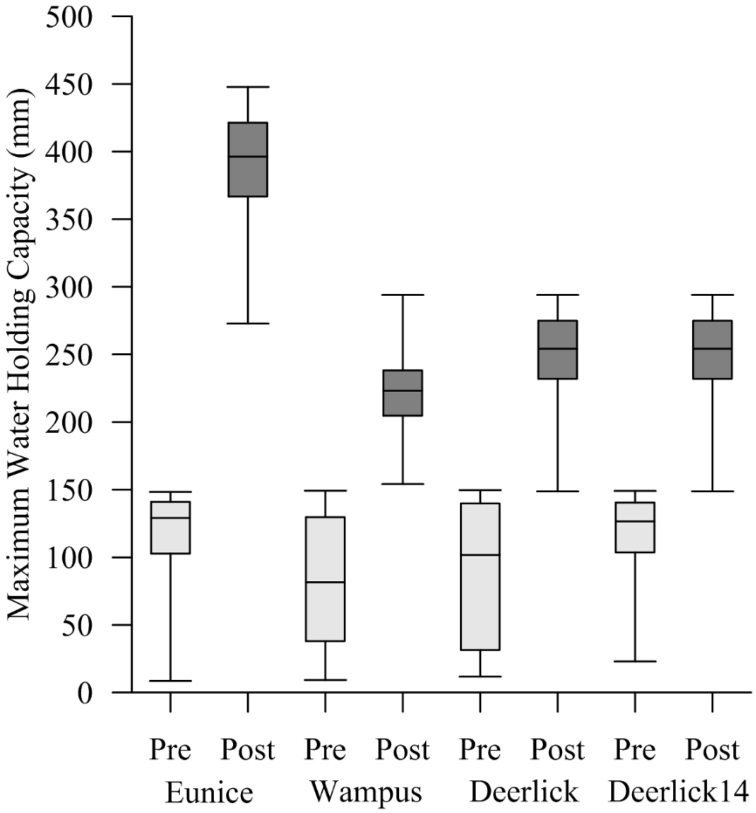

Figure 3.11 Box plots of the distributions of the maximum water holding capacity in the topsoil reservoir for pre-harvest (cool PDO phase) period and post-harvest (warm PDO phase) period. Capacities were calculated using the 100 best parameter values for field capacity (FIELD_CAPACITY) and topsoil reservoir depth (TOPSOIL). For each sample population (n = 100), the line marks the median, the box ends mark the 25th and 75th percentiles, and the bars show non-outlier maximum and minimum values.

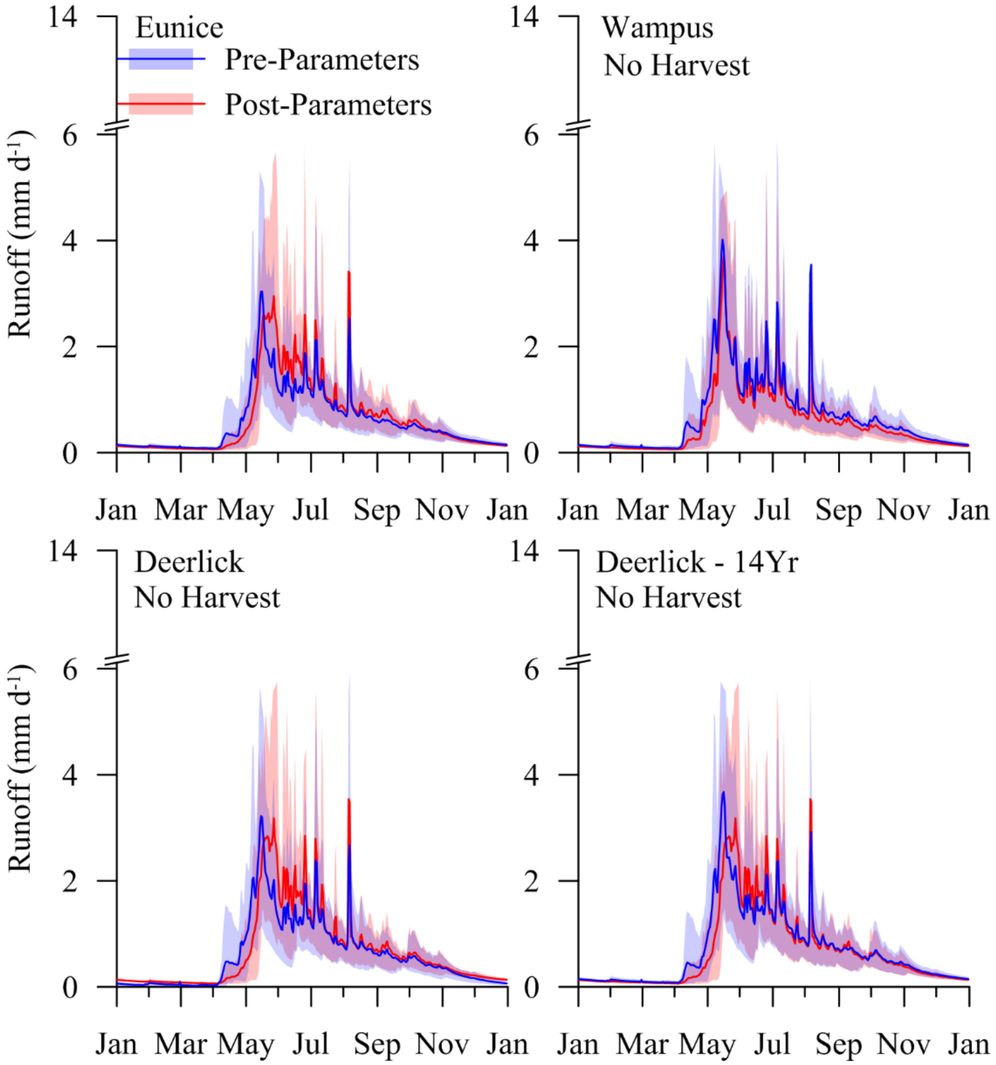

Figure 3.12 Simulated hydrographs for the Tri-Creeks streams reconstructed using the pre- and post-parameters and meteorological input from 1969 – 1975, which compares runoff response to the climate regime shift in the absence of forest harvest. Lines correspond to average daily runoff for the period, while shaded lines correspond to 10th and 90th quantiles. Pre-parameters were calibrated during the cool PDO phase (1969 – 1975) except for Deerlick – 14Yr, which was calibrated during both the cool and warm PDO phases (1969 – 1981). Post-parameters were calibrated during the warm PDO phase/post-harvest condition; however, the model simulations in the treated watersheds reflect the runoff response in the absence of forest harvest.

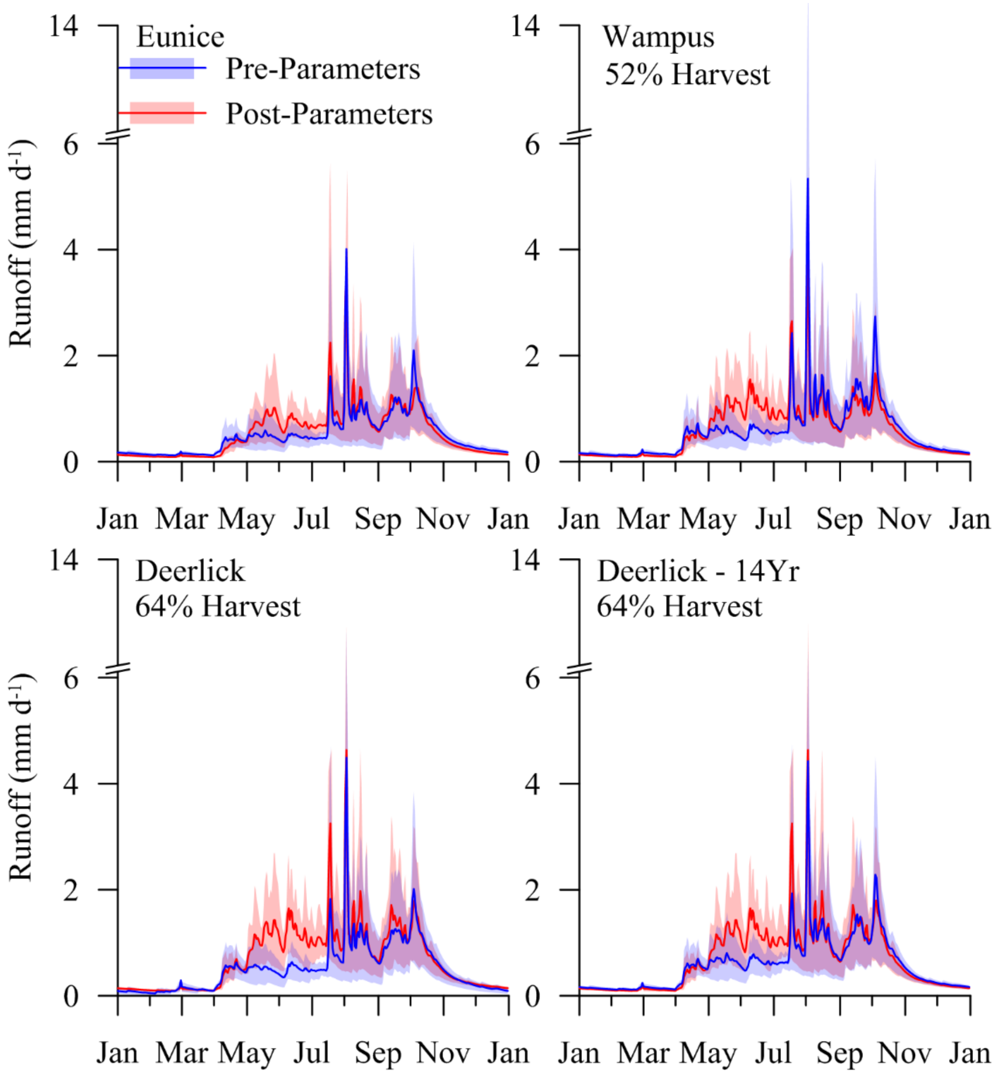

Figure 3.13 Simulated hydrographs for the Tri-Creeks streams reconstructed using the pre- and post-parameters and meteorological input from 1984 – 1988, which compares the runoff response to forest harvest (red line) to the runoff response if there was no harvest (blue line) in the treated watersheds. For Eunice Creek (control), simulated hydrographs compare the runoff response to parameters calibrated in different climate regimes and subsequent runoff generation response. Lines correspond to average daily runoff for the period, while shaded lines correspond to 10th and 90th quantiles. Pre-parameters were calibrated during the cool PDO phase (1969 – 1975) except for Deerlick – 14Yr, which was calibrated during both the cool and warm PDO phases (1969 – 1981). Post-parameters were calibrated during the warm PDO phase/post-harvest condition.

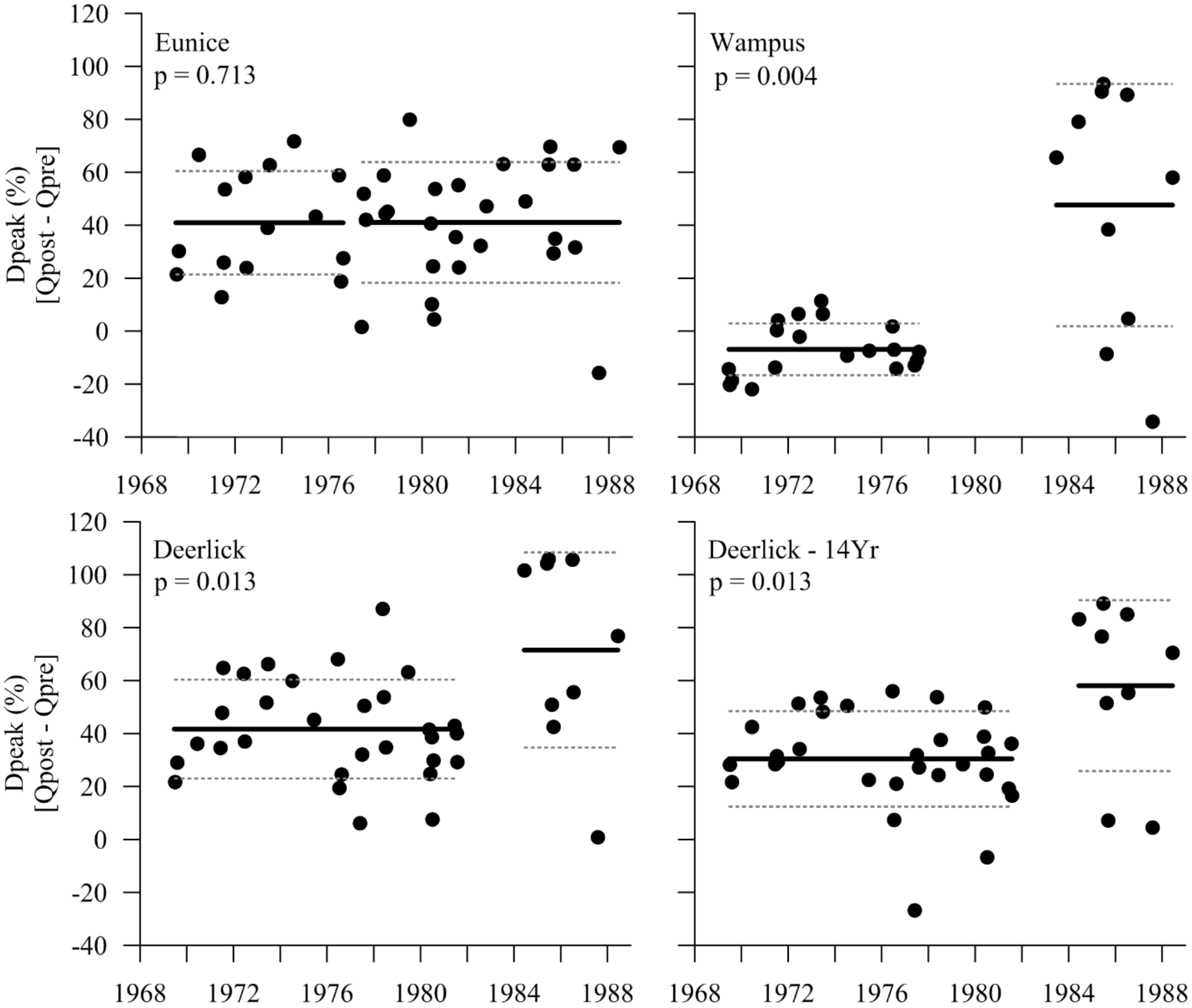

Figure 3.14 The relative difference in rainfall-generated peak runoff events (D_{peak}) simulated with pre- and post-parameters sets during the study period. Black lines indicate the average relative difference in peak runoff events between the cool and warm PDO phases (Eunice) and between the pre- and post-harvest periods (Wampus, Deerlick, Deerlick – 14 Yr). Pre-harvest calibration periods differed for Eunice Creek (1969-1976), Wampus Creek (1969-1977), Deerlick Creek (1969 – 1976) and Deerlick – 14Yr, which included 14 years during both the warm and cold PDO phases (1969 – 1981). The dashed grey lines are the standard deviations. The p-values were calculated using the Wilcoxon rank-sum statistical test.

CHAPTER 4 – EFFECT OF FOREST DISTRUBANCE SCENARIOS ON ATHABASCA RAINBOW TROUT FRY RECRUITMENT IN A FOOTHILLS STREAM

4.1 Introduction

The loss of forest canopy due to mountain pine beetle (MPB) infestation and subsequent forest management strategies could have the potential to affect hydrological processes that change streamflow, alter the physical habitat of streams, and affect in-stream biodiversity. Pine-forested watersheds within western Canada and the United States have seen unprecedented epidemic levels of tree mortality due to MPB (primarily lodgepole pine; Meddens *et al.*, 2012). MPB introduce blue-stain fungi that inhibit sap flow and kill host trees within one year (Hubbard *et al.*, 2013). The needles turn red at tree death (red-attack) and needles fall within three years (grey-attack; Wulder *et al.*, 2006). After five years, the branches begin to drop and trees may start to fall with 90% down after 14 years (Mitchell and Preisler, 1998), which together opens the forest canopy. The canopy openings allow increased throughfall and radiation at the ground surface (Boon, 2012; Winkler and Boon, 2012, Chapter 2). Recent studies suggest reduced overstory tree transpiration and canopy interception losses are compensated by increased snowpack sublimation, increased transpiration of surviving vegetation (non-affected MPB trees) and understory vegetation, and increased soil evaporation as a result of increased soil moisture and subsurface storage (Brown *et al.*, 2013, Biederman *et al.*, 2014a, Biederman *et al.*, 2014b; ; Reed *et al.*, 2014; Reed *et al.*, 2016; Meyer *et al.*, 2017; Chapter 2). The gradual canopy cover loss that follows stand death differs from wildfire and forest harvest because MPB directly affects the overstory without disturbance to the understory vegetation or soil (Adams *et al.*, 2012).

In British Columbia, salvage harvest was motivated by the rapid rate of MPB infestation (BCMoFR, 2005). However, as MPB spreads eastward into Alberta, the provincial management strategy consists of control (i.e. single tree or stand-level harvest of infested pine trees), salvage (i.e. within one year of infestation) or prevention; all of which include forest harvest (ASRD, 2007). The preventative pine reduction strategy was to reduce the number of susceptible pine stands by 75% over the next 20 years through targeted forest harvest (ASRD, 2007). A temporary increase in the Annual Allowable Cut (AAC) was permitted. For example, a management plan in a Foothills region forest management unit (effective 2018) was approved to undertake a 125% accelerated harvest of AAC over the next decade (AAF, 2018). The landscape then becomes a mosaic of dead (MPB grey-attack), alive, and clear-cut harvested stands with varied canopy cover between them. There is a need for forest managers to understand the effect of MPB management strategies on streamflow and the potential negative effects to aquatic life.

Based on decades of forest harvest research, forest cover loss (>20 – 30% watershed area) would lead to increased net precipitation reaching the ground surface, which would presumably increase soil moisture inputs and runoff generated for streamflow (Hibbert, 1967; Bosch and Hewelett, 1982; Stednick, 1996; Moore and Wondzell, 2005). However, studies that document the streamflow response to MPB infestation have provided varied results. Historical paired watershed studies after previous MPB outbreaks in the central Rocky Mountains reported 14-26% greater annual streamflow (Love, 1955; Bethlahmy, 1974; Potts, 1984). However, multi-watershed observations post-MPB epidemic in the western United States show a mix of increased, decreased or unchanged streamflow (Biederman *et al.*, 2015; Slinski *et al.*, 2016). The authors concluded that any changes in streamflow were likely related to climate variability that drives precipitation, snowmelt timing, and streamflow pattern (Biederman *et al.*, 2015; Slinski *et al.*, 2016). The inherent variability makes it difficult to detect forest disturbance from the background climate signal (Burt *et al.*, 2015; Chapter 3), which complicates traditional paired watershed and observational field studies (e.g. Bethlahmy, 1974; Potts, 1984; Slinkski *et al.*, 2016).

A hydrological modelling approach becomes important to detect the effect of forest disturbance if differences are masked by background climate variability in long-term streamflow observations. Model simulations in snow-dominated watersheds (65 to 85% precipitation as snow) found annual streamflow volumes only increased 2% in Alberta (Pomeroy *et al.*, 2012) and 11% in Colorado (Penn *et al.*, 2016). The large snowmelt inputs from the alpine areas and addition of water from adjacent unaffected areas (i.e. healthy forest, non-forested area) likely resulted in the muted forest disturbance signal from MPB (Pomeroy *et al.*, 2012; Penn *et al.*, 2016). More specifically, the increases in streamflow were small relative to inter-annual variability because runoff contributions from unaffected areas muted the watershed-scale response, but also compensatory changes in snow and ET processes mitigated the hillslope-scale response (Penn *et al.*, 2016). Similar compensatory ET processes were found to mitigate the response to MPB in a grey-attack stand in the Alberta Foothills (Chapter 2). However, there is still a need to integrate this hydrological process knowledge with hydrological modelling to understand the streamflow response to MPB and current forest management strategies for fully-forested watersheds.

In snow-dominated forested watersheds, the annual hydrograph is dominated by the spring-early summer snowmelt, which reliably produces much of the annual flow volume and maximum annual peak flow (e.g. Wagner, 2010; Spencer *et al.*, 2019). In contrast, Foothills streams have a lower predictability of seasonal flooding (i.e. maximum annual peak flow) given the stochastic nature of large summer rainfall events (Natural Regions Committee, 2006; Chapter 3). However, both rainfall and snowmelt depth and intensity, in relation to antecedent soil conditions, were strong controls on runoff generation in Foothills watersheds (Chapter 3). In addition, climate variability associated with large-scale ocean-atmosphere circulation, like the Pacific Decadal Oscillation (PDO), drives changes in precipitation and air temperature that could result in different watershed responses in warm (positive) versus cool (negative) PDO phases (Shrestha *et al.*, 2016, Chapter 3). For example, during a cool PDO phase, greater peak SWE and more frequent large rainfall events resulted in wetter antecedent conditions and more of the watershed area was predicted to generate runoff (Chapter 3). Hydrological modelling also predicted significant increases in rainfall-generated peak runoff events and summer runoff following harvest in two Foothills watersheds (Chapter 3). Streamflow changes concern fisheries managers as increased flow can alter physical stream habitat and affect aquatic biodiversity.

Natural disturbances (floods, fires, bark-beetle outbreaks) are part of most intact aquatic ecosystems, which regulate population size and species diversity (Lytle and Poff, 2004). Over time, species evolve life history strategies or behaviours to persist amongst these disturbances. Specifically, salmonid species have evolved their spawning and rearing life stages around annual streamflow patterns (MacIssac, 2010). In addition, salmonids excavate egg pockets into the streambed substrate (i.e. redd) at a depth that limits potential scour of spawning substrates that incubate embryos (DeVries, 1997). During the incubation period, high streamflow can potentially scour the streambed substrate and contribute to egg mortality (i.e. crushing or exposure; Sterling, 1992; Lapointe *et al.*, 2000). Therefore, salmonids could be affected by flow-regime changes that occur outside their normal range of timing, frequency and magnitude (Lytle and Poff, 2004).

Studies have raised concern about the potential scour of redds due to more frequent high flows during the salmonid incubation periods as a result of anthropogenic threats, i.e. human changes to aquatic ecosystems. For example, altered streamflow regimes in future warmer climates may result in increased depth of scour during salmonid incubation that may affect individual year cohorts, but several studies found limited risk to salmonid population decline (Goode *et al.*, 2013;

McKean and Tonina, 2013). The population decline in Bull Trout in an Idaho watershed could not be fully explained by an increase in the frequency and depth of scour due to streamflow changes from forest harvest (Tonina *et al.*, 2008). In Alberta, percent area disturbed from industrial activity (mainly forest harvest) and road density were found to negatively affect the abundance of salmonid species (Bull Trout, Rainbow Trout) compared to reference watersheds (Scrimgeour *et al.*, 2008), but the authors did not investigate the mechanisms by which forest harvest influenced population abundance. However, to my knowledge, no studies have documented the potential streamflow changes due to forest harvest and the direct effect on salmonid fry recruitment.

The Athabasca River population of Rainbow Trout (ARTR), like other salmonids, are sensitive to streamflow changes for successful incubation of embryos and emergence of fry (Sterling, 1992). ARTR fry abundance was found to be inversely correlated with streamflow exceeding a critical discharge (0.731 $m^3 s^{-1}$; r = -0.82, p = 0.0066); the discharge when spawning substrate begins to move downstream (hereafter "ARTR $Q_{0.731}$"; Sterling, 1992). ARTR spawn from late May to early June during the snowmelt recession and construct a redd (10 – 12 cm deep, 3 – 4 egg pits) a short distance upstream of a riffle crest where stream hydraulics provide optimal substrate particle size, water velocity, water depth, and interstitial flow (Dietz, 1971; Sterling, 1986). However, ARTR were observed to locate redds along stream margins if high flows occurred during the spawning period, which were vulnerable to exposure in the event of low summer flow. Conversely, redds were located nearer the channel center if low flow occurred during the spawning period and were vulnerable in the event of high summer flow (Sterling, 1992). Given the unpredictable summer storm events in the Alberta Foothills, ARTR have evolved to cope with extreme flow events and persist in their historical range (Rasmussen and Taylor, 2009). Therefore, some natural variability in timing, magnitude and frequency of extreme events has been tolerated, but events outside the range of natural variability as a result of an unprecedented MPB epidemic or subsequent forest management strategies could lead to poor species success.

Athabasca Rainbow Trout are a unique ecotype found only in the upper Athabasca River watershed and the only native population of rainbow trout in Alberta (COSEWIC, 2014). ARTR were assessed as endangered in 2014 (COSEWIC, 2014) and listed under the *Species at Risk Act* in 2019 (Fisheries and Oceans Canada, 2020). Population abundance data showed declines over 15 years in approximately 54% of streams where data records exist (COSEWIC, 2014). For the ARTR group, the rate of decline was estimated at approximately 96.5% based on a time series of

52 sites (Sinnatamby *et al.*, 2020). ARTR are considered extirpated from Jasper National Park as a result of hybridization with stocked non-native rainbow trout. ARTR population success is threatened by forest harvest according to federal recovery plans (Fisheries and Oceans Canada, 2020); therefore, further research to better understand the effect of forest disturbance on streamflow regimes and ARTR recruitment success is needed, and was a knowledge gap and research priority outlined in the Alberta ARTR recovery plan (Alberta ARTR Team, 2014).

The long-term historical Tri-Creeks Experimental Watershed forestry experiment (Tri-Creeks; Andres *et al.*, 1987; Sterling *et al.*, 2016) and more recent before-after control-impact (BACI) MPB stand-level study (Robb MPB Ecohydrology Site; McIntosh and McDonald, 2010; Piña, 2013; Steinke *et al.*, 2020) provides the opportunity to develop a modelling approach to explore the question: what is the effect of potential streamflow changes from forest disturbance scenarios on Athabasca Rainbow Trout fry recruitment in a Foothills stream? I hypothesized that reduced total evapotranspiration and increased net water input into the soil in clear-cut harvest areas would result in greater streamflow above the ARTR $Q_{0.731}$ during the incubation period compared to MPB grey-attack. I also hypothesized that streamflow above the ARTR $Q_{0.731}$ during the incubation period will be greater in a cool PDO than a warm PDO period. My objectives were to integrate stand-level hydrologic process knowledge (Chapter 2) into a watershed-scale hydrological model (Chapter 3) to quantify the streamflow above the ARTR $Q_{0.731}$ during the incubation period predicted from scenarios that include a reference condition and a combination of clear-cut harvest, MPB grey-attack and undisturbed mature, even-aged lodgepole pine. The last objective was to estimate ARTR fry escapement over 50 years using the relationship between streamflow above the ARTR $Q_{0.731}$ and fry density established in Tri-Creeks (Sterling, 1992). This information will aid in decisions about current MPB strategies in the Alberta Foothills region with respect to the endangered Athabasca Rainbow Trout.

4.2 Study Site

This chapter builds on research from the Robb MPB Ecohydrology site (Chapter 2) and Tri-Creeks (Chapter 3), which are located 31 km apart (Figure 4.1). When Tri-Creeks was active (1965 – 1985), Wampus Creek was one watershed included in the intensive studies to determine whether forest harvest altered the population dynamics of ARTR (Dietz, 1971; Andres, 1974; Sterling, 1978; 1980; 1986; 1990; 1992).

4.2.1 Wampus Creek Watershed

Wampus Creek (28.3 km^2) is located 20 km west of Robb, Alberta (53.157°N, 117.262°W) in the Upper Foothills natural subregion of Alberta (Natural Regions Committee, 2006; Figure 4.1). Topography of the area is gentle to moderate, with slopes of 1 – 40% and elevations range from 1249 – 1690 m.a.s.l. This region consists of folded and fractured sedimentary bedrock that primarily alternates between sandstone, siltstone and shale bedrock (Currie, 1969). The bedrock is overlain at depths of 3 – 21 m with glaciolacustrine deposits at elevations less than 1380 m.a.s.l. and local sandy loam till deposits between elevations of 1380 – 1440 m.a.s.l. (Currie, 1969). At elevations above 1440 m.a.s.l., bedrock is overlain with glacial till deposits at depths of 1.5 m from surface or exposed. Soils are predominantly brunisols and luvisols, with some gleysols and organics (Dumanski *et al.*, 1972). Historical samples of water isotopes, water chemistry and radioactive tritium isotopes collected in Tri-Creeks (1984 – 1986) indicate a groundwater flow system with local and intermediate flow paths with short residence times (i.e. duration of time groundwater remains in subsurface) within the glacial till and sedimentary bedrock units (Andres *et al.*, 1987).

The climate is characterized as continental sub-humid, with long cold winters modified by short periods of chinook winds, and short cool summers with monthly average temperatures ranging from 11°C in July to -13°C in January (Hillman *et al.*, 1978). The warm, dry chinook winds are generated as pacific air masses ascend the leeward side of the Rocky Mountains and can increase the air temperature by 20ºC or more within hours and drop again as rapidly (Jablonski, 1978). Average annual precipitation is 615 mm with 39% falling as snow. Snowfall and winter air temperatures (T_a) in Wampus Creek significantly change dependent on the PDO phase (Chapter 3). A cool PDO phase (warm PDO phase) typically results in a cooler winter T_a (warmer winter T_a) and a greater portion of precipitation falls as snow (rain; Figure 4.2). The largest amount of precipitation falls in July and is highly variable from 6 to 272 mm month^{-1} (Figure 4.3).

The watershed is almost entirely forested with limited bedrock outcropping and small areas of grass and shrub adjacent to stream channels. Major tree species include lodgepole pine (*Pinus contorta* var. latifolia Dougl.), alpine fir (*Abies lasiocarpa* (Hook.) Nutt.), black spruce (*Pinus mariana*), and white spruce (*Picea glauca*). Lodgepole pine is predominant in the headwaters, while black spruce occurs in the valley bottoms, and mature stands consist of white spruce-fir associations (Winkler and Rothwell, 1983).

Prior to the forestry experiment, 0.6% of the Wampus Creek watershed area was select and clear-cut harvested but assumed to not impact the experiment (Andres *et al.*, 1987). The Alberta Forest Service harvesting ground rules (1973) were applied to harvest operations. Haul roads were built from 1975 to 1978 that resulted in a road density of 0.46 km km^{-2} in Wampus Creek. After a 10-year calibration period (1967 – 1977), 52% of Wampus Creek was clear-cut logged over a six-year period (1978 – 1983). Cutblock size ranged from 13 – 200 ha (Nip, 1991). Harvesting was done in the winter to minimize soil disturbance. Silvicultural treatments for reforestation of the cutblocks included drag, ripper or Bracke scarification, which was completed within one year of harvest (Nip, 1991).

During the pre-harvest period, Wampus Creek water year (WY, 1 October – 30 September) runoff ranged from 131 to 357 mm and largely consisted of baseflow (71%; Chapter 3). Snowmelt does not typically generate the maximum annual peak flows, but rather these occur in the summer with large variability in their magnitude and timing due to rainfall events (Figures 4.3 and 4.4). For example, 105 mm of rainfall in one day generated the maximum annual peak flow in 1969, while snowmelt runoff was lower than average (Figure 4.4).

Wampus Creek is a 3rd order stream with a 15.8 km main channel length, 18.9 m km^{-1} mainstem gradient and 2.8 km km^{-2} drainage density. The streambed was classified as gravel with a surface substrate median grain size of 57 mm (Andres, 1974). The mean stream width and depth of the lower fish study section of Wampus Creek were 4.94 m and 0.14 m, respectively (W-A; Figure 4.1; Sterling, 1990).

Fish populations include Bull Trout (*Salvelinus confluentus*) juveniles, while spawning Bull Trout were observed only in August and September (Sterling, 1992). Adult and juvenile Mountain Whitefish (*Prosopium williamsoni*) were seasonally abundant in the lower reaches. Brook Trout (*Salvelinus fontinalis*) were scarce and limited in distribution in the lower reaches prior to 1985. However, subsequent sampling post-1985 indicates Brook Trout abundance has increased in lower Wampus in the past decade (Figure 4.5; Alberta ARTR Team, 2014).

Wampus Creek is dominated by a discrete stream-resident ARTR population (Dietz, 1971; Sterling, 1978). The overlap of the Wampus Creek resident trout population and the McLeod River migrant trout population is assumed to be limited (Sterling, 1980). River-migrant trout were found to use the lower reaches of Wampus Creek to spawn; however, no tagged river-migrant trout were captured more than 2 km upstream (Sterling, 1980). In addition, 0.2% of fin-clipped and tagged stream-resident trout (n = 2,578) were later recaptured in McLeod River by anglers in the 1970s (Sterling, 1980).

Wampus Creek was identified as a benchmark stream to assess the fluctuations in regional ARTR populations over time (Rasmussen and Taylor, 2009). The ARTR population in Wampus Creek has been frequently sampled from 1969 to 2013 and the stream has been closed to recreational fishing since 1965. Population estimates obtained from mark-recapture experiments show ARTR abundance naturally varies with large declines after major flood events, e.g. 1969, 1980 and 1999 (Figure 4.5). Over the period of record, ARTR population abundance has exceeded 100 fish/0.1 ha and rarely fell below 50 fish/0.1 ha (Figure 4.5A; Sterling, 1990). The abundance levels show a consistent pattern of recovery within four to five years from the combined effects of large peak flow events and forest harvest (52% watershed area; Figure 4.5B; Rasmussen and Taylor, 2009; Alberta ARTR Team, 2014).

4.2.2 Robb Mountain Pine Beetle Stand-Level Study

The MPB Ecohydrology site (MPB Robb) is located 11 km east of Robb (53.241ºN, -116.826º W; 1,130 m.a.s.l.) in the Upper Foothills natural subregion of Alberta (Natural Regions Committee, 2006; Figure 4.1). The site represents a region of pure lodgepole pine (*Pinus contorta* var. latifolia Engelm.) forest with mixed conifer stands of white spruce (*Picea glauca* (Moench) Voss) and subalpine fir (*Abies lasiocarpa* (Hook.) Nutt.). The climate is characterized as temperate continental with monthly average temperatures ranging from 15ºC in July to -10ºC in December. Winters are cold, except for occasions with chinook winds. Average annual precipitation is 586 mm with 27% falling as snow. The soils are brunisolic gray luvisols with a silt-loam texture (Piña, 2013).

MPB Robb used a BACI randomized block design to construct controlled tree mortality treatments and simulate MPB attack stand level effects. The overstory included only lodgepole pine. There were very few white spruce, black spruce (*Picea mariana* (Mill.)), trembling aspen (*Populus tremuloides* Michx.), and balsam fir (*Abies balsamea* (L.) Mill.) in the lower canopy. Details of the experimental design and chemical treatment to simulate MPB attack were reported by others (McIntosh and Macdonald, 2013; Steinke *et al.*, 2020) and briefly outlined in Chapter 2. This chapter will only focus on the stand-level process knowledge and detailed measurements collected from the untreated mature, even-aged lodgepole pine (100% pine) control (hereafter

"Pure Pine") and simulated high intensity (100% trees affected) MPB grey-attack treatment (hereafter "MPB Grey").

Concurrent meteorological data and snow surveys (Aug 2015 to Sep 2017) collected at MPB Robb (60 m x 60 m snow grid) and Wampus Creek (60 m long snow course with 30 points) were assessed to reduce uncertainty in model parameters used for forest disturbance scenarios. Meteorological data collected concurrently at MPB Robb and Wampus Creek (Aug 2015 – Sep 2017) indicated an average growing season difference in monthly air temperature. MPB Robb was 17% warmer than Wampus-8 (range 1.1 to 2.3ºC) and 27% warmer than Wampus-A (range 2.4 to 3.2ºC). Average growing season difference in monthly precipitation between MPB Robb and Wampus-8 was 32% (range -51 to 102 mm) and between MPB Robb and Wampus-A was 16% (range -73 to 109 mm). The large variability in monthly rainfall was a result of convective storm systems in the Foothills region. In addition, snow surveys in 2016 and 2017 at MPB Robb (Pure Pine; 1,130 m.a.s.l.) indicate snow water equivalent (SWE) fell within range of that measured in the mature forest at Wampus-H (1,323 m.a.s.l.) and Wampus-8 (1,572 m.a.s.l.). The average relative difference in snowpack SWE within undisturbed mature forest between MPB Robb and Wampus-8 was 21% (range -26 to 44 mm; $n = 6$) and between MPB Robb and Wampus-H was 91% (range 2 to 76 mm; $n = 7$).

4.3 Methods

4.3.1 Data Sources and Processing

Daily climate data (maximum and minimum temperatures, and precipitation) were available from the Tri-Creeks forestry experiment from June 1967 to Dec 1985 at Wampus-C (Figure 4.1). Air temperature (°C) was measured by hygrothermographs located in Stevenson screens with a maximum and minimum thermometer for more accurate daily temperature readings (Figure 4.1). Total daily precipitation was measured and recorded using a Q12M Sacramento automatic weighing gauge (mm d^{-1}).

After Tri-Creeks was decommissioned, long-term climate data from nearby Hinton (Environment and Climate Change Canada; Climate ID 3063526, 1,227 m.a.s.l., 37 km northwest) and Luscar Creek (Alberta Environment and Parks; 1,524 m.a.s.l., 4 km south; Figure 4.1) meteorological stations were used to construct daily precipitation, maximum and minimum air temperature records from January 1986 to October 2019. Air temperature was reconstructed using Hinton (1986 – 2011, monthly linear regressions, average $r^2 = 0.90$) and Luscar (2011 – 2019). A daily precipitation record was constructed using Luscar (2011 – 2019) and the relative (percent) difference in monthly precipitation between Wampus-C and Hinton (1986 – 2011).

4.3.2 Wampus Creek Hydrological Model

Daily streamflows for reference and forest disturbance scenarios were predicted using a previously calibrated and verified hydrological model (Chapter 3). The Raven Hydrological Modelling Framework (v2.9.2, Craig *et al.*, 2020) was used to simulate streamflow in Wampus Creek using a modified version of the HBV-EC model (Appendix B; Bergstrom *et al.*, 1995; Canadian Hydraulics Centre, 2010).

Daily air temperature (minimum, maximum and average) and precipitation were spatially distributed across the watershed using inverse-distance weighting. The model was discretized using hydrological response units (HRUs) that group areas of similar elevation, aspect, slope and landcover. Vertical climate gradients were represented by subdividing the basin into 100 m elevation bands.

Precipitation was partitioned into rain or snow using the HBV-EC algorithm (Bergstrom, 1995) where a linear transition between all snow and rain is determined from the average daily temperature using a rain/snow transition temperature and a rain-snow transition zone (2ºC). Precipitation intercepted by the forest canopy was removed by evaporation and controlled by the leaf area index and vegetation cover in each HRU (Bergstrom, 1995; Hedstrom and Pomeroy, 1998). Snowmelt was simulated using a corrected degree-day approach (Bergstrom, 1995). Rain and snowmelt infiltrated a conceptualized three-layer soil structure based on available water storage. Storm runoff that did not contribute to the topsoil reservoir (stored water that could eventually evaporate), either contributed to streamflow as rapid flow to the stream channel (fast reservoir) or through groundwater recharge (slow reservoir). Groundwater recharge was a function of soil moisture, while soil evaporation and transpiration were a function of soil moisture and potential evapotranspiration (ET). Slight variations to the HBV-EC model included algorithms for forest canopy snow interception (Hedstrom and Pomeroy, 1998), calculation of daily potential ET (Hargreaves and Samani, 1985), and the Variable Infiltration Capacity routine for non-linear baseflow response in the slow reservoir (Clark *et al.*, 2008).

Forest floor interception was determined to be an important hydrological process at the stand-level (Chapter 2). However, rainfall interception by the forest floor layer would have been difficult to incorporate into the model structure at the watershed-scale. Therefore, canopy and forest floor rainfall interception were calculated for storm events during the study period using empirical equations from MPB Robb (Chapter 2). The percent of intercepted rainfall was combined for the canopy and forest floor, which was input as a daily time-series of user-specified parameter values.

Model calibration and verification of the Wampus Creek hydrological model was outlined in Chapter 3. Briefly, the model was calibrated automatically in Ostrich (v17.12.19; Matott, 2019) using dynamically dimensioned search (DDS) optimization (Tolson and Shoemaker, 2007). The DDS – approximation of uncertainty (DDS-AU) algorithm quantified the prediction uncertainty by identifying behavioral parameter sets through repeatedly applying a DDS search from alternative random starting points in the parameter space (Tolson and Shoemaker, 2008). There were 60,000 model evaluations (150 optimization trials). The parameter sets from the 100 optimization trials with the highest values of Nash Sutcliffe model efficiency (NSE) were selected to characterize the prediction bounds. The median value for each parameter was used to predict streamflow.

Streamflow in Wampus Creek was simulated with two hydrological models that represent varied antecedent soil conditions as a result of PDO driven meteorological changes and subsequently the expansion of saturated areas within the watershed that connect to generate runoff (Chapter 3). More runoff was predicted in the cool PDO phase when peak SWE was higher and spring/summer antecedent soil conditions were wetter (hereafter “cool/wet” model; calibrated 1969 - 1975). Less runoff was predicted in the warm PDO phase when peak SWE was lower and winter air temperatures were warmer, which resulted in earlier snowmelt and drier spring/summer antecedent soil conditions (hereafter “warm/dry” model; calibrated 1983 - 1988).

Hydrological model performance indicated good agreement in model efficiency (NSE) and volumetric error (mean percent bias error; PBIAS) between observed and simulated streamflow for the cool/wet model (NSE = 0.76; PBIAS = 1.4%) and warm/dry model (NSE = 0.76; PBIAS = 1.0%; Chapter 3). Simulated snow water equivalent (SWE) showed good agreement with observations, while accumulated seasonal precipitation collected in Sacramento gauges was also well-emulated (Chapter 3).

Additional data were used to evaluate the ability of the hydrological models to predict streamflow. The warm/dry model (calibrated in the post-harvest period) was used to compare simulated to observed streamflow during another warm PDO period (1992 – 1996). This period was 9 to 14 years post-harvest, but full hydrologic recovery of the cutblock vegetation was assumed minimal as canopy cover may not return to pre-disturbance levels for at least 25 years post-harvest (Winkler *et al.*, 2010). This analysis could not be repeated with the cool/wet model as it was calibrated during the pre-harvest period.

4.3.3 Runoff Source Areas

The transport tool in Raven tracks a conservative tracer through storage reservoirs to discriminate between various runoff sources in a watershed. For example, rainfall-sourced or snowmelt-sourced contributions to streamflow. The transport tool could also be used to determine the relative proportion of streamflow generated by different areas of the watershed (Craig *et al.*, 2020). For this specific application, all water that passes through the storage reservoir ‘ponded water’ was tagged with a concentration of 1.0, then implicitly all other water stored elsewhere has a concentration of 0.0. The daily concentration output from specified HRU groups and the watershed hydrograph determine the runoff contribution from the source areas.

The transport tool was used to discriminate between various runoff source areas in Wampus Creek using the reference condition for both models. Different watershed slope aspects and gradients were used to determine areas sensitive to forest disturbance that contribute the most runoff. A slope gradient >9º (hereafter “upper”; 41% total watershed area) and ≤9º (hereafter “lower”; 52% total watershed area) coincides with the natural break in watershed slope (Winkler and Rothwell, 1983). This slope classification corresponds to the upper 2/3 and lower 1/3 of the watershed slope. The slope aspect of the upper watershed was classified into north (337.5º - 67.6º; 24% total area) and south (112.5º - 247.5º; 11% total area).

4.3.4 Forest Disturbance Scenarios

The detailed field measurements and hydrological process knowledge gathered from MPB Robb (Chapter 2) were used to parameterize the process oriented Wampus Creek hydrological model to predict and quantify changes in streamflow using forest disturbance scenarios (Figure 4.6). To integrate stand-level process knowledge into the watershed model, the stand-level model structure was used to test a selection of hydrological model algorithms of varied complexity (i.e. number of parameters) from empirical to physically-based, to determine suitable mathematical representation of potential snowmelt and potential ET in the Pure Pine, MPB Grey and clear-cut harvest stands (Appendix B).

Raven allows a user to interchange model algorithms and evaluate the trade-off between data availability, prediction accuracy, and parameter uncertainty (Craig *et al.*, 2020). Hydrologic process representations that are empirically-based tend to have relatively low data requirements, but may be less accurate if applied outside the conditions for which the relationship was originally developed (Beckers *et al.*, 2009). In contrast, physically-based equations explicitly account for the physical process, but can be highly parameterized and may introduce parameter uncertainty when field data are unavailable or spatially and temporally variable (Beckers *et al.*, 2009).

For all stand-level models, the model structure of the unsaturated zone was kept constant and only differed in the process representation of potential ET, which would allow the process that converted potential ET to actual ET to remain the same. The daily potential ET of a stand was calculated with three algorithms that have been widely reported in the literature and represent the typical range of complexity: 1) Penman-Monteith (Monteith, 1965); 2) net radiation with correction factor for the unmodelled ET driven by vapour deficit (Priestley-Taylor, 1972); 3) temperature-index approach with incoming radiation (Hargreaves and Samani, 1985). A similar approach was used to test the daily energy input to the snowpack. The three potential snowmelt algorithms included: 1) physically-based energy balance (Cold Regions Hydrological Model (CRHM) snowmelt method, Pomeroy *et al.*, 2007); 2) temperature-index with an additive radiation term (restrictive method; Brubaker *et al.*, 1996); and, 3) temperature-index that adjusts melt rates under forest cover (HBV-EC method; Bergstrom, 1995). Performance was evaluated with mean absolute error and mean percent bias error (Figures B.1 and B.2). Simulated snowmelt and actual ET were compared to observed soil moisture (Figures B.3 and B.4), an analytical estimate of actual ET from detailed field measurements (Figures B.5 and B.6) and snow survey data (Figure B.7).

Given the changes in the radiation balance with MPB attack, the potential ET and snowmelt algorithms that best represented the observed water cycling were concluded to be the Priestley-Taylor (1972) potential ET and HBV-EC snowmelt method (Bergstrom, 1995; Appendix B). However, based on the trade-off between data availability, prediction accuracy and parameter uncertainty, Priestley-Taylor (1972) required net radiation to be modelled at the watershed-scale. However, modelled radiation was over-estimated in the winter period compared to measured net radiation (Figure B.8). Given that Hargreaves and Samani (1985) was already implemented in the Wampus Creek hydrological model, a potential ET correction factor was used with the HBV-EC potential snowmelt method to model water cycling at the stand-level (Figure B.9; Table 4.1). This correction factor was then used for the MPB Grey and Pure Pine HRUs in the watershed model, and to inform clear-cut harvest HRUs (Figure B.9). At the stand-level, simulated actual AET showed good agreement with the analytical estimate of actual ET from detailed field measurements in the Pure Pine, MPB Grey and Harvest stands (Figure B.9). Simulated SWE using the HBV-EC potential snowmelt method also provided good agreement with observed SWE collected at the stand-level in the Pure Pine ($r^2 = 0.86$; PBIAS = 12%), MPB Grey ($r^2 = 0.69$; PBIAS = 20%), and Harvest stands ($r^2 = 0.65$; PBIAS = 26%; Figure B.9).

For each model (cool/wet or warm/dry), a baseline streamflow regime was simulated using a reference scenario that represented pristine forest cover where existing cutblocks (52% harvested area) were replaced with mature forest similar to other forest stands (Figure 4.6). Clear-cut harvest scenarios (hereafter “Harvest”) assumed all vegetation was merchantable forest and there was complete removal of the overstory canopy. The impact of roads and soil compaction was not considered. These conditions were held constant with no forest regrowth to evaluate the effect of clear-cut harvest conditions on runoff generation with variable climate and antecedent soil conditions.

Streamflow was predicted for the reference condition and eight additional forest disturbance scenarios: Harvest 52%, Harvest 100%, MPB Grey 52%, MPB Grey 100%, Pure Pine 52% and Pure Pine 100% (Figure 4.6). The Harvest scenarios represent current MPB management strategies in Alberta to either salvage (e.g. within one year after MPB attack) or prevent infestation as part of the pine reduction strategy of susceptible pine stands (ASRD, 2007). MPB Grey scenarios (100% trees affected) represents pine left on the landscape due to inadequate mill capacity or limited access. The Pure Pine scenarios represent stands of mature, even-aged lodgepole pine (100% pine). The Pure Pine scenario contrasts with the reference condition, which represents forests of both mixed species and pine-leading stands (represented by the vegetation parameters in the Wampus Creek model).

Scenarios were used to predict streamflow from 1969 to 2019. The period of study was classified into cool and warm PDO water years using the PDO index (Mantua, 2020). The PDO regime shifts included 1976/77, 1988/89, 1991/92, 1998/99, 2002/03, 2008/14. Daily average streamflow hydrographs were computed for the cool PDO and warm PDO years.

4.3.5 Streambed Substrate Mobility and Fry Escapement

An intensive streambed substrate mobility study conducted in the early 1970s determined the critical velocity at which the median grain size of the streambed surface substrate in Wampus Creek (Wampus-A = 57 mm; Figure 4.1) began to move downstream, which has been reported elsewhere (Andres, 1974; Andres *et al.*, 1987). Briefly, at a stream section the streambed material was removed, painted yellow, replaced and surveyed a year later to observe the amount and distance of painted material that moved downstream. The average critical velocity and discharge necessary to initiate bed movement at riffle crests (i.e. typical location of ARTR spawning) for Wampus-A was 1.4 m s^{-1} and 1.7 m^3 s^{-1}, respectively. Given that spawning location typically occurs on the pool-riffle transition, flow was not uniform, and researchers concluded that average velocity rather than shear stress be used to calculate the initiation of particle motion (Andres, 1974).

Following the streambed mobility study, Sterling (1992) found that the median grain size of spawning substrate (10 mm) was 6 times less than the surface substrate median grain size of Wampus-A (57 mm). Therefore, based on the cross-sectional area of spawning riffles and critical velocity, the critical discharge that contributed to mobility of ARTR spawning substrate at Wampus-A was reported as 0.731 m^3 s^{-1} (Sterling, 1992). To rate the severity of high flows on streambed movement, the streamflow above the ARTR $Q_{0.731}$ during the incubation period was calculated for nine-years based on population data collected during the Tri-Creeks forestry experiment (1969 – 1985).

Estimates of fry recruitment were calculated using population data collected by Sterling (1986) and Sterling (1990) over the period 1969 – 1985. The approach is briefly described here. First, estimates of mature females spawning by May 15 (by age-class; N_{mf}) were obtained:

$$N_{mf} = e^{-zt} \cdot N_0 \cdot F_m \tag{4.1}$$

where, z is the instantaneous mortality rate for time t, $t = 0.75$ (fraction of the year Aug 15 to May 15), N_0 is the estimated age class abundance for Aug 15, and F_m is the ratio of mature females to males (by age class).

The relationship of fecundity to fork length (Sterling, 1986) was used to estimate average fecundity at spawning (by age-class; F_p). Egg production at spawning (by age-class; E) was then estimated:

$$E = N_{mf} \cdot F_p \tag{4.2}$$

The collection of fry emergence data was first reported by Sterling (1986), then Sterling (1992). Spawning areas were visited daily to establish spawning activity starting in mid-May from 1973 to 1985 (except 1980, 1982 and 1983). For each fish study section, egg pits (up to 15) were located. Some egg pits were randomly selected and excavated with a Surber sampler to estimate mean egg deposition (n = 100 over 6 years). Dead and live eggs were enumerated (D_e), and live eggs were held in a streamside incubator (gravity fed stream water) until hatch and released. The timing of 50% hatch in the incubator initiated the fry trap installation (10 – 14 days prior to fry escapement) to determine fry escapement from five randomly selected egg pits. The fry trap was modified to compensate for smaller redd size of the ARTR. The trap apron (buried 20-25 cm below streambed surface downstream of egg pit) measured 1 m^2, and the access sleeve and capture bag measured 30 x 30 x 40 cm. The trap was constructed of 100% Dupont woven soft mesh (circular openings of 1 mm). Traps were monitored twice weekly and were removed if no fry were captured within a one-week period following peak emergence.

Total fry emergence (S_e) from spawning gravel (across 7 study sections in Wampus Creek) was estimated as the ratio (Sterling, 1986; Sterling, 1992):

$$S_e = \sum_{i=1}^{n} F_i / D_e \cdot n \tag{4.3}$$

where, F_i is the number of fry captured in the i^{th} site, D_e is the estimated mean egg deposition per site, and n is the number of sites per section. Mean fry escapement of ARTR in Wampus Creek prior to forest harvest (1973 – 1977) was 36 ± 3.7% (range 3.7 to 83%; Sterling, 1986).

Annual fry recruitment (R), the number of fish that successfully emerge and recruit young of year trout to the population (fry/0.10 ha), was estimated:

$$R = S_e \left(\sum_{i=1}^{n} E_i - E_r \right) \tag{4.4}$$

where, E_i is the egg production for the i^{th} mature female class, and E_r is the estimated egg retention for all year classes.

Fry recruitment data for Wampus Creek were used to develop a relationship between fry density and streamflow (dam^3 per incubation period) above the ARTR $Q_{0.731}$ at Wampus-A (Figure 4.7; Sterling, 1992). Annual fry recruitment in Wampus-A estimated for nine years ranged from

52 fry/0.10 ha to 934 fry/0.10 ha (Figure 4.7; Sterling, 1992). The relationship captures the highest (1980) and third highest (1969) maximum annual peak flows over the 52-year record; however, it does not capture the highest streamflows above the ARTR $Q_{0.731}$ during the incubation period (2010 – 2013 and 2018 – 2019).

The relationship was used to estimate fry recruitment using the average incubation period from peak spawning (May 29) to peak emergence (Aug 3; Sterling, 1992). The relationship between potential streambed scour and fry recruitment is limited to Wampus Creek. Specifically, the ARTR $Q_{0.731}$ is limited to the lower Wampus stream reaches (Wampus-A) because the average riffle characteristics would be extremely variable between streams (Andres, 1974; Andres *et al.*, 1987). Although the critical velocity to initiate movement of the median spawning substrate would likely be similar across streams, the critical discharge would vary greatly between other streams.

4.4 Results

4.4.1 Hydrological Model Verification

As stated previously, hydrological model performance indicated good agreement in model efficiency and volumetric error between observed and simulated streamflow for the cool/wet model and warm/dry model (Chapter 3). In general, both models under-simulated streamflow, particularly the rising limb and peak flow of the snowmelt period, and summer peak flows when antecedent soil conditions between years were highly variable (Chapter 3). In addition, there was good agreement between simulated and observed SWE as well as simulated actual AET and an estimate of actual ET (analytical method) within the Pure Pine, MPB Grey and Harvest stands (Figure B.9).

There was good agreement between observed and simulated streamflow volume (PBIAS = -1.9%) of the warm/dry hydrological model to predict streamflow for another warm PDO period (1992 – 1996) using the median parameter set. However, there was relatively poor agreement between observed and simulated streamflow based on the model efficiency value (NSE = 0.55). The discrepancies between observed and simulated streamflow were primarily attributed to low efficiency in matching peak flow events; the model underestimates observed peak flows. However, given the well-emulated volume of flow by the hydrological model, the models were assumed appropriate to predict streamflow for forest disturbance scenarios in Wampus Creek to quantify the streamflow above the ARTR $Q_{0.731}$.

4.4.2 Runoff Source Areas

For the reference condition in Wampus Creek, runoff source areas were discriminated between different precipitation phases, watershed slope aspects and gradients for both the cool and warm PDO periods. The cool PDO periods typically had a higher proportion of annual precipitation that fell as snow (Figure 4.2). As expected, simulated streamflow concentrations of the conservative tracer indicated the snowpack contributed more to the hydrograph in the cool PDO periods and the contribution of snowmelt had a legacy effect that influenced summer antecedent conditions (Figure 4.8). For the summer (Jun – Aug), the snowpack contributed an average 38% of runoff in the cool PDO period (43 mm summer^{-1}) and 35% of runoff in the warm PDO period (32 mm summer^{-1}). The spring (Apr-May) warm PDO periods also had less snowpack runoff (48%; 37 mm spring^{-1}) compared to the cool PDO (51%; 50 mm spring^{-1}).

Wampus Creek generated similar runoff contributions from upper and lower slopes as well as northern and southern upper slope aspects with small differences between PDO regimes. Compared to the upper slopes (120 mm yr^{-1} cool PDO; 110 mm yr^{-1} warm PDO), annual water yield from lower slopes was 10% greater in the cool PDO period (141 mm yr^{-1}) and 9% greater in the warm PDO period (126 mm yr^{-1}). Compared to the southern upper slope aspects (28 mm yr^{-1} cool PDO; 25 mm yr^{-1} warm PDO), annual water yield from the northern upper slope aspects was 15% greater in the cool PDO period (74 mm yr^{-1}) and 16% greater in the warm PDO period (69 mm yr^{-1}). These results suggest that all Wampus Creek watershed areas would have similar sensitivity to forest disturbance regardless of cutblock distribution within the watershed.

4.4.3 Comparison of Streamflow Response to Different Forest Disturbances

The streamflow response to estimated differences in forest cover, modelled actual ET and snowmelt with the nine scenarios for the cool and warm PDO periods are presented in Figures 4.9 and 4.10. The modelled daily average streamflow with 52% MPB Grey was similar to reference conditions and Pure Pine cover (Figure 4.9). Compared to the reference (250 mm yr^{-1}), annual water yield was 16% greater in the 52% Pure Pine (291 mm yr^{-1}) and 17% greater in the 52% MPB Grey (293 mm yr^{-1}) scenarios for the warm PDO period. However, differences between modelled scenarios were smaller in the cool PDO period simulations, where annual water yield was 7.6% greater in the 52% Pure Pine (298 mm yr^{-1}) and 8.9% greater in the 52% MPB Grey (301 mm yr^{-1}) scenarios compared to the reference (277 mm yr^{-1}). The effect of 52% MPB Grey on summer water yield was small compared to the 52% Pure Pine scenario: the average difference in summer water yield was <1% in the cool (143 mm summer^{-1}) and warm (124 mm summer^{-1}) PDO periods, respectively.

During the warm PDO simulations, there was a larger difference in spring water yield between the reference condition and 100% MPB Grey as a result of larger peak SWE and lower AET. However, the 100% MPB Grey streamflow response closely resembled that of the 100% Pure Pine scenario (Figure 4.9). In addition, the response to 100% MPB Grey indicates little increase in streamflow compared to 100% Pure Pine cover, especially during the summer period (Figure 4.9). The average difference in summer water yield between 100% MPB Grey and 100% Pure Pine was -0.3% (161 mm summer^{-1}) and 1.0% (147 mm summer^{-1}) for the cool and warm PDO periods, respectively. The results suggest tree mortality had little effect compared to snow accumulation and melt on the streamflow response.

The Harvest scenarios showed streamflow increased compared to the reference condition, with greater effect on streamflow in the cool PDO periods (Figure 4.10). Compared to the reference (250 mm yr^{-1}), annual water yield was 33% greater in the 52% Harvest (334 mm yr^{-1}) and 80% greater in the 100% Harvest (451 mm yr^{-1}) scenarios in the warm PDO period. For the cool PDO period, the annual water yield was 29% greater in the 52% Harvest (358 mm yr^{-1}) and 71% greater in the 100% Harvest (472 mm yr^{-1}) scenarios compared to the reference condition (277 mm yr^{-1}). For the summer period, water yield for the 52% Harvest was 33% greater in the warm PDO period (107 mm summer^{-1}) and 30% greater in the cool PDO period (172 mm summer^{-1}). For both Harvest scenarios, the simulated average daily streamflow showed a larger snowmelt peak flow, while the onset of snowmelt was earlier in the warm PDO compared to the cool PDO periods.

Simulated clear-cut forest harvest resulted in more runoff than if dead trees were left standing. The average relative difference between the 52% Harvest and 52% MPB Grey scenarios was 17% (57 mm; cool PDO) and 13% (41 mm; warm PDO), while the average relative difference between the 100% Harvest and 100% MPB Grey scenarios was 34% (136 mm; cool PDO) and 24% (97 mm; warm PDO).

4.4.4 Fry Recruitment

Average annual fry recruitment was lower across all scenarios in the cool PDO years versus warm PDO years as a result of greater streamflow and number of days above the ARTR $Q_{0.731}$ during the incubation period (Tables 4.2 and 4.3). Over the 50-year record, fry recruitment was estimated to occur in all years across all scenarios (Table 4.2; Figure 4.11). Relative to reference conditions, the average annual fry recruitment was 11% less if the stands were harvested (52% Harvest) rather than left as grey-attack (52% MPB Grey), while recruitment was 35% less when harvest occurred at 100% over the total study period (Table 4.3). Consecutive years with high flows resulted in low annual fry recruitment, but subsequent lower flow years produced high recruitment numbers to the population. For example, average densities ranged from 38 - 92 fry/0.1 ha in the 52% Harvest scenario from 2010 – 2013 and 2018 – 2019, but between these high flow periods annual fry recruitment was 343 – 724 fry/0.1 ha. Even in the worst-case scenario (100% Harvest) the same high flow periods (2010 – 2013, 2018 – 2019) resulted in lower fry recruitment (14 – 35 fry/0.1), but the lower flow in 2014 – 2017 had increased fry recruitment (194 – 722 fry/0.1 ha). Over the 50-year record, estimated annual fry recruitment of <100 fry/0.1 ha did not occur for more than three consecutive years for the 52% Harvest scenario and for more than four consecutive years for the 100% Harvest scenario (Figure 4.11).

4.5 Discussion

4.5.1 Streamflow Response to Mountain Pine Beetle and Forest Harvest

The predicted streamflow response to MPB grey-attack fell within the range of inter-annual streamflow variability. Compared to the Pure Pine forest cover, annual water yield was simulated to be only 1% greater for the 52% MPB Grey scenario and 2% greater for the 100% MPB Grey scenario. Differences in simulations between the Pure Pine and MPB Grey HRUs within the Wampus Creek hydrological model reflected the observed differences found in the detailed stand-level field study (Chapter 2). Differences in canopy cover were also reflected in the HRUs average snowpack depth. Average peak SWE in the reference HRU (104 mm) was 16% lower than the Pure Pine HRU (121 mm) and 17% lower than MPB Grey HRU (123 mm). Average annual actual ET in the reference HRU (344 mm yr^{-1}) was 27% greater than the Pure Pine HRU (249 mm yr^{-1}), and 28% greater than the MPB Grey HRU (247 mm yr^{-1}). For the MPB Grey scenarios, the reduced overstory transpiration and canopy interception losses were compensated by increased understory evapotranspiration as a result of increased net radiation reaching the forest floor (Chapter 2), which likely mitigated the potential increases in streamflow response to MPB grey-attack (Biederman *et al.*, 2015; Penn *et al.*, 2016), and MPB effects on streamflow between PDO phases were small. Streamflow was also found not to be significantly altered by early grey-phase MPB attack in 32 watersheds (16-3355 km^2; 21 to 90% affected) in seven western United States (21-72% precipitation as snow), which analyzed some watersheds outside the Rocky Mountain region

(Slinski *et al.*, 2016). Their results found that any changes in streamflow were likely related to climate variability that drives snowmelt timing and streamflow pattern rather than MPB grey-attack (Slinski *et al.*, 2016). Climate variability was also found to offset the increases in annual water yield from MPB (70% affected) and subsequent salvage harvest in another non-alpine watershed in British Columbia's interior (1570 km^2; 34% precipitation as snow; Zhang and Wei, 2012). The results from MPB scenarios in Wampus Creek reflect findings from stand-scale studies and suggest that the effect of MPB grey-attack on streamflow falls within the range of natural variability.

Clear-cut harvest scenarios in response to MPB infestation (pine reduction strategy or salvage harvest) resulted in increased water yield. The average annual water yield was 15% greater than the MPB scenario across 52% of the watershed area. During the growing season, reduced transpiration and canopy interception that follows forest harvest should allow soils to wet up to a greater depth than would be observed under a MPB grey-attack canopy (Chapter 2) or an undisturbed mature forest canopy (Elliot *et al.*, 1998; Winkler *et al.*, 2010). The transfer of these net soil water inputs to the stream is governed by the amount of subsurface storage (Redding and Devito, 2010; Smith *et al.* 2014). The antecedent soil conditions, in relation to climate, were strong controls on runoff generation in Wampus Creek (Chapter 3). Historical harvest in Wampus Creek was predicted to significantly increase summer runoff and rainfall-generated peak runoff events using a change-detection hydrological modelling method (Chapter 3). Results from this study show runoff generation in Harvest scenarios was larger during cool PDO periods, which was likely enhanced by larger snowmelt input and wetter antecedent soil conditions. Therefore, how fully-forested Foothills watersheds respond to forest harvest will likely be a function of climate variability and antecedent watershed storage that acts as a buffer between water inputs and streamflow response.

4.5.2 Wampus Creek Fry Recruitment

Athabasca Rainbow Trout are adapted to and have evolved with episodic extreme flow events (COSEWIC, 2014). Results show that some incubation mortality due to spawning substrate scour already existed for the reference condition and Pure Pine forest cover. Observed population abundance data show consecutive high recruitment years after a large flood year (e.g. low recruitment in 1969 and 1980) helped to stabilize the population, and the ARTR population in Wampus Creek returned to pre-flood numbers within five years (Sterling, 1990). Population assessments during the historical forest harvest in Wampus Creek (52% watershed area) indicated that ARTR possess the ability to adapt to changes in streamflow as there was no significant change in the amount of fry escapement between pre- and post-harvest (Sterling, 1992). Increased streamflow due to forest harvest and reduced fry recruitment did not translate into reduced ability for the ARTR population to persist over time.

Density-dependence in fry survival once emerged was observed in Wampus Creek (Sterling, 1990) and could mitigate for losses incurred during the incubation period due to streambed scour. The survival of fry appeared highly dependent on fry densities ($n = 5$ years; $r = -0.9841$, $p<0.01$; Sterling, 1986). Strong density-dependent compensation in survival rates shortly after Rainbow Trout fry emerged (~2 months post-hatch) mitigated the incubation losses incurred due to increases in flow fluctuations from a Colorado River dam (Korman *et al.*, 2011). Other studies of salmonid populations have shown that most density-dependent mortality occurs when fry first emerge from their incubation environment and compete for limited feeding territories (Elliot, 1985; Nislow *et al.*, 2004; Einum and Nislow, 2005). Therefore, estimates of fry density that recruit to the population may also be affected by density-dependence.

The estimates of fry recruitment only address changes in the streamflow regime due to forest disturbance; however, forest disturbance changes in sediment supply may also affect fry survival during their incubation phase. Salmonid embryo mortality through increased supply of fine sediment deposition could smother gravel spawning beds and reduce intra-gravel oxygen flow (Greig *et al.*, 2007; May *et al.*, 2009; Tonina and Buffington, 2009). In a review of the effects of suspended sediment on aquatic ecosystems, measurable negative effects on Rainbow Trout included reduction in egg viability and development, and reduced fry survival (Newcombe and MacDonald, 1991). However, higher pulses of flow can increase Rainbow Trout fry habitat quality and food availability (Korman *et al.*, 2011). Except under extreme conditions (e.g. riparian clearcutting or landslides; Tschaplinski and Pike, 2017), contemporary forest logging best management practices may not increase sediment delivery to streams (Rachels *et al.*, 2020). For example, suspended sediments increased 12% post-harvest in Wampus Creek (range -10 to 30%; Nip, 1991), but no change was detected in sediment deposition in spawning habitat (Sterling, 1992). Spawning substrate quality showed large inter-annual variation, but spawning habitat degradation was not confirmed post-harvest, and fine sediments associated with higher streamflow during snowmelt and summer storms were assumed to be transported from the study stream sections (Andres *et al.*, 1987; Sterling, 1992). Therefore, the broader risk to egg survival in Wampus Creek may be streambed scour rather than sediment deposition.

Increased streambed scour and reduced ARTR fry recruitment due to forest harvest is likely to be absorbed by a relatively resilient ARTR population like that in Wampus Creek; however, changes in the magnitude of fry recruitment may make a difference between stability and long-term decline in ARTR populations affected by other multiple anthropogenic threats. Threats were limited in Wampus Creek as it is a benchmark for ARTR population assessment because of limited landscape disturbance, superior logging road restoration techniques, restricted angling, and limited habitat loss and alteration with no historical stocking of non-native fish species (Andres *et al.*, 1987; Rasmussen and Taylor, 2009). However, temporal assessment of population abundance data has shown declines in over half the streams surveyed in the last 15 years as a result of multiple anthropogenic threats that overlap with their native range (COSEWIC, 2014; Sinnatamby *et al.*, 2020). For example, recent work in an Alberta stream downstream of a coal mine tailings release showed increased fine sediment and invasive populations of Brook Trout were the largest threats to ARTR abundance (Medinski, 2018). Brook Trout were stocked into several streams of Alberta's Foothills (1940 – 1964) and non-native trout can impact trout populations through competition and/or hybridization (Rasmussen and Taylor, 2009; COSEWIC, 2014). For example, Brook Trout have several competitive advantages over ARTR, which includes fall spawning that avoids the scouring summer peak flows as well as faster growth and earlier sexual maturity that results in more recruitment (Fausch, 2008). In addition, recent restrictive regulations on angling (catch-and-release instated 2012) have been designed to sustain the ARTR populations, but it is possible that post-release hooking mortality and poaching could contribute to the cumulative anthropogenic threats (Sinnatamby *et al.*, 2020). Access to angling and more use of off-highway vehicle trails will also continue to increase as industrial development occurs (e.g. oil and gas exploration/extraction, logging, coal mining), which results in increased angling pressure and increased available sediment and erosion to streams (Gunn and Sein, 2000; Howard, 2018). Lastly, climate change is considered a future threat to ARTR populations (Fisheries and Oceans Canada, 2020). These cumulative anthropogenic threats are of concern for declining ARTR populations.

The relationship between spawning substrate scour and fry recruitment is limited to Wampus Creek, and uncertainty exists for estimates of fry recruitment. The uncertainties in the measured parameters used to establish the scour-fry recruitment relationship were not quantified, which included the estimates of mature females, number of eggs deposited per pit, and estimates in streamflow measurements (Sterling, 1992). In addition, the choice to use the average incubation period (date of peak spawning to peak emergence) could overestimate or underestimate the streamflow above the ARTR $Q_{0.731}$ for each specific year, and subsequently the density of fry. For example, in 1969, the average incubation period (May 29 – Aug 3) did not capture the maximum annual peak flow on August 5th; however, reconnaissance stream surveys indicate fry continued to emerge until mid-August and fry densities were overestimated (369 fry/0.1 ha) compared to reported values (52 fry/0.1 ha; Dietz, 1971; Sterling, 1992). Conversely, the average incubation period underestimated fry densities (607 fry/0.1 ha) in 1977 compared to reported values (680 fry/0.1 ha; Sterling, 1992), which may be a result of over-estimation of the maximum annual peak flow that occurred on May 29th or did not capture the accurate dates of the incubation period. Given that stream surveys were not available for the 50-year record, the average incubation period provided the best estimate to capture the variability in ARTR incubation dates. Altogether, the average incubation period and the scour-fry recruitment relationship were derived from the best available data and provides the most useful model to explore the effects of streamflow on ARTR fry recruitment.

4.5.3 Management Implications

4.5.3.1 Current Mountain Pine Beetle Management Strategies

Mountain pine beetle has affected 43.6% of the susceptible pine in Alberta (C. Whitehouse, pers. communications, December 22, 2020). However, unlike British Columbia, much of the susceptible pine in the Alberta Foothills grows in mixed stands with other softwood and hardwood species (Schneider *et al.*, 2010). Mixed-species stands (<50% pine) make up 62% of the forested area in six forest management areas within the Foothills (2.46 million total forested acres), while 26% of the area is pure pine-leading stands (>= 80% pine; Schneider *et al.*, 2010). Pure pine stands affected by MPB would have greater changes in water cycling as a result of higher MPB intensity compared to that observed in mixed-species stands. The stands affected by MPB explored in the MPB Grey scenarios (100% pine) would represent a smaller portion of the forested landscape. In addition, simulated MPB grey-attack within Wampus Creek at both moderate (52%) and severe (100%) watershed levels only resulted in a 1-2% change in annual water yield relative to Pure Pine forest cover: a change that would likely be smaller for mixed-species stands affected by MPB. The Alberta MPB Management Strategy is intended to contain the infestation and all elements include forest harvest (ASRD, 2007). However, if a forest management goal is to reduce potential changes in streamflow, then MPB affected trees should be left to stand rather than the use of a salvage or pine reduction strategy.

Fully-forested watersheds like Wampus Creek are sensitive to changes in streamflow due to forest harvest regardless of cutblock distribution within the watershed. Streamflows sourced from north or south slope aspects and upper or lower slope gradients were similar if the 11% greater lower slope area and 13% greater northern slope aspect distribution in the watershed was considered. These results contrast the literature from alpine watersheds (e.g. Green *et al.*, 2012). The snowpack in the alpine zone is known to be the main source of runoff that contributes to the annual hydrograph in snow-dominated watersheds (e.g. Schnorbus and Alila, 2004; Fang *et al.*, 2016; Spencer *et al.*, 2019). However, for Wampus Creek, runoff generation was dependent on the inter-annual variability in antecedent soil conditions and snowpack depth (i.e. PDO regime; Chapter 3). Snowmelt functions to satisfy soil storage prior to spring and summer rain events that typically generate the maximum annual peak flow; a hydrologic response like that observed in the Boreal Plains (e.g. Devito et al, 2005; Redding and Devito, 2011). In addition, increased proportions of permeable or fractured sedimentary bedrock found along the eastern slopes of the Rocky Mountains and Foothills region have been suggested to attenuate precipitation inputs for streamflow generation (Jensco *et al.*, 2011; Harder *et al.*, 2015; Spencer *et al.*, 2019). Therefore, climate variability and antecedent watershed storage will play a larger role on changes in streamflow than cutblock distribution.

4.5.3.2 Athabasca Rainbow Trout Fry Recruitment

Forest disturbance increased streamflow above the ARTR $Q_{0.731}$ during the incubation period and reduced fry recruitment, but annual fry recruitment was estimated to occur over the 50-year simulated streamflow record. The observed streamflow record also indicated flows naturally exceeded the critical discharge threshold due to episodic high flow events and ARTR population assessments over 30 years post-harvest shows the population continues to persist. These results show that increased spawning substrate mobility as a result of streamflow changes due to forest harvest would not likely produce a measurable change in ARTR fry recruitment at the population level. A similar conclusion was found for an Idaho watershed (20% forest harvest) that showed increased scour resulted in an estimated 15% increase in incubation mortality of Bull Trout, but was not likely the sole contributor of species extirpation from the area (Tonina *et al.*, 2008).

However, pervasive scour events over time (e.g. 1:2 year flood frequency) may affect a generation (~5 years) of ARTR. The population growth rate of ARTR is sensitive to changes in fry survival; however, sensitivity modelling analyses suggests that ARTR may be able to sustain a positive population growth rate with small decreases in the survival rate of ARTR fry (i.e. 41% decrease in annual survival rate in perpetuity; Caskenette and Koops, 2018). However, decreases in the survival rate of ARTR fry caused by changes in streambed scour and concurrent changes in other vital rates (e.g. fecundity or survival rates of other life stages) may combine to drive the population growth rate below 1 (Caskenette and Koops, 2018). While results from Wampus Creek suggest that ARTR fry recruitment could have been aggravated by forest harvest, increased streambed scour due to forest harvest is unlikely to play a lead role in the long-term decline of the population in Wampus Creek. ARTR have successful adaptations to survive high flows, but ARTR may be poorly adapted to angling pressure or competition from introduced fish species.

4.5.4 Conclusions

Mountain pine beetle and current forest management scenarios indicate that MPB had little effect on streamflow during the ARTR incubation period, while forest harvest (52% watershed area) increased summer water yield 16% and 32% compared to the MPB grey-attack and reference scenarios, respectively. Overall, summer streamflow in the Harvest scenarios was higher during cool PDO periods when there was larger snowmelt input and wetter antecedent soil conditions. However, increased streamflow above the ARTR $Q_{0.731}$ during the incubation period could be large in the warm PDO periods due to the stochastic nature of heavy summer rainfall events observed in the Foothills. Athabasca Rainbow Trout would appear to be adapted to and have evolved with these episodic extreme flow events as summer flow regimes in the observed streamflow and simulated reference conditions indicate that streamflow above the ARTR $Q_{0.731}$ occurred often. Population abundance data 30 years after harvest indicate fry recruitment and the ARTR population have persisted despite streamflow changes from historical forest harvest in Wampus Creek (Sterling, 1992; Alberta ARTR Team, 2014). Over the 50-year simulated streamflow record, fry recruitment was estimated to occur in all years, even despite an extreme worst-case scenario of 100% clear-cut harvest. These results show that increased spawning substrate mobility due to forest harvest would not likely produce catastrophic mortality to ARTR fry as similar conditions have occurred naturally in this Foothills stream. However, further population modelling is needed to understand if reduced fry recruitment due to forest harvest with additional cumulative anthropogenic threats (e.g. angling pressure, increased sedimentation, and competition with Brook Trout) translates into ARTR population decline. However, this study shows that there is little effect on ARTR fry recruitment from MPB grey-attack and forest harvest in Wampus Creek relative to natural variability.

Table 4.1 List of median model parameters used in the 'wet/cool' model ('dry/warm' model parameters in brackets if different; Chapter 3). Vegetation/landuse parameters for MPB Grey and Control HRUs were collected from MPB Robb (Chapter 2).

Parameter Name	Definition	Units	Wampus Creek HRUs			
			Undisturbed	Harvest	MPB Grey	Control
ADIABATIC_LAPSE	Adiabatic temp. lapse rate	°C km^{-1}	6.2 (5.1)	6.2 (5.1)	6.2 (5.1)	6.2 (5.1)
RAINSNOW_TEMP	Rain/snow transition temp	°C	1.2 (0.6)	1.2 (0.6)	1.2 (0.6)	1.2 (0.6)
MAX_HEIGHT	Maximum vegetation height	m	25	0.5	0.5	23.5
MAX_LAI	Maximum leaf area index	m^2 m^{-2}	4.6 (3.7)	1.2	3.9	3.4
MAX_CAPACITY	Max. canopy storage capacity	mm	15 (15)	0	40.3	37.2
MAX_SNOW_CAPACITY	Maximum canopy SWE storage	mm	20 (20)	0	17.0	14.7
RAIN_ICEPT_PCT^A	Percent rainfall interception	-	0.27 (0.18)	0	0.77	0.80
SNOW_ICEPT_PCT	Percent snowfall interception	-	0.39 (0.28)	0	0.47	0.47 (0.50)
PET_VEG_CORR	Parameter to modify evap.	-	-	0.52	0.42	0.42
FOREST_ SPARSENESS	Canopy cover	%	0.85 (0.89)	0	0.63	0.46
MELT_FACTOR	Maximum snowmelt factor	mm/d °C	4.0 (3.8)	2.7	2.8	2.3
MIN_MELT	Minimum snowmelt factor	mm/d °C	1.9 (1.3)	1.1	0.01	0.2
HBV_MELT_FOR_CORR	Snowmelt forest correction	-	0.89 (0.87)	0	1	1
HBV_MELT_ASP_CORR	Snowmelt aspect correction	-	0.96 (0.86)	0.46	0.96 (0.86)	0.96 (0.86)
REFREEZE	Maximum refreeze factor	mm/d °C	0.03 (1.2)	0.26	1.2	2.0
FIELD_CAPACITY	Field capacity saturation	[0..1]	0.95 (0.96)	0.95 (0.96)	0.95 (0.96)	0.95 (0.96)
SAT_WILT	Minimum saturation	[0..1]	0.09 (0.03)	0.09 (0.03)	0.09 (0.03)	0.09 (0.03)
TOPSOIL	Thickness soil layer	m	0.40 (0.92)	0.40 (0.92)	0.40 (0.92)	0.40 (0.92)
SOIL 1 (Fast Reservoir)	Thickness soil layer	m	1.36 (1.41)	1.36 (1.41)	1.36 (1.41)	1.36 (1.41)
SOIL 2 (Slow Reservoir)	Thickness soil layer	m	0.57 (0.52)	0.57 (0.52)	0.57 (0.52)	0.57 (0.52)
HBV_BETA	Infiltration exponent	-	0.52 (1.3)	0.52 (1.3)	0.52 (1.3)	0.52 (1.3)
MAX_CAP_RISE_RATE	Maximum capillary rise rate	mm d^{-1}	0.83 (0.65)	0.83 (0.65)	0.83 (0.65)	0.83 (0.65)
MAX_PERC_RATE	Maximum percolation rate	mm d^{-1}	8.9 (8.9)	8.9 (8.9)	8.9 (8.9)	8.9 (8.9)
BASEFLOW_COEFF	Linear baseflow storage	-	0.47 (0.43)	0.47 (0.43)	0.47 (0.43)	0.47 (0.43)
BASEFLOW_N	Baseflow exponent (Fast Res.)	-	1.3 (4.0)	1.3 (4.0)	1.3 (4.0)	1.3 (4.0)
BASEFLOW_N	Baseflow exponent (Slow Res.)	-	8.9 (9.8)	8.9 (9.8)	8.9 (9.8)	8.9 (9.8)

Table 4.2 Absolute values of streamflow and number of days above the critical discharge threshold during the incubation period (IP) and estimated number of fry escapement averaged over the cool PDO years (n = 21) and warm PDO years (n = 30). Maximum and minimum values are presented in brackets.

Scenario	Streamflow above $Q_{0.731}$ (dam^3/IP)		No. Days/IP		Fry Density (No./0.1 ha)	
	Cool PDO	Warm PDO	Cool PDO	Warm PDO	Cool PDO	Warm PDO
Reference	849 (0-2740)	469 (0-2788)	9 (0-24)	7 (0-29)	434 (80-724)	551 (77-724)
Harvest 52%	1344 (7-3343)	825 (0-3579)	15 (1-28)	11 (0-32)	316 (49-719)	455 (40-724)
MPB Grey 52%	1122 (0-3207)	756 (0-3692)	10 (0-25)	8 (0-30)	369 (55-724)	477 (37-724)
Pure Pine 52%	1133 (0-3219)	768 (0-3698)	11 (0-25)	8 (0-30)	365 (54-724)	474 (37 -724)
Harvest 100%	2345 (490-5262)	1510 (2-4743)	27 (12-42)	19 (1-40)	168 (10-487)	316 (16-723)
MPB Grey 100%	1542 (0-3885)	1183 (0-4943)	12 (0-26)	9 (0-31)	291 (32-724)	399 (13 -724)
Pure Pine 100%	1602 (2-3916)	1215 (0-4951)	13 (1-29)	9 (0-31)	282 (31-722)	392 (13-724)

Table 4.3 Percent difference in streamflow above the ARTR critical discharge threshold during the incubation period (IP) and estimated number of fry escapement relative to reference conditions averaged over the cool PDO years (n = 21), warm PDO years (n = 30), and total study period (1969 – 2019).

Scenario	Streamflow above $Q_{0.731}$/IP (%)			Fry Density (%)		
	Cool PDO	Warm PDO	Avg.	Cool PDO	Warm PDO	Avg.
Harvest 52%	74	93	84	-39	-28	-34
MPB Grey 52%	41	53	47	-22	-23	-23
Pure Pine 52%	42	55	49	-23	-24	-24
Harvest 100%	116	148	132	-102	-74	-88
MPB Grey 100%	74	98	86	-53	-52	-53
Pure Pine 100%	84	107	96	-57	-55	-56

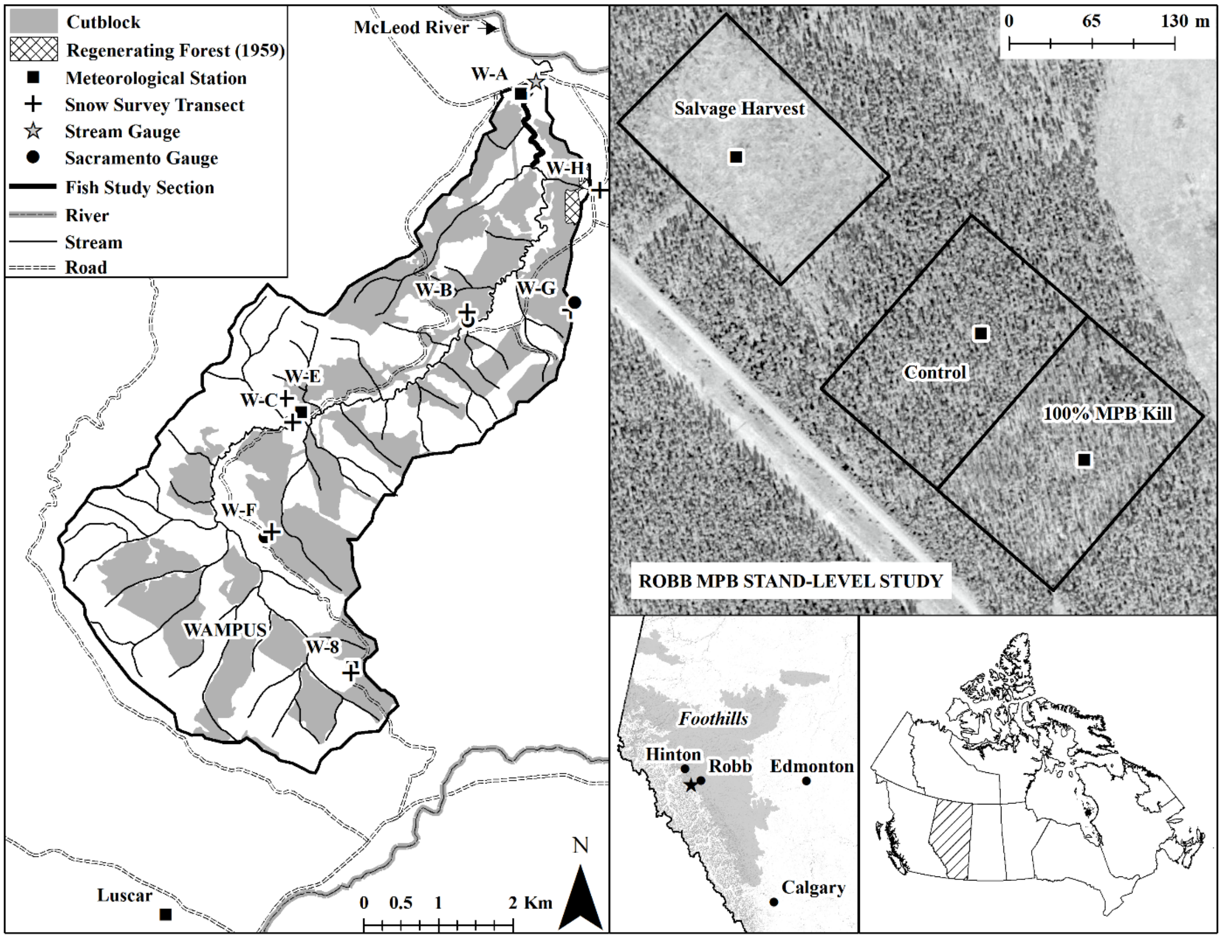

Figure 4.1 Study area and locations of Wampus Creek (part of the Tri-Creeks Experimental Watershed; marked by a star on the provincial map) and the MPB before-after control-impact stand-level study near Robb, Alberta, Canada, which are both located within the Foothills Natural Sub-Region (dark grey). The Foothills are adjacent to the eastern slopes of the Rocky Mountains (west) and the Boreal Plain (northeast).

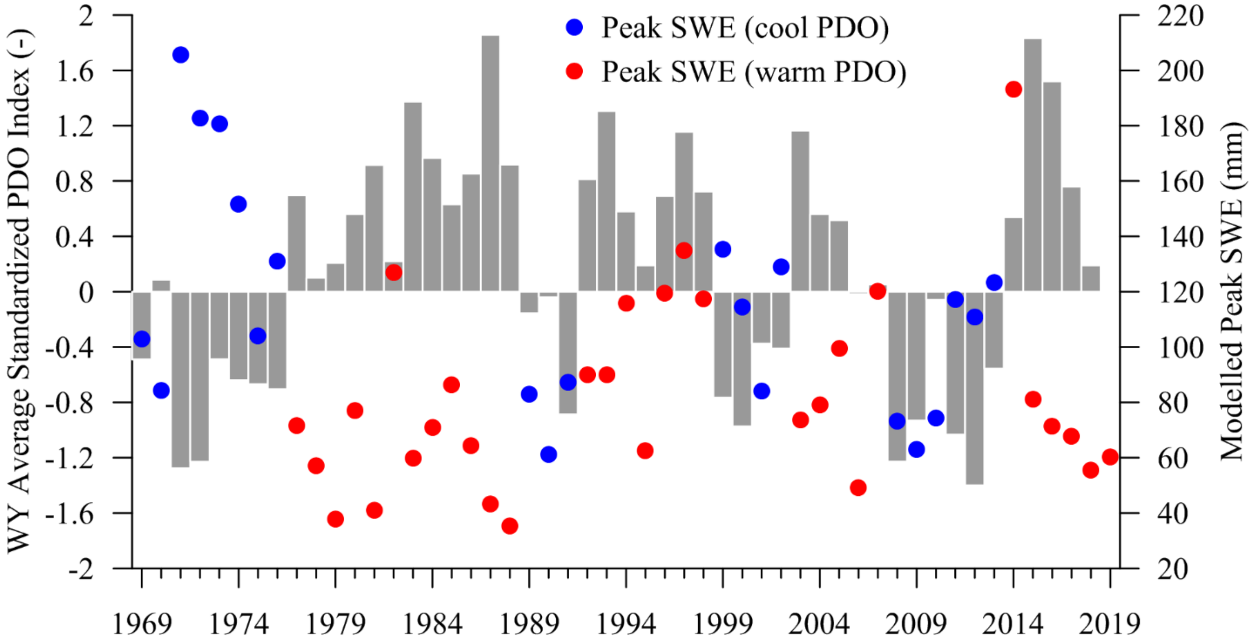

Figure 4.2 Water year average (October – September) standardized PDO index (grey bars; no data available for 2019; Mantua, 2020) plotted over the study period with modelled average watershed peak snow water equivalent (SWE) for the undisturbed reference condition.

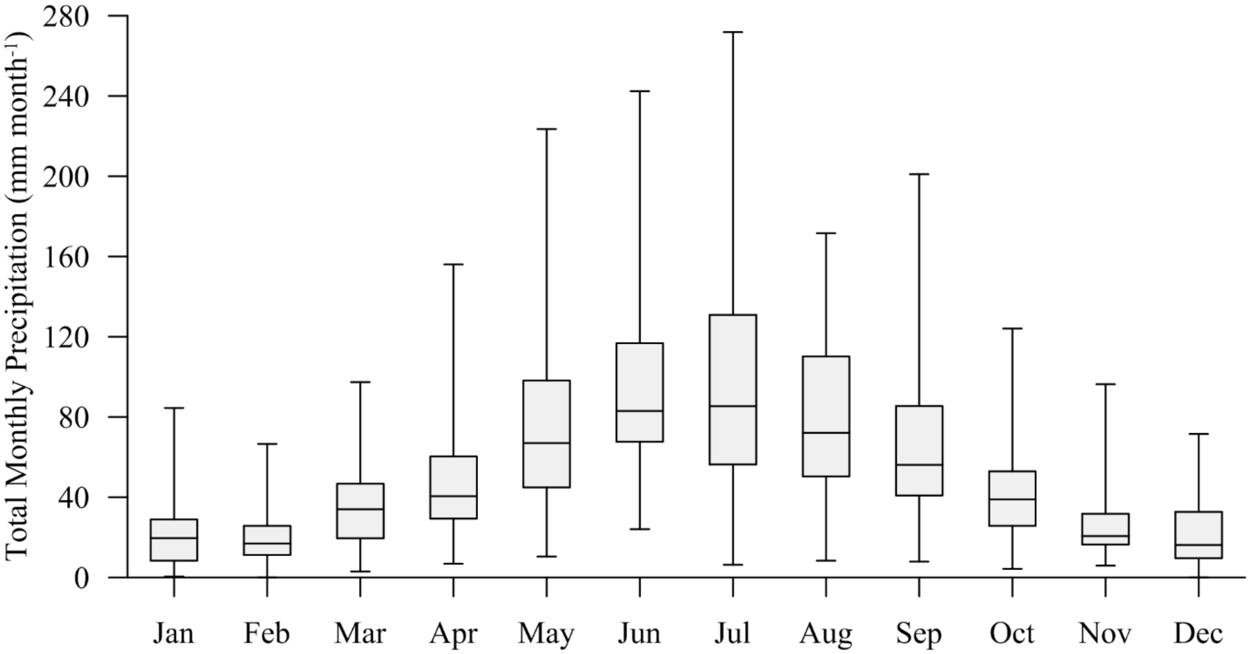

Figure 4.3 Box plot of total monthly precipitation in Wampus Creek from 1967 to 2019. For each month, the horizontal line within the box indicates the median, the box ends mark the 25th and 75th percentiles, and the bars show maximum and minimum values.

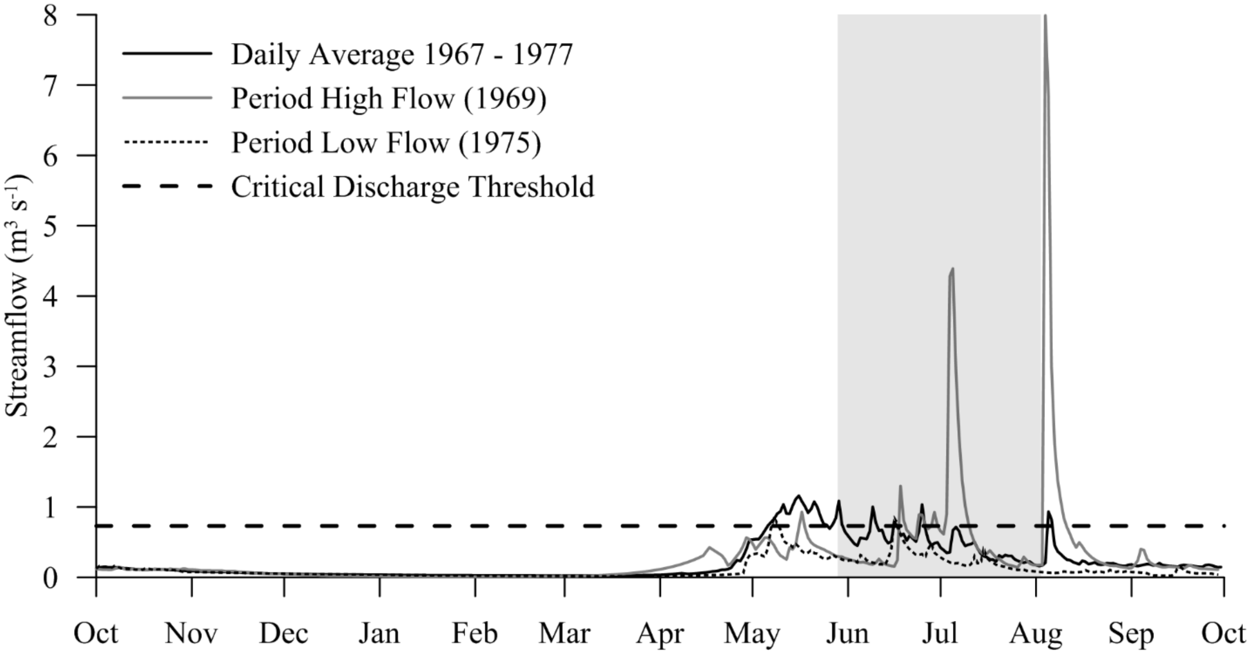

Figure 4.4 Wampus Creek hydrograph for the pre-harvest period, 1967 – 1977. The maximum annual flow recorded in 1969 was the third highest discharge over the 52-year record (1967 – 2019). The stream discharge that was found to scour Athabasca Rainbow Trout spawning substrates is indicated by the critical discharge threshold line (0.731 m^3 s^{-1}; Sterling, 1992). The average incubation period of Athabasca Rainbow Trout from peak spawning (May 29) to peak fry escapement (Aug 3) is indicated by the grey box (Sterling, 1992). The portion of the hydrograph above the critical discharge threshold within the incubation period represents the stream discharge that could contribute to scour of the spawning substrates and embryo mortality.

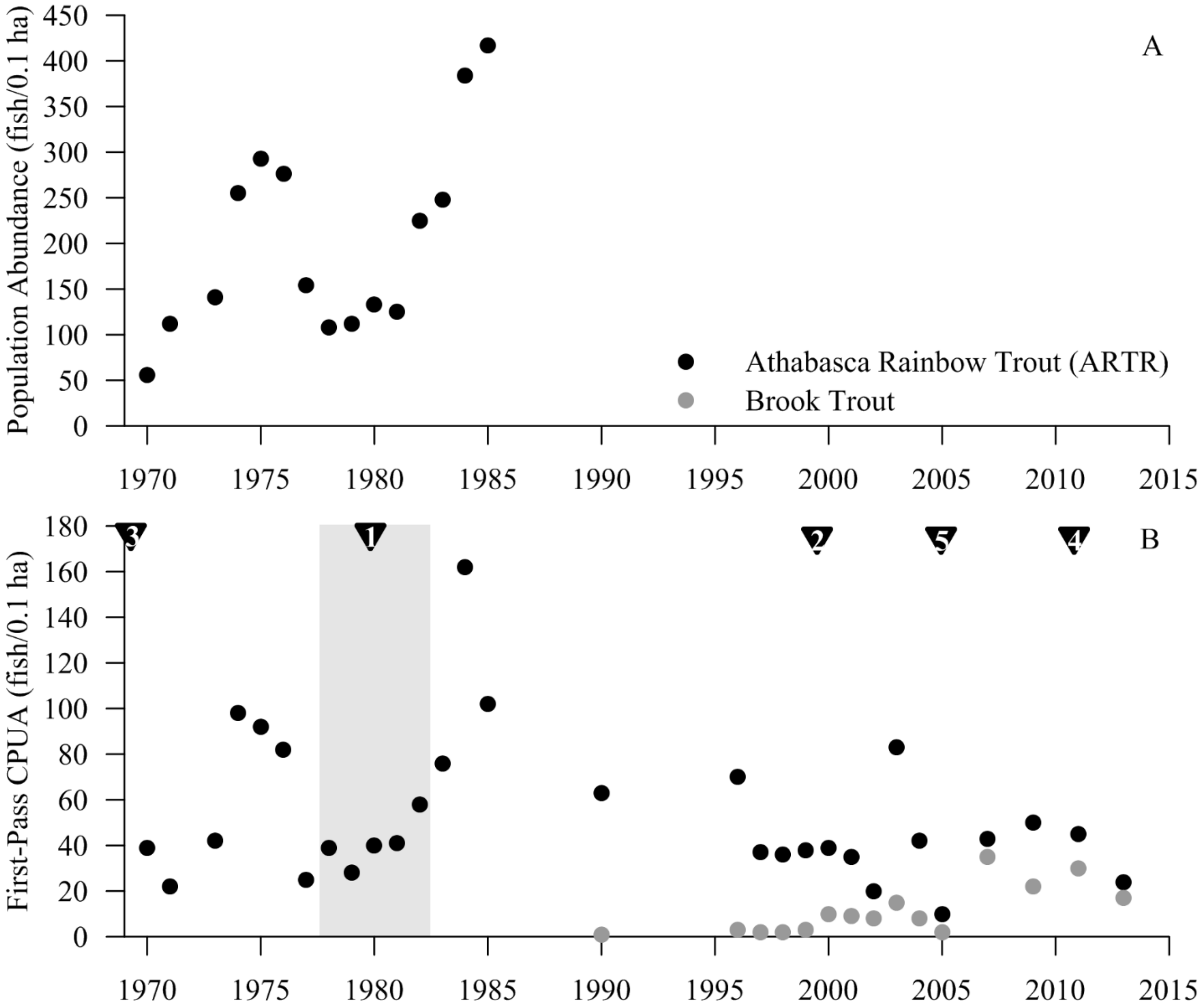

Figure 4.5 Wampus Creek (lower study section) population abundance of ARTR from 1970 to 1985 (top panel A; data from Sterling, 1990) and standardized to first-pass catch per unit area (CPUA) for comparison between 1970 – 1985 and data collected after the Tri-Creeks watershed experiment (1990 – 2013; bottom panel B; data from Alberta ARTR Team, 2014). Harvest period in Wampus Creek is indicated by the grey box. The black triangles indicate the top five maximum annual peak flows recorded over the 52-year streamflow record in descending order: 1980, 1999, 1969, 2011 and 2005. To clarify, these ranked floods do not indicate the order of years for maximum streamflow above the ARTR critical discharge during the incubation period.

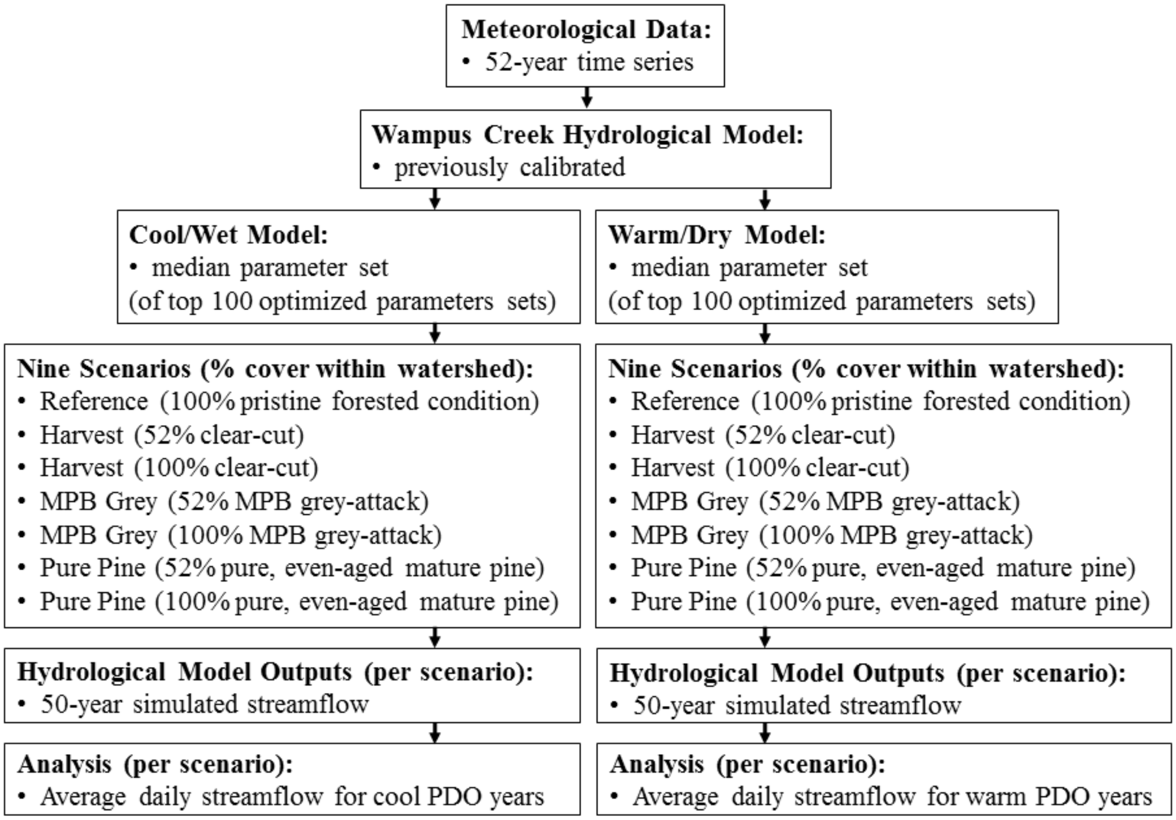

Figure 4.6 Flowchart that illustrates the method used for hydrological model simulations and analysis of model outputs.

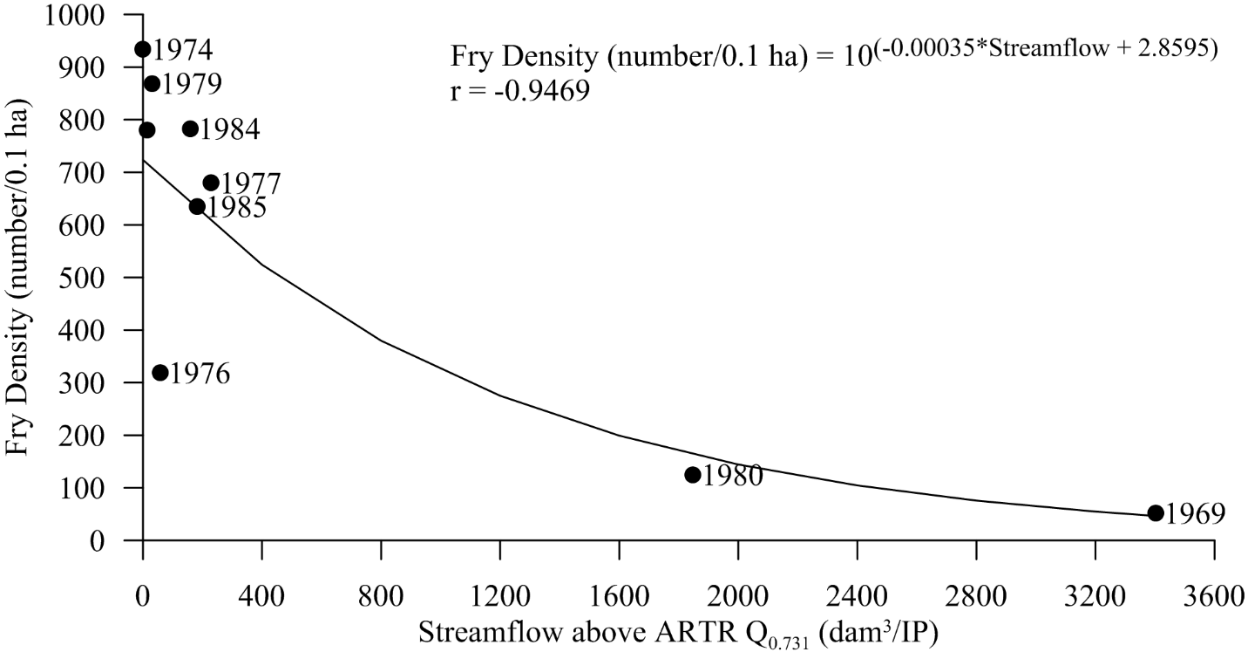

Figure 4.7 Relationship of fry density to streamflow above the ARTR critical discharge threshold (0.731 m^3 s^{-1}) during the incubation period (IP; ~May to Aug) in Wampus Creek from 1969 to 1985 (data from Sterling, 1992). The data point with no year label is 1975. The highest maximum annual peak flow over the 52-year Wampus Creek streamflow record occurred in 1980, while 1969 was the third highest.

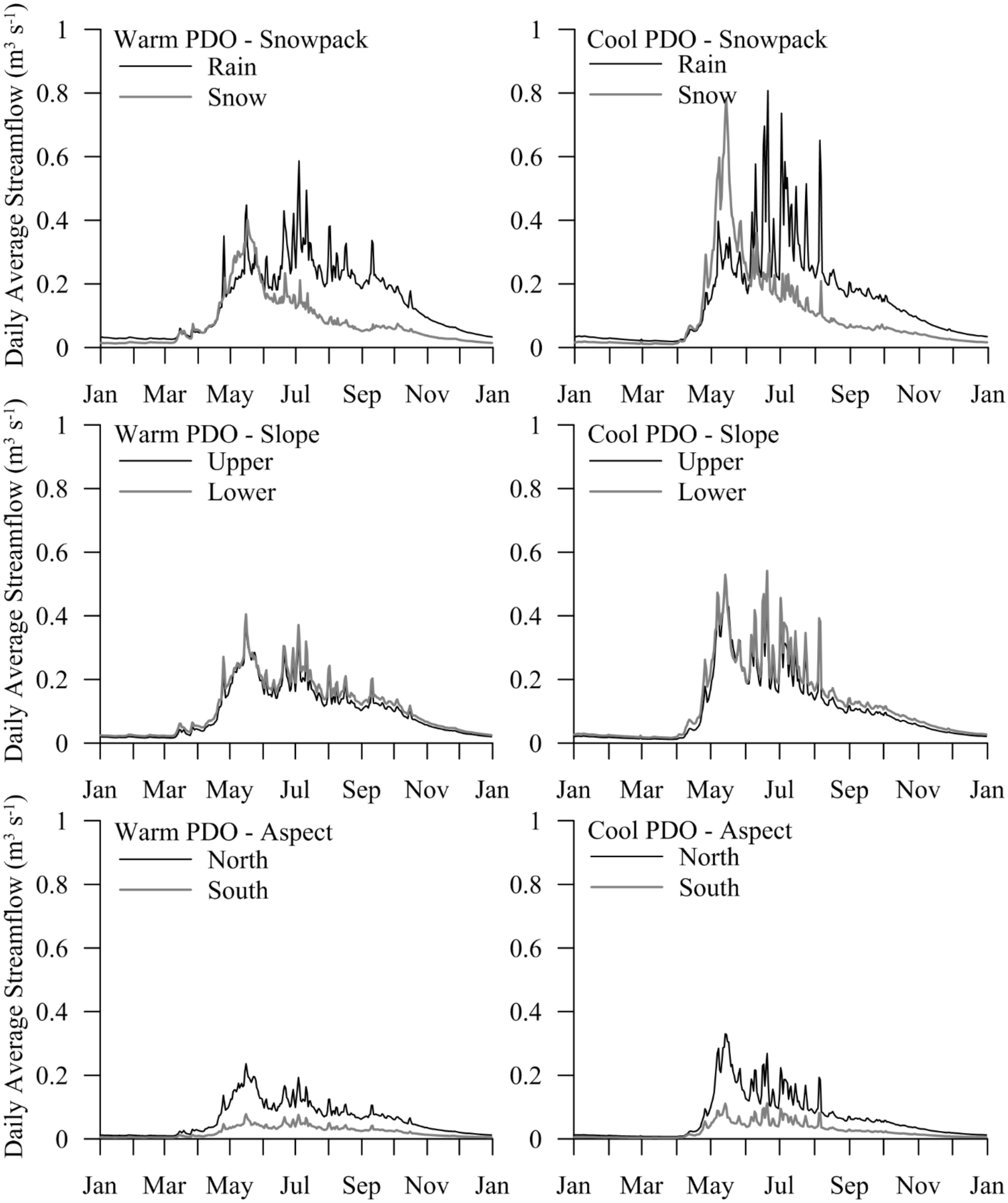

Figure 4.8 Tracking runoff source areas from precipitation and watershed sections for modelled reference condition in Wampus Creek using the conservative tracer in the Raven transport function. Plots show predicted average daily streamflow for the cool PDO periods (using ‘cool/wet model’ output) and warm PDO periods (using the ‘warm/dry’ model output) during the period 1969 – 2019. Runoff source areas include 1) snowpack versus rainfall, 2) slope: upper 2/3 (>9º; 41% total area) and lower 1/3 (≤9º; 52% total area) watershed slope gradients, and 3) aspect: upper watershed north (337.5º - 67.6º; 24% total area) and south (112.5º - 247.5º; 11% total area) aspects.

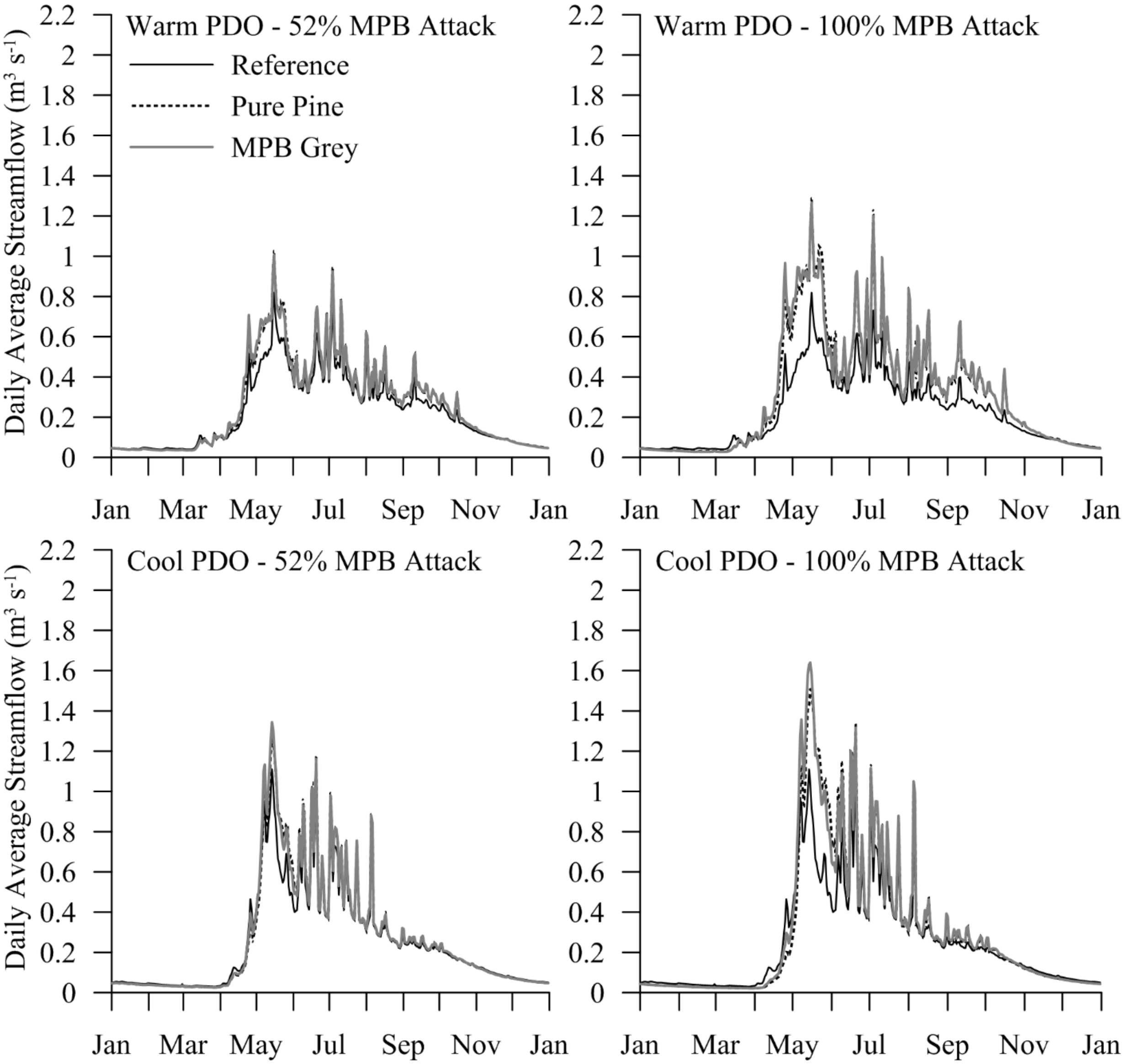

Figure 4.9 Predicted average daily streamflow hydrographs for Wampus Creek for the cool PDO periods (using 'cool/wet model' output) and warm PDO periods (using the 'warm/dry' model output) during the period 1969 – 2019 for 52% and 100% MPB grey-attack compared to the reference condition. Streamflow was also compared to the Pure Pine model scenario over 52% and 100% of the watershed area. The Pure Pine scenario contrasts the reference condition, which represents forests of both mixed-species (pine with other softwoods/hardwoods) and pine-leading stands.

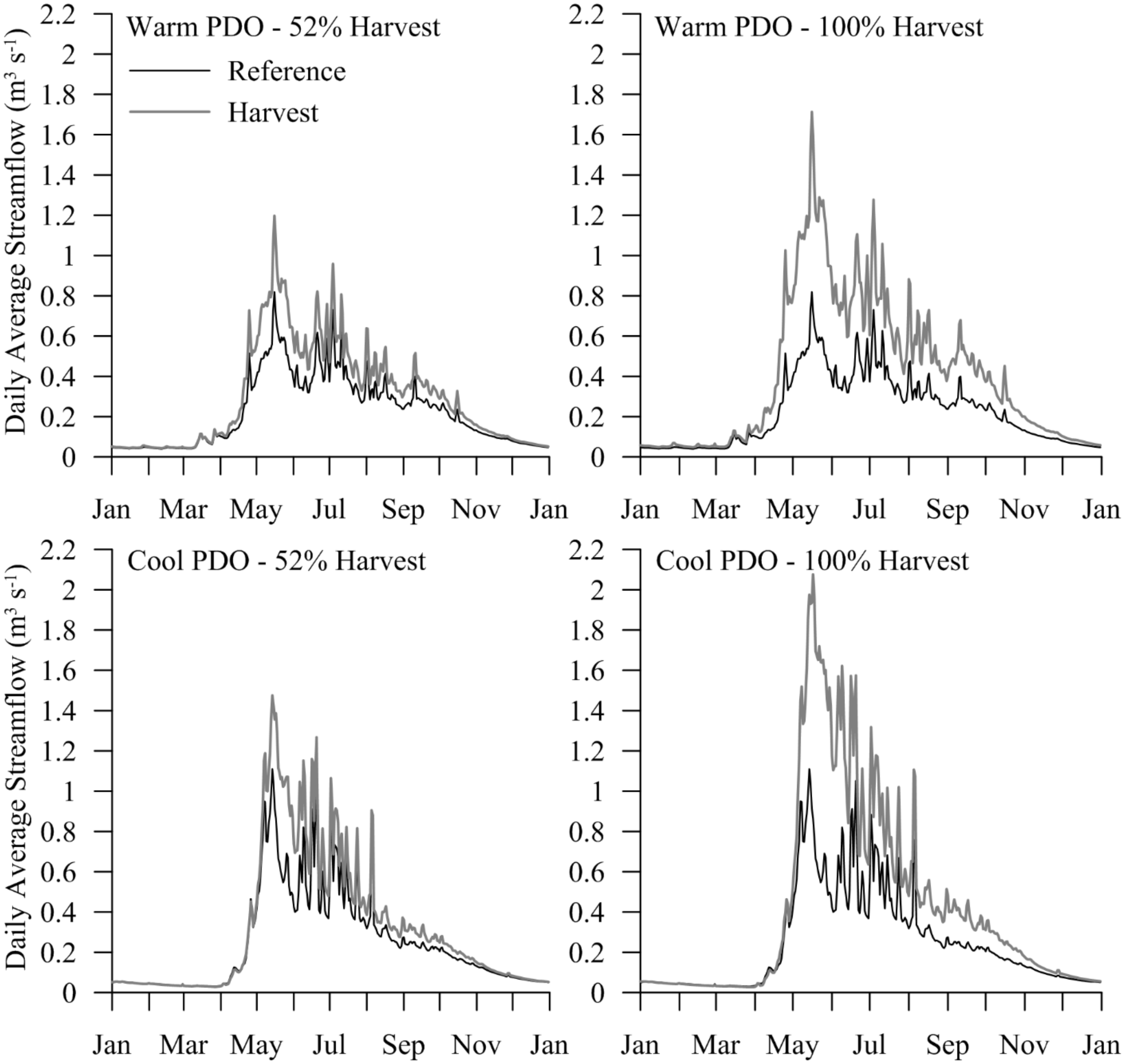

Figure 4.10 Predicted average daily streamflow hydrographs for Wampus Creek for the cool PDO periods (using 'cool/wet model' output) and warm PDO periods (using the 'warm/dry' model output) during the period 1969 – 2019 for 52% and 100% clear-cut harvest compared to the reference condition.

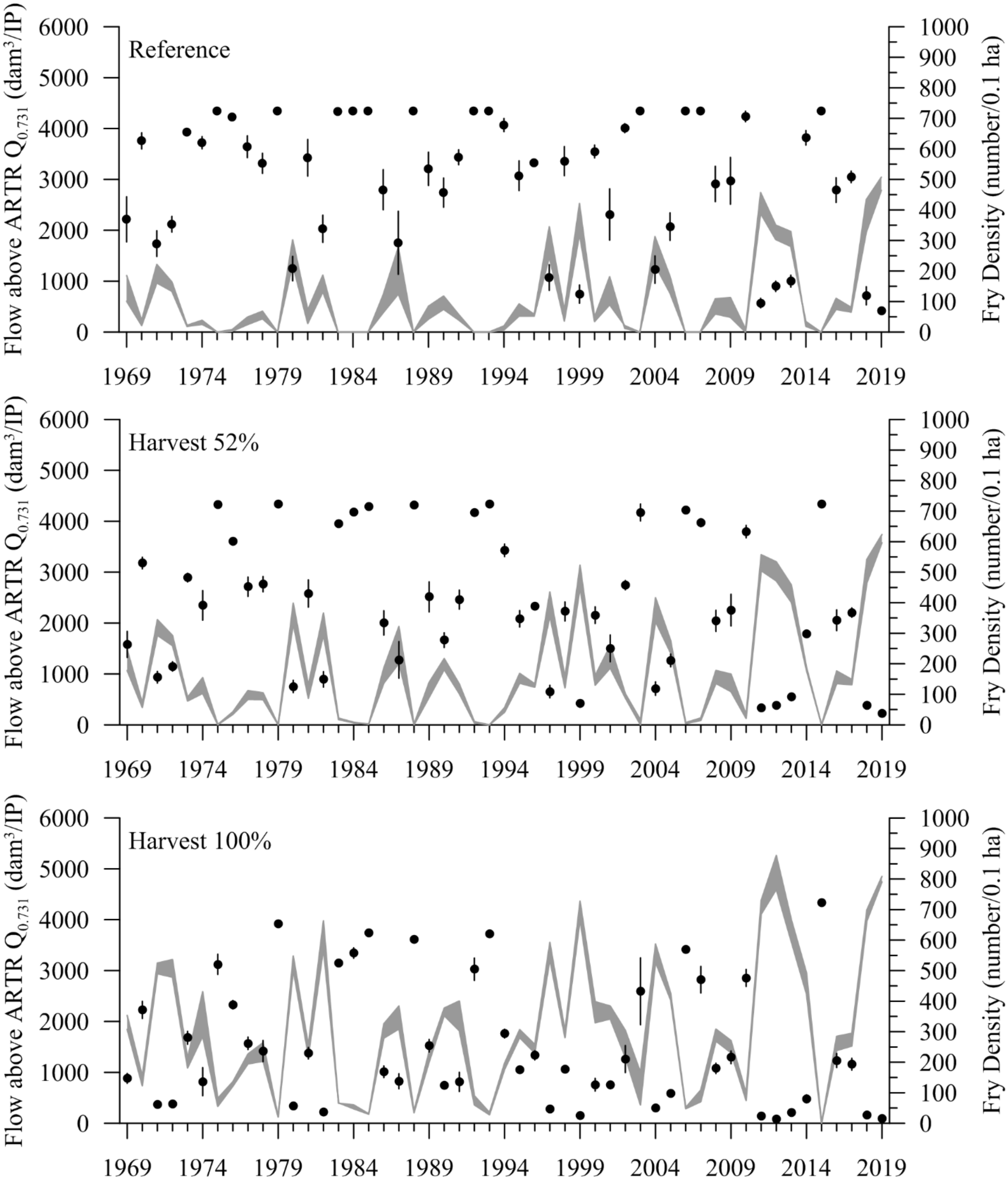

Figure 4.11 Time series of annual predicted streamflow (flow) above the ARTR critical discharge threshold during the average incubation period (IP) plotted for the reference watershed condition, 52% clear-cut harvest (historical cutblock area), and 100% clear-cut harvest as worst-case scenario. The grey band indicates the maximum ('wet/cool' model output) and minimum ('dry/warm' model output) streamflow. Fry densities (black dots) are the average values estimated from the predicted streamflows and bars indicate the maximum/minimum estimated fry density.

CHAPTER 5 - SYNTHESIS

This thesis serves to update, fill knowledge gaps, and introduce new concepts as to the effects of mountain pine beetle (MPB) and forest harvest on hydrologic processes, streamflow response and Athabasca Rainbow Trout (ARTR) fry recruitment in the Alberta Foothills region. The three chapters make novel contributions to forest hydrology, forest and water resource management described in the following sections.

5.1 Mountain Pine Beetle and Forest Harvest Effects on Hydrologic Processes

In chapter 2, I analyzed three years of field data collected from the Robb MPB Ecohydrology before-after control-impact study (MPB Robb) in an undisturbed mature lodgepole pine (i.e. alive) stand, clear-cut salvage harvested stand, and two MPB stands with varied simulated grey-attack intensity. The detailed stand-level measurements were then used to parameterize water balance models that quantified the magnitude of responses exhibited by the individual components of total evapotranspiration (i.e. overstory transpiration, canopy interception loss, understory evapotranspiration, soil evaporation) and root zone drainage. The results add to the literature that provides context for the stand-scale hydrologic response to MPB that range across geo-climate regions within the MPB epidemic from British Columbia (e.g. Winkler *et al.*, 2014) and Alberta (Piña, 2013) to Arizona (Morehouse *et al.*, 2008), and could be used to better understand interrelated feedbacks on nutrient cycling and water quality (e.g. Mikkelson *et al.*, 2013; Cigan *et al.*, 2015).

The hydrometeorological data and water balance modelling results did not support the hypothesis that root zone drainage increases in MPB grey-attack in even-aged mature lodgepole pine stands. As expected, compared to an undisturbed mature stand, within the canopy cover of the MPB grey-attack stands, canopy interception decreased and canopy windspeed increased, while radiation transmitted to the forest floor increased, and soil moisture in the upper soil horizons increased. Compensatory increases in understory evapotranspiration were also observed. Within the 50% Kill stand, the increase in available soil moisture due to partial overstory mortality led to increased transpiration from the neighboring live trees within the stand (Piña, 2013). For the 100% Kill stand, decreased overstory transpiration and canopy rainfall interception losses were compensated by increased understory evapotranspiration as a result of increased net radiation reaching the forest floor, with the net result in minimal change to total evapotranspiration. In all stands, the highest evapotranspiration rates occurred in the summer months with the greatest proportion of annual precipitation, which resulted in snowmelt as the dominant input to soil moisture with additional small increases observed after infrequent large rainfall events. The results of this chapter show that the regional differences in water cycling within MPB grey-attack and salvage harvest stands need to be considered to better understand changes in runoff generation in other geoclimatic regions as MPB continues to spread outside its natural ecological range.

5.2 Forest Harvest Effects on Streamflow

In Chapter 3, I used a combination of statistical and hydrological modelling methods to reanalyze the effect of historical forest harvest in the Tri-Creeks Experimental Watershed (Tri-Creeks) and attempt to isolate the streamflow response from climate variability. The forest harvest experiment coincided with a large-scale ocean-atmosphere circulation phase change of the Pacific Decadal Oscillation (PDO; 1976/77), which was not uncommon in several other historical paired watershed experiments in the Pacific Northwest (Golding, 1980; King and Tennyson, 1984; Troendle and King, 1987; Andres *et al.*, 1987; Cheng, 1989; King, 1989), but not well known or realized until the mid-1990s (Mantua *et al.*, 1997). The climate variability associated with PDO driven changes in precipitation and air temperature obscured the streamflow record as watersheds were found to respond differently in the warm and cool PDO phases. The background climate variability made it difficult to detect measurable change in the streamflow response to forest harvest using linear regression models in the pre-harvest period to predict post-harvest streamflow with the modified double mass curve method (Wei and Zhang, 2010) and a hydrological modelling change detection method (Zégre *et al.*, 2010). I found that a significant forest harvest signal was only detected when a hydrological modelling approach was used that accounted for antecedent soil storage and did not assume hydrological model and linear regression parameters were consistent between the pre- and post-harvest periods. Pre- and post-parameters sets used to reconstruct streamflow driven by the same meteorological data in the post-harvest period assessed the integrated watershed response and could remove additional uncertainty as a result of climate variability (Seibert and McDonnell, 2010). The results of Chapter 3 show that greater caution is needed to evaluate the effect of forest harvest on streamflow when the response is not solely the result of forest harvest operations. To detect forest harvest effects on streamflow, the length of the initial control period with respect to climate variation (e.g. PDO, ENSO) and antecedent storage within watersheds should not be overlooked.

A change-detection hydrological modelling approach that calibrated parameters separately in the pre- and post-harvest periods (Seibert and McDonnell, 2010; Seibert *et al.*, 2010) predicted significant measurable increase in rainfall-generated peak runoff events and summer runoff in the post-harvest period within Deerlick Creek and Wampus Creek, which was not detected in the control watershed. By applying the same change detection approach to the control watershed, it was possible to eliminate unexplained variation as the cause for changes in streamflow and attribute the increases detected from forest harvest with greater certainty. Storm runoff increased in the treatment watersheds in the post-harvest period, but may have been attenuated by the drier antecedent conditions in the warm PDO phase and large potential for subsurface storage given Tri-Creeks' geologic setting. The results of this chapter provided insight into the dominant controls on runoff generation in a region with complex glacial tills underlain by folded and faulted permeable sedimentary bedrock with a more continental climate (i.e. seasonal snowpack with a larger proportion of growing season precipitation). Climate, in relation to antecedent soil condition, remained a strong control on runoff generation even with forest harvest at 52% (Wampus Creek) and 64% (Deerlick Creek) watershed area. Therefore, how Foothills watersheds respond to forest harvest will likely be a function of climate variability, antecedent watershed storage, and subtle differences in actual watershed storage that act as a buffer between water inputs and streamflow response.

This is one of the first studies to explicitly include antecedent watershed storage and subtle differences in actual watershed storage between watersheds in a conceptual model to understand changes in the streamflow regime due to forest harvest. According to Green and Alila's (2012) conceptual model that predicts changes in peak flows due to forest harvest, the more net precipitation that enters the soil after harvest in meso-scale, fully-forested conifer watersheds with no alpine, seasonal snowpack and >50% harvest would be predicted to result in an increase in the mean and variability of peak flows. Their conceptual model focuses on stand-scale changes in snowmelt processes as a result of canopy cover loss and physical characteristics of the watershed that include stand density, slope gradient and aspect, aspect distribution, elevation, percent alpine area, watershed size and drainage density. However, in Tri-Creeks, the streamflow variability appears to be strongly controlled by its geological setting and large potential for subsurface water storage. The distribution of deep (>8 m) glacial soil permeability and water input timing and intensity may exert greater control than topography on runoff generation (Redding and Devito, 2008, 2010; Smith *et al*, 2014; Hokanson *et al.*, 2019). Subsurface runoff from the glacial till was shown to be a large component of streamflow from historical water quality and isotopes samples in Tri-Creeks and is likely an important storage reservoir that fills and drains on a multi-annual basis to deliver water to streamflow and underlying bedrock aquifers (Andres *et al.*, 1987). In addition, increased proportions of permeable or fractured sedimentary bedrock found along the eastern slopes of the Rocky Mountains, like that found in the Foothills, has been suggested to attenuate precipitation inputs for streamflow generation (Jensco *et al.*, 2011; Harder *et al.*, 2015; Spencer *et al.*, 2019). Therefore, the results from Chapter 3 provide further insight into the controls on streamflow response to forest harvest of conifer trees in watersheds with seasonal snowpack.

To my knowledge, this is the only study in a meso-scale watershed relevant to regional management application that simulated the streamflow regime between different historical PDO states as an analogue to anticipated projected climate change impacts on streamflow in western North America. The only other study is at the large continental scale, Fraser River basin (~230,000 km^2), British Columbia (Shrestha *et al.*, 2016): a size where changes on the overall effects to the hydrologic system in relation to climate variability from large-scale ocean-atmosphere circulation patterns may be obscured as opposing and buffering factors emerge at larger scales.

Projected climate changes in precipitation and air temperature may be less than those observed in the historical warm PDO phase in Tri-Creeks; however, the control watershed model (Eunice Creek; 16.8 km^2) was able to reasonably simulate the magnitude and timing of climate-driven differences in the warm PDO condition when streamflow was reconstructed with parameters calibrated in the cool PDO phase (i.e. pre-parameters). For example, pre-parameters used to reconstruct streamflow for the warm PDO period (1977 – 1988) in the control watershed under-predicted spring streamflow and did not capture the timing of advanced snowmelt. The hydrological model's ability to simulate future hydrologic changes based on potential climate changes scenarios may be important for watershed management (e.g. environmental surface water baseline assessments; environmental flow needs studies). The results of this chapter demonstrate that caution is needed when using a hydrological model to assess potential future climate change on streamflow regimes in the Alberta Foothills, especially when quantifying values of ecological flow needs for forest management planning or infrastructure design.

5.3 Mountain Pine Beetle and Forest Harvest Effects on ARTR Fry Recruitment

Chapter 4 results showed that MPB had little effect on streamflow during the ARTR incubation period (May 29 to Aug 3), while forest harvest (52% watershed area) increased summer water yield 16% and 32% compared to MPB grey-attack and reference scenarios, respectively. Overall, summer streamflow in the forest harvest scenarios was higher during cool PDO periods when there was larger snowmelt input and wetter antecedent soil conditions (i.e. expansion of saturated areas within the watershed). However, increased streamflow above the ARTR critical discharge threshold of 0.731 $m^3 s^{-1}$ during the incubation period could be large even in the warm PDO periods due to the stochastic nature of heavy summer rainfall events in the Foothills region.

ARTR are adapted to and have evolved with these episodic extreme flow events, and fry recruitment within this population has adapted to streamflow changes from historical forest harvest in Wampus Creek (1978 – 1983) as population abundance data indicate the ARTR population continued to persist 30 years later (Sterling, 1992; Rasmussen and Taylor, 2009; Alberta ARTR Team, 2014). Over the 50-year simulated streamflow record, fry recruitment was estimated to occur in all years, even despite an extreme worst-case scenario of clear-cut harvest across the entire watershed. These results show that increased spawning substrate mobility as a result of streamflow changes due to forest harvest would not likely produce a measurable change in ARTR fry recruitment at the population level. To my knowledge, this is the first study to have documented the potential streamflow changes due to forest harvest and the direct effect on salmonid fry recruitment. These results could factor into decisions about current MPB strategies in the Alberta Foothills region with respect to the endangered Athabasca Rainbow Trout (Fisheries and Oceans Canada, 2020).

5.4 Future Research

This thesis made use of decadal and multi-decadal datasets collected at both the stand-scale (MPB Robb) and watershed-scale (Tri-Creeks), which demonstrates the need for continued long-term monitoring to better understand forestry management and the watershed response. For example, the 2nd pass harvest started in Wampus Creek in December, 2018. Presently, the assumption in Wampus Creek is that after 35 years post-harvest the cutblocks have established adequate canopy cover for hydrologic recovery to pre-harvest levels. However, studies of streamflow data in a snowmelt-dominated watershed with conifer forests in Colorado suggested that hydrologic recovery of cutblocks occurs slowly and may take as long as 80 years post-harvest

(Troendle and King, 1985; Green and Alila, 2012). Therefore, further research in Foothills watersheds made up of regenerating forest and clear-cut harvested stands and the effects on streamflow are needed. Continued streamflow monitoring in Wampus Creek (Water Survey of Canada) and a nearby meteorological station (Luscar Creek; Alberta Environment and Parks) could be used to explore such questions in the future. However, that being said, there is a need in the literature for better understanding of water cycling in regenerating/juvenile stands and what stand attribute (e.g. leaf area index, canopy cover, tree height, etc.) is the primary driver to the return of hydrologic recovery in the stand. For example, in the British Columbia interior, rainfall interception losses in a 4-m tall lodgepole pine stand were not similar to an adjacent mature forest until 25 years post-harvest, while maximum snow water equivalent was only 43% recovered in a 4.5-m tall stand with 28% canopy cover (Winkler *et al.*, 2005; Winkler *et al.*, 2010). Further research is needed in the geo-climate of the Foothills region in regenerating stands with stand attributes commonly assessed using the Alberta forest and vegetation inventory datasets.

Similarly, there is a need to understand stand water cycling as the MPB grey-attack stands age and most dead trees fall to the ground (~15 years post-attack). The MPB grey-attack stands that were not salvaged across the geographic extent of MPB infestation will either regenerate into new forest or be rehabilitated (e.g. Steinke *et al.*, 2020; Rhoades *et al.*, 2020). A study within a MPB grey-attack stand in British Columbia used hydrological modelling to project changes in water cycling into the next decade with changes in stand succession (Meyers *et al.*, 2017). Natural succession in MPB grey-attack stands may favour shade tolerant or semi shade tolerate species in even-aged pine forests (Dhar and Hawkins, 2011), but salvage harvest stands that are replanted with nursery-grown tree seedlings (with or without silviculture intervention) may have a much more simplified stand structure and composition. Data collection in these stand types would be useful to quantify changes in the magnitude of response in individual evapotranspiration components and root zone drainage, as well as to parameterize hydrological watershed models.

The results of this thesis suggest rainfall and snowmelt depth and intensity, in relation to soil storage capacity (i.e. antecedent conditions), are likely strong controls on groundwater response, similar to that observed in soils developed from deep (>8 m) glacial tills (Redding and Devito, 2008, 2010; Smith *et al.*, 2014). However, further research is needed to better understand the first order controls on rainfall (snowmelt) – runoff relationships and how and when hillslopes connect to streams, especially with the influence of PDO driven meteorological changes. A detailed groundwater study in Tri-Creeks would provide further understanding into the runoff generation processes in Foothills watersheds that have complex glacial deposits underlain by permeable bedrock, such as specific thresholds that control vertical and lateral subsurface flow (i.e. storage and transmission properties of the soil, subsoil and bedrock). Further knowledge of subsurface flow pathways and how they change with forest disturbance would have implications for biogeochemical assessments into nutrient cycling, contaminant fluxes or water quality.

Lastly, integration between forest hydrology and aquatic ecology disciplines is needed to develop a comprehensive understanding of the potential impacts of watershed disturbance and the response of the endangered ARTR population success. For example, further population modelling is needed to understand if reduced fry recruitment due to forest harvest and changes in the streamflow regime with additional cumulative anthropogenic threats (e.g. angling pressure, increased sedimentation, and competition with Brook Trout) translate into ARTR population decline.

REFERENCES

(AAF) Alberta Agriculture and Forestry. (2018). Forest management plan approval decision (2018–2027): forest management unit R13: West Fraser Mills Ltd. (Edson). Government of Alberta, Ministry of Agriculture and Forestry. Edmonton. 20 pp.

(Alberta ARTR Team) Alberta Athabasca Rainbow Trout Recovery Team. (2014). Alberta Athabasca Rainbow Trout Recovery Plan, 2014-2019. Alberta Environment and Sustainable Resource Development, Alberta Species at Risk Recovery Plan No. 36. Edmonton, AB. 111 pp.

(ASRD) Alberta Sustainable Resource Development. (2007) Mountain Pine Beetle action plan, Edmonton, Alberta, Canada, 8 pp.

(BCMoFR) British Columbia Ministry of Forests and Range. (2005). Merritt timber supply area. Rationale for annual allowable cut (AAC) determination, effective 1 July 2005. http://www.for.gov.bc.ca/hts/tsa/tsa18/tsr3/18ts05ra.pdf (Accessed 2 February 2017).

Adams, H. D., Luce, C. H., Breshears, D. D., Allen, C. D., Weiler, M., Hale, V. C., Smith, A. M. S. & Huxman, T. E. (2012). Ecohydrological consequences of drought- and infestation-triggered tree die-off: insights and hypotheses. *Ecohydrology*, 5, 145–159.

Adams, R.S. (1990). Evapotranspiration and surface conductance for a high elevation, grass covered forest clearcut. MSc thesis, Univ. of Alberta, Edmonton, Alberta. 42 pp.

Alila, Y., Bewley, D., Kuraś, P., Marren, P., Hassan, M., Luo, C., & Blair, T. (2009). Effects of pine beetle infestations and treatments on hydrology and geomorphology: Integrating stand-level data and knowledge into mesoscale watershed functions. Natural Resources Canada, Canadian Forest Service, Pacific Forestry Centre, Victoria. Mountain Pine Beetle Working Paper 2009-06. 69 pp.

Andres, D., van der Vinne, G., & Sterenberg, G. (1987). Hydrologic, hydrogeologic, thermal, sediment and channel regimes of the Tri-Creeks Experimental Basin. Alberta Research Council, Report No. SWE-87/01. Vol. 1. 418 pp.

Andres, D. (1974). Tri Creek bed mobility study. Alberta Environment, Technical Services Division. 72 pp.

Australian Bureau of Meteorology. (2015). S.O.I. (Southern Oscillation Index) archives – 1876 to present. http://www.bom.gov.au/climate/ current/soihtm1.shtml (Accessed 9 July, 2015).

Baldocchi, D.D., Vogel, C.A., & Hall, B. (1997). Seasonal variation of carbon dioxide exchange rates above and below a boreal jack pine forest. *Agricultural and Forest Meteorology*, 83, 147–170.

Barr, A. G., Van der Kamp, G., Black, T. A., McCaughey, J. H., & Nesic, Z. (2012). Energy balance closure at the BERMS flux towers in relation to the water balance of the White Gull Creek watershed 1999–2009. *Agricultural and Forest Meteorology*, 153, 3-13.

Bates, C.G. (1921). First results in the streamflow experiment Wagon Wheel Gap, Colorado. *Journal of Forestry*, 19, 402-408.

Baylis, A. D. (2000). Why glyphosate is a global herbicide: strengths, weaknesses and prospects. *Pest Management Science*: formerly *Pesticide Science*, 56(4), 299-308.

Beckers, J., Smerdon, B., Redding, T., Anderson, A., Pike, R., & Werner, A. T. (2009). Hydrologic models for forest management applications: Part 1: Model selection. *Watershed Management Bulletin*, 13(1), 35-44.

Beckingham, J.D., Corns, I.G.W., & Archibald, J.H. (1996). Field guide to ecosites of West-Central Alberta. UBC Press, Vancouver, BC.

Bergström, S. (1995). The HBV model. In Singh,V.P. (Ed.), Computer models of watershed hydrology (pp. 443–476). Highlands Ranch, CO: Water Resources Publications.

Bethlahmy, N. (1974) More streamflow after a bark-beetle epidemic. *Journal of Hydrology*, 23(3-4), 185-189, doi:10.1016/0022-1694(74)90001-8.

Bewley, D., Alila, Y., & Varhola, A. (2010). Variability of snow water equivalent and snow energetics across a large catchment subject to Mountain Pine Beetle infestation and rapid salvage logging. *Journal of Hydrology*, 388(3), 464-479.

Biederman, J. A., Somor, A. J., Harpold, A. A., Gutmann, E. D., Breshears, D. D., Troch, P. A., Gochis, D.J., Scott, R.L., Meddens, A.J.H. & Brooks, P. D. (2015). Recent tree die-off has little effect on streamflow in contrast to expected increases from historical studies. *Water Resources Research*, 51(12), 9775-9789.

Biederman, J. A., Harpold, A. A., Gochis, D. J., Ewers, B. E., Reed, D. E., Papuga, S. A., & Brooks, P. D. (2014a). Increased evaporation following widespread tree mortality limits streamflow response. *Water Resources Research*, 50(7), 5395-5409.

Biederman, J. A., Brooks, P. D., Harpold, A. A., Gutmann, E., Gochis, D.J., Reed, D.E., & Pendall, E. (2014b), Multi-scale observations of snow accumulation and peak snowpack following widespread, insect-induced lodgepole pine mortality. *Ecohydrology*, 7(1), 150–162, doi: 10.1002/eco.1342.

Bladon, K. D., Silins, U., Landhäusser, S. M., & Lieffers, V. J. (2006). Differential transpiration by three boreal tree species in response to increased evaporative demand after variable retention harvesting. *Agricultural and Forest Meteorology*, 138(1-4), 104-119.

Bond-Lamberty, B., Gower, S. T., Amiro, B., & Ewers, B. E. (2011). Measurement and modelling of bryophyte evaporation in a boreal forest chronosequence. *Ecohydrology*, 4(1), 26-35.

Boon, S. (2012). Snow accumulation following forest disturbance. *Ecohydrology*, 5(3), 279-285.

Boon, S. (2009). Snow ablation energy balance in a dead forest stand. *Hydrological Processes*, 23(18), 2600-2610.

Boon, S. (2007). Snow accumulation and ablation in a beetle-killed pine stand in Northern Interior British Columbia. *Journal of Ecosystems and Management*, 8(3), 1-13.

Bosch, J. M., & Hewlett, J. D. (1982). A review of catchment experiments to determine the effect of vegetation changes on water yield and evapotranspiration. *Journal of Hydrology*, 55(1), 3-23.

Brabender, B. (2005). Scaling leaf area index and rainfall interception in lodgepole pine. MSc thesis, Univ. of Alberta, Edmonton, Alberta. 91 pp.

Brown, M. G., Black, T. A., Nesic, Z., Foord, V. N., Spittlehouse, D. L., Fredeen, A. L., Bowler, R., Grant, N.J., Burton, P.J., Trofymow, D.L. & Meyer, G. (2013). Evapotranspiration and canopy characteristics of two lodgepole pine stands following mountain pine beetle attack. *Hydrological Processes*, 28(8), 3326-3340.

Brown, M. J., & Parker, G. G. (1994). Canopy light transmittance in a chronosequence of mixed-species deciduous forests. *Canadian Journal of Forest Research*, 24(8), 1694-1703.

Brubaker, K. A. Y. E., Rango, A., & Kustas, W. (1996). Incorporating radiation inputs into the snowmelt runoff model. *Hydrological Processes*, 10(10), 1329-1343.

Burles, K., & Boon, S. (2011). Snowmelt energy balance in a burned forest plot, Crowsnest Pass, Alberta, Canada. *Hydrological Processes*, 25, 3012–3029. doi:10.1002/HYP.8067

Burt, T. P., Howden, N. J. K., McDonnell, J. J., Jones, J. A., & Hancock, G. R. (2015). Seeing the climate through the trees: observing climate and forestry impacts on streamflow using a 60-year record. *Hydrological Processes*, 29(3), 473–480. https://doi.org/10.1002/hyp.10406

Campbell Scientific (2015). Instruction manual for CS616 and CS625 water content reflectometers. Campbell Scientific, Inc. 46 pp.

Canadian Hydraulics Centre. (2010). Green Kenue reference manual. Ottawa, ON: National Research Council. 340 pp.

Carey, S. K., Tetzlaff, D., Seibert, J., Soulsby, C., Buttle, J., Laudon, H., McDonnell, J., McGuire, K., Caissie, D., Shanley, J., Kennedy, M., Devito, K., & Pomeroy, J.W. (2010). Inter-comparison of hydro-climatic regimes across northern catchments: Synchronicity, resistance and resilience. *Hydrological Processes*, 24(24), 3591-3602.

Carlyle-Moses, D.E., Lishman, C.E., & McKee, A.J. (2014) A preliminary evaluation of throughfall sampling techniques in a mature coniferous forest. Journal of Forestry Research, 25, 407–413. doi:10.1007/S11676-014-0468-8

Carroll, AL, Regniere, J., Logan, J.A., Taylor, S.W., Bentz, B., & Powell J.A. (2006). Impacts of climate change on range expansion by the mountain pine beetle. Mountain Pine Beetle Initiative Working Paper 2006-14, Natural Resources Canada, Canadian Forest Service, Victoria, British Columbia, Canada. 27 pp.

Caskenette, A.L. & Koops M.A. (2018). Recovery Potential Modelling of Rainbow Trout, Oncorhynchus mykiss (Athabasca River Populations). DFO Can. Sci. Advis. Sec. Res. Doc. 2018/021. iv. 30 pp.

Cheng, J. D. (1989). Streamflow changes after clearcut logging of a pine beetle infested watershed in southern British Columbia, Canada. *Water Resources Research*, 25(3), 449–456. https://doi.org/10.1029/WR025i003p00449

Chernos, M., MacDonald, R., & Craig, J. (2017). Efficient semi-distributed hydrological modelling workflow for simulating streamflow and characterizing hydrologic processes. *Confluence: Journal of Watershed Science and Management*, 1, 1-13 doi: 10.22230/jwsm.2017v1n1a3

Cigan, P. W., Karst, J., Cahill, J. F., Sywenky, A. N., Pec, G. J., & Erbilgin, N. (2015). Influence of bark beetle outbreaks on nutrient cycling in native pine stands in western Canada. *Plant and Soil*, 390(1-2), 29-47.

Clark, M. P., McMillan, H. K., Collins, D. B., Kavetski, D., & Woods, R. A. (2011). Hydrological field data from a modeller's perspective: Part 2: process-based evaluation of model hypotheses. *Hydrological Processes*, 25(4), 523-543.

Clark, M.P., Slater, A.G., Rupp, D.E., Woods, R.A., Vrugt, J.A., Gupta, H.V., Wagener, T., & Hay, L.E. (2008). Framework for understanding structural errors (fuse): a modular framework to diagnose differences between hydrological models. *Water Resources Research*, 44(12), 1-14.

Clow, D. W., Rhoades, C., Briggs, J., Caldwell, M., & Lewis, W. M. (2011). Responses of soil and water chemistry to mountain pine beetle induced tree mortality in Grand County, Colorado, USA. Applied Geochemistry, 26, S174-S178.

Collins, B. J., Rhoades, C. C., Underhill, J., & Hubbard, R. M. (2010). Post-harvest seedling recruitment following mountain pine beetle infestation of Colorado lodgepole pine stands: a comparison using historic survey records. *Canadian Journal of Forest Research*, 40(12), 2452-2456.

COSEWIC (2014). COSEWIC assessment and status report on the Rainbow Trout Oncorhynchus mykiss in Canada. Committee on the Status of Endangered Wildlife in Canada. Ottawa. xi, 60 pp.

COSEWIC (2012). COSEWIC assessment and status report on the Bull Trout Salvelinus confluentus in Canada. Committee on the Status of Endangered Wildlife in Canada. Ottawa. iv, 103 pp.

Craig, J. R., Brown, G., Chlumsky, R., Jenkinson, W., Jost, G., Lee, K., Mai, J., Serrer, M., Sgro, N., Shafii, M., Snowdon, A., & Tolson, B. (2020). Flexible watershed simulation with the Raven hydrological modelling framework. Environmental Modelling & Software, 104728.

Craig, J.R., Huang,, S., Khedr, A., Pearson, S., Spraakman, S., Stonebridge, G., Werstuck, C., & Zhang, C. (2019). Raven: user's and developer's manual. Raven Version 2.9.2. URL: http://raven.uwaterloo.ca/ (Accessed July, 2019).

Creed, I. F., Spargo, A. T., Jones, J. A., Buttle, J. M., Adams, M. B., Beall, F. D., Booth, E.G., Campbell, J.L., Clow, D., Elder, K., Green, M.B., Grimm, N.B., Miniat, C., Ramlal, P., Saha, A., Sebestyen, S., Spittlehouse, D., Sterling, S., Williams, M.W., Winkler, R., & Yao, H. (2014). Changing forest water yields in response to climate warming: results from long-term experimental watershed sites across North America. *Global Change Biology*, 20(10), 3191-3208.

Currie, D.V. (1969). Hydrogeology of the Tri Creeks Basin, Alberta. MSc thesis, Univ. of Alberta, Edmonton, Alberta. 67 pp.

Devito K.J., Creed, I.F., & Fraser, C. (2005). Controls on runoff from a partially harvested aspen forested headwater catchment, Boreal Plain, Canada. *Hydrological Processes*, 19, 3-25.

DeVries P. (1997). Riverine salmonid egg burial depths: a review of published data and implications for scour studies. *Canadian Journal of Fisheries and Aquatic Sciences*, 54, 1685-1698.

Dhar, A., & Hawkins, C. D. (2011). Regeneration and growth following mountain pine beetle attack: A synthesis of knowledge. *Journal of Ecosystems and Management*, 12(2).

Dingman S.L. (2002). Physical hydrology, 2nd edn. Prentice-Hall Inc., Upper Saddle River, New Jersey 07458, USA

Dumanski, J., Macyk, T.M., Veavvy, C.F., and J.D. Lindsay. (1972). Soil survey and land evaluation of Hinton-Edson area, Alberta. Alberta Institute of Pedology, Report No. S-72-31. 119 pp.

Eckhardt, K. (2012). Analytical sensitivity analysis of a two parameter recursive digital baseflow separation filter. *Hydrology and Earth System Sciences*, 16(2), 451.

Einum, S., and K. H. Nislow. (2005). Local-scale density-dependent survival of mobile organisms in continuous habitats: an experimental test using Atlantic salmon. *Oecologia*, 143, 203-210.

Elliott, J. A., Toth, B. M., Granger, R. J., & Pomeroy, J. W. (1998). Soil moisture storage in mature and replanted sub-humid boreal forest stands. *Canadian Journal of Soil Science*, 78(1), 17-27.

Elliott, J. M. (1985). Population regulation for different life-stages of migratory trout Salmo trutta in a Lake District stream, 1966-83. *Journal of Animal Ecology*, 617-638.

Ellis, C. R., Pomeroy, J. W., Essery, R. L. H., & Link, T. E. (2011). Effects of needleleaf forest cover on radiation and snowmelt dynamics in the Canadian Rocky Mountains. *Canadian Journal of Forest Research*, 41(3), 608-620.

Environment Canada. (2016). Historical climate data. URL: http://climate.weather.gc.ca/ (Accessed February 3, 2016).

Fang, X., & Pomeroy, J. W. (2016). Impact of antecedent conditions on simulations of a flood in a mountain headwater basin. *Hydrological Processes*, 30(16), 2754-2772.

Fausch, K. D. (2008). A paradox of trout invasions in North America. *Biological Invasions*, 10, 685-701.

Fettig, C. J., Reid, M. L., Bentz, B. J., Sevanto, S., Spittlehouse, D. L., & Wang, T. (2013). Changing climates, changing forests: a western North American perspective. *Journal of Forestry*, 111(3), 214-228.

Fielder, P., & Comeau, P. (2000). Construction and testing of an inexpensive PAR sensor. Resources Branch, Ministry of Forests, Victoria, BC. Working Paper 53/2000. URL: http://www.for.gov.bc.ca/hfd/pubs/Docs/Wp/Wp53.htm (Accessed May 15, 2015).

Fisheries and Oceans Canada. (2020). Recovery Strategy for the Rainbow Trout (Oncorhynchus mykiss) in Canada (Athabasca River populations). Species at Risk Act Recovery Strategy Series. Fisheries and Oceans Canada, Ottawa. vii, 90 pp.

Goeking, S. A., & Tarboton, D. G. (2020). Forests and water yield: a synthesis of disturbance effects on streamflow and snowpack in western coniferous forests. *Journal of Forestry*, 118(2), 172-192.

Golding, D.L. (1980). Calibration is the pre-treatment relationship between the streamflow characteristic of interest and some other variable or variables. Proceedings of the Helsinki Symposium, June 1980: IAHS-AISH Publ. no. 130, 3-7.

Golding, D.L., & Stanton, C. R. (1972). Water storage in the forest floor of subalpine forests of Alberta. *Canadian Journal of Forest Research*, 2(1), 1-6.

Gomi, T., Moore, R. D., & Dhakal, A. S. (2006). Headwater stream temperature response to clear-cut harvesting with different riparian treatments, coastal British Columbia, Canada. *Water Resources Research*, 42, W08437, doi:10.1029/2005WR004162.

Goode, J. R., Buffington, J. M., Tonina, D., Isaak, D. J., Thurow, R. F., Wenger, S., Nagel, D., Luce, C., Tetzlaff, T., & Soulsby, C. (2013). Potential effects of climate change on streambed scour and risks to salmonid survival in snow-dominated mountain basins. *Hydrological Processes*, 27(5), 750-765.

Granier, A. (1987). Evaluation of transpiration in a douglas-fir stand by means of sap flow measurements. *Tree Physiology*, 3(4), 309-319.

Granier, A. (1985). A new method of sap flow measurement in tree stems. *Annales Des Sciences Forestieres*, 42(2), 193-200.

Green, K. C., & Alila, Y. (2012). A paradigm shift in understanding and quantifying the effects of forest harvesting on floods in snow environments. *Water Resources Research*, 48(10), W10503.

Greig, S. M., Sear, D. A., & Carling, P. A. (2007). A review of factors influencing the availability of dissolved oxygen to incubating salmonid embryos. *Hydrological Processes*, 21(3), 323-334.

Guillemette, F., Plamondon, A. P., Prévost, M., & Lévesque, D. (2005). Rainfall generated stormflow response to clearcutting a boreal forest: peak flow comparison with 50 world-wide basin studies. *Journal of Hydrology*, 302(1-4), 137-153.

Gunn, J., & Sein, R. (2000). Effects of forestry roads on reproductive habitat and exploitation of lake trout. *Canadian Journal of Fisheries and Aquatic Sciences*, 57, 97-104.

Harder, P., Pomeroy, J. W., & Westbrook, C. J. (2015). Hydrological resilience of a Canadian Rockies headwaters basin subject to changing climate, extreme weather, and forest management. *Hydrological Processes*, 29(18), 3905–3924. https://doi.org/10.1002/hyp.10596

Hargreaves, G. H., & Samani, Z. A. (1985). Reference crop evapotranspiration from temperature. *Applied Engineering in Agriculture*, 1(2), 96-99.

Hedstrom, N., & Pomeroy, J. (1998). Measurements and modelling of snow interception in the boreal forest. *Hydrological Processes*, 12(1011), 1611–1625.

Hendry, M. J. (1982). Hydraulic conductivity of a glacial till in Alberta. *Groundwater*, 20(2), 162-169.

Hibbert, A. (1967). Forest treatment effects on water yield. In International symposium on forest hydrology, Sopper, W.A.L.H. (ed.). Pergamon, Oxford.

Hill T., & Lewicki, P. (2007). Statistics Methods and Applications. StatSoft: Tulsa, OK, 800 pp.

Hillman, G.R., Powell, J.M., & Rothwell, R.L. (1978). Hydrometeorology of the Hinton-Edson area, Alberta, 1972-75. Canadian Northern Forestry Centre, Edmonton, Alberta. Inf. Rep. NOR-X-202. 171 pp.

Hokanson, K.J., Mendoza, C.A., & Devito, K.J. (2019). Interactions between regional climate, surficial geology, and topography: Characterizing shallow groundwater systems in subhumid, low-relief landscapes. *Water Resources Research*, 55, 284–297, doi: 10.1029/2018WR023934

Howard, M.J. (2018). Erosion and erodibility from off highway vehicle trails in Alberta's Southern Rocky Mountains. MSc thesis, Univ. of Alberta, Edmonton, Alberta. 139 pp.

Hubbard, R. M., Rhoades, C. C., Elder, K., & Negron, J. (2013). Changes in transpiration and foliage growth in lodgepole pine trees following mountain pine beetle attack and mechanical girdling. *Forest Ecology and Management*, 289, 312-317.

IPCC (2013), Climate change 2013: the physical science basis, in Contribution of Working Group I to the Fifth Assessment Report of the Inter-governmental Panel on Climate Change, edited by T. F., D. Qin, *et al.*, Cambridge University Press, Cambridge, U. K., doi: 10.1017/CBO9781107415324. 1535 pp.

Jablonski, P.D. (1978). Mesoclimate of the Tri-Creeks Region. The Tri-Creeks Watershed Study Rep. No. 3. Alberta Energy and Natural Resources, Forest Land Use Branch. 28 pp.

Jencso, K. G., & McGlynn, B. L. (2011). Hierarchical controls on runoff generation: topographically driven hydrologic connectivity, geology, and vegetation. *Water Resources Research*, 47(11), W11527, doi:10.1029/2011WR010666.

Jones, J. A., Creed, I. F., Hatcher, K. L., Warren, R. J., Adams, M. B., Benson, M. H., Boose, E., Brown, W.A, Campbell, J.L., Covich, A., Clow, D.W., Dahm, C.N., Elder, K., Ford, C.R., Grimm, N.B., Henshaw, D.L., Larson, K.L., Miles, E.S., Miles, K.M., Sebestyen, S.D., Spargo, A.T., Stone, A.B., Vose, J.M., & Williams, M.W. (2012). Ecosystem processes and human influences regulate streamflow response to climate change at long-term ecological research sites. *BioScience*, 62(4), 390-404.

Jones, J. A., & Post, D. A. (2004). Seasonal and successional streamflow response to forest cutting and regrowth in the northwest and eastern United States. *Water Resources Research*, 40(5), W05203, doi:10.1029/2003WR002952.

Karpyshin, S. (2019). Transpiration response of residual lodgepole pine after partial-cut and strip-shelterwood harvesting in Alberta's southern Rocky Mountains. MSc thesis, Univ. of Alberta, Edmonton, Alberta. 101 pp.

Kelliher, F.M., Leuning, R., & Schulze, E.D. (1993). Evaporation and canopy characteristics of coniferous forests and grasslands. *Oecologia*, 95(2), 153–163.

King, J. G. (1989). Streamflow responses to road building and harvesting: a comparison with the equivalent clearcut area procedure. Res. Pap. INT-401. Ogden, UT: U.S. Department of Agriculture, Forest Service, lntermountain Research Station. 13 pp.

King, J. G., & Tennyson, L. C. (1984). Alteration of Streamflow Characteristics Following Road Construction in North Central Idaho. *Water Resources Research*, 20(8), 1159–1163.

Korman, J., Kaplinski, M., & Melis, T. S. (2011). Effects of fluctuating flows and a controlled flood on incubation success and early survival rates and growth of age-0 rainbow trout in a large regulated river. *Transactions of the American Fisheries Society*, 140(2), 487-505.

Lapointe, M., Eaton, B., Driscoll, S., & Latulippe, C. (2000). Modelling the probability of salmonid egg pocket scour due to floods. *Canadian Journal of Fisheries and Aquatic Sciences*, 57(6), 1120-1130.

Love, L. D. (1955). The effect on streamflow of the killing of spruce and pine by the Engelmann spruce beetle, EOS, *Transactions American Geophysical Union*, 36(1), 113–118, doi:10.1029/TR036i001p00113.

Lytle, D. A., & Poff, N. L. (2004). Adaptation to natural flow regimes. *Trends in Ecology & Evolution*, 19(2), 94-100.

MacIsaac, E. A. (2010). Salmonids and the hydrologic and geomorphic features of their spawning streams in British Columbia. Compendium of forest hydrology and geomorphology in British Columbia. British Columbia Ministry of Forests and Range, 66, 461-478.

Mahat, V., Anderson, A., & Silins, U. (2015). Modelling of wildfire impacts on catchment hydrology applied to two case studies. *Hydrological Processes*, 29(17), 3687-3698.

Mangiafico, S. S. (2017). Package ‘rcompanion’. Retrieved from https://cran.rproject.org/web/packages/rcompanion/rcompanion.pdf

Mantua N. (2020). PDO Index. University of Washington Joint Institute for the Study of the Atmosphere and Ocean. http://research.jisao.washington.edu/pdo/PDO.latest (Accessed Nov 2020)

Mantua N. (2016). PDO Index. University of Washington Joint Institute for the Study of the Atmosphere and Ocean. http://research.jisao.washington.edu/pdo/PDO.latest (Accessed May 2016)

Mantua, N. J., Hare, S. R., Zhang, Y., Wallace, J. M., & Francis, R. C. (1997). A Pacific interdecadal climate oscillation with impacts on salmon production. *Bulletin of the American Meteorological Society*, 78, 1-11.

Matott, L.S. (2019). OSTRICH: An optimization software tool: documentation and user‘s guide. v17.12.19. URL: http://www.eng.buffalo.edu/~lsmatott/Ostrich/OstrichMain.html (Accessed July 1, 2019).

May, C. L., Pryor, B., Lisle, T. E., & Lang, M. (2009). Coupling hydrodynamic modeling and empirical measures of bed mobility to predict the risk of scour and fill of salmon redds in a large regulated river. *Water Resources Research*, 45(5). W05402, doi:10.1029/2007WR006498

McIntosh, A. C., & Macdonald, S. E. (2013). Short-term resistance of ecosystem properties and processes to simulated mountain pine beetle attack in a novel region. *Ecosphere*, 4(6), 1-28.

McKean, J., & Tonina, D. (2013). Bed stability in unconfined gravel bed mountain streams: With implications for salmon spawning viability in future climates. *Journal of Geophysical Research: Earth Surface*, 118(3), 1227-1240.

Meddens, A. J., & Hicke, J. A. (2014). Spatial and temporal patterns of Landsat-based detection of tree mortality caused by a mountain pine beetle outbreak in Colorado, USA. *Forest Ecology and Management*, 322, 78-88.

Medinski, N.A. (2018). Assessing the impacts of multiple ecological stressors on an endangered native salmonid, the Athabasca Rainbow Trout, in the foothills of the Canadian Rocky Mountains. MSc thesis, Univ. of Alberta, Edmonton, Alberta. 107 pp.

Meyer, G., Black, T. A., Jassal, R. S., Nesic, Z., Grant, N. J., Spittlehouse, D. L., Fredeen, A.L., Christen, A., Coops, N.C., Foord, V.N., & Bowler, R. (2017). Measurements and simulations using the 3-PG model of the water balance and water use efficiency of a lodgepole pine stand following mountain pine beetle attack. *Forest Ecology and Management*, 393, 89-104.

Mikkelson, K., Bearup, L. A., Maxwell, R. M., Stednick, J. D., McCray, J. E., & Sharp, J. O. (2013). Bark beetle infestation impacts on nutrient cycling, water quality and interdependent hydrological effects. *Biogeochemistry*, 115, 1–21, doi:10.1007/s10533-013-9875-8.

Millions, E. L. (2015). Physiological and morphological responses of pine and willow saplings to post-fire salvage logging. MSc thesis, Univ. of Lethbridge, Lethbridge, Alberta. 81 pp.

Mitchell, R. G., & Preisler, H. K. (1998). Fall rate of lodgepole pine killed by the mountain pine beetle in central Oregon. *Western Journal of Applied Forestry*, 13(1), 23-26.

Mitton, J. B., & Ferrenberg, S. M. (2012). Mountain pine beetle develops an unprecedented summer generation in response to climate warming. *The American Naturalist*, 179(5), E163-E171.

Monteith, J. (1965). The state and movement of water in living organisms. Vol. 17. Academic Press Inc., New York, Ch. Evaporation and Environment, 205–234.

Moore, R. D., & Scott, D. F. (2005). Camp Creek revisited: streamflow changes following salvage harvesting in a medium-sized, snowmelt-dominated catchment. *Canadian Water Resources Journal*, 30(4), 331–344. https://doi.org/10.4296/cwrj3102135

Moore, R.D., & Wondzell, S. M. (2005). Physical hydrology and the effects of forest harvesting in the pacific northwest: a review. *Journal of the American Water Resources Association*, 41(4), 763–784.

Morehouse, K., Johns, T., Kaye, J., & Kaye, A. (2008). Carbon and nitrogen cycling immediately following bark beetle outbreaks in south-western ponderosa pine forests. *Forest Ecology Management*, 255(7), 2698–2708, doi:10.1016/j.foreco.2008.01.050.

Nash, J. & Sutcliffe, J.V. (1970). River flow forecasting through conceptual models part I: a discussion of principles. *Journal of Hydrology*, 10(3), 282–290.

Natural Regions Committee. (2006). Natural regions and subregions of Alberta. Complied by D.J. Downing and W.W. Pettapiece. Government of Alberta. Pub. No. 1/005. 264 pp.

Newcombe, C. P., & MacDonald, D. D. (1991). Effects of suspended sediments on aquatic ecosystems. *North American Journal of Fisheries Management*, 11(1), 72-82.

Newton, B.W., Prowse, T.D., & Bonsal, B.R. (2014). Evaluating the distribution of water resources in western Canada using synoptic climatology and selected teleconnections. Part 1: winter season. *Hydrological Processes*, doi:10.1002/hyp.10233.

Nip. A.M.-K. (1991). The Tri-Creeks Experimental Watershed: changes in hydrology and water quality following forest harvesting and their impact on salmonid fishes in the Tri-Creeks Basin. Research Branch Technical Report No. 4. Alberta Forestry, Lands and Wildlife. Edmonton. 66 pp.

Nislow, K. H., Einum, S., & Folt, C.L. (2004). Testing predictions of the critical period for survival concept using experiments with stocked Atlantic salmon. *Journal of Fish Biology*, 65 (Supplement A), 188-200.

Penman, H. (1948). Natural evaporation from open water, bare soil and grass. Royal Society of London Proceedings, Series A 193, 120–145.

Penn, C. A., Bearup, L. A., Maxwell, R. M., & Clow, D. W. (2016). Numerical experiments to explain multiscale hydrological responses to mountain pine beetle tree mortality in a headwater watershed. *Water Resources Research*, 52(4), 3143-3161.

Piña, P. (2013). Impact of mountain pine beetle attack on water balance of lodgepole pine forests in Alberta. PhD thesis, Univ. of Alberta, Edmonton, Alberta. 162 pp.

Pinheiro, J., Bates, D., DebRoy, S., & Sarkar, D. (2012). nlme: linear and nonlinear mixed effects models. R package version 3. 1–105. https://CRAN.R-project.org/package=nlme.

Pomeroy, J., Fang, X., & Ellis, C. (2012). Sensitivity of snowmelt hydrology in Marmot Creek, Alberta, to forest cover disturbance. *Hydrological Processes*, 26(12), 1891-1904.

Pomeroy, J. W., Gray, D. M., Brown, T., Hedstrom, N. R., Quinton, W. L., Granger, R., & Carey, S. (2007). The cold regions hydrological model: a platform for basing process representation and model structure on physical evidence. *Hydrological Processes*, 21, 2650–2667.

Pomeroy, J. W., Marsh, P., & Gray, D. M. (1997). Application of a distributed blowing snow model to the Arctic. *Hydrological Processes*, 11(11), 1451-1464.

Potts, D. F. (1984), Hydrologic impacts of a large-scale mountain pine beetle (Dendroctonus Ponderosae Hopkins) epidemic. *Water Resources Bulletin*, 20(3), 373–377, doi:10.1111/j.1752-1688.1984.tb04719.x.

Priestley, C., & Taylor, R. (1972). On the assessment of surface heat flux and evaporation using large-scale parameters. *Monthly Weather Review*, 81–92.

Pugh, E., & Small, E. (2012). The impact of pine beetle infestation on snow accumulation and melt in the headwaters of the Colorado River. *Ecohydrology*, 5(4), 467-477.

R Core Team. (2020). R: a language and environment for statistical computing. R Foundation for Statistical Computing, Vienna,Austria. R version 4.0.1. URL: https://www.R-project.org/ (Accessed July, 2020).

R Core Team (2019). R: A language and environment for statistical computing. R Foundation for Statistical Computing, Vienna, Austria. R version 3.6.1. URL: https://www.R-project.org/ (Accessed June, 2019).

Rachels, A. A., Bladon, K. D., Bywater-Reyes, S., & Hatten, J. A. (2020). Quantifying effects of forest harvesting on sources of suspended sediment to an Oregon Coast Range headwater stream. *Forest Ecology and Management*, 466, 118123.

Raffa, K. F., Aukema, B. H., Bentz, B. J., Carroll, A. L., Hicke, J. A., Turner, M. G., & Romme, W. H. (2008). Cross-scale drivers of natural disturbances prone to anthropogenic amplification: the dynamics of bark beetle eruptions. *Bioscience*, 58(6), 501-517.

Rasmussen, J.B., & Taylor, E.B. (2009). Status of the Athabasca rainbow trout (Oncorhynchus mykiss) in Alberta. Alberta Sustainable Resource Development and Alberta Conservation Association. Wildlife Status Report No. 66. Edmonton, AB. 32 pp.

Redding, T.E., & Devito, K.J. (2011). Aspect and soil textural controls on snowmelt runoff on forested Boreal Plain hillslopes. *Hydrology Research*, 42(4), 250-267.

Redding, T.E, & Devito, K.J. (2010). Mechanisms and pathways of lateral flow on aspen-forested, luvisolic soils, Western Boreal Plains, Alberta, Canada. *Hydrological Processes*, 24(21), 2995-3010.

Redding, T.E, & Devito, K.J. (2008). Lateral flow thresholds for aspen forested hillslopes on the Western Boreal Plain, Alberta, Canada. *Hydrological Processes*, 22(21), 4287–4300.

Reed, D. E., Ewers, B. E., Pendall, E., Frank, J., & Kelly, R. (2016). Bark beetle-induced tree mortality alters stand energy budgets due to water budget changes. *Theoretical and Applied Climatology*, 131(1-2), 153-165.

Reed, D. E., Ewers, B. E., & Pendall, E. (2014). Impact of mountain pine beetle induced mortality on forest carbon and water fluxes. *Environmental Research Letters*, 9(10), 105004.

Reid, D. E. B., Silins, U., & Lieffers, V. J. (2006). Sapwood hydraulic recovery following thinning in lodgepole pine. Annals of Forest Science, 63(4), 329-338.

Reinelt, E.R. (1970). On the role of orography in the precipitation regime of Alberta. *The Albertan Geographer*, 6, 45–58.

Rhoades, C. C., Hubbard, R. M., Elder, K., Fornwalt, P. J., Schnackenberg, E., Hood, P. R., & Tinker, D. B. (2020). Tree regeneration and soil responses to management alternatives in beetle-infested lodgepole pine forests. *Forest Ecology and Management*, 468, 118182.

Schindler, D. W., & Donahue, W. F. (2006). An impending water crisis in Canada's western prairie provinces. Proceedings of the National Academy of Sciences, 103(19), 7210-7216.

Schmidt, R.A., & Gluns, D.R. (1991). Snowfall interception on branches of three conifer species. *Canadian Journal of Forest Research*, 21, 1262–1269.

Schneider, R. R., Latham, M. C., Stelfox, B., Farr, D., & Boutin, S. (2010). Effects of a severe mountain pine beetle epidemic in western Alberta, Canada under two forest management scenarios. *International Journal of Forestry Research*, doi:10.1155/2010/417595.

Schnorbus, M., & Alila, Y. (2004). Forest harvesting impacts on the peak flow regime in the Columbia Mountains of southeastern British Columbia: An investigation using long-term numerical modeling. *Water Resources Research*, 40, 1–16. https://doi.org/10.1029/2003WR002918.

Scrimgeour, G. J., Hvenegaard, P. J., & Tchir, J. (2008). Cumulative industrial activity alters lotic fish assemblages in two boreal forest watersheds of Alberta, Canada. *Environmental Management*, 42, 957–970.

Seibert, J., & McDonnell, J. J. (2010). Land-cover impacts on streamflow: a change-detection modelling approach that incorporates parameter uncertainty. *Hydrological Sciences Journal*, 55(3), 316–332. https://doi.org/10.1080/02626661003683264

Seibert, J., McDonnell, J. J., & Woodsmith, R. (2010). Effects of wildfire on catchment runoff responses: a modelling approach to detect changes in snow-dominated forested catchments. *Hydrology Research*, 41(5), 378–390, doi:10.2166/nh.2010.036.

Shapiro, S.S., Wilk, M.B., & Chen, H.J. (1968). A comparative study of various tests for normality. *Journal of The American Statistical Association*, 63(324), 1343–1372.

Shrestha, R. R., Schnorbus, M. A., & Peters, D. L. (2016). Assessment of a hydrologic model's reliability in simulating flow regime alterations in a changing climate. *Hydrological Processes*, 30(15), 2628-2643.

Singh, T. (1983). A proposed method for preliminary assessment of erosion hazards in west-central Alberta. Environment Canada, Canadian Forestry Service, Canadian Northern Forestry Centre, Edmonton, Alberta. Inf. Rep. NOR-X-2Sl. 17 pp.

Sinnatamby, R.N., Cantin, A., & Post, J.R. (2020). Threats to at-risk salmonids of the Canadian Rocky Mountain region. *Ecology of Freshwater Fish*, 29, 477–494. doi: 10.1111/eff.12531.

Slinski, K. M., Hogue, T. S., Porter, A. T., & McCray, J. E. (2016). Recent bark beetle outbreaks have little impact on streamflow in the Western United States. *Environmental Research Letters*, 11(7), 074010.

Smerdon, B. D., Redding, T., & Beckers, J. (2009). An overview of the effects of forest management on groundwater hydrology. *Journal of Ecosystems and Management*, 10(1). 23-44.

Smith, R. S., Moore, R. D., Weiler, M., & Jost, G. (2014). Spatial controls on groundwater response dynamics in a snowmelt-dominated montane catchment. *Hydrology and Earth System Sciences*, 18(5), 1835-1856.

Som, N. A., Zégre, N. P., Ganio, L. M., & Skaugset, A. E. (2012). Corrected prediction intervals for change detection in paired watershed studies. *Hydrological Sciences Journal*, 57(1), 134-143.

Spencer, S. A., Silins, U., & Anderson, A. E. (2019). Precipitation-runoff and storage dynamics in watersheds underlain by till and permeable bedrock in Alberta's Rocky Mountains. *Water Resources Research*, 55(12), 10690-10706, doi:10.1029/2019WR025313.

Spittlehouse, D.L. (2006). Annual water balance of high elevation forests and clearcuts. In: Proceedings 27th Conference Agricultural and Forest Meteorology, May 21–25, 2006, San Diego, Calif., American Meteorological Society, Boston, Mass.

St Jacques, J. M., Sauchyn, D. J., & Zhao, Y. (2010). Northern Rocky Mountain streamflow records: global warming trends, human impacts or natural variability? *Geophysical Research Letters*, 37(6), L06407, doi:10.1029/2009GL042045.

Stednick, J.D. (1996). Monitoring the effects of timber harvest on annual water yield. *Journal of Hydrology*, 176(1), 79-95.

Steinke, J., McIntosh, A. C., Schroeder, L., & Macdonald, S. E. (2020). Understory vegetation responses to simulated mountain pine beetle attack and salvage logging in grey attack stage lodgepole pine stands. *Forest Ecology and Management*, 474, 118373.

Steinke, J.A. (2018) Vegetation responses following mountain pine beetle attack in lodgepole pine forests of west-central Alberta. MSc thesis, Univ. of Alberta, Edmonton, Alberta. 116 pp.

Sterling, G., Goodbrand, A., & Spencer, S. A. (2016). Tri-Creeks Experimental Watershed. *The Forestry Chronicle*, 92(1), 53-56.

Sterling, G. (1992). Fry emergence survival of rainbow trout, Oncorhynchus mykiss (Walbaum), following timber harvest in two Foothill streams of west-central Alberta. MSc. Thesis, University of Alberta, Edmonton, Alberta. 116 pp.

Sterling, G. (1990). Population dynamics of rainbow trout (Oncorhynchus mykiss) in the Tri-Creeks experimental watershed of west-central Alberta; a post-logging evaluation. Tri-Creeks Experimental Watershed, Research Report 10. Alberta Forestry Lands and Wildlife, Fish and Wildlife Division, 68 pp.

Sterling, G. (1986) An evaluation of spawning habitat and fry escapement of rainbow trout (Salmo gairdneri RICHARDSON) before logging in the Tri-Creeks watershed of west-central Alberta. Tri-Creek Experimental Watershed, Research Report Number 8. Alberta Energy and Natural Resources, Fish and Wildlife Division, 74 pp.

Sterling, G. (1980) Migratory behavior of the major salmonid fishes, rainbow trout, Dolly Varden char and mountain whitefish in the Tri-Creek watershed, 1969 – 1978. Tri-Creek Experimental Watershed, Research Report Number 6. Alberta Energy and Natural Resources, Fish and Wildlife Division, 64 pp.

Sterling, G. (1978) Population dynamics, age and growth of rainbow trout (Salmo gairdneri) and dolly varden (Salvelinus malma) in the Tri-Creek watershed, 1971 to 1977. Tri-Creek Experimental Watershed, Research Report Number 2. Alberta Energy and Natural Resources, Fish and Wildlife Division, 86 pp.

Strittholt, J. R., Staus, N. L., Heilman Jr, G., & Bergquist, J. (2007). Mapping high conservation value and endangered forests in the Alberta Foothills using spatially explicit decision support tools. Conservation Biology Institute. 73 pp.

Tague, C., & Grant, G. (2004). A geological framework for interpreting the low-flow regimes of Cascade streams, Willamette River Basin, Oregon. *Water Resources Research*, 40(4), 1-9.

Tolson, B.A., & Shoemaker, C.A. (2008). Efficient prediction uncertainty approximation in the calibration of environmental simulation models. *Water Resources Research*, 44(4), W04411, doi:10.1029/2007WR005869.

Tolson, B.A., & Shoemaker, C.A. (2007). Dynamically dimensioned search algorithm for computationally efficient watershed model calibration. *Water Resources Research*, 43(1), W01413, doi:10.1029/2005WR004723.

Tonina, D., & Buffington, J. M. (2009). A three-dimensional model for analyzing the effects of salmon redds on hyporheic exchange and egg pocket habitat. *Canadian Journal of Fisheries and Aquatic Sciences*, 66(12), 2157-2173.

Tonina, D., Luce, C. H., Rieman, B., Buffington, J. M., Goodwin, P., Clayton, S. R., Clayton, S. R., Ali, S.M., Barry, J.J., & Berenbrock, C. (2008). Hydrological response to timber harvest in northern Idaho: implications for channel scour and persistence of salmonids. *Hydrological Processes*, 22(17), 3223-3235.

Topp, G. C., Davis, J. L., & Annan, A. P. (1980). Electromagnetic determination of soil water content: measurements in coaxial transmission lines. *Water Resources Research*, 16(3), 574-582.

Troendle, C. A., & King, R. M. (1987). The effect of partial and clearcutting on streamflow at Deadhorse Creek, Colorado. *Journal of Hydrology*, 90(1-2), 145–157.

Troendle, C. A., & King, R. M. (1985). The effect of timber harvest on the Fool Creek watershed, 30 years later. *Water Resources Research*, 21(12), 1915-1922.

Tschaplinski, P. J., & Pike, R. G. (2017). Carnation Creek watershed experiment—long-term responses of coho salmon populations to historic forest practices. Ecohydrology, 10(2), doi 10.1002/e1812.

Vogel, R. M., & Kroll, C. N. (1996). Estimation of baseflow recession constants. *Water Resources Management*, 10(4), 303-320.

Wagner, M.J.N. (2010). Hydrologic risk assessment framework for Alberta's Green Zone. MSc thesis, Univ. of Alberta, Edmonton, Alberta. 181 pp.

Water Survey of Canada. (2016). Water office. URL: http://wateroffice.ec.gc.ca. (Accessed February 2, 2016).

Watson, F. G. R., Vertessy, R., McMahon, T., Rhodes, B., & Watson, I. (2001). Improved methods to assess water yield changes from paired-catchment studies: application to the Maroondah catchments. *Forest Ecology and Management*, 143(1–3), 189–204.

Wei, X., Liu, W., & Zhou, P. (2013). Quantifying the relative contributions of forest change and climatic variability to hydrology in large watersheds: a critical review of research methods. *Water*, 5(2), 728-746.

Wei, X., & Zhang, M. (2010). Quantifying streamflow change caused by forest disturbance at a large spatial scale: a single watershed study. *Water Resources Research*, 46, W12525, doi:10.1029/2010WR009250.

Westerling, A. L., & Swetnam, T. W. (2003). Interannual to decadal drought and wildfire in the western United States. EOS, *Transactions American Geophysical Union*, 84(49), 545-555.

Whitehouse, C. (2020). Forest health specialist. Government of Alberta. Personal communications, December 22, 2020.

Whitfield, P.H., Moore, R.D., Fleming, S.W., & Zawadzki, A. (2010). Pacific decadal oscillation and the hydroclimatology of Western Canada – review and prospects. *Canadian Water Resources Journal*, 35, 1-28. doi:10.4296/cwrj3501001.

Williams, C. H., Silins, U., Spencer, S. A., Wagner, M. J., Stone, M., & Emelko, M. B. (2019). Net precipitation in burned and unburned subalpine forest stands after wildfire in the northern Rocky Mountains. *International Journal of Wildland Fire*, 28(10), 750-760.

Williams, A. P., Allen, C. D., Macalady, A. K., Griffin, D., Woodhouse, C. A., Meko, D. M., Swetnam, T.W., Rauscher, S.A., Seager, R., Grissino-Mayer, H.D., Dean, J.S., Cook, E.R., Gangodagamage, C., Cai, M., & McDowell, N. G. (2013). Temperature as a potent driver of regional forest drought stress and tree mortality. *Nature Climate Change*, 3(3), 292-297.

Winkler, R.D., Boon, S., Zimonick, B., & Spittlehouse, D. (2014). Snow accumulation and ablation response to changes in forest structure and snow surface albedo after attack by mountain pine beetle. *Hydrological Processes*, 28(2), 197-209.

Winkler, R. D., Moore, R. D., Redding, T. E., Spittlehouse, D. L., Smerdon, B. D., & Carlyle-Moses, D. E. (2010). The effects of forest disturbance on hydrologic processes and watershed. Compendium of forest hydrology and geomorphology in British Columbia. British Columbia Ministry of Forests and Range, 66, 179-212.

Winkler, R. D., & Moore, R. D. (2006). Variability in snow accumulation patterns within forest stands on the interior plateau of British Columbia, Canada. *Hydrological Processes*, 20(17), 3683-3695.

Winkler, R.D., Spittlehouse, D.L., & Golding, D.L. (2005). Measured differences in snow accumulation and melt among clearcut, juvenile and mature forests in southern British Columbia. *Hydrological Processes*, 19, 51-62.

Winkler, R. D., & Rothwell, R. L. (1983). Biogeoclimatic classification system for hydrologic interpretations. *Canadian Journal of Forest Research*, 13(6), 1043-1050.

Wulder, M. A., Dymond, C. C., White, J. C., Leckie, D. G., & Carroll, A. L. (2006). Surveying mountain pine beetle damage of forests: A review of remote sensing opportunities. *Forest Ecology and Management*, 221(1-3), 27-41.

Yasunaka, S., & Hanawa, K. (2003). Regime shifts in the Northern Hemisphere SST field: Revisited in relation to tropical variations. *Journal of the Meteorological Society of Japan*. Ser. II, 81(2), 415-424.

Zégre, N., Skaugset, A. E., Som, N. A., McDonnell, J. J., & Ganio, L. M. (2010). In lieu of the paired catchment approach: hydrologic model change detection at the catchment scale. *Water Resources Research*, 46, W11544, doi:10.1029/2009WR008601.

Zhang, M., & Wei, X. (2012). The effects of cumulative forest disturbance on streamflow in a large watershed in the central interior of British Columbia, Canada. *Hydrology and Earth System Sciences*, 16(7), 2021-2034, doi:10.5194/hess-16-2021-2012.

APPENDIX A – SOIL MOISTURE RELATIONSHIPS AT MPB ROBB STANDS

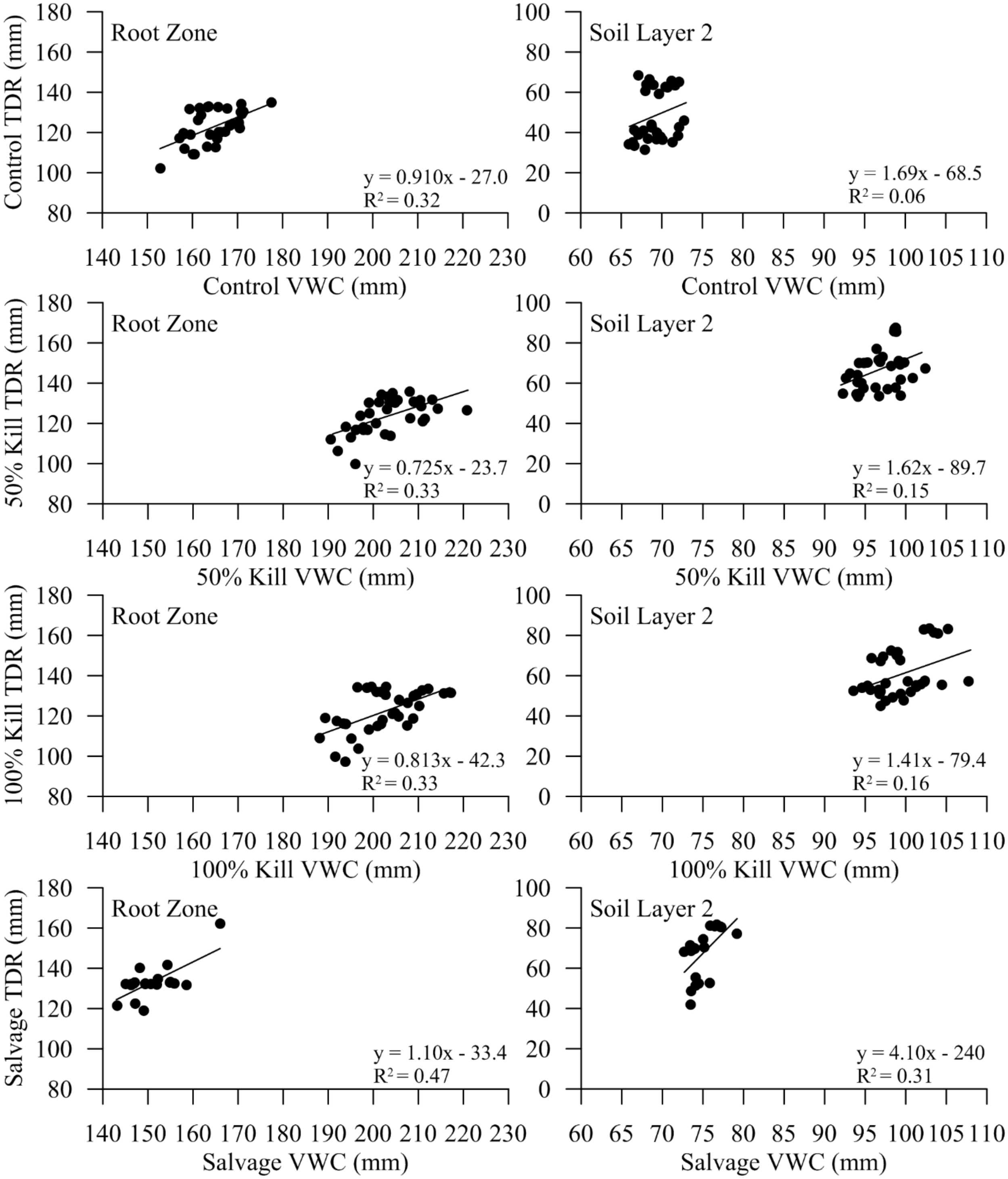

Figure A.1 Linear relationships between mean daily soil moisture measured with CS616 sensors (Campbell Scientific; volumetric water content, VWC) at one-point in each stand and time domain reflectometry (TDR) at eight locations within each stand during the 2008 – 2010 growing seasons for the Control, 50% Kill and 100% Kill stands, and during the post-harvest period in the Salvage stand (growing seasons 2009 – 2010).

APPENDIX B – HYDROLOGIC PROCESS REPRESENTATION FOR MOUNTAIN PINE BEETLE GREY-ATTACK STANDS AND SCALING TO A WATERSHED MODEL

Refer to Chapter 2 for the stand-scale water balance approach (section 2.2.8) for model structure, forcing functions, parameter optimization, and method to quantify parameter uncertainty. Refer to Chapter 2, section 2.2.7 for method to estimate analytical actual ET.

B.1 Potential Evapotranspiration Equations

The model structure of the unsaturated zone was kept constant for all models and only differed in the formulation of potential ET, which would allow the process that converted potential ET to actual ET to remain the same.

B.1.1 Penman-Monteith (Monteith, 1965)

Monteith (1965) modified the Penman equation to represent the daily *ET* rate from a vegetated surface by incorporating canopy conductance:

$$PET_{PM} = \frac{1}{\lambda_v \rho_w} \cdot \left[\frac{\Delta}{\Delta + \gamma \cdot (1 + c_{atm}/c_{can})} R_n + \frac{\rho_a c_{atm} c_a}{\Delta + \gamma \cdot (1 + c_{atm}/c_{can})} (e_s - e) \right] \tag{B.1}$$

$$c_{atm} = v \cdot \frac{k^2}{ln\left(\frac{z_{ref} - z_o}{z_{rough}}\right) ln\left(\frac{z_{ref} - z_o}{z_{vap}}\right)} \tag{B.2}$$

$$c_{can} = 0.5 \cdot c_{leaf} \cdot LAI \tag{B.3}$$

where λ_v (MJ kg^{-1}) is the latent heat of vaporization of water, ρ_w (kg m^{-3}) is the density of water, $\Delta = de_s/dT$ is the slope of the saturated vapour pressure curve, $R_n = S_n + L_n$ (MJ m^{-2} d^{-1}) is the net radiation to the system equal to the sum of net incoming and outgoing shortwave and longwave radiation, ρ_a is the air density (kPa), c_{atm} (m d^{-1}) is the atmospheric conductance, c_a is the specific heat of air (1.012 x 10^{-3} MJ kg^{-1} K^{-1}), e is the vapour pressure of the atmosphere, $e_s(T)$ (kPa) is the current saturated vapour pressure of the atmosphere, a function of temperature, γ (kPA K^{-1}) is the psychrometric constant, c_{can} (m d^{-1}) is the canopy conductance, k is the von Karman constant (0.42), z_{ref} is the reference height (m) at which the wind velocity (v; m d^{-1}) is reported, z_o (m) is the zero-plane displacement height, z_{rough} is the roughness height (m), and z_{vap} is the vapour roughness height (m), c_{leaf} is the leaf conductance (m d^{-1}). Refer to Craig *et al.* (2019) for equations to calculate $\lambda_{v,}$ Δ, $e_s(T)$, and γ.

B.1.2 Priestley-Taylor (1972)

Only net radiation explicitly drives daily *ET* with a correction factor for the unmodelled *ET* driven by vapour deficit (α) as:

$$PET_{PT} = \alpha \cdot \frac{1}{\lambda_v \rho_w} \left[\frac{\Delta}{\Delta + \gamma^*} R_n \right] \tag{B.4}$$

B.1.3 Hargreaves and Samani (1985)

An empirical approach based on air temperature and incoming extraterrestrial shortwave radiation (S_{ET}; MJ m^{-2} d^{-1}):

$$PET_{HS} = \frac{1}{\lambda_v \rho_w} \cdot S_{ET} \cdot 0.0023 \cdot \sqrt{T_{max} - T_{min}} \left(T_{avg} + 17.8 \right) \tag{B.5}$$

where T_{avg}, T_{max}, and T_{min} are the average, maximum, and minimum daily air temperature (ºC), respectively.

B.2 Potential Snowmelt Equations

The model structure of the unsaturated zone was kept constant for all models and only differed in the formulation of potential snowmelt; however, given that potential ET influences canopy interception and sublimation losses, each potential snowmelt method was tested with each potential ET equation resulting in a combination of nine models.

B.2.1 CRHM Energy Balance Snowmelt Method (Pomeroy et al., 2007)

The potential melt rate M_{CRHM} (mm d^{-1}) is a parameter-free energy-based potential melt model from the CRHM:

$$M_{CRHM} = \frac{1}{\lambda_v \rho_w} \cdot \left(S_n + L_n + Q_h + Q_p \right) \tag{B.6}$$

$$Q_h = -0.92 + 0.076 \cdot v + 0.19 \cdot T_{max} \tag{B.7}$$

$$Q_P = c_p \rho_w \cdot R \cdot max(T, 0.0)/1000 \tag{B.8}$$

where Q_h (MJ m^{-2} d^{-1}) is the convective/conductive heat transfer, Q_p (MJ m^{-2} d^{-1}) is the energy content of the rainfall, *R* (mm d^{-1}) is the rainfall rate/1000 (m d^{-1}), *T* (ºC) is the air temperature, c_p (MJ kg^{-1} K^{-1}) is the specific heat capacity of water. M_{CRHM} was applied to the snowpack with a single-layer energy balance snow model that tracked liquid water content, snow water equivalent (SWE), and the energy in the snowpack as implemented in CRHM (Pomeroy *et al.*, 2007).

B.2.2 Restricted Snowmelt Method (Brubaker et al., 1996)

The potential melt rate M_{RES} (mm d^{-1}) is a temperature-index method plus a correction term for net radiation:

$$M_{RES} = M_m \cdot (T - T_f) + \frac{S_n + L_n}{\lambda_f \rho_w} \quad \text{(B.9)}$$

where M_m is the potential melt factor (mm d^{-1} ºC^{-1}; MELT_FACTOR), λ_f (MJ kg^{-1}) is the latent heat of fusion and T_f is the freezing temperature (0ºC). M_{RES} was simply applied to the snowpack until disappearance.

Potential refreeze (M_{FZE}) of water in the snowpack was accounted for using a degree day method (Bergstrom, 1995) and a potential refreeze factor (K_f; mm d^{-1} ºC^{-1}; REFREEZE_FACTOR):

$$M_{FZE} = K_f \cdot min(T_f - T, 0) \quad \text{(B.10)}$$

B.2.3 HBV-EC Snowmelt Method (Bergstrom, 1995)

The potential melt rate M_{HBV} (mm d^{-1}) is a modified version of the temperature-index approach with a corrected melt factor (M_a; mm d^{-1} ºC^{-1}) to account for forest cover, aspect and slope angle:

$$M_a = C_f \cdot C_{asp} \left(M_{a.min} + (M_{a.max} - M_{a.min}) \cdot \frac{1.0 - cos(\Gamma - \Gamma_s)}{2} \right) \quad \text{(B.11)}$$

$$C_f = (1.0 - F_c) \cdot (1.0 + F_c \cdot M_{RF}) \quad \text{(B.12)}$$

where C_f is the forest correction factor (-), C_{asp} is the aspect correction factor (-), $M_{a.max}$ is the maximum potential melt rate (mm d^{-1} ºC^{-1}; MELT_FACTOR) and $M_{a.min}$ is the minimum potential melt rate (mm d^{-1} ºC^{-1}; MIN_MELT). Γ is the day angle and Γ_s is the winter solstice angle (23.5º). M_{RF} is the forest melt correction (-; HBV_MELT_FOR_CORR). C_{asp} (which includes the slope factors) was set to equal 1 given the flat topography of the study site. M_{HBV} was simply applied to the snowpack until disappearance as per the Raven input file for HBV-EC emulation (Craig *et al.*, 2019). Potential refreeze of water in the snowpack was accounted for using Eq. 2.17.

B.3 Evaluation of Hydrologic Process Algorithms

Based on model performance (Figures B.1 and B.2) and agreement with observed soil moisture data (Figures B.3 and B.4), the best combination of potential snowmelt and potential ET equations to represent water cycling in MPB grey-attack stands would be Priestley-Taylor (1972) and HBV-EC snowmelt (Bergstrom, 1995), which considers the trade-off between prediction accuracy and parameter uncertainty.

Simulated actual ET using the Penman-Montieth (1965) and Priestley-Taylor (1972) compared well with the estimated actual AET using the analytical method (Figure B.5). More variability was shown with Hargreaves and Samani (1985), and this equation over-estimated winter actual ET (Figure B.6). Over-estimated winter actual ET was due to three times greater evaporation of interpreted snow in the forest canopy compared to estimated actual AET using the analytical method. Therefore, the best equations to represent water cycling in MPB grey-attack stands were equations with net radiation data as input.

The similarity in modelled snowmelt using the CRHM and Restricted snowmelt methods indicate that the MPB forest snow balance is dominated by net radiation (Figure B.7). However, the HBV-EC method was in good agreement with observed SWE for the MPB attacked stands if winter actual ET was not over-estimated (i.e. with Hargreaves and Samani (1985) equation). In addition, the timing of snowmelt was best represented by the HBV-EC method (Figure B.7), which is important to capture antecedent soil moisture conditions correctly.

B.4 Scaling to Watershed Hydrological Model

Priestley-Taylor (1972) requires net radiation to be modelled at the watershed-scale. However, modelled radiation was over-estimated in the winter period compared to measured net radiation (Figure B.8). Based on the trade-off between data availability, prediction accuracy, and parameter uncertainty, Hargreaves and Samani (1985) instead of Priestley-Taylor (1972) was used to estimate potential ET in the Pure Pine, MPB Grey and Harvest HRUs (Chapter 4). In addition, Hargreaves and Samani (1985) was already part of the model structure of the watershed hydrological model (Chapter 3). Therefore, a correction factor (PET_VEG_CORR) was used with the Hargreaves and Samani (1985) potential ET equation to test model performance at the stand-level. These model simulations also include the combined forest floor and canopy rainfall interception without the litter layer in the soil model structure. There was good agreement between the estimate of actual AET using the analytical method and simulated AET as well as observed and simulated SWE (Figure B.9). Therefore, Hargreaves and Samani (1985) with a PET correction factor and the HBV-EC snowmelt method was used to model MPB grey-attack at the watershed-scale.

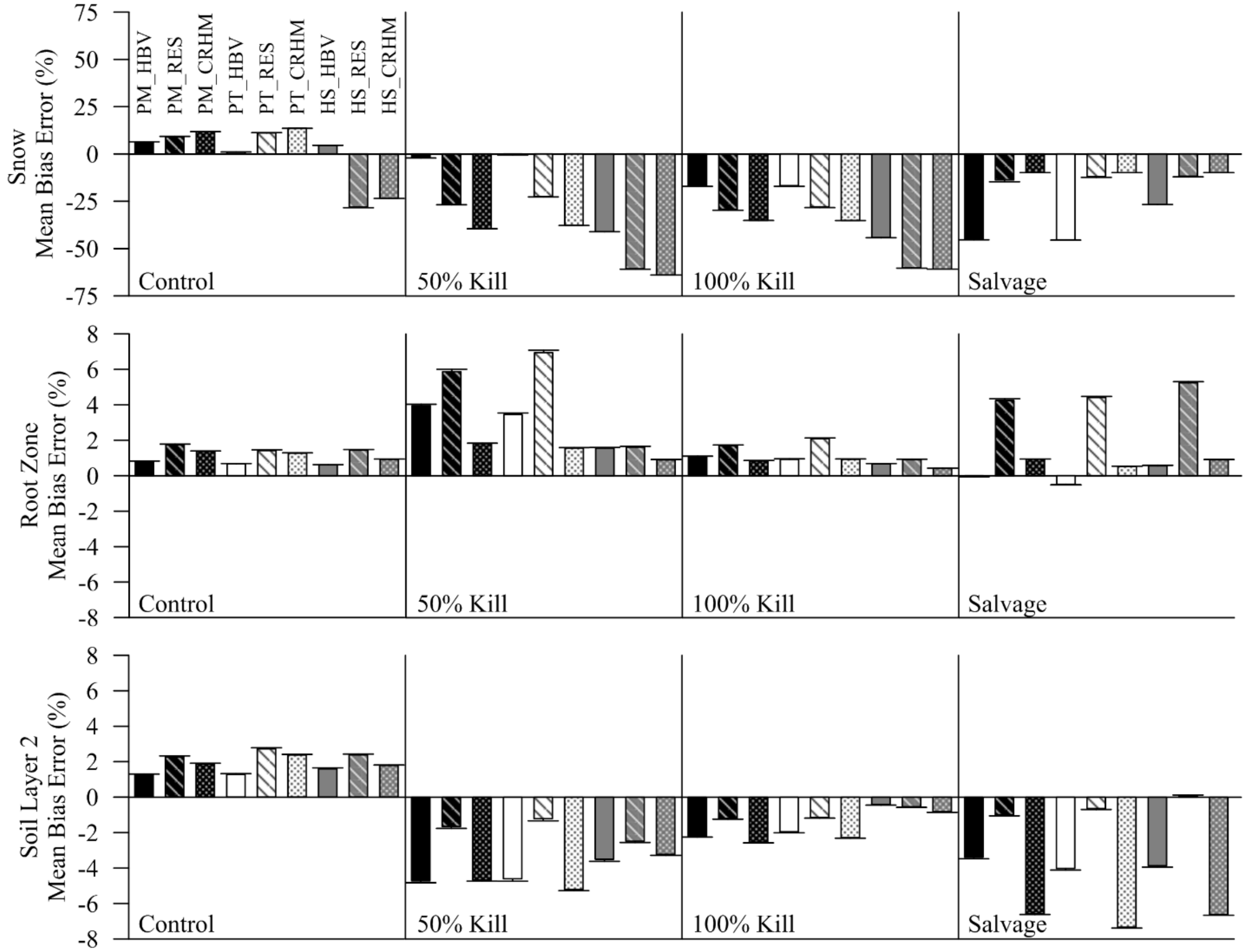

Figure B.1 Agreement between observations and model predictions of snow water equivalent, root zone (0 – 0.4 m below ground surface) storage and soil layer 2 (0.4 – 0.6 m.b.g.s) storage for all nine combination of models for each treatment. Each bar represents the average mean bias error of 100 simulations. Error bars represent standard error of the mean. PM, Penman-Monteith; PT, Priestley-Taylor; HS, Hargreaves and Samani; HBV, HBV-EC snowmelt; RES, restricted snowmelt; CRHM, Cold Regions Hydrological Model snowmelt.

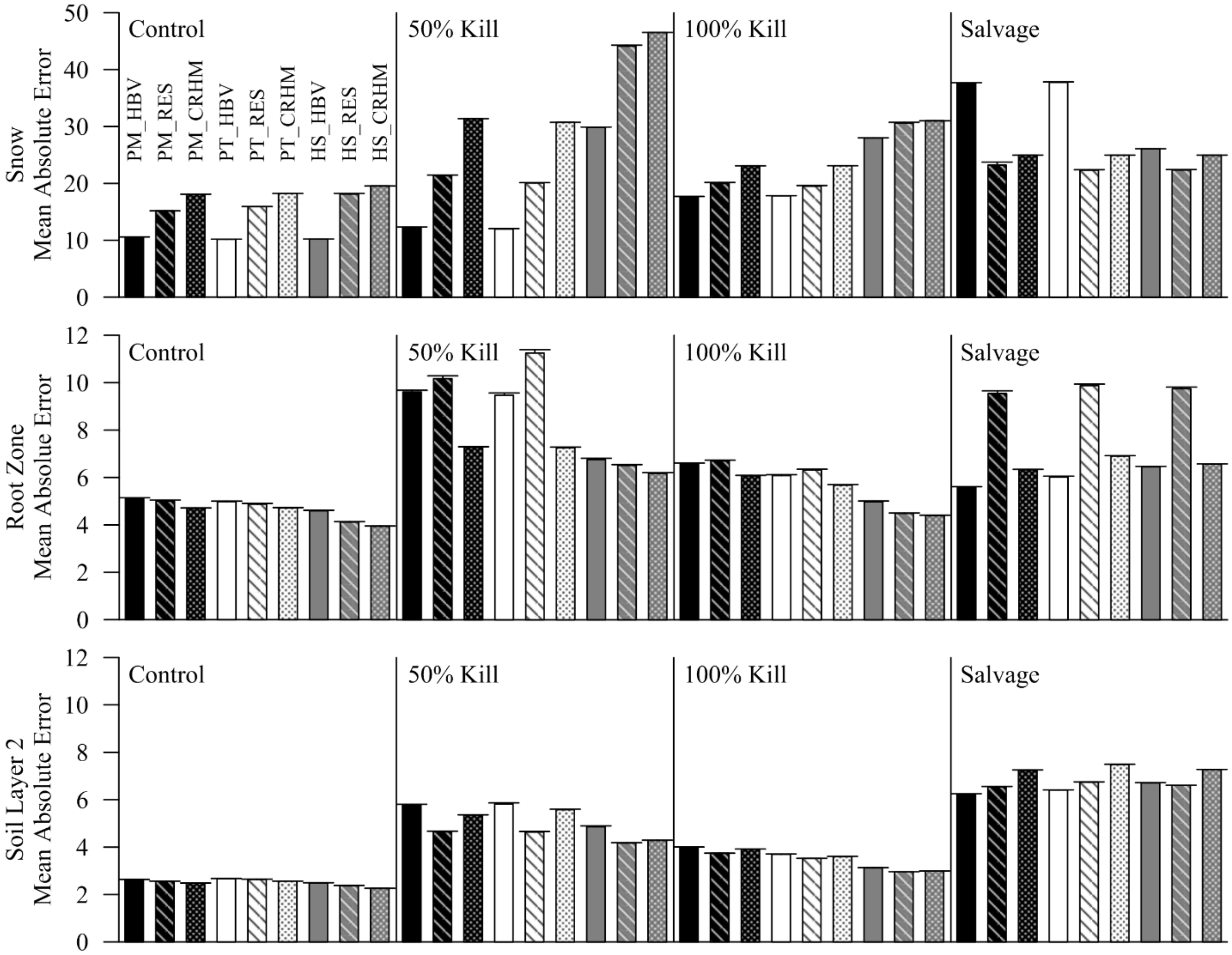

Figure B.2 Agreement between observations and model predictions of snow water equivalent, root zone (0 – 0.4 m below ground surface) storage and soil layer 2 (0.4 – 0.6 m.b.g.s) storage for all nine combination of models for each treatment. Each bar represents the average mean absolute error of 100 simulations. Error bars represent standard error of the mean. PM, Penman-Monteith; PT, Priestley-Taylor; HS, Hargreaves and Samani; HBV, HBV-EC snowmelt; RES, restricted snowmelt; CRHM, Cold Regions Hydrological Model.

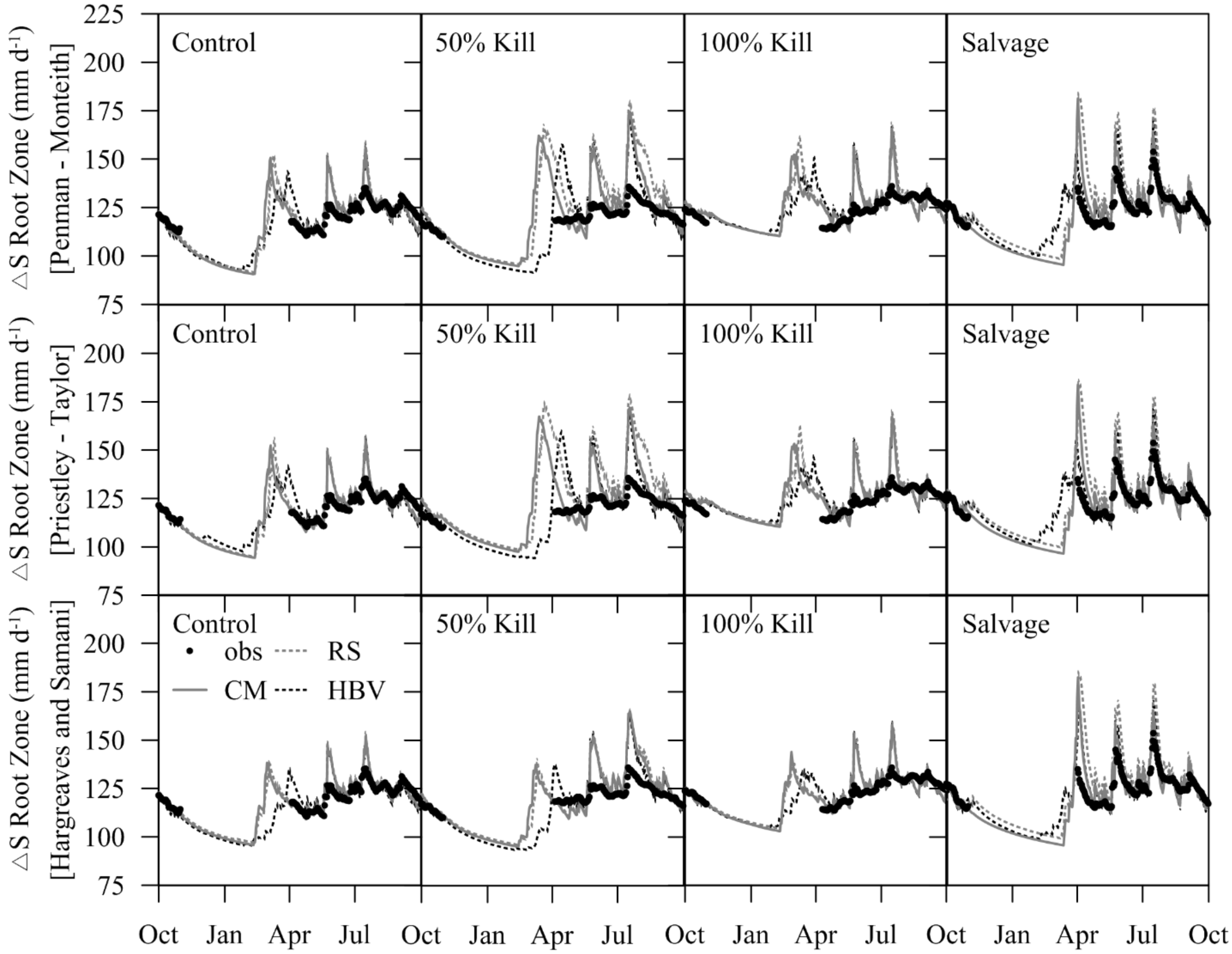

Figure B.3 Predictions of change in storage in the root zone (0 – 0.4 m below ground surface) for the 2016 water year compared to observed soil water content for each model combination in the treatment stands. Measured soil water content when soil temperature was below 0ºC was excluded due to inaccuracy associated with the presence of frozen soil water. HBV, HBV-EC snowmelt; RS, restricted snowmelt; CM, Cold Regions Hydrological Model snowmelt.

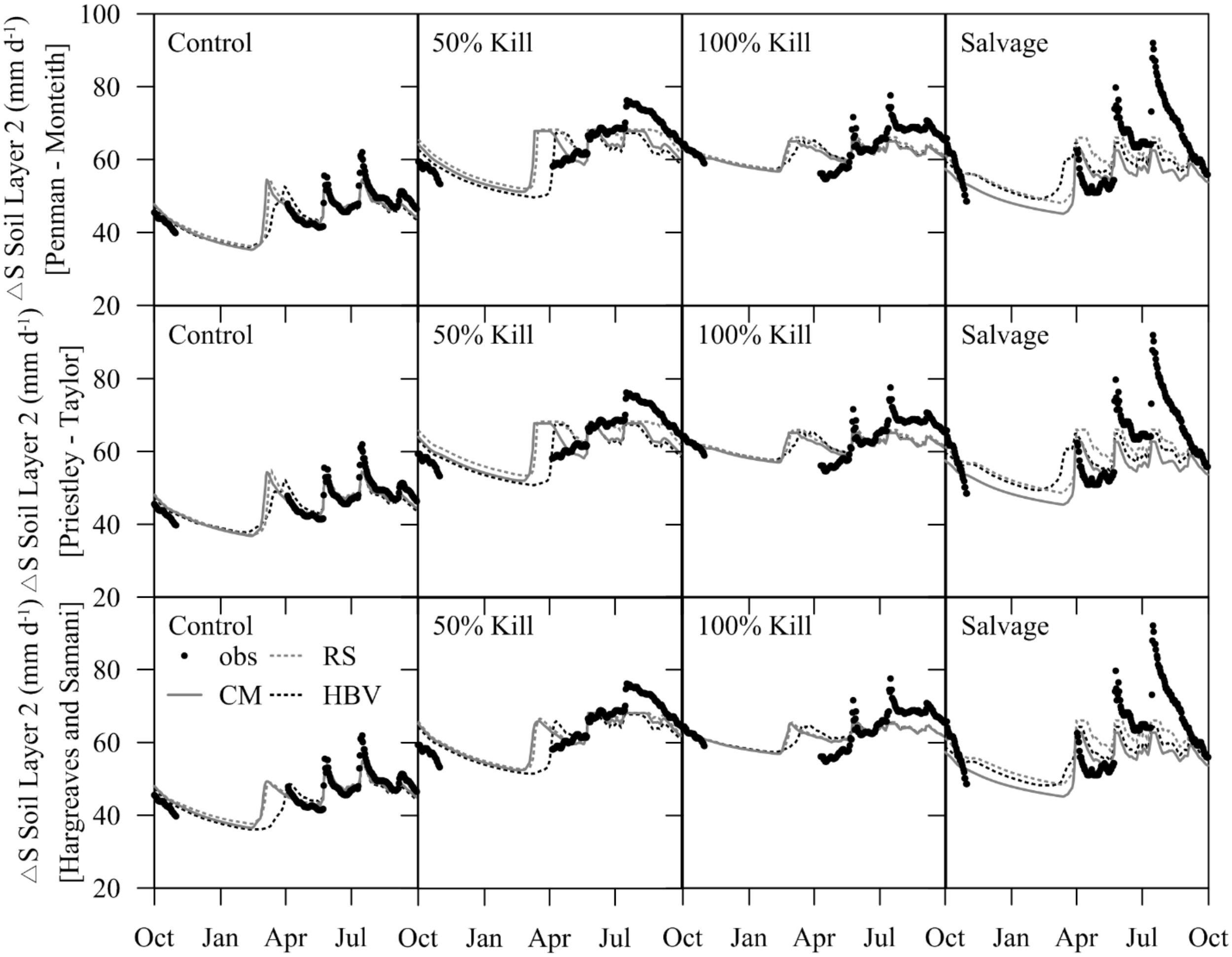

Figure B.4 Predictions of change in storage within soil layer 2 (0.40 – 0.60 m below ground surface; below the root zone soil layer) for the 2016 water year compared to observed soil water content for each model combination in the treatment stands. Measured soil water content when soil temperature was below 0ºC was excluded due to inaccuracy associated with the presence of frozen soil water. HBV, HBV-EC snowmelt; RS, restricted snowmelt; CM, Cold Regions Hydrological Model snowmelt.

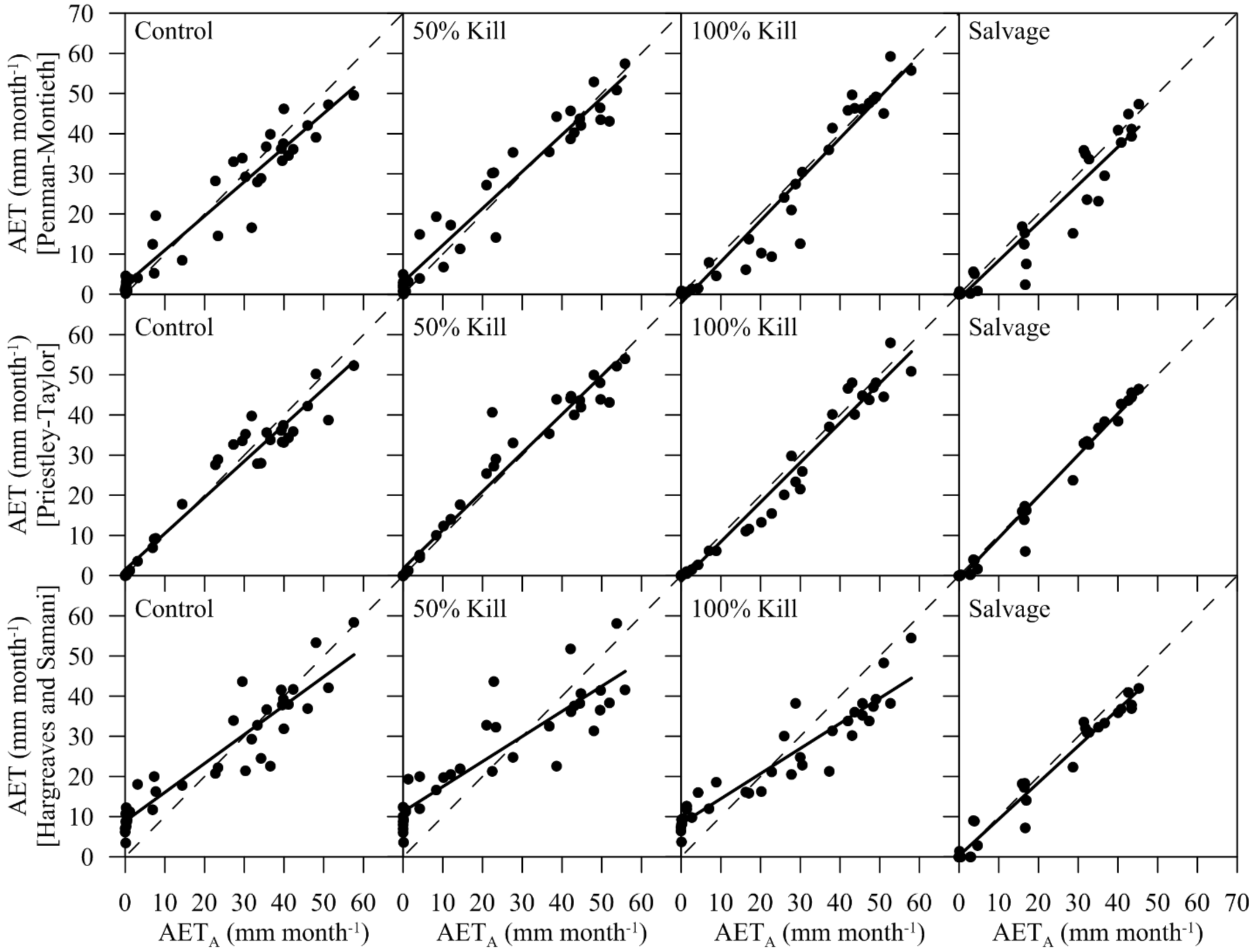

Figure B.5 Predictions of monthly actual evapotranspiration using the three potential ET algorithms compared to AET estimated using an analytical method (AET_A) with measured data for each treatment stand over the study period (1 Oct 2014 – 30 Sep 2017).

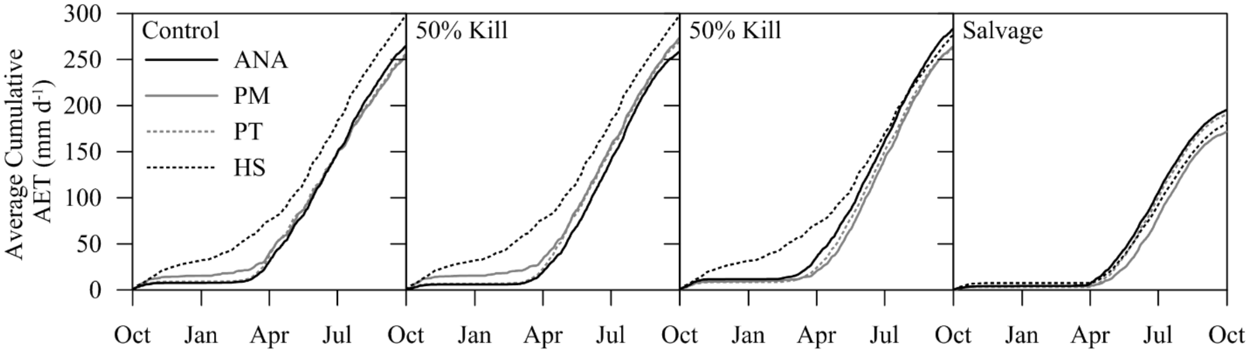

Figure B.6 Mean daily cumulative AET (three water years) of AET estimated with the four methods for each treatment stand. PM, Penman-Monteith; PT, Priestley-Taylor; HS, Hargreaves and Samani; ANA, analytical method.

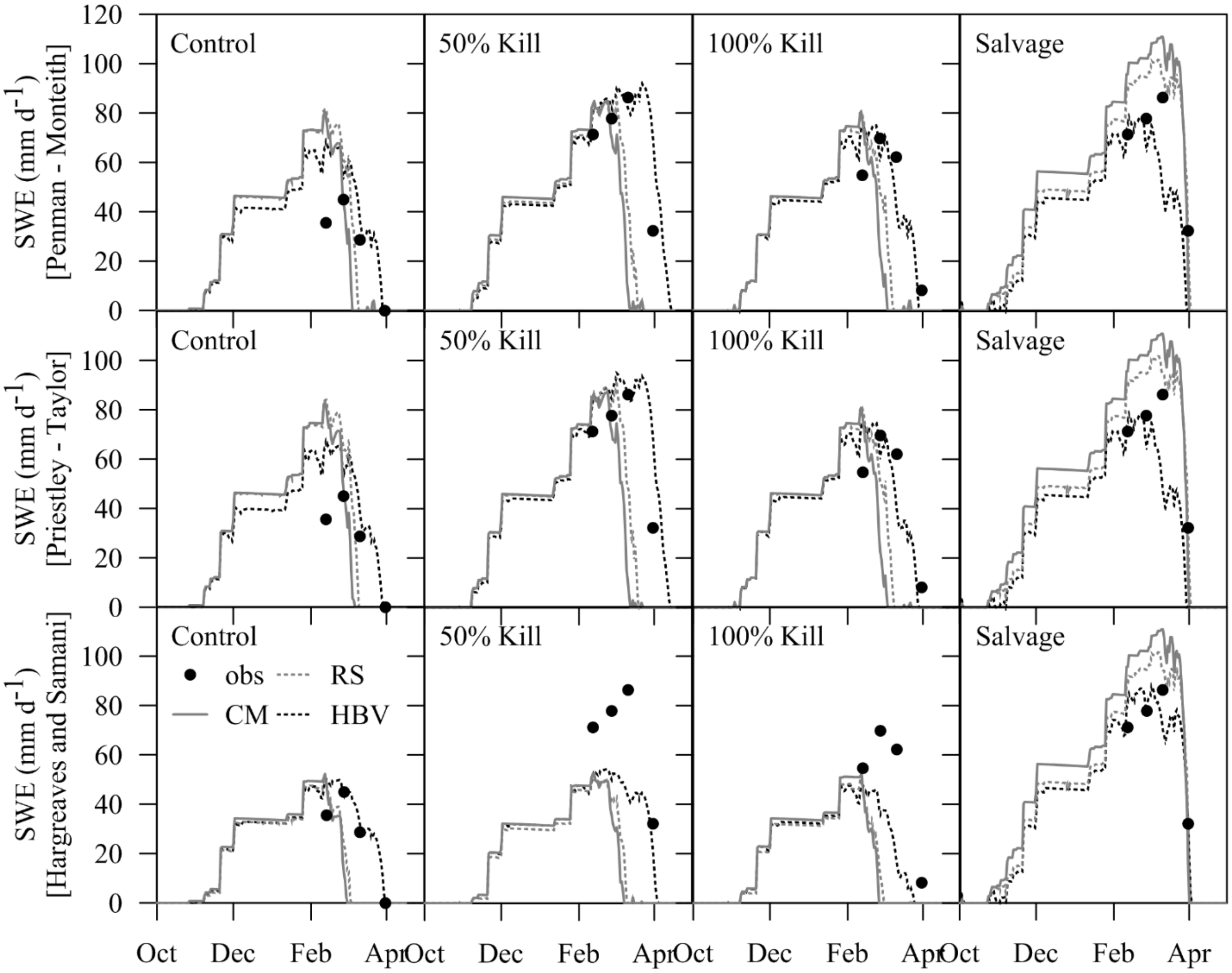

Figure B.7 Predictions of SWE for the 2016 water year compared to observed snow survey data for each model combination in the treatment stands. HBV, HBV-EC snowmelt; RS, restricted snowmelt; CM, Cold Regions Hydrological Model snowmelt.

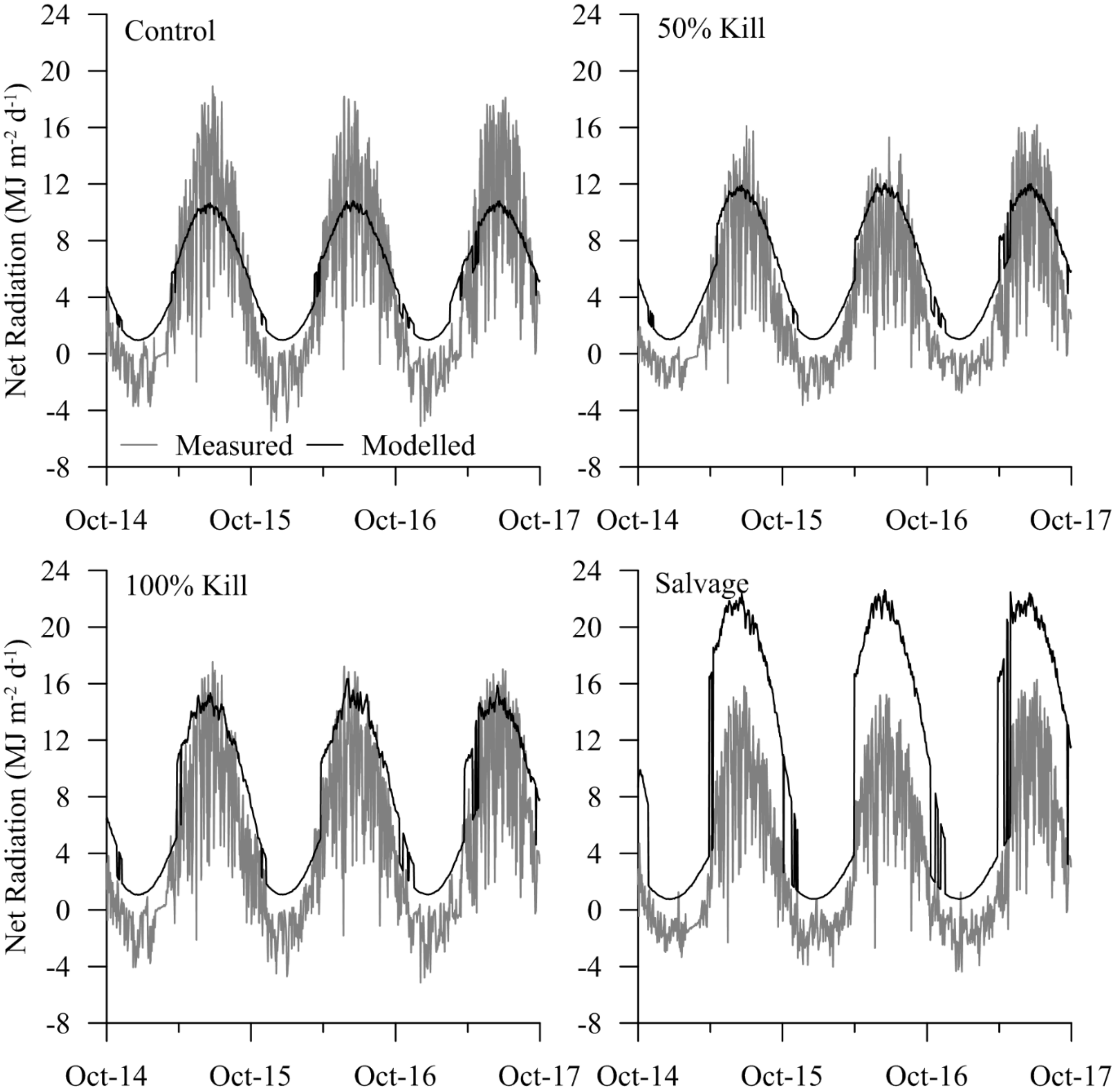

Figure B.8 Comparison of measured radiation and modelled net radiation (with field measured extinction coefficient) during the detailed MPB Robb stand-level study.

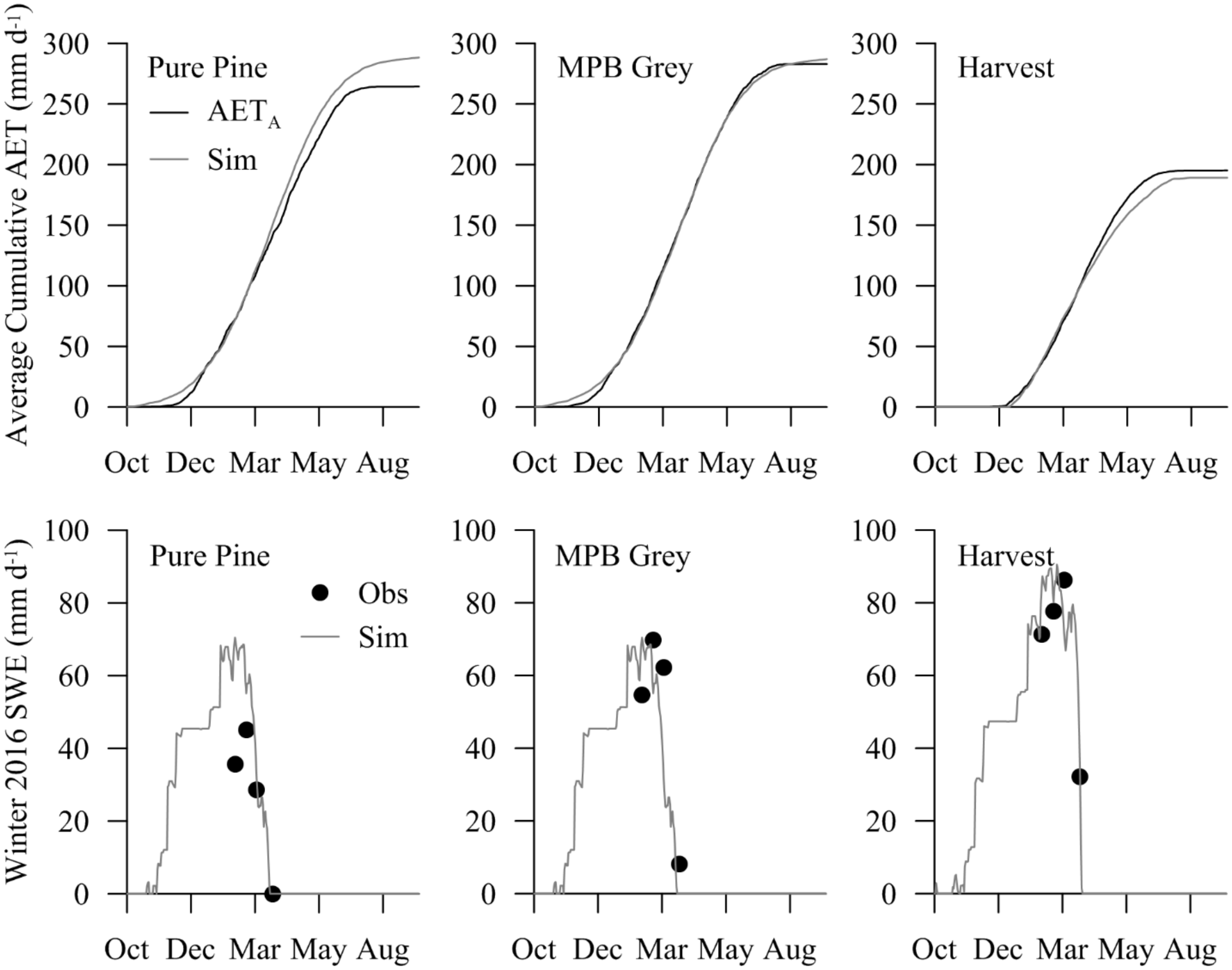

Figure B.9 Mean daily cumulative actual ET (three water years) estimated for the Pure Pine (100% pine trees), MPB Grey (100% affected trees) and Harvest (100% clear-cut) hydrologic response units (HRUs) using Hargreaves and Samani (1985) potential ET method with a correction factor compared to estimates of analytical actual ET (AET$_A$). The bottom panel is the modelled snowmelt for a selected winter using the corrected potential ET. These model simulations also include the combined forest floor and canopy rainfall interception without the litter layer in the soil model structure.